Rho GTPases Required for Angiogenesis: Role and Regulation of RhoG

Margherita Scarcia

Submitted in accordance with the requirements for the degree of
Doctor of Philosophy

The University of Leeds
School of Medicine

August 2013

The candidate confirms that the work submitted is her own and that appropriate credit has been given where reference has been made to the work of others.

I dedicate this work to whoever fights every day with passion and dedication, dressed in just the shield of knowledge, to make the world a better place.

Acknowledgements

Many people have contributed to the completion of my degree. I especially thank my family for believing in me. My mother, Caterina, for her constant love and encouragement and my father, Nino, for giving me words of guidance when I felt lost. I surely can't forget my fiancée, Giulio, who constantly stood on my side with his patience and love.

I want to thank my supervisor, Dr Georgia Mavria, whose extensive knowledge and passion for science has inspired me and helped me to develop an independent thinking. I am also grateful to my co-supervisor, Professor Pam Jones, for all the wise advice she gave me, the right support and help with the thesis. I also would like to thank Sabu Abraham and Maggie Yeo for training me at the beginning of my PhD and for generation of the preliminary data that led to my thesis.

I big thanks goes to all my colleagues, whoever shared the lab with me. In particular I thank Tracey Harvey, who was not just help in the lab but a sister to me; Kat McMahon and Andy Benest, for all the crazy moments we shared, the laughter and the tears and of course, the assistance and help that I received from each one of them.

I would like to thank Professor Chris Marshall at the Institute of Cancer Research London for the time I spent training in his laboratory and Dr Gareth Howell at FBS for help with confocal microscopy. I am thankful to Professors Martin Schwartz for the DOCK9 expression construct, Dr Len Stephens for the RhoG expression construct, Dr Jean-François Côté for GST-ELMO, Dr Hironori Katoh for flag-tagged DOCK4, Dr Vijay Yajnik for EGFP-tagged and DOCK4 deletion mutants and Dr Rick Bagshaw for the GST-DOCK4-SH_3 and GST-empty vector constructs.

Abstract

Angiogenesis is the formation of new blood vessels from pre-existing ones and it is necessary for physiological processes such as normal development, and pathological conditions like cancer growth and metastatic cell dissemination. In order to form new blood vessels, endothelial cells, the cells that line the blood vessels, must go through a number of distinct cellular processes. In order to sprout, cells have to initially detach from the vessel wall, migrate and divide. Endothelial cells must then establish new cell junctions and form functional lumens. During these processes the endothelial cell actin cytoskeleton and cell morphology change dramatically. The Rho family of small GTPases are key regulators of such morphological changes. Whilst the prototypical family members Rho, Rac and Cdc42 have been implicated in different aspects of endothelial cell behavior such as migration and cell assembly, other Rho GTPase family members are less characterized.

The aim of this study has been to understand the role of the Rho GTPase RhoG in vessel formation and to identify its regulators and downstream effectors. For this purpose organotypic co-culture system was employed of endothelial cells and fibroblasts that gives rise to three-dimensional capillary-like tubes as an *in vitro* tool to model vessel development. Using RNAi-mediated knockdown in the endothelial cells in the *in vitro* co-culture system, the role of putative regulators (guanine nucleotide exchange factors) and downstream effectors in angiogenesis was analysed and players that control lateral filopdia formation were identified. Pulldown assays that determine the activation status of Rho GTPases and gene overexpression and protein co-immunoprecipitation assays were then used to confirm phenotypic results seen in the co-culture assay. Using this system, a novel non-canonical SGEF-RhoG-DOCK4-Rac1-DOCK9-Cdc42 signaling module was identified that controls filopodia formation during endothelial cell assembly and sprouting. Knockdown of components of this signaling module block lateral filopodia formation, while tip filopodia persist suggesting that that different sub-populations of endothelial cell filopodia exist that are regulated independently during tubule morphogenesis. Mechanistic studies carried out in the course of this study showed that DOCK4 and DOCK9 interact with each other and with the RhoG effector ELMO. Complex formation of DOCK9 with ELMO is through DOCK4 whereas DOCK4 interacts directly with DOCK9. Domain deletion studies showed that DOCK4 interacts with DOCK9 via its SH3 domain.

In summary, this work has identified a new signaling cascade that drives vessel formation *via* lateral filopodia formation and sprouting and demonstrated for the first time an interaction between a Rac1 exchange factor (DOCK4) and a Cdc42 exchange factor (DOCK9). In addition to providing new information about the process of angiogenic sprouting and functional interaction between different GEFs, the signaling components identified in this study may constitute useful therapeutic targets in pathological angiogenesis in cancer and other diseases.

Table of Contents

List of Figures

Appendix

List of Tables

List of Abbreviations

Å: Angstrom

aa: amino acid

Ang: Angiopoietin

BCA: Bicinchoninic Acid

BDNF: Brain derived Neurotrofic factor

bFGF: Basic Fibroblast Growth Factor

BSA: Bovine Serum Albumin

C-Terminal: Carboxyl-Terminal

C57BL/6: C57 Black 6 mice

CRIB: Cdc42 and Rac interacting binding

Dll4: Delta like 4

DMEM: Dulbecco's modified eagles medium

DMSO: Dimethylsulfoxide

DNA: Deoxyribonucleic acid

DTT: Dithiothreitol

E.coli: Escherichia coli

ECL: enhanced chemiluminescence

ECM: Extracellular matrix

ECs: Endothelial cells

EDTA:Ethylenediaminetetraacetic acid

EGFP: Enhanced Green Fluorescent Protein

EMT: Endothelial to Mesenchymal transition

EV: Empty vector

F12: Ham's F-12 nutrient mix

FACS: Fluorescence activated cell sorting

FCS: Fetal Calf Serum

FGFR: Fibroblast Growth Factor Receptor

g: gravitational acceleration

GAP: GTPase activating protein

GAPDH: Glycerinaldehyde-3-phosphate-Dehydrogenase

GDI: GDP-dissociation inhibitor

GDP: Guanosine Diphosphate

GEF: Guanine nucleotide exchange factors

GFP: Green Fluorescent Protein

GOF: gain of function

GST: Glutathione Sepharose Transferase

GTP: Guanosine Triphosphahate

HDF: Human Dermal Fibroblast

HEK 293T: Human Embryonic Kidney cells

HEPES: (4-(2-hydroxyethyl)-1-piperazineethanesulfonic acid)

HIFs: Hypoxia Inducible Factors

HSPG: Heparan Sulphate Proteoglycans

HUVEC: Human Umbilical Vein Endothelial Cells

IL2: interleukin2

IPTG: Isopropyl-β-D-thiogalactopyranoside

IRDye: Infrared Dye

KO: Knockout

LB: Lysogeny Broth

LOF: loss of function

LVEM: Large Vessel endothelial Medium

MBC: MyoBlast City

MES: [2-(N-Morpholino) ethanesulfonic Acid]

MLEC: Mice Lung Endothelial cells

MMP: metalloproteinases

MOP: 3-(N-morpholino)propanesulfonic acid

mRNA: messenger Ribonucleic acid

N-Terminal: Amino-Terminal

^{o}C: Centigrade

PAK: P21 activated Kinase

PBS: Phosphate Buffer Saline

PDGFB: Platelet Derived Growth Factor B

PDGFR-β: Platelet Derived Growth Factor Receptor beta

PFA: Paraformaldehyde

PMSF: Phenylmethylsulfonylfluoride

PVDF: Polyvinylidenfluoride

RFPECs: Rat Fat Pad Endothelial Cells

rpm: revolutions per minute

RT: room temperature

SDS-PAGE: Sodium Dodecyl Sulfate Polyacrylamide Gel Electrophoresis

siRNA: small interfering Ribonucleic acid

shRNA: short hairpin Ribonucleic acid

SMC: Smooth muscle cells

TBS: Tris-buffered saline

TBST: Tris-buffered saline+Tween 20

VEGF: Vascular Endothelial Growth Factor

VEGFRs: Vascular Endothelial Cell Receptors

vSMC: Vascular Smooth muscle cells

WT: Wild Type

Chapter 1

Introduction

1. The vascular system

Primitive or small organisms rely on simple diffusion to control oxygen and nutrient distribution. In contrast, multicellular organisms need a functional circulatory system to fuel tissues with oxygen and nutrients and lymphatic vessels to collect the excess of interstitial fluids. The circulatory system is mainly composed by the heart and ramified vessel network that begins to form during vasculogenesis. Vessels arising by vasculogenesis are later organized into a more complex network of mature blood vessels, *via* angiogenesis. Vasculature has multiple roles: it is the main organ that distributes and exchanges chemicals, gases, nutrients and metabolic waste in tissues; it maintains cell homeostasis, balancing the body pH and temperature (Murakami, 2011). The circulatory system also acts as vehicle for the distribution of hormones, cytokines, growth factors and cells of the immune system that can quickly travel throughout the body to reach sites of inflammation (Adams and Alitalo, 2007; Aird, 2007).

Formation of a vascular network is a complex process that requires endothelial cells to proliferate, migrate, form cellular junctions and organize lumens for blood flow. These processes require endothelial cells to undergo complex cytoskeletal rearrangements that must be controlled spatially and temporally during expansion of the vascular network and establishment of blood vessel functionality. Several angiogenic factors and cell surface receptors that control angiogenesis have been identified and characterized. However, less is understood about the signaling pathways they activate and the precise cellular processes they control. There is increasing evidence that members of the Rho family of small GTPases act downstream of angiogenic receptors to regulate the process of angiogenesis through control of the endothelial cytoskeleton (Bryan and D'Amore, 2007). Rho GTPases are key regulators of the actin cytoskeleton, thereby influencing actin-dependent cellular processes such as cell motility, polarity and adhesion. Rho GTPases also participate in signaling pathways that control the cell cycle, apoptosis and gene transcription. The first study was published on the role of RhoA and Rac1 in 1992, showing that RhoA controls actin stress fibres while Rac1 regulates membrane ruffles in response to growth factor stimulation (Ridley et al., 1992). Since then the number of studies on the function of the prototypical Rho family members Rho, Rac1 and Cdc42 in numerous cellular systems

including endothelial cells has progressively increased. However, many studies in endothelial cells have been carried out in 2-dimensional cell culture systems that do not recapitulate the process of new vessel formation. Moreover, while studies have focused on Rho, Rac and Cdc42, the role of non-prototypical Rho family members in angiogenesis is largely unknown. In addition, it is not known how Rho GTPases are regulated during angiogenesis.

1.1 Blood Vessels

Blood vessels constitute the first organ to develop in the embryo (Carmeliet, 2003) and are essential for transport of blood and oxygen around the developing fetus. The blood vasculature consists of three major types of vessels: the arteries, which distribute the oxygenated and nutrient rich blood from the heart to the rest of the body; the veins that return deoxygenated blood to the heart; and the capillaries, the smallest vessels in the vasculature, that provide a large surface area and low pressure to maximize exchange of chemicals between blood and the surrounding tissues. The only exceptions to this general organization of the blood vasculature are the pulmonary arteries that pump de-oxygenated blood out from the heart to the lungs, and pulmonary veins that transport oxygenated blood from the lungs to the heart. Arteriolar vessels, venular vessels and capillaries are lined by a contiguous monolayer of endothelial cells. Capillaries are supported by variable coverage of pericytes (ranging from high coverage in the nervous system to low coverage in somatic vessels), which serve to keep the ECs in a stable, quiescent state. Arteries are sheathed by a thicker supporting layer of pericytes compared to veins (Adams and Alitalo, 2007). To withstand the high pressure caused by the shear force of the blood flow, arteries are further strengthened by a compact, homogeneous layer of smooth muscle cells (SMCs), with the thickest SMC layer found in the larger caliber vessels (Risau and Flamme, 1995; Aird, 2007).

1.1.1 Lymphatic Vessels

Lymphatic vessels and blood vessels arise in parallel and have complementary functions. The lymphatic system transports lymph to the heart and is involved in balancing the volume of interstitial fluids and removal of waste products (Alitalo and Carmeliet, 2002; Adams and Alitalo, 2007). The lymphatic system consists of lymphatic capillaries (small endothelial-lined tubes) and lymphatic tissues (spleen, lymph nodes, thymus, Peyers patches). Lymphatic capillaries that are adjacent to the blood capillaries are also covered by a single layer of specialized endothelial cells. The larger lymphatic vessels have layers of tunica intima, media (that contains SMCs) and adventitia (fibrous tissue and SMCs), similar to the covering seen in blood vessels. However, lymphatic and blood vessels are quite dissimilar. Lymphatic vessels lack a basement membrane. This characteristic, together with gaps between ECs, makes them highly permeable while ECs in blood vessels usually have tight junctions. To maintain stability when the surrounding tissue pressure rises, lymphatic vessels are provided with anchoring filaments. Overall, the lymphatic system has a lower flow rate and lower pressure than the vascular system.

1.1.2 Vasculogenesis

Vasculogenesis is the process of *de novo* blood vessel formation (Risau and Flamme, 1995; Aird, 2007) occurring from endothelial cell precursors. The process of vasculogenesis starts outside the embryo proper, in the yolk sac, where aggregation of mesenchymal cells forms blood islands (Risau and Flamme, 1995). Blood islands are surrounded by a peripheral layer of angioblasts (endothelial cells precursors) and hemangioblasts (endothelial and hematopoietic cell precursor) (Munoz-Chapuli et al., 1999) which form the inner mass. Angioblasts respond to VEGF released by the surrounding mesenchyme by sprouting and subsequently fusing with another sprouting blood island, creating the primitive capillary plexus (Risau and Flamme, 1995). The primitive capillary plexus is characterized by a uniform distribution of evenly sized vessels, which are later remodeled through angiogenesis, to produce mature vasculature, characterized by a more complex branching architecture of large and small vessels and capillaries (Jain, 2003; Ferguson et al., 2005). A schematic illustration of the process is shown in Figure 1.1.

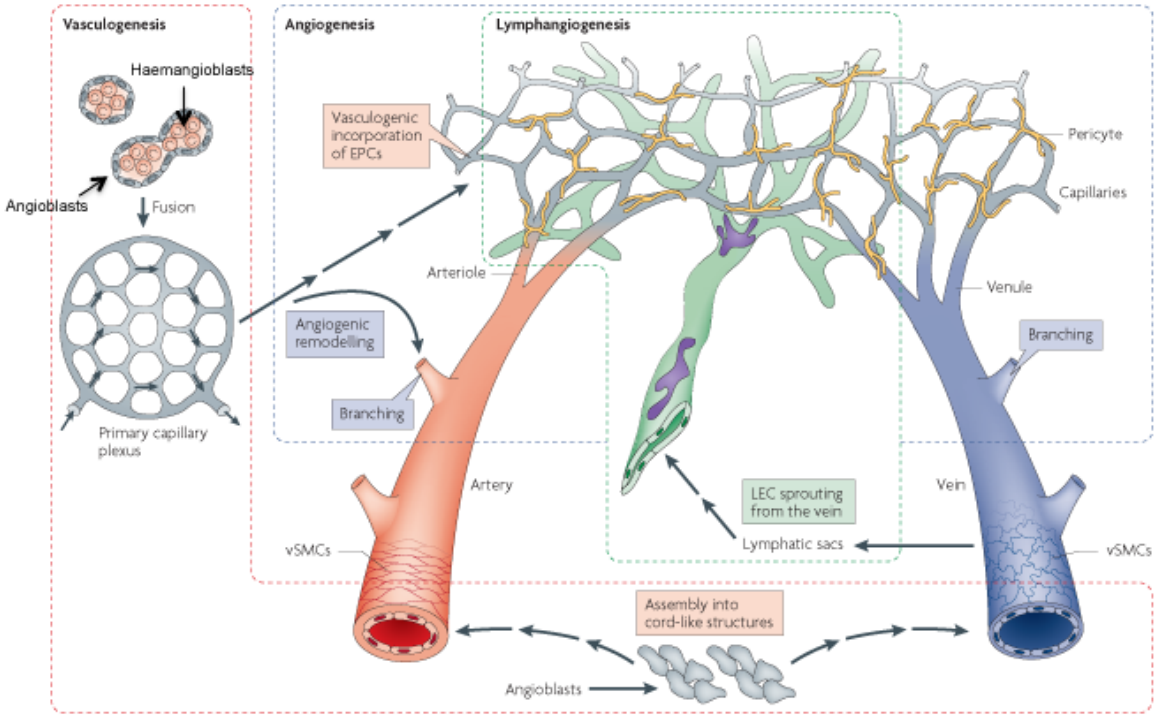

Figure 1.1 Schematic of vasculogenesis, sprouting angiogenesis and lymphatic angiogenesis
Mesodermal cells in the yolk sac differentiate into endothelial progenitor cells (EPCs), aggregate to form blood islands and reorganise into the primitive plexus (left, red dotted area). Blood circulation is established and primary plexi remodel to form a network of arterioles and arteries (red), capillaries (grey), and venules and veins (blue). Arteries and veins are covered by vascular smooth muscle cells (vSMC), whereas capillaries are covered by pericytes (yellow). From the embryonic veins the first lymphatic endothelial cells (LECs) sprout and migrate to form lymphatic sacs. During lymphangiogenic sprouting, branching and proliferation of lymphatic endothelial cells lead to differentiation and remodelling of the lymphatic vessels. Figure modified from Adams and Alitalo, 2007.

The capillary plexus rearranges under the influence of hemodynamic factors released by the embryo proper until the newly formed extraembryonic vessels penetrate the embryo. Intra-embryonic angioblasts cluster, migrate, spread and quickly start interacting to form a lumen. Lumenised vessels that orientate longitudinally form the dorsal aortae. The heart is the first functional organ to appear in the embryo (Ferguson et al., 2005). In addition to the yolk sac and embryo, vasculogenesis also occurs in the allantois, a fetal membrane that lies just outside the amniotic cavity. This results in formation of the umbilical vessels that connect the maternal circulation to fetal circulation (Downs, 2003; Downs et al., 2009).

1.1.3 Angiogenesis

Angiogenesis is formation of new blood vessels from pre-existing ones. During developmental angiogenesis, the vascular network arises from expansion and remodeling of the primitive vascular plexus (Section 1.1.2). This expansion of the vasculature is necessary since the primitive vascular plexus is not sufficient to deliver oxygen to the growing tissues. The formation of new blood vessels from pre-existing ones takes place through a number of different events that include sprouting of new vessels (sprouting angiogenesis), pruning of excess vasculature and longitudinal division of existing blood vessels (intussusceptive angiogenesis). Ultimately, vessels become stable and quiescent, and acquire functionality through formation of vascular lumens (Conway et al., 2000). Depending on the ultimate type of vessels that need to be produced (artery, vein, capillary), activated endothelial cells migrate and divide, connect with each other through the process of anastomosis and become surrounded by layers of peri-endothelial cells, pericytes or SMCs. The peri-endothelial cells stabilize the newly formed vessel network by generating a layer of extracellular matrix around them (Conway et al., 2001).

1.1.4 Lymphangiogenesis

Lymphangiogenesis refers to the formation of new lymphatic vessels; it occurs during embryogenesis and also during wound healing in the adult. The function of

lymphangiogenesis is to regulate tissue fluid homeostasis (Tammela and Alitalo, 2010) but the mechanism through which lymphatic vessels are formed is still unclear. It was originally thought that primitive lymph sacs develop from endothelial budding from embryonic veins, and then the lymphatic system develops by sprouting into the surrounding tissues and organs (Oliver and Detmar, 2002). An alternative theory is that lymph sacs arise from 'lymphangioblasts' (mesenchymal precursor cells), and these then form vascular connections. This latter theory has been supported by the identification of lymphangioblasts contributing to the lymphatic system development in the avian wing bud (Schneider et al., 1999). It is likely that the formation of new lymphatic vessels in the embryo arises from a combination of these two mechanisms.

1.2 Mechanisms of angiogenesis

Angiogenesis arises from a combination of four tightly regulated processes: sprouting angiogenesis, intussusception, regression and anastomosis.

1.2.1 Sprouting angiogenesis and branch formation

Sprouting angiogenesis can be divided into two phases, an activation phase and a resolution phase (Folkman and D'Amore, 1996; Carmeliet, 2003). The activation phase is initiated by genetic programs and signaling mechanisms that follow a series of sequential activation steps. When tissues become oxygen deficient, soluble VEGF is released, which attracts endothelial cells and stimulates blood vessel formation. Activated endothelial cells degrade the extracellular matrix through release of matrix metallo-proteinases (MMPs) such as MT1-MMP, specifically expressed by endothelial cells. Endothelial cells then migrate away from the parental vessel into the surrounding matrix towards the pro-angiogenic stimulus, proliferate and sprout. A summary of the different events occuring during sprouting angiogenesis is shown in Figure 1.2. The sprouting vessel can be subdivided into two types of specialized endothelial cell with distinct cellular fate specifications: tip cells and stalk cells (Blum et al., 2008; Gerhardt et al., 2003). The front situated cell, termed tip-cell,

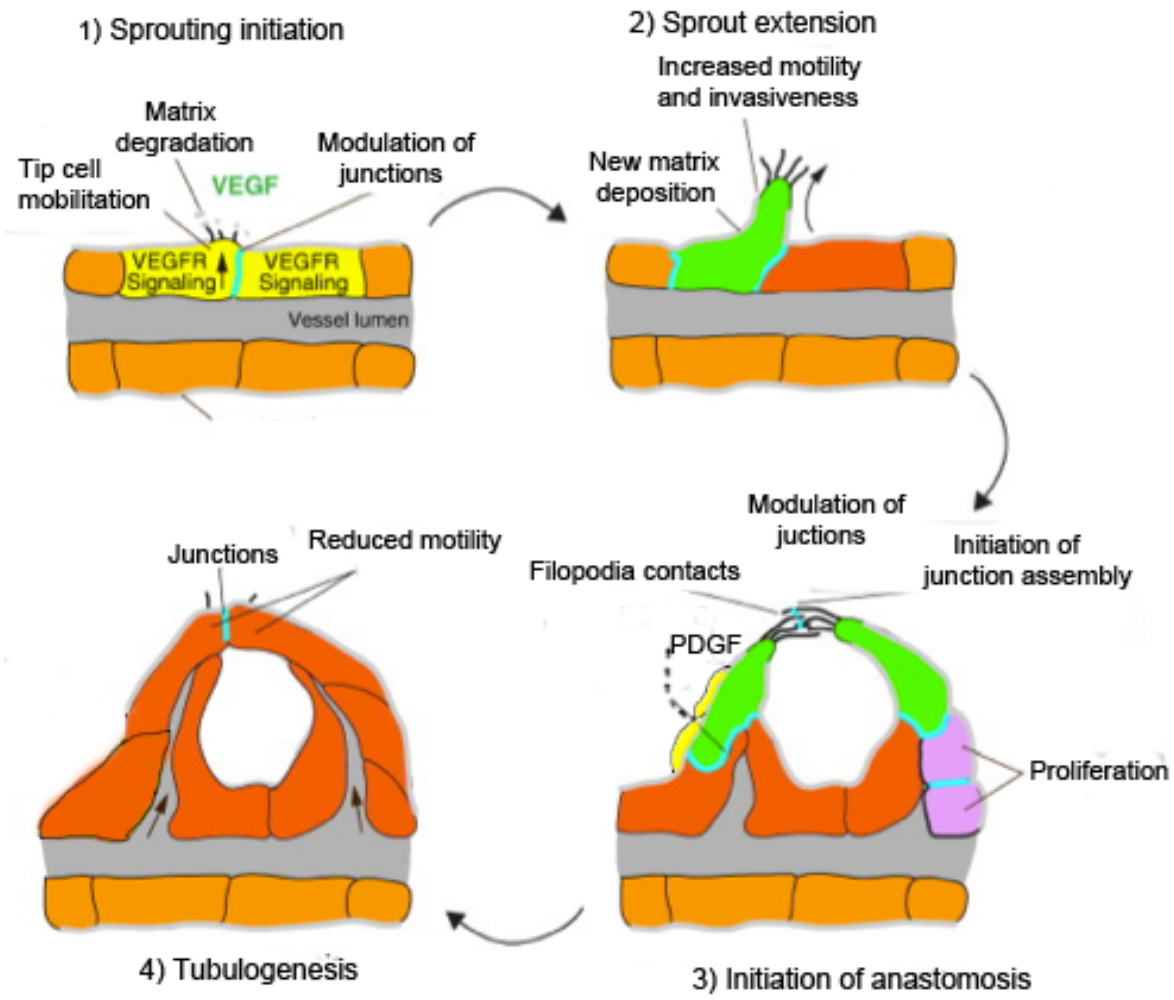

Figure 1.2 Steps of sprouting angiogenesis
Sprouting angiogenesis requires dynamic changes regarding cell-cell and cell-matrix interaction. During endothelial sprouting, tip cell (1, 2; yellow to green conversion) acquires a motile and invasive behaviour by detaching from adjacent endothelial (stalk) cells (red) and by altering apical-basal polarity. Sprouting also requires breakdown of the sub-endothelial basement membrane (1; dark gray) and formation of new basement membrane deposited around the growing sprout (2). Release of platelet-derived growth factor (PDGF) B by the tip cell recruits the pericytes to the newly formed sprouts. Fusion of sprouts and vessel formation is mediated by attraction that occurs between tip cells when encounter each other (3). As lumens start to form (4) blood flows, increasing lumen size and improves oxygen delivery and thereby reduces pro-angiogenic signals that are hypoxia-induced. Perfusion promotes vessel maturation, stabilization and cell junction, deposition of new matrix and tight pericyte attachment. Figure modified from Eilken and Adams, 2010.

utilizes numerous extensions of the plasma membrane called filopodia (Section 1.4.1) for sensing and responding to guidance cues in the micro-environment, such as VEGF (Gerhardt et al., 2003). Endothelial cells that are located behind the tip cell are termed stalk cells, and are essential for the elongation of the vessel branch, which results from EC proliferation. Coordination between tip and stalk cells is highly regulated by multiple factors, the main ones being the VEGF gradient and Dll4/Notch signaling (Section 1.3.1.2). Tip cells from the newly formed sprouts connect to neighbouring vessels of another sprout (Carmeliet, 2003) through filopodia to form a functional vessel. Newly formed blood vessels are stabilized by the vascular basement membrane and recruitment of mural cells, such as SMCs and pericytes. Many signaling pathways contribute to the control of this blood vessel maturation process. Upon VEGF stimulation, platelet derived growth factor (PDGF) B is primarily secreted by endothelial cells thereby mediating the recruitment of pericytes, which express its receptor PDGFR-β. A schematic of different events occuring during sprouting angiogenesis is shown in Figure 1.2.

Another signaling system involved in vessel growth and stabilization is the angiopoietin/Tie system, which consists of the angiopoietins (Ang-1 and Ang-2) and their tyrosine kinase receptors (Tie-1 and Tie-2) (Augustin et al., 2009). Binding of Ang-1 to the receptor Tie-2 is implicated in cell quiescence and vessel stability (Brindle et al., 2006), while the binding of Ang-2 to Tie-2 controls vascular homeostasis through an autocrine loop mechanism (Augustin et al., 2009). Recent studies however have shown that interaction of Ang-1 to Tie2 can also promote endothelial cell migration depending on the cellular context (Abdel-Malak et al., 2008).

1.2.2 Endothelial cell dynamics during sprouting

Generation of a sprout is a dynamic process. Once junctional proteins are loosened and a protrusion emerges, the sprout elongates as a result of a “pull-push” system between the tip and stalk cells (Qutub and Popel, 2009). As the tip cell moves forward to extend the vessel, it applies a pulling force causing the stalk cells to migrate out of the existing capillary. This pulling force causes the adjacent stalk cell segment to proliferate (Qutub and Popel, 2009).

Stalk cell proliferation in turn pushes the tip cell forward, resulting in tip cell migration. The process is cyclic as the tip cell then migrates along a gradient of an angiogenic growth factor, pulling along the adjacent stalk cell segment, which elongates. Diverse stimuli including different angiogenic growth factors, cell-to-cell contacts and internal retraction forces that generate mechanical stretch of adjacent cells affect this process (Merks et al., 2006). The main factor that drives endothelial cell motion and directionality *in vivo* is the VEGF gradient. Directionality of a sprout is maintained through the leading tip cell that senses the surrounding microenvironment to lead the way supported by proliferating stalk cells.

In 2011 Arima and colleagues analyzed the spatiotemporal dynamics of endothelial cell movement using a combination of live cell imaging of the aortic ring angiogenesis assay, and computational analysis (Arima et al., 2011). They found that endothelial cell behaviour during angiogenesis is both complex and heterogeneous. Analysis of endothelial cell behaviour during migration showed that endothelial cells individually migrate at different speeds, with the same cell navigating across the vessel, going back to front and front to back (Arima et al., 2011). Cells also change their position along the branch network (cell-mixing), moving about and overtaking other cells within the stalk area or moving to the tip of the vessel. That allows a new EC to occupy the leading position as the vessel grows. Arima and co-workers' findings indicate that stalk and tip cells are interchangeable, although a cell that occupies the leading position shows specific phenotypic features (del Toro et al., 2010). For instance, tip cells are enriched in proteases, basal membrane components, ADAM family members and cathepsin S, which are known to facilitate cell migration and angiogenesis *via* degradation of the ECM (del Toro et al., 2010).

1.2.3 Intussusceptive angiogenesis

Intussusception is a process that is distinct to sprouting angiogenesis but that also leads to vessel remodelling and angiogenesis (Carmeliet and Jain, 2000). Whereas sprouting angiogenesis involves the active sprouting and formation of new vessels, intussusceptive angiogenesis is the remodelling of existing vessels into a network of smaller vessels by cell

migration. During intussusceptive angiogenesis, endothelial cells, predominantly in venules or capillaries, invaginate into existing vessels creating a zone of contact between endothelial cells that lying opposite each other in the endothelium, forming inter-endothelial bridges (Djonov et al., 2002). In the next stage, the endothelial bilayer is reorganized with a perforation inwards, forming an inner lumen that is stabilized by invading pericytes producing collagen fibres. An interstitial pillar core is then formed and penetrated by myofibroblasts, pericytes and interstitial fibres which results in longitudinal division of one vessel into two (Djonov et al., 2002).

1.2.4 Vessel Regression

During angiogenesis, endothelial cells can undergo changes that lead to vessel regression. Experiments in tissue culture models have shown that vessel regression is consequence of withdrawal of vascular growth factors (Ausprunk et al., 1978; Benjamin et al., 1999) and macrophage-induced endothelial cells apoptosis (Lang and Bishop, 1993). In the latter case it is yet not clear whether regression is a direct consequence of endothelial cell death within the vessel or whether regression is followed by apoptosis (Saunders et al., 2005; Bayless and Davis, 2004). In a more recent report it was demonstrated that vessels formed in a 3-dimensional model regressed even in the presence of VEGF and bFGF (Im and Kazlauskas, 2006) indicating that regression is an intrinsic component of the angiogenic program that does not necessarily result from growth factor withdrawal (Im and Kazlauskas, 2006). Studies have shown that phospholipase C-γ 1 (PLCγ) participates to vessel regression through competition with phosphoinositide 3 kinase (PI3K) for the binding to membrane lipids necessary for vessel stability (Im and Kazlauskas, 2006).

1.2.5 Anastomosis

Anastomosis refers to the mechanism through which tip cells of different vessels fuse. It has been shown that macrophages are involved in bridging tip cells that are in close proximity and then guiding their fusion (Fantin et al., 2009). Upon anastomosis, endothelial

tip cells undergo changes to ensure that the connection between the newly formed vessels is maintained. The changes involve reversing the endothelial cell dynamic and migratory nature into a more passive behaviour in which cells are tightly bound to one another through junctions. Conversion of the endothelial cell phenotype is promoted by the release of VEGFC by macrophages, localized at the vessel branch points (point within stalk cells where the branch originates). Data reported in the literature support a model in which VEGFC-producing macrophages stimulate VEGFR3-positive tip cells to activate Notch target genes which leads to decreased sensitivity to VEGF and facilitate vessel anastomosis (Tammela et al., 2011). This hypothesis is generated based on the phenotype of endothelial deletion of VEGFR3 which results in increased number of tips cells, resembling the phenotype of genetic deletion of Notch (Tammela et al., 2011).

1.3 Regulation of angiogenesis

Angiogenesis is regulated by growth factors released by hypoxic tissues or degradation of the ECM. VEGFA and bFGF represent the major growth factors involved in vessel formation and remodeling (Risau and Flamme, 1995).

1.3.1 VEGF and its receptors

The VEGF family members are key regulators of both vasculogenesis and angiogenesis in vertebrates. To date the VEGF family includes 5 different members, from VEGFA to VEGFD and the related placenta growth factor (PLGF) which has been shown to stimulate angiogenesis in ischemic heart and limb with a comparable efficiency to VEGF (Luttun et al., 2002). The VEGF family members show different affinity towards the receptors (VEGFR1 (Flt-1) and VEGFR2 (KDR, Flk1), almost exclusively expressed on endothelial cells and VEGFR3 (Flt-4), primarily expressed by lymphatic endothelial cells in healthy adult) and co-receptors (Heparan sulphate proteoglycans (HSPGs) and neuropilins). Figure 1.3 summarizes binding of VEGF family members with the corresponding receptors.

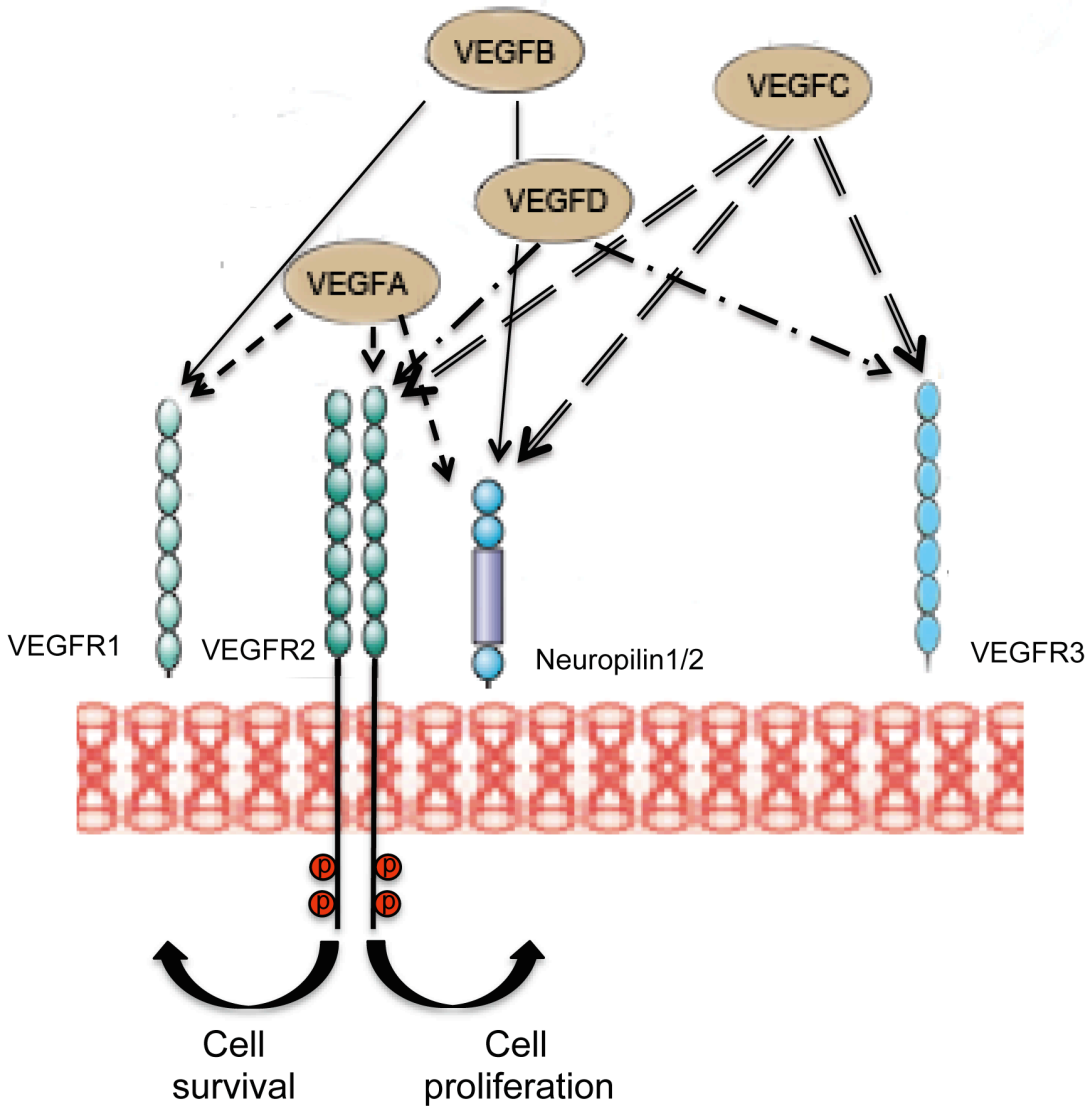

Figure 1.3 VEGF family members and their receptors
The VEGF family members and their interaction with VEGFRs and co-receptor Neuropilins. Binding of VEGFs to VEGFR2 induces phosphorylation of tyrosine kinase residues of the intracellular domain and activation of signaling cascades that control cell proliferation and survival. Figure modified from Ferrara et al., 2003.

Upon binding to the ligand, VEGF receptors form homo- and heterodimers which mediate activation *via* the auto-phosphorylation of several tyrosine residues located in the intracellular domain (Ferrara et al., 2003) and regulation of many downstream biological events including cell survival and proliferation (Gerber et al., 1988; Bernatchez et al., 1999). VEGFA, the most important angiogenic growth factor, has been found to have 5 isoforms: VEGF121, VEGF145, VEGF165, VEGF 189 and VEGF 206, whose biological activity is dictated by their capacity to interact with VEGF co-receptors. Another VEGF isoform, called VEGF165b, it has been found to negatively regulate VEGF activity (Woolard et al., 2004). VEGFA is crucial for vasculogenesis; deletion of one VEGF allele resulted in embryonic lethality between embryonic day (E) 11 and E12 (Carmeliet et al., 1996; Ferrara et al., 1996); whereas knockout of both alleles leads to an even earlier lethal phenotype (E9.5-E10.5) with severe vascular malformations (Ferrara, 2004). Knockout of VEGFR2 showed similar defects than those seen with loss of VEGFA gene in a transgenic mouse model (Tammela et al., 2005).

1.3.1.1 VEGF isoforms and their role in filopodia formation

A newly formed sprout needs a VEGF gradient to direct vessel growth (Gerhardt, 2008). In the absence of such a gradient, tip cell filopodia become randomly orientated and regressive, with angiogenesis resulting in poorly organized tubules (Gerhardt et al., 2003). The VEGF isoforms regulate filopodia formation, filopodia morphology and ultimately vascular patterning. For instance, studies of the mouse hindbrain vasculature solely expressing VEGF188 showed a predominance of tip cells extending long and numerous filopodia (Ruhrberg et al., 2002). In contrast, in the presence of VEGF120, while the vessel diameter was enlarged, tip cells were scarce and filopodia were significantly reduced in length, resulting in a poorly branched network of vessels.

The balance between the VEGFR members and their ligands is important. Jakobsson and colleagues have demonstrated that the level of VEGFR1/VEGFR2 in EC affects tip cells (Jakobsson et al., 2010). Reduction of VEGFR2 expression inhibits cells from adopting the tip position whereas EC with lower VEGFR1 expression dominate the tip cell position.

VEGFR3, which is also expressed in endothelial tip cells, negatively regulates tip cells. It was observed that cells with lower VEGFR3 levels (heterozygous for VEGFR3) dominate the tip position in competition with wild-type cells. VEGFR3, stimulated by VEGFC, appears to promote the conversion of tip into stalk cells through reinforcing Notch signaling (Tammela et al., 2010).

1.3.1.2 Tip cell selection and Notch signaling

Tip cells observed and analysed in many sprouting angiogenesis models possess a number of features, such as forefront position of the vessel branch, sensitivity to external cues, and highly polarized structure. In contrast with the stalk cells, tip cells do not proliferate and do not form lumen. Members of the VEGF receptor family have major roles in controlling sprouting angiogenesis along with Dll4 (ligand)/Notch (receptor) signaling, which coordinates endothelial tip cell/stalk cell fate. After binding of VEGFA to its receptor VEGFR2, endothelial cells increase the level of Dll4 synthesized (Lobov et al., 2007). It has been suggested that differences in VEGF level affects the level of Dll4 in ECs and this is the basis on which tip and stalk cell selection is determined (Lobov et al., 2007; Siekmann and Lawson, 2007). The cells with higher expression levels of Dll4 positioned at the tip and activate the Notch receptor in the stalk cells. Activation of Notch results in transcription of genes, such as Hes and Hey, that encode proteins that function as transcriptional repressors of VEGFR2, VEGFR3 and Dll4 (Henderson et al., 2001; le Noble et al., 2005). This results in a decreased responsiveness of the stalk cells to the VEGF environmental stimulus (Hellstrom et al., 2007). Stalk cells, prevented from acting as tip cells, gather around the leading cell, and divide and elongate. The balance between proliferative stalk cells and the selected leading tip cell is essential for the formation of an optimal blood vessel network (Lobov et al., 2007; Leslie et al., 2007). It was shown that inhibition of Notch signaling using γ-secretase inhibitors or endothelial-specific genetic deletion of Notch promoted increased numbers of tip cells (Boulton et al., 2008; Lobov et al., 2007; Leslie et al., 2007). In the absence of Notch, however, the sprouting vessels look thinner, showing a phenotype typical of immature vessels. In contrast, when the Notch signaling pathway is activated, the number of tip cells is significantly reduced and the

vascular network is less dense (Scehnet et al., 2007).

1.3.2 FGF and its receptors

The FGF family is composed of 22 members, most of which are single-chain peptides of 16-18 kDa that share up to 70% similarity (Ornitz and Itoh, 2001). FGFs are highly conserved and are found in many organisms (Ornitz and Itoh, 2001). FGFs stimulate a variety of cellular functions by binding to cell surface FGF receptors. So far, 5 members of the FGF receptor family have been identified (FGFR1, FGFR2, FGFR3, FGFR4 and FGFR6) and all are single-chain receptor tyrosine kinases. The FGFRs contain two or three immunoglobulin-like domains and a heparin-binding sequence (Ornitz and Itoh, 2001). The receptors are activated by dimerization induced by FGF binding. This leads to receptor auto-phosphorylation and activation of downstream signaling cascades with different biological responses including cell differentiation (Kanda et al., 1996), proliferation (McAvoy and Chamberlain, 1989) and mitogenic activity towards endothelial cells (Rusnati et al., 1996; Boilly et al., 2000), fibroblasts and SMCs (Couper et al., 1997; Wang et al., 1994). Another class of FGF receptors is Syndecans (Syndecan 1, Syndecan 2, Syndecan 3 and Syndecan 4), the main form of heparan sulphate proteoglycans (HSPG) receptors synthesized by many cells through which FGFs control physiological and pathological cell behaviour (Khan et al., 2008).

While the FGF family regulates a plethora of developmental processes, including limb development (Marin et al., 1998) and brain patterning (Marin et al., 2000) aFGF (FGF1) and bFGF (FGF2) have been found to play a central role in angiogenesis. aFGF has been found to regulate branching and survival of myocardial arteries (Carmeliet, 2000) whereas bFGF regulates endothelial cell migration and survival (Kottakis et al., 2011). In particular, they are important for new blood vessel growth as determined by wound healing assays (Broadley et al., 1989; Risau, 1990), proliferation of endothelial cells (Gualandris et al., 1994) or, in the case of tumour angiogenesis, *via* paracrine signaling through aFGF and bFGF released by tumour and stromal cells, or mobilization from the ECM (Presta et al., 2005).

1.3.3 Regulation of expression of VEGF

1.3.3.1 Tissue Oxygenation and VEGF

Hypoxia has been described as a potent stimulator of angiogenesis (Harris, 2002), triggered in response to a loss of homeostasis and represents a link between vascular oxygen supply and metabolic demand. In presence of oxygen prolylhydroxylases activate a proteasomal degradation pathway which degrades the HIF (Hypoxia Inducible Factor) family (HIF1, HIF2 and HIF3). In tissues lacking oxygen, the HIF1 accumulates, its α and β subunits dimerize, and consequentially HIF-1 migrates to the nucleus where it regulates transcription of downstream targets. In particular HIF-1 binds to Hypoxia Regulated/ Responsive Element/Enhancer sequences in the 5' and 3' regions of the VEGFA gene (Ryan et al., 2000; Dachs and Tozer, 2000). Expression of VEGFA is upregulated and soluble VEGFA is released to stimulate angiogenesis in order to compensate for the absence of oxygen.

1.4 Characterization of filopodia and their role in cellular processes

1.4.1 Filopodia architecture and molecular composition

Filopodia are thin (0.1–0.3 μm), tight bundles of filamentous actin with a finger-like structure, inserted in or protruding from the actin network at the plasma membrane (Small and Celis, 1978; Svitkina et al., 2003). Once bulged out these filaments elongate to maintain cell movement pushing the leading edge forward, and they are involved in promoting cell migration or extension (Pollard and Borisy, 2003; Chhabra and Higgs, 2007). Depending on the external stimuli and cell type, filopodia vary in number, length and distribution around the cell (Gupton and Gertler, 2007).

For example, fibroblast filopodia and nerve growth cone filopodia rarely exceed 10μm in length, but in sea-urchin embryos filopodia extend up to 40μm (Welch and Mullins, 2002). A large number of proteins that regulate the actin cytoskeleton have been shown to localize at filopodia sites and to regulate filopodia formation. Although many of these proteins are specific only to certain cell types, others are more broadly expressed. The best characterized actin-regulatory proteins that are involved in filopodia formation and maintenance are listed in Table 1.1.

Actin-regulatory proteins	Activity
Cdc42	Small GTPase that stimulaes filopodia formation (Nobes and Hall, 1995)
Myoxin-X	Concentrated at the tip filopodia, converge filament barbed end together (Bohil et al., 2006)
Fascin	Actin-binding protein (Kureishy et al., 2002)
ENA/VASP	Actin regulatory proteins that antagonize filament capping (Krause et al., 2003)
WASP/WAVE	Scaffolds that link upstream signals to the activation of the ARP2/3 complex (Stradal and Scita, 2006)
ARP2/3 complex	Proteins that serve as nucleation sites for new actin filaments
RIF	Small GTPase that stimulates filopodia formation through activation of Dia2 protein (Pellegrin and Mellor, 2005)

Table 1.1 Proteins involved in filopodia formation
Table 1.1 lists a number of commonly expressed proteins involved in filopodia formation.
Table modified from Mattila and Lappalainen, 2008.

1.4.2 Function of filopodia

Filopodia have been described as ‘antennae’ that cells use to scrutinize the microenvironment around them (Gupton and Gertler, 2007), through a variety of receptors that trigger diverse signaling pathways and cellular responses (del Toro et al., 2010). This supports the role of filopodia in both sensing the surroundings and acting as sites of signal transduction. The roles of filopodia are diverse and yet to be fully understood; they have been implicated in several physiological processes, of which cell migration is the best characterized (Figure 1.4).

The first description of how contractile filopodia influence cell movement was published in 1974 (Izzard, 1974). The analysis was carried out through *in vivo* visualization of a class of cells in the tunic of the ascidian *Botryllus schlosser*. Using timelapse microscopy it was found that active filopodia contractions and stretching influenced the whole body movement.

Filopodia mediate adhesion to the extracellular matrix to support the inter-change between cell migration and adhesion (Galbraith et al., 2007). This is through expression of integrins that accumulate at the filopodia sites in their active state. Integrin-containing filopodia at the leading edge promote the initial adhesion to the surrounding matrix generating the tension that acts to pull the cell forward.

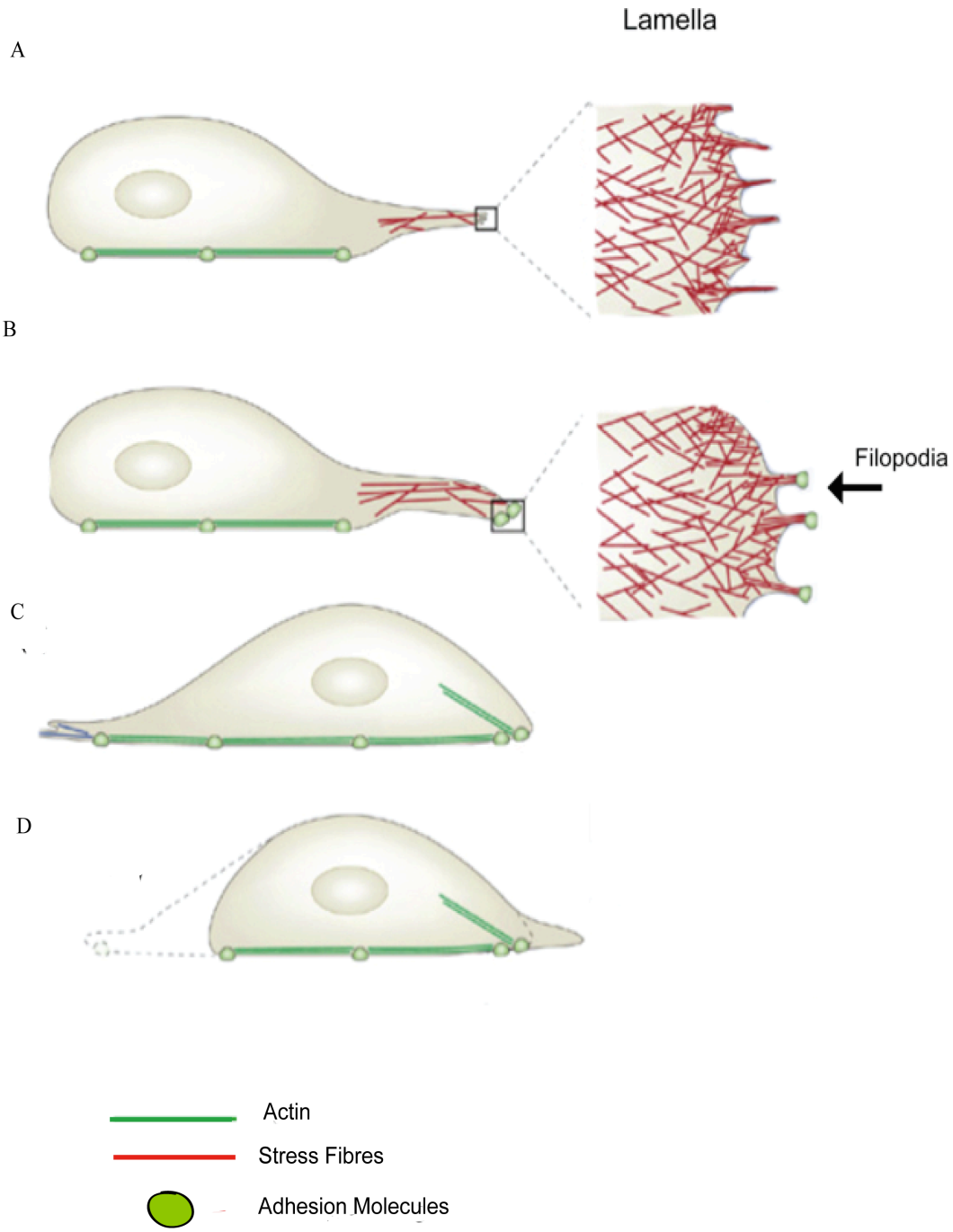

Figure 1.4 Changes in actin cytoskeleton during cell migration
A) Actin dynamics at the leading edge of the cell (cone-like structure (lamellipodium, Section 1.5.5.3), and filopodia formation) drive cell movement. B) Filopodia mediate the "pull-push" mechanism through active interaction with the matrix lying underneath the cell layer. This mediates extension of the cell body and adhesion with the substratum. C) Focal adhesion stress fibers and consequent cell contraction move the cell body and the nucleus forward until D) retraction fibers pull the rear of the cell closer to the rest of the cell body, increasing adhesion to the substrate and trailing edge retraction. Figure modified from Mattila and Lappalainen, 2008.

1.4.3 Roles of filopodia in different cell types

Filopodia play different roles, depending upon the cell type. The main function of filopodia in endothelial cells occurs during sprouting angiogenesis where filopodia probe the surrounding environment, sense the VEGF gradient and lead the ECs towards it as described in Section 1.2.1. The most significant example of how filopodia impact on endothelial cell behaviour *in vivo* was described by Gerhardt and colleagues (Gerhardt et al., 2003) through analysis of the mammalian retina plexus showing the role of filopodia in sensing VEGF released by the astrocytes. Binding to the extracellular matrix is an essential step in controlling cell viability. Endothelial cell filopodia form focal adhesion points connecting the cytoskeleton to the extracellular matrix (Defilippi et al., 1999). In addition, filopodia play a role in endothelial cell-cell contact (Hoelzle and Sviktina, 2012). According to the model proposed, once ECs interact with one another through sheet-like extensions of the cytoplasm (lamellipodia), this interaction is maintained by filopodia formation that create bridge-like structures between endothelial cells. The formation of cell-cell junction is a major process in controlling cell homeostasis and cell permeability in physiological conditions as well as during pathologies.

In macrophages, many filopodia are scattered around the cell body. Their role is to explore the environment and tightly bind pathogens and particles the cell needs to eliminate in order to maintain cell homeostasis (Kress et al., 2007). This process is mediated by formation of phagocytic cups, actin based membrane structures formed by filopodia.

In *Drosophila* and *C. elegans,* sheets of epithelial cells interact and subsequently fuse together to control embryo dorsal closure, a process mediated by filopodia. Cells recognize one another in a position-dependent manner through filopodia extension allowing epithelial cell sheets to align and adhere, a process known as adhesion zippering (Raich et al., 1999; Vasioukhin et al., 2000; Millard and Martin, 2008).

In neurons, filopodia sense neurite outgrowth promoting stimuli (Gallo and Letourneau, 2004; Zheng et al., 1996). Filopodia are also necessary for the development of dendritic spines, small protrusions along the neuron's dendrite, important in brain functions such as memory (Dent et al., 2007; Kwiatkowski et al., 2007; Zheng et al., 1996).

1.4.4 Mechanisms of filopodia formation

The initial step in the formation of an actin filament (nucleation) and successive combination of monomers to form a new filament has yet to be clarified. Two models have been proposed to explain how filopodia form: the convergent elongation model and the tip nucleation model.

In the convergent elongation model, the filopodium is generated by actin filaments that extend and grow out of the initial cone-like structure (lamellipodium) that surrounds the plasma membrane and the process is initiated by the actin nucleator ARP2/3 complex. In contrast, the tip nucleation model emphasizes the activity of the actin nucleator formin family proteins that nucleate actin filament at the tip of the filopodium.

The convergent elongation model was proposed based on the kinetic structural analysis of filopodial initiation in B16F1 melanoma cells (Svitkina et al., 2003). Observation of EGFP-(enhanced green fluorescent protein) expressing filopodia led to the postulation that filopodia originate from a reorganization of the lamellipodia network. The major difference between lamellipodia and filopodia therefore is that the actin filaments that form filopodia continuously elongate whereas lamellipodia are capped after a short period of filament extension. Filopodia are protected from capping by the action of the Ena/VASP family, which are enriched at tip filopodia (Lanier et al., 1999). The Ena/Vasp proteins have been found to antagonize capping molecules *in vitro* (Bear et al., 2002). Svitnika and colleagues also hypothesized that filaments with pre-bound Ena/VASP are selected within the actin filaments in the lamellipodium and brought together to assemble filopodia (Svitkina et al., 2003). Differences in filopodia width also suggested that these protrusions eventually cluster together, through their uncapped barbed ends (actin monomers linked with Myosin). Filopodia clustering is mediated by proteins such as Dia2 (Diaphanous-related (mDia) formins) and Myosin-X. The model also suggests that elongated actin bundles which are joined together are crosslinked by fascin (an actin cross linking protein) to produce the typical filopodia protrusion architecture (Gupton and Gertler, 2007).

The tip nucleation model suggests that filament assembly is initiated by Formin homology 2 (FH2). FH2 is persistently associated with the barbed end during their rapid growth, supporting fast assembly of actin subunits while protecting the end from capping proteins. The adjacent Formin homologous 1 (FH1) domain is recruited to quicken filament elongation by gathering the actin binding protein Profiling to the tip end. There is evidence that supports both models and it may be possible that, at least partially, the role of ARP2/3 and Formin in generation of filopodia overlap (Dent et al., 2007).

1.5 Rho GTPases: Regulators of Actin Dynamics

1.5.1 Introduction

Rho GTPases are a class of proteins principally known for regulating cytoskeletal dynamics and other cellular processes related to adjustment of the actin cytoskeleton, including cell polarity, migration, vesicle trafficking and cytokinesis.

1.5.2 Rho GTPases belong to Ras superfamily of small GTP binding proteins

The Rho GTPases are a family of small (~21 kDa) signaling G proteins that belong to the Ras surperfamily of small GTPases (Madaule and Axel, 1985). In higher vertebrates, the Ras superfamily consists of over 100 members, subdivided into Ras, Rab, Arf, Ran, and Rho subgroups each with distinct functions (Ridley, 2001). The Rho family consists of 23 members that can be sub-divided into eight subgroups: Rho (RhoA, B and C), Rac (Rac1, 2, 3 and RhoG), Cdc42, (Cdc42, TC10, TCL, Chp, Wrch-1), Rnd (Rnd1, 2 and Rnd3/RhoE), RhoD (RhoD and Rif), RhoH/TTF, RhoBTB (RhoBTB1, and 2), Miro (Miro1 and 2). The Rho GTPase family is evolutionary conserved, with members identified in yeast, plants, worms, and flies (Jaffe and Hall, 2005). Figure 1.5 shows a phylogenetic tree of the Ras superfamily.

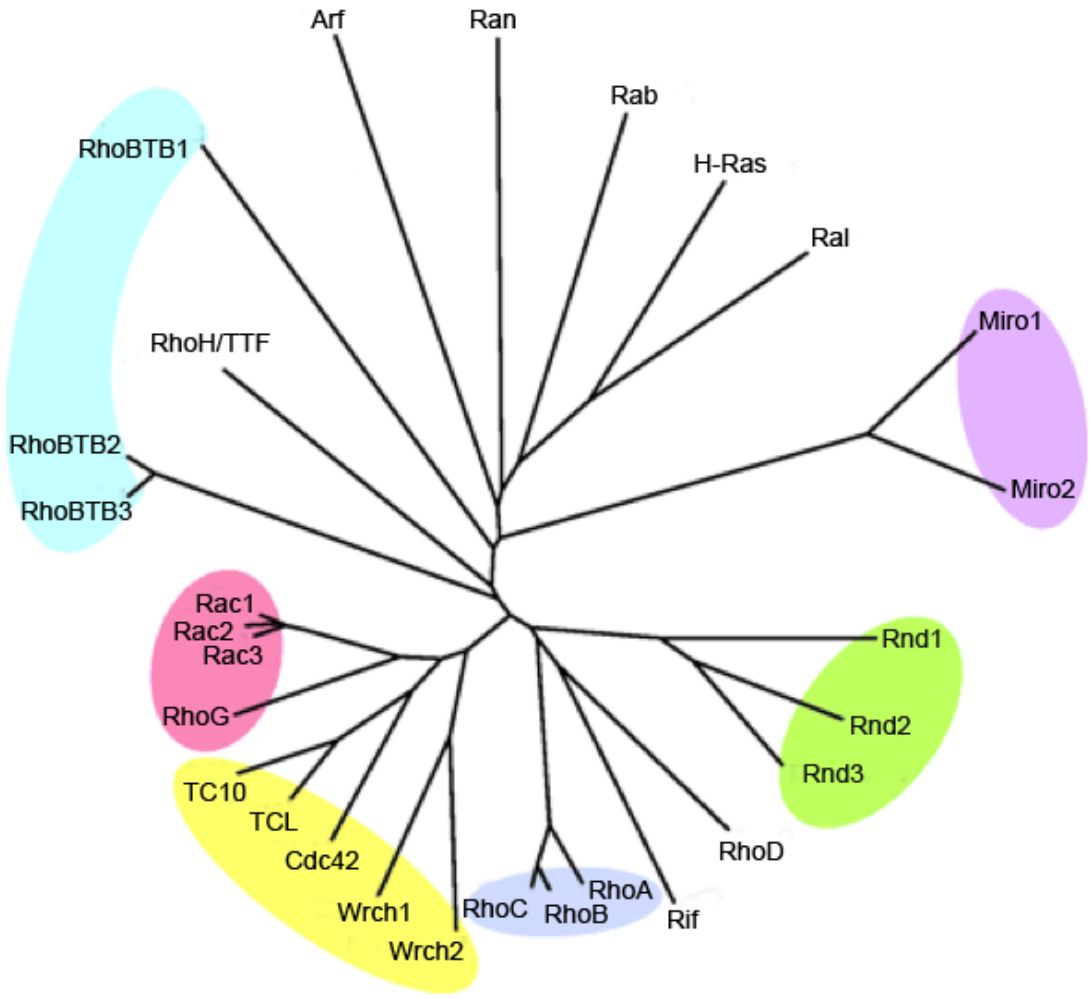

Figure 1.5 Phylogenetic tree of Rho GTPase family
Phylogenetic tree of the 23 Rho GTPase members and representative of Ras superfamily GTPases. Rho family GTPases are divided in six branches (from light blue to purple) based on sequence similarity and functional data. Figure modified from Wennerberg and Den, 2004.

Rho GTPases are known to control actin dependent processes such as migration, adhesion and axon guidance (Kaibuchi et al. 1999; Chimini and Chavrier 2000; Yuan et al., 2003). However a number of reports demonstrated their involvement in other cellular activities such control of cell polarity, gene expression and cell cycle progression (Van Aelst and D'Souza-Schorey 1997; Etienne-Manneville and Hall 2002). Through the regulation of these cellular processes, Rho GTPases play pivotal roles in tumourigenesis and although they are not mutated, they are deregulated in a large number of cancers (Vega and Ridley 2008). In addition, there is increasing evidence that Rho GTPases play important roles in angiogenesis (Abraham et al., 2009; Bryan et al., 2007; Cascone et al., 2003; Hoang et al., 2004; Mavria et al., 2006). New blood vessels in tumours may be formed both by sprouting of existing blood vessels (Ergun et al. 2001) and/ or assembly of recruited endothelial cells (Flamme et al., 1997). During these processes endothelial cells undergo complex morphological changes, such as spreading and extension of protrusions during migration and sprouting (Gerhardt et al. 2003; Gerhardt and Betsholtz, 2005) and cell contraction during assembly (Abraham et al., 2009) that are dependent on the actin cytoskeleton and are therefore regulated by Rho GTPases.

The best characterized members are Rho, Rac and Cdc42. RhoA, RhoB and RhoC, members of the same family that share around 80% of sequence similarity are referred to as Rho (Etienne-Manneville and Hall, 2002). Similarly, the Rac family members (Rac1, Rac2 and Rac3) are referred to as Rac (Etienne-Manneville and Hall, 2002).

In fibroblasts, gain of function (GOF) of Rho has been demonstrated to be responsible for stress fibres and focal adhesion (Chrzanowska-Wodnicka and Burridge, 1996) while activated Rac promotes lamellipodia formation and ruffles of the plasma membrane inducing de novo actin polymerization at the cell periphery (Ballestrem et al., 2000). Active Cdc42, on the other hand, promotes reorganization of actin polymerization to form filopodia or microspikes (Allen et al., 1997).

1.5.3 Structure of Rho GTPases

Crystallographic analyses of members of the Rho GTPase family revealed a 20kDa catalytic domain that is solely expressed in this family of proteins (Bourne et al., 1990). This domain comprises five alpha helices (α1-α5), six beta-strands (β1-β6) and five polypeptide loops (G-1-G-5) (Bourne et al., 1990). The polypeptide loops that form the guanine nucleotide binding site are the most highly conserved regions in this domain, hence the term G protein superfamily. Figure 1.6 shows a schematic of the main motifs present on Rac1 protein structure. The P-loop (also called the G-loop) is responsible for the binding of the phosphate groups of the GTP, therefore allows activation of the protein.

The analysis of the structure assumed by the protein when in the active and inactive state brought to light two functional regions: switch I and switch II. The switch I region, corresponding to the G-2 loop, incorporates the Rho GTPases downstream effector and it is therefore defined as the effector loop (Pai et al., 1989). This region is present in all the Ras superfamily GTPases but is the most diverse region amongst all the Rho GTPase members (Hirshberg et al., 1997; Ihara et al., 1998).

The hydrolysis of GTP in GDP and P_i (Section 1.5.4) driven by Rho GTPases requires the appropriate positioning of a water molecule for a nucleophilic attack on the γ-phosphate of the GTP (Feuerstein et al., 1989) and of Mg^{2+} that acts as a enzyme cofactor. Direct hydrogen bonding of the catalytic water molecule and amino acid take place in the switch II region, corrisponding to the G-3 loop, and it is necessary to ensure correct orientation for GTPase hydrolysis (Hirshberg et al., 1997; Ihara et al., 1998). Amino acid mutations in the G loops alter the ultimate Rho GTPase activity. In particular, mutation of the Gln61 in the switch II region to leucine generates a form of constitutively active Rho GTPases (Der et al., 1986). Substitution of the Gly12 in the P phosphate binding loop with valine also constitutively activates the Ras superfamily of GTPases. Such constitutively active mutants have proven to be an invaluable experimental tool in studying the role of the Rho family GTPases (Bishop and Hall, 2000). The G-4 and G-5 loops also contribute to stabilization of the Rho GTPase structure mediating interaction through the α and β helices and acting as a recognition site for the guanine base of the GTP (Paduch et al., 2001).

A

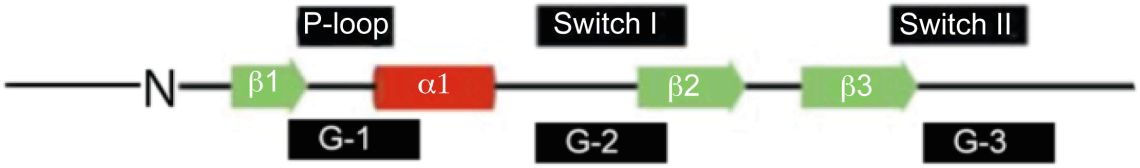

B

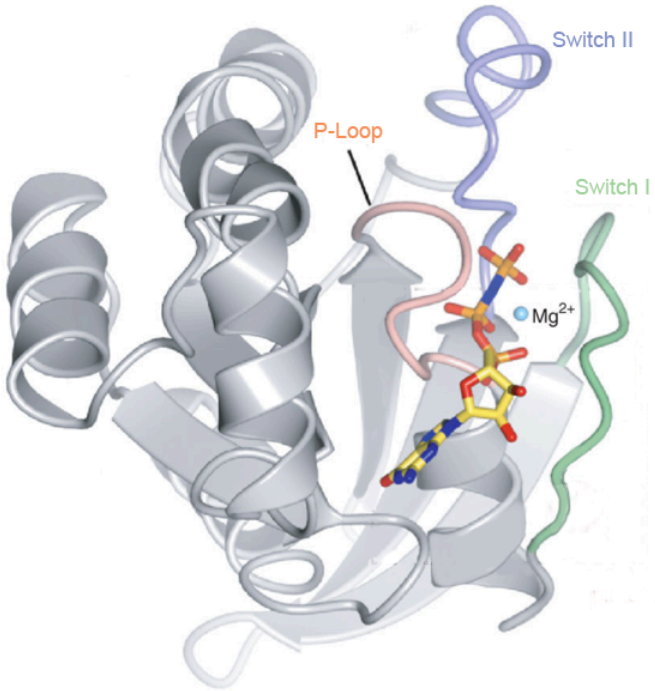

Figure 1.6 Structure of Rac1 protein
Figure shows secondary (A) and 3-dimensional (B) structure elements and sequence motifs of the Rac1 protein. Secondary structure (A) is illustrated as red barrels (α-helices) and green arrows (β-strands). Black boxes show characteristic motifs conserved in Rho GTPase proteins. Figure modified from Haeusler et al., 2003. (B) The crystal structure of Rac1 highlights the main domains. Switch I region is colored in green and it is shown to incorporate the downstream effector (colored pentagon); switch II region is colored in purple and the magnesium is coloured in cyan. The pink helix represents the loop P. Figure modified from Krauthammer et al., Nature, 2012.

1.5.4 The Rho GTPase cycle

To be activated, Rho GTPases need to cycle from a GDP bound form to a GTP bound active form. Spontaneous activation of Rho GTPases is a slow process due to a low off rate (K_{off}) for bound GDP (Bourne et al., 1991). Therefore, nucleotide exchange is thought to be the rate limiting step of the GTPase cycle (Erickson and Cerione, 2004). A faster activation of Rho GTPases is stimulated by positive regulators (Guanine nucleotide exchange factors, GEFs) that trigger the switch from Rho GDP to GTP. The maintenance of the active conformation is modulated by the Rho GTPases activating proteins (GAPs) that stimulate the intrinsic activity of Rho GTPase to hydrolysate GTP in GDP and phosphate to reverse the active state. Guanine dissociation inhibitors (Rho GDIs) maintain Rho proteins in the inactive state sequestering them in the cytosol (Michaelson et al., 2001). Figure 1.7 shows a schematic of the GTPase cycle.

Approximately 80 GEFs, 70 GAPs and 3 Rho GDIs have been identified in mammals (Etienne-Manneville and Hall, 2002) indicating that the many different cellular processes controlled by Rho GTPases are tightly organized and responses in different cell types, stimuli and biological activities are regulated by different mechanisms.

Despite a few exceptions where GAPs are expressed following preferential tissue expression and tissue specific function, these proteins are ubiquitously expressed, showing activity towards multiple Rho GTPases (Vigil et al., 2010).

A number of GAPs have been identified as having a key role in angiogenesis including p73RhoGAP (Su et al., 2004) and p190RhoGAP, that contributes to formation of capillary-like structure *in vitro* (Guegan et al., 2008). An example of Rho GDI involved in vessel integrity and endothelial cell behaviour is Rho GDI1 that regulates vessel barrier and permeability (Gorovoy et al., 2007) but also RhoG activation and cell migration downstream of bFGF signaling (Elfenbein et al., 2009).

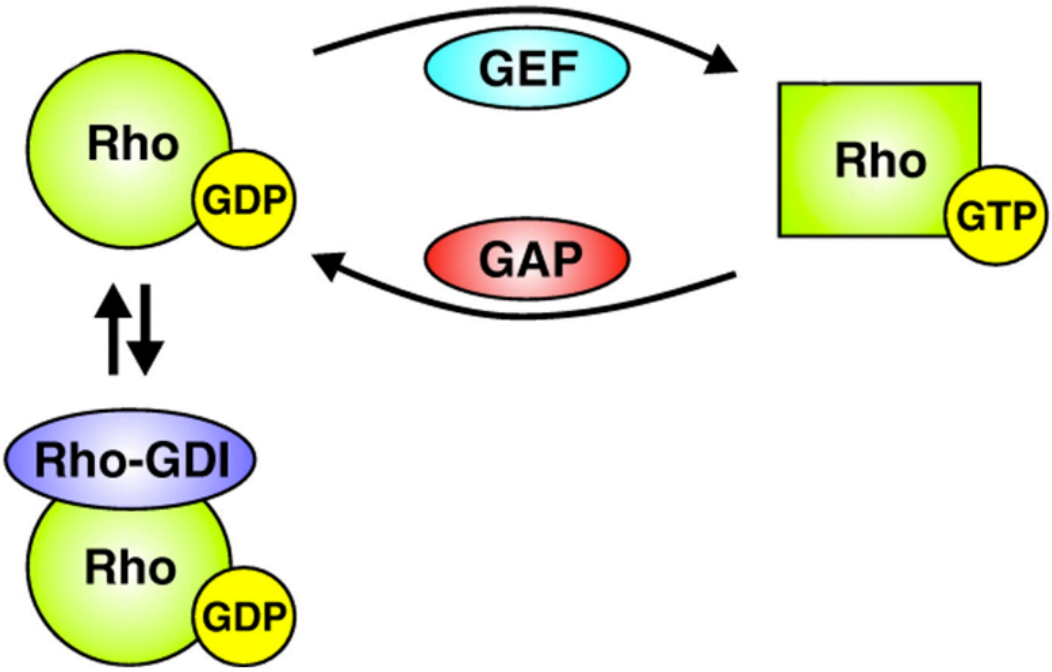

Figure 1.7 The Rho GTPase cycle
Rho GTPases cycle between Rho-GTP bound, active and Rho-GDP bound, inactive states. Their activation state is controlled by Guanine nucleotide exchange factors (GEFs) and GTPase-activating proteins (GAPs). Rho Guanine nucleotide dissociation inhibitors (GDIs) prevent their translocation to the plasma membrane and subsequent activation by GEFs.
Figure modified from Huveneers and Danen, 2002.

1.5.5 Rho family members

A precise spatial and sequential control of the actin filaments is necessary for many cellular functions including motility, cell divisions and endocytosis (Devreotes and Zigmond, 1988; Bretscher, 1991). Rho GTPases are regulators of cytoskeleton dynamics involved in several cellular processes. Studies on Rho GTPases have demonstrated that these proteins are well coordinated to achieve balance in movement and migration (Machacek et al., 2009). It has been suggested that RhoA acts to initiate protrusive events in the lamellipodial region, whereas sequential Cdc42 and Rac1 activation stabilizes the newly expanded membrane (Machacek et al., 2009). Cells can then adhere and migrate following a pull and push module (Section 1.2.2).

1.5.5.1 Rho

Rho is a sub-class of Rho GTPases comprising of RhoA, RhoB and RhoC. These members are structurally closely related and can potentially interact with the same downstream effectors, but elicit substantially different effects on cell shape and migratory properties, as observed in cancer cells (Ridley, 2013). RhoA plays a key role in the regulation of cell contractility. RhoB, primarily localized on endosomes, has been shown to regulate cytokine trafficking and cell survival, while RhoC may be more important in cell locomotion (Wheeler and Ridley, 2004). RhoA was the first member to be identified (Madaule et al., 1985) although its cellular functions were not elucidated until later (Ridley and Hall, 1992). Constitutively activated (Val14rhoA) mutants of RhoA expressed in a fibroblast cell line (Swiss 3T3) induced the assembly of contractile actin and myosin filaments (called stress fibres; Ridley and Hall, 1992). Similar events were seen in neuronal cells (Kozma et al., 1997) where RhoA caused growth cone collapse and neurite retraction. Balance between cell contraction and spreading is the main mechanism adopted by cells in forward movement. RhoA is also responsible for assembly of focal adhesion, stress fibres attached to the plasma membrane *via* adaptor molecules (i.e. vinculin and talin; Burridge and Connel, 1983a; Burridge and Connel, 1983b) that maintain cells anchored to the extracellular matrix, promote cell invasion and control cell behaviour in response to changes at the plasma membrane (Wehrle-Haller et al., 2012). The role of RhoA in

development is crucial as shown by the various conditional knockout phenotypes (Melendez et al., 2011; Jackson et al., 2011; Herzog et al., 2011). In particular, a conditional RhoA gene reducing expression in the developing mouse brain has shown lethality at late embryonic stages due to premature neuronal progenitor cell differentiation and increased apoptosis in the neuronal tube (Katayama et al., 2011).

1.5.5.2 Expression of RhoA in endothelial cells and function in angiogenesis

Rho signaling is essential for VEGF-dependent *in vivo* angiogenesis and *in vitro* capillary formation. To visualize neovascularization *in vivo*, a mouse skin angiogenesis model was engineered where VEGF was continuously delivered (Hoang et al., 2002). Ablation of endothelial RhoA using dominant negative mutants inhibited neovascularization when vessels were stimulated with VEGF, indicating a specific activity of RhoA downstream of VEGF signaling. In contrast, VEGF stimulated vessels expressing constitutively active RhoA developed an angiogenic network more prominent than VEGF stimulated vessels alone (Hoang et al., 2002). The role of RhoA in angiogenesis and vasculogenesis has been partially addressed through *in vitro* experiments. HUVEC plated in a 3-dimensional extracellular matrix (ECM) environment form capillary-like structures resembling ECs organization during angiogenesis (Nakatsu et al., 2003). It was shown that the cytoskeletal changes promoted by RhoA are sufficient to induce migration and motility of HUVEC in the absence of any external stimulus. In particular, tight binding with the ECM and consequent cell cytoskeleton retraction stimulates cell movement and helps to maintain cell-cell interactions. This is thought to be a key process in capillary-like structure formation *in vitro* as well as *in vivo* during neo-angiogenesis.

It has been shown that VEGF stimulates RhoA activation in ECs and blockage of RhoA and its downstream kinase (Rho kinase (ROCK) I/II) results in ablation of VEGF-induced cytoskeletal changes (Bryan et al., 2010). Moreover Y27632 (a ROCK inhibitor) inhibits vasculogenesis as demonstrated through cystic embryoid body models and is responsible for disruption of angiogenesis in *ex vivo* and *in vitro* models (Bryan et al., 2010). However in an oxygen-induced retinopathy mouse model it was shown that inhibition of ROCKI/II increased neovascularization suggesting that ROCKI/II acts as a negative regulator of

VEGF induced angiogenesis. The role of RhoA and its downstream effector ROCK in angiogenesis is still to be fully characterized.

1.5.5.3 Rac and lamellipodia formation

The term Rac indicates a subclass of Rho GTPases comprising of Rac1, Rac2 and Rac3. Rac1 is ubiquitously expressed whereas Rac2 is solely found in hematopoietic cells and Rac3 in the developing nervous system. Rac is known to control actin rearrangements, umbrella like structures called lamellipodia and formation of ruffles at the plasma membrane in a variety of cell types (Hall, 1998). Together with other protrutions, lamellipodia are involved in adhesion to the substrate and cell migration and as ruffle lamellipodia play a role in phagocytosis (Small et al., 2002). Studies on neutrophils using live imaging techniques have shown that Rac1 localises at the sites of lamellipodia formation and also at the rear of the cells even though no actin based activity was visualized. This suggests that Rac1 may play several roles in cell depending upon the spatial-sequential localization (Gardiner et al. 2002). Rac1 also plays roles in cell division (Michaelson et al., 2008), cell adhesion (Guo et al., 2006) and cell polarity (Liu et al., 2007).

1.5.5.4 Expression of Rac1 in endothelial cells and function in angiogenesis

The role of Rac1 in ECs has been investigated using a conditional Rac1 knockout (Cre/Flox approach), where the Rac1 gene was solely deleted in ECs (Tan et al., 2008). *In vitro* experiments using primary ECs from these conditional knockout mice showed that Rac1 deletion reduced cell migration, adhesion, tubulogenesis and permeability in response to VEGF, which was probably due to the inability of Rac1-deficient ECs to form lamellipodia structures and focal adhesions, and to remodel cell-cell contacts. More importantly, Rac $^{-/-}$ ECs resulted in embryonic lethality in mid-gestation (around E9.5), and defective development of major vessels and complete lack of small branched vessels were readily observed in these endothelial Rac1-deficient embryos and their yolk sacs.

The evidence provided by Tan and colleagues shows that expression of endothelial Rac1 is indispensable for vessel formation and angiogenesis.

1.5.5.5 Cdc42

Cdc42 has been found to influence cell behaviour in many ways including cell polarity, migration and actin cytoskeleton remodeling (Erickson et al., 2001). Cdc42 was first identified in *S. cerevisiae* as a cell-cycle mutant (Miller and Johnson, 1997) and loss of Cdc42 prevents budding and mating projections (Etienne-Manneville, 2004).

The Cdc42 full knockout mice showed that the knockout was embryonic lethal with mice dying at embryonic age of E7.5, earlier than seen with Rac1 knockout (Chen et al., 2000). Embryonic stem cells (ESCs) analysed *in vitro* showed defects in cell morphology. Further analysis showed an increased actin nucleation in the absence of Cdc42, causing disruption of cell shape. Cdc42 controls the formation of filopodia, which are important for cell–cell contact and sensing the environment as described in Section 1.4.2. Cdc42-null ESCs show defects in number and length of filopodia-like protrusions (Chen et al., 2000); also Cdc42-null neurons appeared to have less filopodia around the cell body (Garvalov et al., 2007). Therefore, as for Rac1, the small GTPase Cdc42 is necessary to guarantee full embryonic development.

1.5.5.6 Expression of Cdc42 in endothelial cells and function in angiogenesis

The phenotype of endothelial-specific Cdc42 deficient mice resembled the Cdc42 full knockout, embryonic lethal (Hu et al., 2011) with smaller embryos with fewer vessels compared to wild type, suggesting that Cdc42 is crucial for vessel development. During EC migration, many Rho GTPases are activated to control cell morphology. This results in forward movement and simultaneous disruption of adhesion forces at the rear of cell to maintain the cell contacts to the extracellular matrix. Cdc42 is involved in controlling

migration of ECs through filopodia formation that sense the VEGF gradient (Section 1.4.3). Studies using human foreskin microvascular endothelial cells (hMECs) have shown that reduction of the level of active Cdc42 through overexpression of its GAP (Cdc42GAP) results in reduction of capillary-like structures in a 3-dimensional fibrin matrix (Engelse et al., 2008) underlining the importance of Cdc42 in tube formation. Studies using ECs have shown that Cdc42 plays a key role in the control of cell polarity through binding to the downstream proteins Par3 and Par6. Cdc42 is involved in lumen formation in endothelial cells (Davis and Camarillo, 1996; Davia et al., 2007). In addition, constitutively active Cdc42 (V12Cdc42) selectively expressed in endothelial cells resulted in increased endothelial cell adhesiveness and lung vascular barrier integrity (Ramchandran et al., 2008). V12Cdc42 increased the interaction between α- and β-catenin, suggesting that Cdc42 strengthens the endothelial barrier and reduces vascular permeability.

1.5.5.7 RhoG

RhoG shares significant homology with Rac1 and Cdc42 (72% and 62% sequence identity, respectively, Vincent et al., 1992). It is ubiquitously expressed and evolutionarily conserved, with homologues identified in mammals, *Drosophila* and *C. elegans* (Estrach et al., 2002). RhoG, as with other Rho GTPases, has a varied role depending upon the upstream signaling pathway, the positive regulator and the downstream effector.

In lymphocytes RhoG regulates gene expression throughout remodeling of the actin cytoskeleton (Vigorito et al., 2003). Downstream of the haematopoietic lineage positive regulator Vav1, RhoG stimulates the interferon-γ promoter and the nuclear factor of activated T cells (NFAT). In addition Vav2 and Vav3 co-operate to stimulate the rapid activation of RhoG downstream of EGF signaling pathway in HeLa cells (Samson et al., 2010).

There are inconsistent reports describing the downstream pathway following RhoG activation; in REF-52 (a fibroblast cell line), constitutively active RhoG (RhoGv12) elicits filopodia protrusion similar to the overexpressed Cdc42 constructs and lamellipodia

formation, typical of Rac1 phenotype (Gauthier-Rouvière et al., 1998). Overexpression of RhoGv12 in presence of dominant negative Rac1 maintains filopodia formation while Cdc42 does not abolish lamellipodia, indicating that RhoG can activate Rac1 and Cdc42 through two distinct, independent signaling cascades (Gauthier-Rouvière et al., 1998). Recent reports demonstrated that RhoG activates Rac1 and Cdc42 through the same signaling pathway (Franke et al., 2012). It has been shown in rat pheochromocytoma PC12 (neuronal cell line) that RhoGv12 increases the endogenous Rac1 and Cdc42 activation and suggests that RhoG acts upstream of Rac1 and Cdc42 (Katoh et al., 2000). Differences in the RhoG downstream pathway might be related to the cell type.

The canonical mechanism triggered by RhoG to activate the downstream protein Rac1 suggests a binding between RhoG and its downstream effector ELMO (Katoh and Negishi, 2003; Hiramoto et al., 2006) followed by a ternary complex with a member of the DOCK superfamily (Section 1.7) (Lu et al., 2004; Lu and Ravichandran, 2006). Formation of this complex has been shown to occur during many different cellular processes such as cell migration in fibroblasts (Hiramoto et al., 2006) and neurite outgrowth in neuronal cells (Namekata et al., 2012).

1.5.5.8 Expression of RhoG in endothelial cells and function in angiogenesis

To date there is no evidence linking RhoG with angiogenesis, although its activity in endothelial cells, under certain conditions, has been reported. It has been shown that RhoG activity is essential to regulate trans-endothelial cell migration in the course of inflammation (van Buul et al., 2007). During inflammation endothelial RhoG elicits dynamic membrane protrusions, forming docking structures that partially cover the adherent leukocyte and allow them to penetrate the endothelial layer (van Buul et al., 2007). Ablation of RhoG activity by small interfering RNA leads to a dramatic reduction of protrusions formed at the plasma membrane and the trans-endothelial cells migration is compromised. It has also been reported that RhoG regulates endothelial cell migration downstream of Syndecan 4 by promoting Rac1 activation (Elfenbein et al., 2009).

1.5.6 Rho GTPases downstream effectors

1.5.6.1 ROCK

The mechanism through which stress fibres and focal adhesions are mediated depends on effectors downstream of RhoA. There are numerous downstream effectors that have been linked to Rho proteins with no catalytic domains such as Rhophilin, Rhotekin and Citron (Madaule et al., 1995; Reid et al., 1996; Watanabe et al., 1996) or serine threonine kinases such as PKN (Protein Kinase N; Amano et al., 1996) or ROCK. ROCK is the major contributor to RhoA-induced actin cytoskeleton dynamics (Chrzanowska-Wodnicka and Burridge, 1996). ROCK regulates phosphorylation of the myosin-binding subunit (MBS) of myosin phosphatase (myosin phosphatase target subunit 1; MPYPT1) on the threonine residue 697 and serine residue 854. Phosphorylation of the residues coincides with inactivation of the enzyme (Feng et al., 1999; Kawano et al., 1999) and phosphorylation of myosin light chain. Rho-kinase and myosin-binding subunit are involved in many cellular processes downstream of RhoA, including stress fibres and focal adhesion organization, smooth muscle contraction and neurite retraction (Amano et al., 2000; Kaibuchi et al., 1999).

A recent report has suggested that both Rho-kinase and myosin light chain kinase play important roles in cellular behaviour, such as the regulation of cadherin-based adhesion (Thomas et al., 2013) and the regulation of morphological and permeability changes of endothelial cells (McKenzie and Ridley, 2007).

1.5.6.2 ELMO proteins

The ELMO family of proteins are a class of downstream effectors specifically activated by RhoG. The mammalian ELMO was first identified as a gene regulating engulfment of apoptotic cells during embryonic development and cell motility (Gumienny et al., 2001). The *C.elegans* orthologue of ELMO, ced-12, was first identified as a protein required for cell migration and engulfment of apoptotic cells during embryonic development. In mammals, three ELMO proteins (ELMO1, 2 and 3) have been identified (Brzostowski et al., 2009).

Out of the three ELMO proteins, ELMO1 is by far the best characterized. ELMO1 is highly conserved amongst different species and human and mouse share 98% amino acid identity also seen for ELMO2. ELMO1 and ELMO2 share the 75% identity and 88% sequence similarity and ELMO1 and ELMO2 have about 44% similarity to the *C. elegans* ced-12 and 65% similarity to the *Drosophila* ced-12. An important part of the ELMO structure is the pleckstrin homology (PH) domain that mediates the binding with lipids at the plasma membrane and with the Src homology 3 (SH_3) domain of DOCK (Dedicator of cytokinesis) family members (Brugnera et al., 2002; Grimsley et al., 2004).

It has been shown that the ELMO proteins bind to DOCK GEFs including DOCK180, DOCK3 and DOCK4 (Brugnera et al., 2002; Grimsley et al., 2004; Lu and Ravichandran, 2006) and it has been debated whether the DOCK-ELMO binding is needed for Rho GTPase activation. It has been suggested that ELMO is essential for DOCK180 to act as Rac1 positive regulator (Brugnera et al., 2002; Grimsley et al., 2004) but it has also been shown that DOCK proteins or the DHR2 domain alone activate Rho GTPases *in vitro* in the absence of ELMO (Côté and Vuori, 2007; Lu et al., 2005). A role for ELMO in the localization of DOCK proteins has emerged (Kobayashi et al., 2001; Côté et al., 2005) and it is plausible that ELMO mediates some protein-protein interaction required for DOCK180 localization or function. Extensive studies using ELMO deletion mutants have suggested that the ELMO PH domain may directly contact the DHR2 domain of DOCK180, possibly stabilizing the binding of Rac to DOCK180 (Lu et al., 2004). Binding of ELMO1 to the DOCK180 SH_3 domain appears to unblock the auto-inhibited conformation by removing this steric block to facilitate Rac binding (Komander et al., 2008).

1.5.6.3 P21-Activated Kinase (PAK)

PAKs (p21 activated kinases) were the first Rho GTPase effectors to be identified. These are a family of serine/threonine kinases activated downstream of Rac1 and Cdc42 to regulate a variety of cellular activities derived from actin cytoskeleton remodelling (Arias-Romero and Chernoff, 2008). The PAK family can be sub-divided into two groups. Group I

PAKs (PAK1-3), that binds to Rac and Cdc42 through a CRIB containing domain (Cdc42 and Rac interactive binding) and group II PAKs, that consists of PAK4-6 (Arias-Romero and Chernoff, 2008). Conserved residues within the N-terminal PBD (p21-binding domain) are primarily involved in binding and activation by Rac and Cdc42. In the absence of a stimulus, the kinase activity of the PAK members is inactive due to the interaction of flanking KI (kinase inhibitory) regions (Lei et al., 2000) of one molecule packed against the kinase domain of the others (Parrini et al., 2002). Structural data (Morreale et al., 2000) and biochemical studies (Benner et al., 1995) suggest that GTPase binding causes a major change in the conformation of the KI domain that disrupts its interaction with the catalytic domain, allowing auto-phosphorylation that is required for full kinase activity (Lei et al., 2000). Downstream of Rac1 and Cdc42, PAK proteins have been shown to influence endothelial cytoskeleton dynamics including assembly of focal adhesion (Stoletov et al., 2001) and endothelial cell behaviour including migration and tube formation *in vitro* (Kiosses et al., 2002).

1.5.6.4 Other Rho GTPases downstream effectors

Rho GTPases have a variety of downstream effectors including other serine/threonine kinases (MLK, MEKK), SH_3 domain-containing proteins, lipid kinases (PI3-kinase) and scaffolding proteins. An example of the latter is represented by WASP and WAVE, downstream of Cdc42 and Rac1 respectively, to promote the formation of filopodia and lamellipodia through orientation of polymerized actin filaments leading to formation of membrane protrusions (Takenawa et al., 2007). WASP contains a WH1 domain (also known as the Ena-VASP-homology-1 (EVH1) domain) that is followed by a basic region and a CRIB domain (Rudolph et al., 1998).

Other examples of Rho GTPase downstream effectors are IQGAP1 and 2 (named GAPs because of some homology with Ras GAP). These effectors for Rac and Cdc42 are thought to be involved in actin polymerization (Briggs and Sacks, 2003) since IQGAP is found complexed with F-actin and Cdc42 or F-actin and Rac1 (Briggs and Sacks, 2003). Another effector, POR-1 (Partner of Rac), has been implicated in Rac-induced lamellipodia

formation, since truncations act as dominant negative constructs (D'Souza-Schorey et al., 1997).

1.6 Guanine Nucleotide Exchange Factors (GEFs) and their structure

As described in Section 1.5.4, the guanine nucleotide exchange factors (GEFs) catalyse Rho GTPase activation, triggering the switch from GDP to GTP. The first mammalian Rho GEF was identified as a transforming gene from diffuse B cell lymphoma and was therefore designated Dbl (Eva et al., 1988; Hart et al., 1991). Dbl was subsequently shown to function as a GEF for human Cdc42.

The main regions forming the GEF structure are a ~200-residue Dbl homology (DH) domain and an adjacent, C-terminal, ~100-residue pleckstrin homology (PH) domain. All Rho GEFs contain a DH domain and an adjacent PH domain (Cherfils and Chardin, 1999). The DH domain is responsible for catalysing the exchange of GDP for GTP within Rho GTPases while the PH domain has been proposed to localize the GEF to the plasma membranes by binding phosphoinositides (Erickson and Cerione, 2004). Isolated DH domains are functional *in vitro*, although the PH domain is required for maximal GEF activity (Rossman et al., 2002) and stabilization of the DH domain. Amino acid substitutions within the DH domain have been found to influence the affinity towards Rho GTPases. Some Rho GEFs (Sos1, Tiam1) act exclusively on specific Rho GTPases while others (the Vav family members) appear to act on multiple GTPases.

Outside the DH–PH domains, Dbl-family proteins have well-defined nucleotide and Mg^{2+}-binding pockets. The form of nucleotide (GDP or GTP) that is bound modulates the GEF activity whereas the Mg^{2+} is required for high-affinity binding of guanine nucleotides in Rho GTPases. The other domains vary depending upon the GEF, showing significant divergence amongst the family and justifying the unique cellular functions of the different family members.

1.6.1 SGEF and TRIO: regulation of Rho GTPases and control of endothelial cell behaviour

1.6.1.1 SGEF

SGEF and Trio represent two types of GEFs that, despite the differences in domains, are both RhoG GEFs involved in controlling endothelial cell dynamics. The human SGEF gene, identified in a two-hybrid screen, is localized on chromosome 3 and encodes a protein of around 100kDa. The gene encodes two transcripts: one (SGEF) has structural features typical of a Rho GEF and is expressed in several human tissues while the second transcript (CSGEF), an N-terminal truncated form of around 88 kDa, lacks the functional domain for the catalytic exchange of GDP to GTP and is found in the prostate and liver (Qi et al., 2003). Other than the typical PH-DH domains, SGEF also possesses a SH_3 domain which could mediate protein-protein interaction. In addition to its role in controlling remodeling of the endothelium under certain conditions, SGEF has been found overexpressed in prostate cancer where it enhances cancer development and progression (Wang et al., 2012). SGEF knockout mice are viable and fertile, showning no gross defects; however, under specific pathological conditions, SGEF plays a crucial role in inflammation (Samson et al., 2013).

1.6.1.2 Trio

In contrast to SGEF, Trio is important during embryonic development and knockout mice die soon after birth (Peng et al., 2010), showing important neurological defects, and defects in secondary myogenesis, suggesting a role for Trio in this late developmental process (O'Brien et al., 2000). Trio is a complex molecule with two GEF domains, a PH domain next to each DH domain and a PSK (protein serine/threonine kinase) domain with IgG-like repeats adjacent to it. The PH domain is thought to play a role in anchoring Trio to the plasma membrane or in stabilizing the GEF structure for protein-protein interaction. Trio is a RhoG positive regulator (Blangy et al., 2000) that controls signaling pathways involved in many cellular activities including phagocytosis through RhoG-ELMO complex fomation (O'Brien et al., 2000). The role of Trio in influencing the final conformation of the

cytoskeleton is reinforced by its interaction with Filamin A (protein that crosslinks actin filaments) and Focal Adhesion Kinase (FAK) (Seipel et al., 2001) to control cellular attachment to the plasma membrane, cell spreading, migration and cell survival (Medley et al., 2003).

1.6.1.3 Expression of SGEF and Trio in endothelial cells and function in angiogenesis

There is no evidence as yet linking SGEF with angiogenesis *in vitro* or *in vivo*. However it has been shown that SGEF is highly expressed in the endothelium and studies reported by van Buul and colleagues have shown that SGEF plays a key role during trans-endothelium migration of leukocytes (van Buul et al., 2007).

As with SGEF, Trio has also been linked with rearrangement of the ECs cytoskeleton and leukocyte trans-endothelial migration (van Rijssel et al., 2012) leading to ECs docking membrane structures that favour leucocytes adhesion and migration across the endothelium.

1.6.1.4 Other GEFs involved in endothelial cell behaviour and angiogenesis

SGEF and Trio have been shown to control leucocyte transendothelial migration by promoting docking structure (van Buul et al., 2007; van Rijssel et al., 2012); however it is to date unclear which signaling pathway they act upon to control those cellular changes. VEGF is the major growth factor responsible for endothelial cell behaviour and function. Few GEFs have been reported to act downstream of VEGF signaling cascade; Vav2 represents one example. It has been shown that Vav2 is responsible for Rac1 activation downstream of VEGF stimulation *in vitro* leading to endothelial cell migration by induction of Rac1-stimulated lamellipodia formation (Garrett et al., 2007). It has also been shown that the Vav family of GEFs is responsible for regulation of corneal angiogenesis induced by Ephrin A1 stimulation (Hunter et al., 2006). Loss of Vav proteins inhibited Rac1 activity and the angiogenic response *in vivo* and *in vitro* (Hunter et al., 2006).

Two other GEFs with pro-angiogenic function are Arhgef15 and Tiam1. Arhgef15

promotes actin polymerization and cell motility (Kusuhara et al., 2012) whereas Tiam1 controls endothelial cell permeability and Rac1 dependent cell migration (Knezevic et al., 2009).

Contrary to these GEFs discussed above, FGD5 has been reported to have an anti-angiogenic role *in vitro* and *in vivo* (Cheng et al., 2012) although it has been shown to control a wide range of EC regulatory activities including cell permeability, directional migration and proliferation (Kurogane et al., 2012).

1.7 DOCK superfamily of GEFs

In addition to Dbl proteins, an unrelated class of GEFs has been described to activate Rho GTPases: DOCK (Dedicator of cytokinesis) family members of proteins (Meller et al., 2005). The DOCK family adds to the diversity of proteins that function as GEFs and activators of Rho GTPases.

However, compared to the well characterized PH-DH GEFs, where there are structure and biochemical data, relatively little is known about the mechanism of action of DOCKs. The prototype of this family, DOCK1 (or DOCK180 as more commonly named), was originally identified as a binding partner for the SH_3 domain of the adaptor protein Crk by far western blotting (Matsuda et al., 1996). Localization of DOCK180 to the plasma membrane was shown to drive changes in cell morphology that were consistent with Rac activation (Hasegawa et al., 1996). Plasma membrane recruiting of DOCK180 was subsequently shown to occur downstream of integrin signaling in a pathway involving the adaptor Crk and another previously characterized adaptor protein, p130Cas, culminating in the activation of Rac (Kiyokawa et al., 1998). This pathway was shown to be functionally relevant in cell motility downstream of integrin-mediated adhesion at the leading edge (Klemke et al., 1998; Cheresh et al., 1999). At the same time, genetic studies in *C. elegans* and *Drosophila* demonstrated that DOCK proteins are evolutionary conserved regulators of Rac driven cell migration. The DOCK superfamily of proteins can be subdivided into four groups, designated A, B, C and D. A schematic diagram of the superfamily and the domain structures of its subfamilies is shown in Figure 1.8.

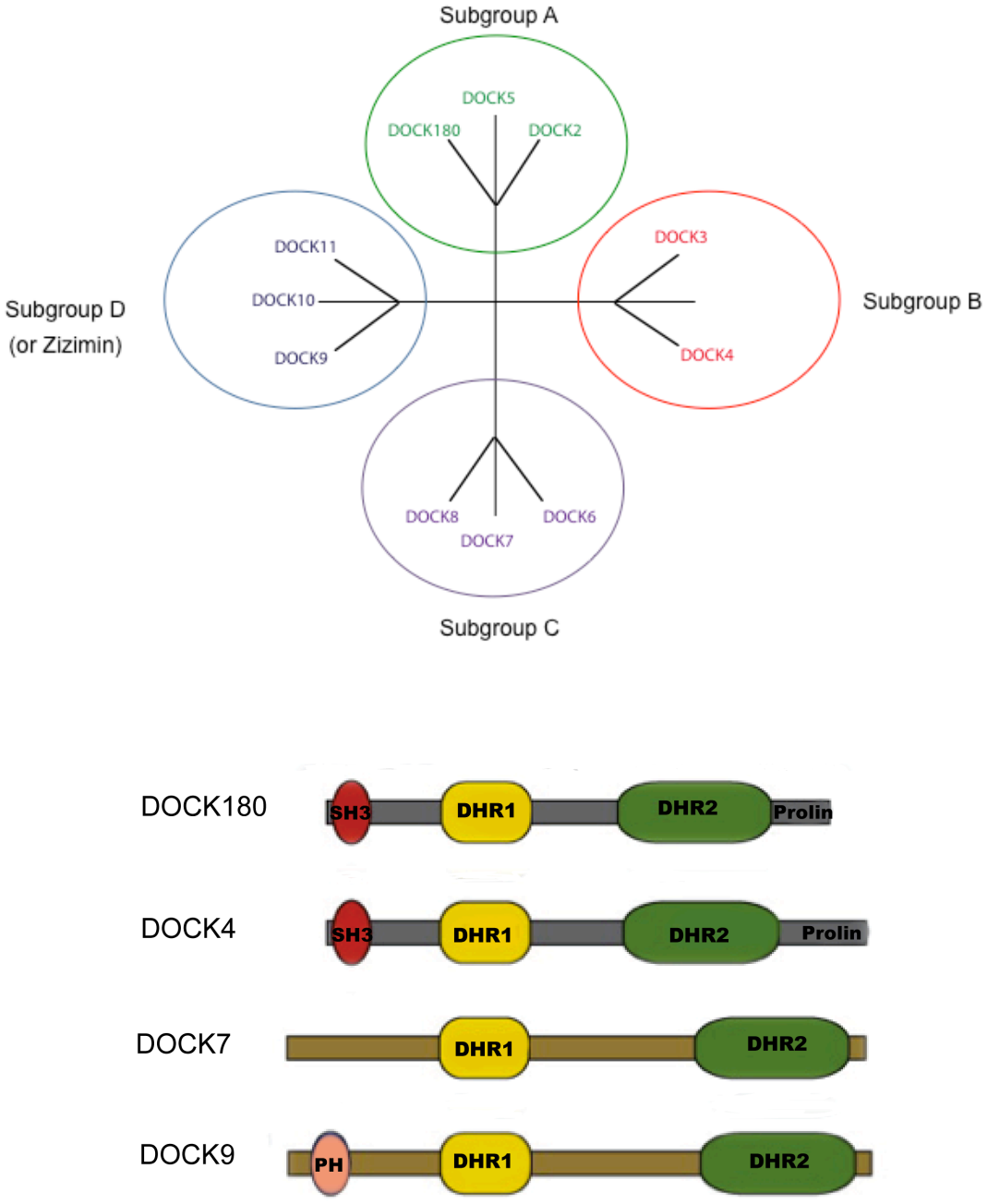

Figure 1.8 Identification of the DOCK family of GEFs
Top panel: Phylogenetic tree of the DOCK family of GEFs, where members have been divided in 4 subgroups based on their amino acid sequence similarity.
Bottom panel: Schematic diagram of the structure of representative members of each DOCK subgroup. Highlighted in yellow is the DHR1 binding domain, in green the DHR2 domain, in red the SH_3 domain and in pink the PH domain. Figure modified from Côté and Vuori, 2002.

Significantly, DOCK proteins are very large (~2000 amino acids) and very little is known about the function of their different domains. The homology between the DOCKA/B and the DOCKC/D subfamilies is restricted to the DHR1/DHR2 domains (Côté and Vuori, 2002). The subfamilies show trends of selectivity towards the Rho GTPases. For instance DOCKA and DOCKB subfamilies activate Rac while the DOCKD subfamily seems to be specific for Cdc42. The substrates of the DOCKC subfamily are less clear and seem to be both Rac1 and Cdc42 (Miyamoto et al., 2007). Extensive structural, functional and biochemical data for most of these proteins is still lacking.

1.7.1 The DHR1 and DHR2 domain of DOCKs

The most striking feature of the DOCK family is the presence of two conserved domains, DHR1 (DOCK homology region 1) and DHR2 (DOCK homology region 2) (Côté and Vuori, 2002) highlighted in Figure 1.9. DHR1, ~200 residues, is located at the N-terminus of the DOCK structure and binds to phosphatidylinositol 3,4,5-trisphosphate (Yang et al., 2009). The DHR-2 domain is the GEF catalytic domain, formed by ~ 400 residues located within the C terminus. This is organized into three lobes of roughly equal size (A, B, and C), with the Rho-family binding site and catalytic centre generated entirely from lobes B and C. Lobe C, the most conserved region of DHR2 domains, contains an area called the nucleotide sensor (α helix insert) that stabilises the DHR2 domain when binding the Rho GTPases. An example of DHR1 and DHR2 domains is shown in Figure 1.9.

1.7.1.1 DOCK4

DOCK4 and DOCK9 are two examples of DOCKs that belong to different sub-groups of the DOCK superfamily and control Rac1 and Cdc42 respectively.

DOCK4 presents a sequence of 200 amino acids highly homologous to other members of the DOCK family. DOCK180 and DOCK4 proteins have a N-terminal SH_3 domain and a divergent C-terminal containing proline rich motifs that bind SH_3 domains to mediate intra or inter-molecular protein interactions (Mayer and Baltimore, 1993). The first report

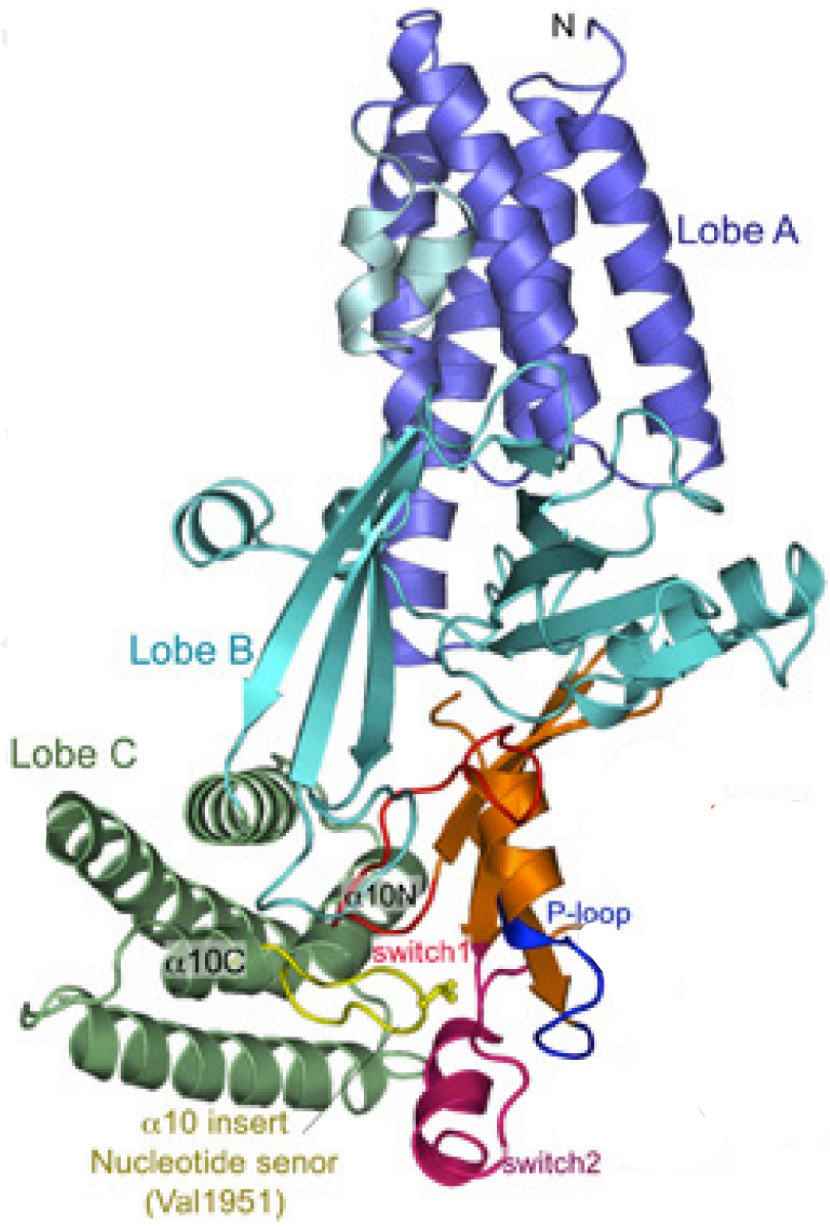

Figure 1.9 Summary of the DHR2 domain of GEFs involved in the interaction with a Rho GTPase

The lobe A (purple), lobe B (light blue) and lobe C (green) constitute the main body of the domain. Note the α10 region in the lobe C that contains the nucleotide sensor responsible for the binding with the Rho GTPase. Figure modified from Yang et al, 2009.

linking the mammalian DOCK4 and its nucleotide exchange activity to a Ras superfamily member (Yajnik et al., 2003) also linked DOCK4 with tumourogenesis. Specifically, injection of an osteosarcoma cell line in a mouse model of DOCK4 homozygous deletion mouse model (Yajnik et al., 2003) showed that DOCK4 plays a key role in cell junction and tumour extravasation controlling the downstream GTPase Rap. A DOCK4 GOF in the mouse osteosarcoma cell line showed restoration of the adherent junction and reduction of tumour cell migration.

Another Rho GTPase controlled by DOCK4 is Rac1. Overexpression in NIH3T3 (fibroblast cell line) showed that DOCK4 controls Rac1 activation (Hiramoto et al., 2006). Overexpression of DOCK4 DHR2 deletion constructs in HEK 293T cells showed reduced interaction between DOCK4 and Rac1. Mutation in the DOCK4 SH_3 domain showed enhanced Rac1-GTP binding. Activation of Rac1 *via* DOCK4 seems to be mediated by a binding between DOCK4 and the scaffolding protein ELMO (Section 1.5.6.2). Rac1 is activated by DOCK4 *via* ELMO, which binds *via* the SH_3 domain (Hiramoto et al., 2006). The ternary complex (RhoG/ELMO/DOCK4) translocates from the cytosol to the plasma membrane where Rac1 is activated to mediate cell migration (Hiramoto et al., 2006). A similar mechanism has been shown in hippocampal neurons (Ueda et al., 2013). The RhoG/ELMO/DOCK4 signaling module has been shown to promote cell migration and invasion in breast cancer downstream of Ephexin4 and EphA2 (Hiramoto-Yamaki et al., 2010).

1.7.1.2 DOCK9

DOCK9 (also known as Zizimin1) is known to activate Cdc42. DOCK9 was identified using an affinity proteomic approach to identify novel activators of Cdc42 in fibroblasts (Meller et al., 2002) and has been shown to be expressed in many tissues (Meller et al., 2002). DOCK9 belongs to the subgroup D of the DOCK superfamily and, consistent with the other DOCK family members, contains a DHR1 and DHR2 domains (Meller et al., 2002). DOCK9 shows high affinity for nucleotide-depleted Cdc42 *in vivo* and *in vitro*

(Kwofie and Skowronski, 2008). In contrast to the subgroup of DOCK A, B, C, DOCK9 contains a N-terminal PH domain that mediates its interaction with the plasma membrane (shown in Figure1.8). As for DOCK180 (subgroup A) and DOCK4 (subgroup B), binding with ELMO proteins is indispensable to open the structure of DOCK9 (subgroup D), to enable Cdc42 binding (Yang et al., 2009). The role of DOCK9 has been characterized in neurons, showing regulation of dendritic growth through activation of Cdc42 (Kuramoto et al., 2009) and in glioblastoma cells, in which DOCK9 stimulates pseudopodia formation and invasion (Hirata et al., 2012).

1.7.1.3 Expression of DOCK4 and DOCK9 in endothelial cells and function in angiogenesis

To date there are no reports describing the role of either DOCK4 or DOCK9 in angiogenesis nor are knockout models yet available making functional studies more difficult.

1.7.1.4 DOCKs in angiogenesis

DOCK180 is the only DOCK reported to have a role in angiogenesis *in vivo* and *in vitro*. Morpholino knockout models in zebrafish have shown that ELMO/DOCK180 complex regulates Rac1 activation and plays a role in angiogenesis (Epting et al., 2010). DOCK180 knockout mice die just before birth showing multiple vessel abnormalities (Laurin et al., 2008).

1.8 Preliminary Data leading to this thesis

1.8.1 DOCK4 and Rac1 control filopodia formation

An RNAi screen previously performed in the laboratory identified DOCK4 as a regulator of lateral branches. A similar phenotype was visualized in Rac1 siRNA transfected endothelial cells.

To gain insight into the role of DOCK4 and Rac1 in regulating branch formation, HUVEC were infected with EGFP expressing retrovirus harboring DOCK4 shRNA (short hairpin RNA) or Rac1shRNA and co-cultured with confluent fibroblasts.. Co-cultures of fibroblasts and EGFP-HUVEC were monitored by time-lapse microscopy. Wild type (WT) tubules branched and remodeled actively to form a network of tubules, whereas tubules formed with EC knocked-down for DOCK4 remained as cords that did not branch or remodel (Figure 1.10A). Endothelial cells lacking Rac1 showed similar phenotypes to DOCK4 knockdown, forming short and unbranched tubules (Figure 1.10A).

Interestingly, initiation of sprouts was observed occasionally when DOCK4 expression was reduced; however those were not viable and failed to form branches. The formation of cords suggests that in absence of DOCK4 cells can still interact in a head-to- tail manner. The time-lapse movies showed that tubules anastomosed normally when DOCK4 was absent supporting the hypothesis that DOCK4 is necessary for lateral cell-cell adhesion but not for head-to-tail association. High resolution confocal imaging showed that, in contrast to control endothelial cells, cells lacking DOCK4 were unable to form lateral filopodia, whereas tip filopodia persisted (Figure 1.11).

Altogether, the data show that DOCK4 and Rac1 are necessary for lateral cell-cell adhesion and branching but dispensable for head–to-tail interaction.

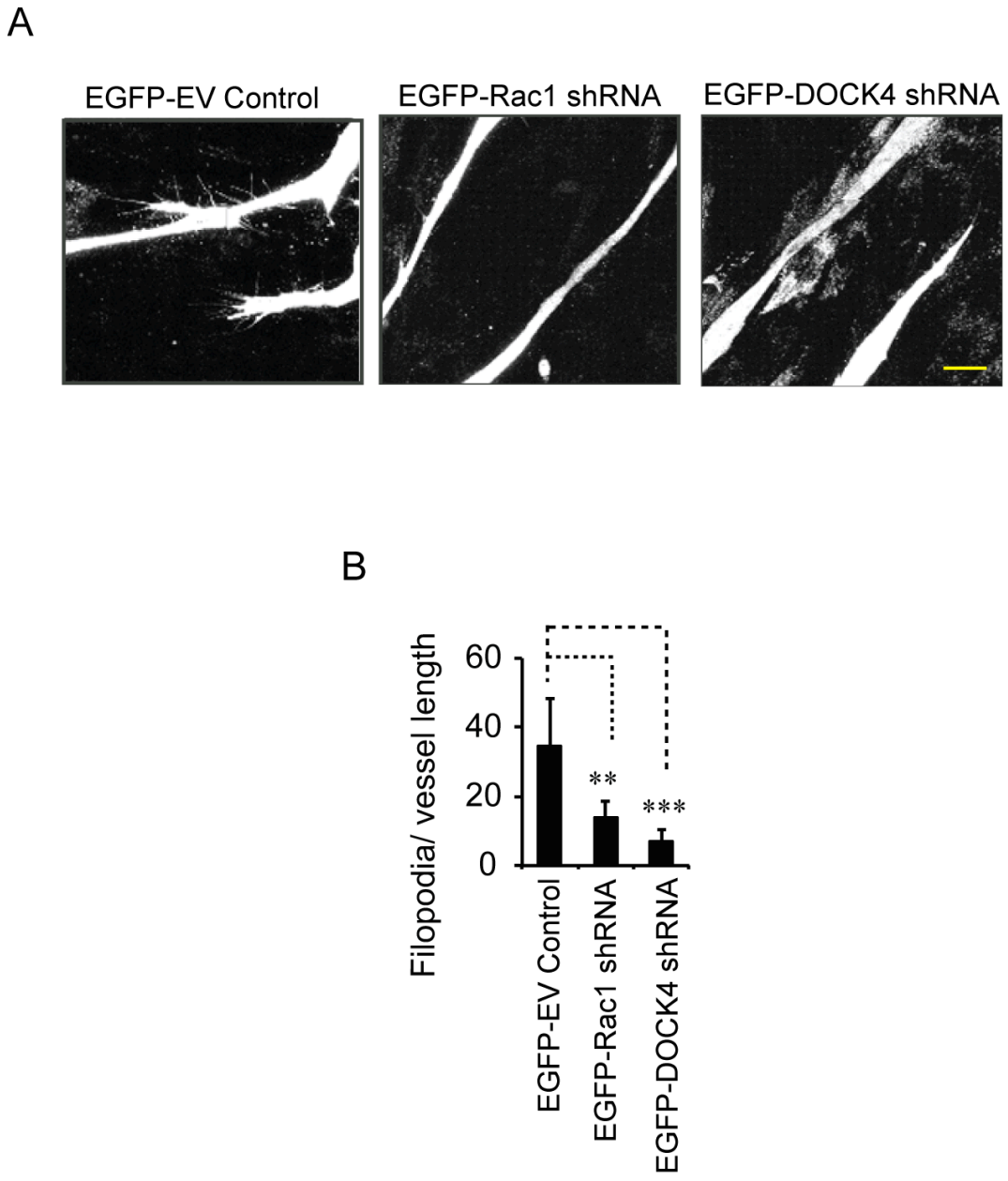

Figure 1.10 Loss of filopodia formation with knockdown of DOCK4 or Rac1
EGFP expressing HUVEC were co-cultured with fibroblasts, treated with VEGF (25ng/ml) and imaged day 6 after seeding. (A) Confocal images of filopodia in the presence of VEGF (25ng/ml) 6 days after seeding onto confluent fibroblasts and after depletion of Rac1 or DOCK4 (EGFP Rac1shRNA or DOCK4 shRNA; EGFP-EV (empty vector) control). Scale bar: 50μm. Note abundant filopodia in control tubules (EGFF EV control) and absence of filopodia in tubules lacking Rac1 or DOCK4. (B) Bar chart shows number of filopodia divided by tubule length (error bars indicate S.E.M.; n=6 microscopic fields each a 3x3 tiled confocal image from a representative experiment). Data generated by Sabu Abraham.

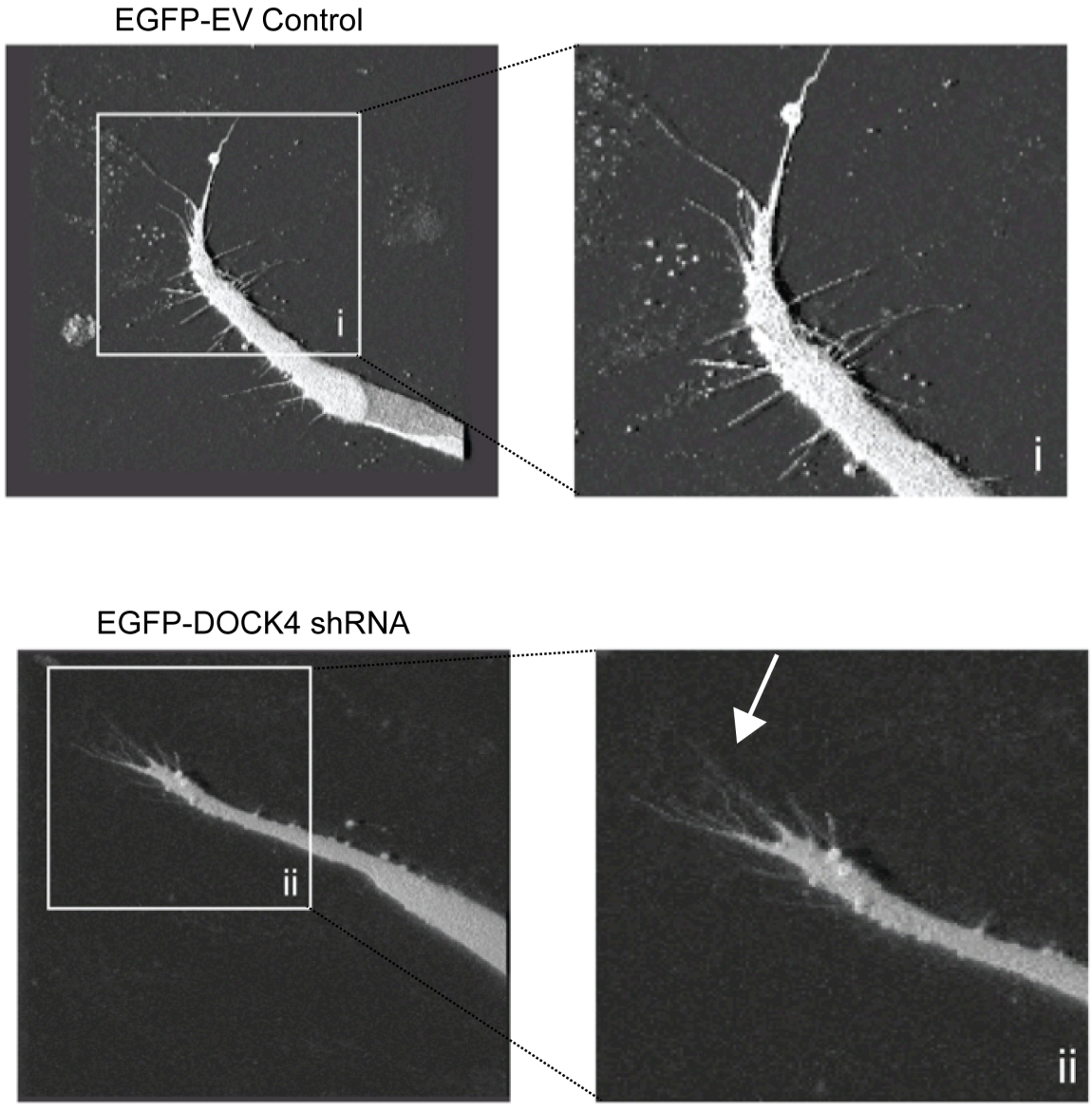

Figure 1.11 Tip filopodia persist in the absence of DOCK4
Still images from timelape movies of filopodia in the co-culture assay following DOCK4 depletion (EGFP-DOCK4 shRNA or EGFP EV (empty vector) control) and VEGF treatment for 6 days. Note that tip filopodia persist in the absence of DOCK4 (white arrow). Scale bar: 20μm. Data generated by Sabu Abraham.

1.8.2 DOCK4 acts as a Rac1 guanine nucleotide exchange factor in ECs

The Rac1 and DOCK4 knockdown phenotypes in the co-culture model are comparable. Knockdown of either protein ablated lateral branches, cells lacked filopodia formation and lateral cell-cell adhesion. Since DOCK4 is a Rac1 GEF in HEK 293T cells (Upadhaya et al., 2008) and MDA-MB 231 (breast cancer cell line) cells (Kawada et al., 2009), pulldown assays to quantitate active Rac1 following VEGF stimulation in the presence or absence of DOCK4 were performed in HUVEC. Cells were plated on fibronectin-coated dishes and transfected the following day with Standard pool siRNA for DOCK4 or mock transfected. Active Rac1 was pulled down accordingly with the method described in Section 2.3.7. Data in Figure 1.12 (A and B) show that, as previously demonstrated, VEGF stimulates Rac1 activation (Garrett et al., 2007), and that knockdown of DOCK4 blocks VEGF-mediated Rac1 activation at all the time points followed. Therefore DOCK4 acts as a GEF for Rac1 downstream VEGF signaling pathway in HUVEC.

1.8.3 RhoG is necessary for tube formation in an organotypic angiogenesis system

In other cell systems DOCK4 is regulated by RhoG (Hiramoto et al., 2006; Hiramoto-Yamaki et al., 2010). The effects of knocking down individual members of the Rho GTPases in HUVEC using siRNAs were investigated. This showed which members had the greatest phenotypic effects on angiogenesis and hence would be of interest for further studies. Representative images showing the effects of knocking down Rac1 and RhoG in a HUVEC organotypic assay (Section 2.4) are shown in Figure 1.13. While control endothelial cells showed a branched network of long tubules, HUVEC lacking Rac1 developed short vessels, thinner in appearance and sparsely localized in the wells, forming a network of vessels that did not branch. Given that Rac1 has been reported to be a regulator of multiple cellular processes, this phenotype was not unexpected. Knockdown of RhoG showed it contributes to vessel development to a similar extent as of Rac1; knockdown of RhoG also resulted in shorter tubules with no branches.

Different angiogenenic parameters (number of branches, number of tubules and branch

A

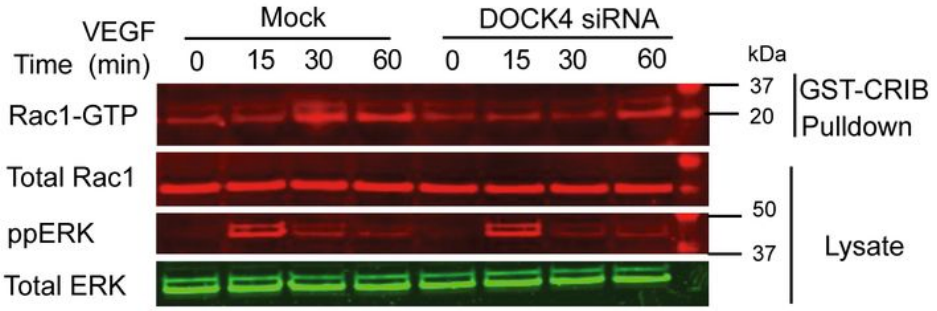

B

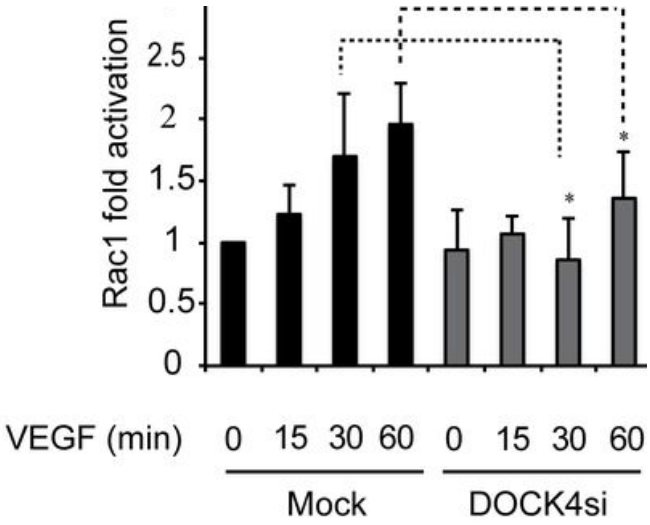

Figure 1.12 DOCK4 controls Rac1 activation downstream of VEGF
HUVEC growing on fibronectin-coated dishes were transfected using DOCK4 Standard pool siRNA or mock transfected HUVEC. Cells were then serum starved for 3 hours and stimulated with VEGF (25ng/ml) for 15, 30 and 60 minutes. After stimulation cells were lysed and Rac1 activation was analyzed using a Rac1 pulldown assay (Section 2.3.7). (A) Western Blots of Rac1-GTP, total Rac1, ppERK and total ERK from one representative experiment are shown.
Levels of Rac1-GTP are shown as fold stimulation compared to un-stimulated control after normalization for total Rac1.
(B) Bar chart shows Rac1 fold activation from three independent experiments. Error bars are S.E.M., p values from unpaired student's t-test compared to unstimulated control (0 timepoint). *, $P<0.05$. Data generated by Maggie Yeo.

points) were quantified in organotypic cultures with knockdown of Rac1 or RhoG (Figure 1.13B). The number of tubules formed in absence of RhoG and Rac1 was diminished compared to tubules formed by control cells (non targeting control siRNA transfected cells) and were shorter in length. In addition, the branch point index (number of branch points per tubule length) in tubules with reduced expression of RhoG or Rac1 was significantly diminished compared to control (Figure 1.13C). The results suggested a possible role for RhoG in vessel sprouting.

Altogether the data showed that DOCK4 is a Rac1 GEF downstream of VEGF in endothelial cells and controls branching through regulation of filopodia formation. The preliminary studies also showed that knockdown of RhoG in endothelial cells results in a phenotype similar to that seen in absence of Rac1 suggesting that, like in other systems, RhoG may control Rac1 activation in endothelial cells.

Given that RhoG has been reported to activate Rac1 upstream of DOCK4 and that its role in vessel formation has not previously been investigated, the aim of this thesis was to clarify the function played by RhoG in endothelial cells, to establish whether RhoG contributes to angiogenesis and through which molecular mechanism. This involved i. determining which steps of the VEGF signaling cascade are controlled by RhoG to regulate endothelial cell behaviour and which RhoG GEFs are involved (Chapter 3); delineating the RhoG signaling module that controls filopodia formation and hence cell-cell interaction (Chapter 4) and iii. determining the role of two GEFs, DOCK4 and DOCK9 in regulation of that RhoG signaling module (Chapter 5).

A

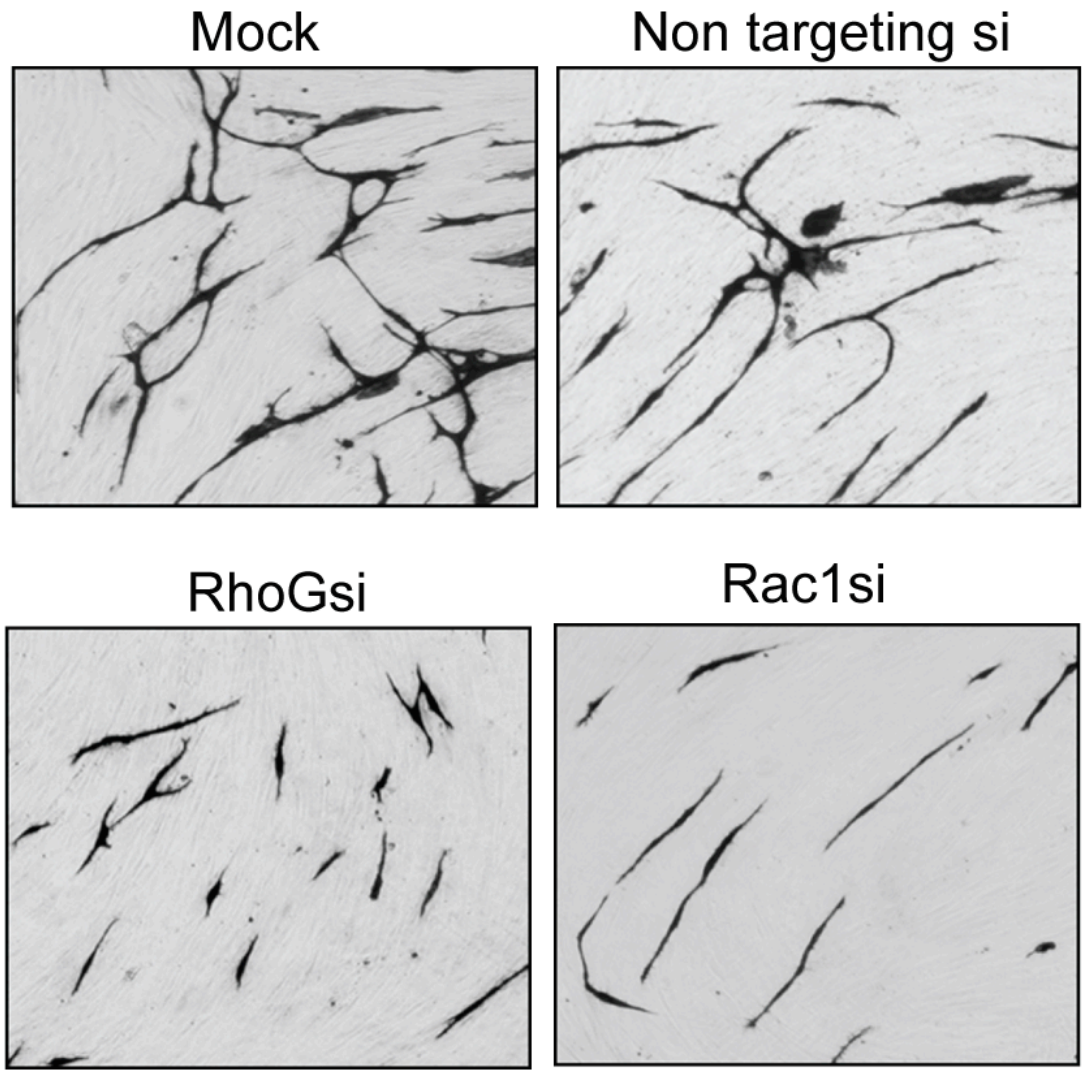

B

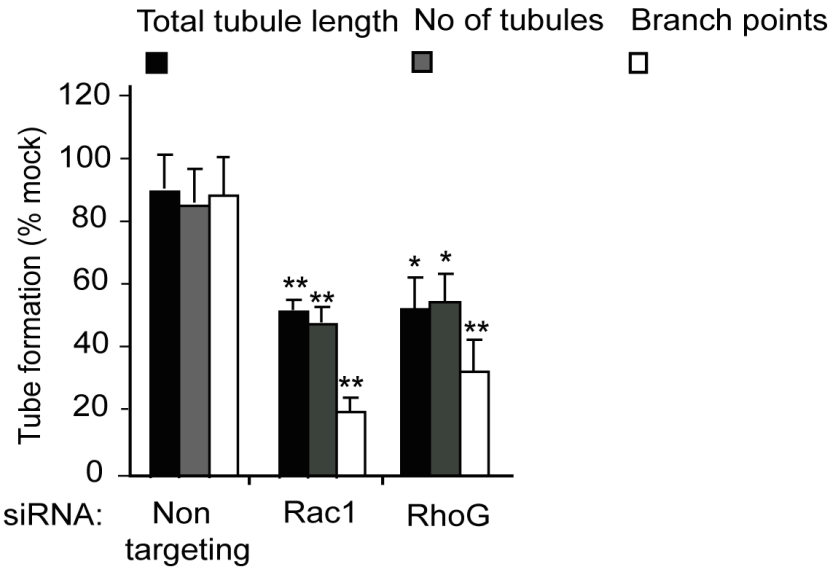

C

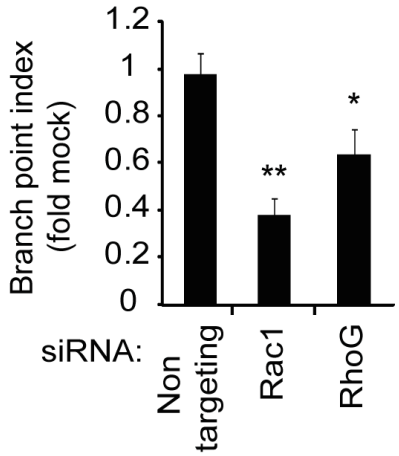

Figure 1.13 Rho GTPases required for angiogenesis
HUVEC were transfected with Standard pool siRNAs or mock transfected, and after 24 hours they were seeded onto confluent fibroblasts. Tube formation was assessed by CD31 staining 5 days after seeding. (A) Representative Western Blots of Rac1-GTP and total Rac1 are shown. Scale bar: 100μm. Straight tubule morphology was observed with knockdown of RhoG or Rac1. (B) Quantification of total tubule length, number of tubules and branch points represented as mean ±S.E.M. from three independent experiments. Quantifications were carried out using the angiosys software (Section 2.4). (C) Bar chart represents the branch point index as fold increase compared to mock transfected control. Error bars represent S.E.M., p values from unpaired student's t-test compared to non targeting control from three independent experiments. *, $P<0.05$; **, $P<0.01$; ***, $P<0.001$. Data generated by Sabu Abraham.

Chapter 2

Materials and Methods

2.1 Cell culture and Treatments

2.1.1 Cell lines

Human Dermal Fibroblasts (HDF) and Human Umbilical Vein Endothelial Cells (HUVEC) were purchased from TCS CellWorks. HEK 293T cells (originally generated by transforming Human Embryonic Kidney cells with sheared adenovirus 5 DNA (Graham et al., 1977)) were purchased from Clontech Laboratories.

2.1.2 Coating culture plates

Fibronectin coating for pulldown assays in HUVEC and HEK 293T cells: Fibronectin solution from human plasma (1mg/ml, Sigma-Aldrich) was diluted with Phosphate Buffered Saline (PBS) to a final concentration of 10μg/ml. Dishes were left for 3 hours at 37^{o}C before washing with PBS. Fibronectin-coated dishes were used for pulldown and immunoprecipitation assays.

Collagen I coating for HEK 293T cell expansion: 100mm plastic dishes were coated with filter-sterilized 50 μg/ml Collagen I Rat Tail (BD Biosciences) diluted from 5mg/ml stock with 0.02M glacial acidic acid. The solution was applied straight into dishes and incubated for 1 hour at room temperature (RT) to solidify. Plates were then rinsed 3x with PBS. Collagen I coated dishes were used for thawing HEK 293T cells.

Gelatin coating for fibroblasts on glass bottom plates: 2% gelatin solution (Sigma-Aldrich) was diluted to 0.1% with PBS. Plates were kept at RT for 30 minutes before excess gelatin was rinsed off with PBS. Gelatin-coated glass-bottomed plates were used for live cell imaging.

2.1.3 Cell culture conditions

HDF were cultured in Dulbecco's Modified Eagle Medium (DMEM) containing 10% fetal calf serum (FCS, Biosera Ltd) supplemented with 100mg/ml glutamine and 100 μg/ml

penicillin (Sigma-Aldrich). HDF (purchased at passage 8) were quickly thawed and cultured in a plastic-bottomed T75 cm^2 flask. After approximately 5 days, when confluence reached 80%, cells were harvested as follows: medium was removed and the cell layer was washed with PBS to eliminate traces of serum. 0.5%Trypsin/EDTA (5% diluted with sterile PBS, Sigma-Aldrich) was then added to cover the monolayer and cells were gently rocked for few seconds at RT. When the entire cell population was detached, cells were collected into culture medium and plated onto a plastic bottomed T150 cm^2 flask. Cells were then successively split at a ratio of 1:2 onto T150 cm^2 flasks when confluent as stated above. Cells were used in assays up to passage 11.

HUVEC were cultured in Large Vessel Endothelial Medium (LVEM, TCS CellWorks) complete with endothelial supplements (TCS CellWorks) and 100 μg/ml penicillin. HUVEC (purchased at passage 2) were quickly thawed and cultured in a plastic-bottomed T75 cm^2 flask. Medium was changed every 48 hours. At 80% confluence, cells were harvested with 0.5% Trypsin-EDTA as outlined for HDF. Cells were collected into culture medium and plated onto a plastic bottomed T150 cm^2 flask. Cells were then successively split at a ratio of 1:5 onto T150 cm^2 flasks when confluent as stated above. Cells were used up to passage 5 in assays and were cultured for no longer than a total 30 days from thawing. Where required, cells were stimulated with 25ng/ml recombinant human VEGFA (Vascular Endothelial Growth Factor A, Sigma-Aldrich) or 50ng/ml bFGF (basic Fibroblast Growth Factor, PeproTech).

HEK 293T cells were cultured in DMEM supplemented with 10% FCS (Biosera Ltd), 100mg/ml glutamine and 100μg/ml penicillin (Sigma-Aldrich). Cells (stored at passage 2) were first thawed onto Collagen I coated 100mm dishes. When confluence reached 90%, cells were harvested with 0.5% Trypsin-EDTA and expanded at a 1:10 ratio onto on plastic bottomed T150 cm^2 flasks.

All cell types were cultured in a humidified chamber with 5% CO_2 at 37^oC.

2.1.4 Thawing and freezing cell stocks

Stocks of all cell types were kept in liquid nitrogen. For use, vials were quickly thawed at 37^{o}C as described for each cell type in Section 2.1.3.

Cell stocks for freezing were prepared as follows: cells were grown to 80% confluence and the medium was changed 24 hours prior to freezing. Cells were then harvested with 0.5% Trypsin/EDTA, washed with PBS, re-suspended in 15mls of culture medium and counted either using a Beckman Coulter Z1 Dual Cell and Particle Counter (Beckman Coulter) or manually using a haemocytometer. Cells were then centrifuged (300g for 5 minutes at RT), the supernatant was discarded and the pellet was re-suspended in culture medium containing 20% FCS and 10% DMSO (Invitrogen) to give a final cell count of 10^{6}/ml. 1 ml cell suspension was then transferred to a 1.5 ml cryovial (Corning Incorporated) and stored at -80°C overnight before being transferred to liquid N_2 for long-term storage.

2.1.5 Standard Solutions

A list of standard solutions is shown in Table 2.1.

Standard Solutions	**Company**	**Recipe**
DMEM (Dulbecco's Modified Eagle's Medium)	Sigma-Aldrich	
Freezing medium		Cell culture medium supplemented with 20% FCS (Biosera Ltd) and 10% DMSO (Invitrogen).
LB (Luria Broth) medium	Sigma-Aldrich	20g of LB powder in 1L distilled water. Solution was autoclaved.
LB (Luria Broth) agar		15g of Agar powder (Sigma-Aldrich) dissolved in 1L of LB medium.
LVEM (Large Vessel endothelial Medium)	TCS CellWorks	
PBS (Phosphate Buffered Saline)	Sigma-Aldrich	
4% PFA (Paraformaldehyde) solution		Diluted from 39% solution (Sigma-Aldrich) with sterile PBS.
TE (Tris-EDTA) buffer	Qiagen	
TBS (Tris Buffer Saline) pH8		50mM Tris, 150 mM NaCl
TBST (Tris Buffer Saline Tween)		TBS with 0.1% Tween® 20 (Sigma-Aldrich)
0.5%Trypsin-EDTA (Ethylenediaminetetraacetic acid)		Diluted with PBS from 5% Trypsin-EDTA stock (Sigma-Aldrich)
Transfer Buffer		25mM Tris, 190mM glycine, 20% methanol, 0.01% SDS
5X siRNA Buffer	Thermoscientific	Diluted to 1X with RNAse free sterile water (Fisher Scientific)
RhoGTPase Lysis Buffer		100mM NaCl, 50 mM Tris-HCl pH 7.4, 10% glycerol, 1% NP-40, 5mM $MgCl_2$, EDTA-Free complete protease inhibitors (Roche), 1mM DTT
NP-40 Lysis Buffer		150nM NaCl, 20mM Tris-Cl pH 7.5, 1% NP-40, EDTA-free complete protease inhibitors (Roche), 0.1% phosphatase inhibitor (Sigma-Aldrich)

Table 2.1 List of standard solutions used in this thesis, their sources and recipes.

2.1.6 Transfection

2.1.6.1 Small interfering RNA

The small interfering RNA (siRNA) oligonucleotides used in this thesis were purchased from Dharmacon (Thermo Scientific) and Qiagen (Qiagen House). Transfections were performed using either Standard pools of 4 siRNAs (SMARTpool) targeting different parts of the mRNA, or individual On-Target siRNAs (ON-TARGET plus) that they target different regions of the mRNA to the Standard pools. On-Target siRNAs harbour a chemical substitution that reduces off target effects (Jackson et al., 2006). Pools and individual siRNAs were double-stranded RNA oligonucleotides with a 3'-UU overhanging on both strands and 5' phosphate on the antisense strand. siRNA oligonucleotides were supplied lyophilised and were re-suspended in 1x siRNA Buffer (Dharmacon; 20 mM KCl, 6 mM HEPES-pH 7.5, 0.2 mM $MgCl_2$) to obtain standard stock concentrations of 20μM. These were then aliquoted in RNase-free tubes in aliquots of 5μl and stored at -20^{o}C. The sequences of the oligonucleotides are shown in Table 2.2.

2.1.6.2 siRNA transfection

siRNA oligonucleotides were transfected into HUVEC using GeneFECTOR (VennNova), according to the manufacturers protocol. HUVEC were plated overnight onto 6 well plates ($1.5x10^5$ cells/ well) or for biochemistry onto fibronectin-coated 60mm dishes ($5x10^5$ cells) in complete LVEM. 0.5μl or 1μl of 20μM siRNA stock in siRNA buffer was added to 100μl or 200μl of reduced serum Optimem medium (Invitrogen) for transfection in 6 well plates and 60mm dishes respectively. 6μl or 12μl of GeneFector (VennNova) was added to equal amount of reduced serum Optimem medium. The siRNA-Optimem and GeneFector-Optimem solutions were mixed, vortexed for 10 seconds and left at RT for 5 minutes. The solution was then added dropwise onto cell cultures that had been washed four times with reduced serum Optimem medium and left with 1ml or 2 mls of reduced serum Optimem medum (for 6 well plates and 60mm dishes respectively). The cell cultures were then left at 37°C in 5% CO_2 for 3 hours before the transfection medium was replaced with complete LVEM. Cells were trypsinised for plating onto the organotypic angiogenesis assay 24 hours

siRNA / pool name	Oligonucleotide number	Sequence/ catalogue number
Rac1 SMARTpool	1	5'-(CGGCACCACUGUCCCAACA)
	2	5'-(UAAAGACACGAUCGAGAAA)
	3	5'-(UAAGGAGAUUGGUGCUGUA)
	4	5'-(AGACGGAGCUGUAGGUAAA)
Rac1 ON-TARGETplus		5'-(CGGCACCACUGUCCCAACA)
RhoG SMARTpool	1	5'-(CUACACAACUAACGCUUUC)
	2	5'-(CCAGUCCGCCGUCCUAUGA)
	3	5'-(GCAACAGGAUGGUGUCAAG)
	4	5'-(CGUCAUCUGUUUCUCCAUU)
RhoG ON-TARGETplus	5	5- CUACACAACUAACGCUUUC)
	7	5'-(GCUGUGCGCUACCUCGAAU)
Cdc42 SMARTpool	1	5'-(GGAGAACCAUAUACUCUUG)
	2	5'-(GAUUACGACCGCUGAGUUA)
	3	5'-(GAUGACCCCUCUACUAUUG)
	4	5'-(CGGAAUAUGUACCGACUGU)
DOCK4 SMARTpool	1	5'-(CAAAGGGUCUGGAGCAUUA)
	2	5'-(UAAGAGAGCUGAUGCUUGA)
	3	5'-(GGAAAUAGAUGUGAUAGUG)
	4	5'-(CCUCUUAUAUGACGAGCUA)
DOCK4 ON-TARGETplus	11	5'-(GGAGAAAAUUGCACGAUUA)
DOCK9 SMARTpool	1	5'-(GUAAACGAACGUCUGAUUA)
	2	5'-(ACUCAGAAGUUUCGAGAUA)
	3	5'-(CAGCUUGACUACUCAUUAA)
	4	5'-(CGGCAUUGCUUCUCCAUAU)
DOCK9 ON-TARGETplus	10	5'-(UCUGGAAAGCCGAGCGCUA)
	11	5'-(GCACAAUGGUUCACGGGAU)
SGEF SMARTpool	1	GAGAUGAUGUACACAAUUA)
	2	5'-(GAAGGAAGUUAGCAAGUUG)
	3	5'-(CAAAUGGCCUUGCCGCUAA)
	4	5'-(GAAAGGACAAGGAACAUUU)
SGEF ON-TARGETplus	5	5'-(CAAAUGGCCUUGCCGCUAA)
	6	5'-(UUGGAGAUCUUGAUACGAA)
Trio SMARTpool		Dharmacon: M-005047-00-0005
Trio ON-TARGETplus	5	5'-(GUAAAGAAGUGAAAGAUUC)
	7	5'-(GGAAUACAACCACGAAGAA)
FLJ10665 SMARTpool		Dharmacon: M-020318-01-0005
Non targeting		Allstars (Qiagen; 1027281)

Table 2.2 Sequences Standard pool siRNAs (Dharmacon SMARTpool) or individual On-Target oligonucleotide duplexes (Dharmacon ON-TARGETplus) used in the study.

after transfection, or lysed for biochemical analyses 48 hours after transfection. The transfection efficiency was determined either by Western Blot where antibodies were available (Section 2.3.5), or by qRT-PCR (Section 2.2.2) at 48 or 72 hours after transfection.

siRNA oligonucleotides were transfected into HEK 293T cells using Lipofectamin 2000 (Invitrogen), according to the manufacturer's protocol. HEK 293T cells were plated overnight onto 24 well plates ($1x10^5$ cells), or for biochemistry onto fibronectin-coated 60mm dishes ($5X10^5$ cells) in DMEM 10%FCS. 0.5µl or 2.5µl of 20µM siRNA stock in siRNA buffer (Dharmacon) was added to 50µl or 250µl of reduced serum Optimem medium for transfection in 24 well plates and 60mm dishes respectively. 1µl or 5µl of Lipofectamin 2000 was added to equal amount of reduced serum Optimem medium. The siRNA-Optimem and Lipofectamine-Optimem solutions were mixed, vortexed for 10 seconds and left at RT for 30 minutes. The solutions were then added dropwise onto cell cultures that had been washed 4x with antibiotic-free DMEM 10% FCS and left with 500µl or 2 mls of antibiotic-free DMEM 10% FCS (for 24 well plates and 60mm dishes respectively). The cell cultures were then incubated at 37°C in 5% CO_2 for 48 hours without change of medium. Cells were fixed and stained for immunohistochemistry analysis or lysed for biochemical analysis 48 hours after transfection. The transfection efficiency was determined either by Western Blot or qRT-PCR as described above for HUVEC.

2.1.6.3 Transfection of plasmid DNA

DNA plamids were transfected into HEK 293T cells using Lipofectamin 2000 (Invitrogen) according to the manufacturers protocol. HEK 293T cells were plated overnight onto 24 well plates ($1x10^5$ cells) or for biochemistry onto fibronectin-coated 60mm dishes ($5x10^5$ cells) or 100mm dishes ($1x10^6$ cells) in DMEM 10%FCS. 200ng or 800ng or 5µg DNA plasmids was added to 50µl, 250µl or 500µl of reduced serum Optimem medium for transfection in 24 well plates, 60mm and 100mm dishes respectively. 1µl or 5µl or 20µl of Lipofectamin 2000 was added to equal amount of reduced serum Optimem medium. The two solutions were combined and vortexed for 10 seconds and left at RT for 30 minutes.

The solution was then added dropwise onto cell cultures that had been washed 4x with antibiotic-free DMEM 10% FCS and left with 500µl or 2 mls or 10mls of antibiotic-free DMEM 10% FCS for 24 well plates, 60mm or 100mm dishes respectively. The cell cultures were then incubated at 37^{o}C in 5% CO_2 for 48 hours without changing the medium. Cells were fixed and stained for immunohistochemistry analysis or lysed for biochemical analysis 48 hours after transfection. The transfection efficiency was determined either by Western Blot or qRT-PCR as stated above (Section 2.1.6.2). Plasmid constructs used in this thesis are listed in Table 2.3.

2.1.6.4 siRNA and DNA plasmid co-transfection

siRNA oligonucleotides and DNA plasmids were co-transfected into HEK 293T cells following the protocols described in Section 2.1.6.2 and 2.1.6.3.

0.5µl or 2.5µl of 20µM siRNA were combined to 200ng or 800ng of DNA plasmid and added to 50µl or 250µl of reduced serum Optimem medium for transfection in 24 well plates or 60mm dishes respectively. 1µl or 5µl of Lipofectamin 2000 was added to equal amount of reduced serum Optimem medium. Solutions were then mixed and added onto cultures following the procedure described above. The cell cultures were then incubated at 37^{o}C in 5% CO_2 for 48 hours without changing the medium. Cells were fixed and stained for immunohistochemistry analysis or lysed for biochemical analysis 48 hours after transfection. The transfection efficiency was determined as stated above (Section 2.1.6.2).

DNA plasmid constructs	Source
GST-PAK-CRIB (Sanz-Moreno et al., 2008)	Professor Christopher Marshall, ICR, London, UK
GST-ELMO (Côté et al., 2007)	Dr Jean Francois Côté, McGill University, Canada
GST-DOCK4-SH_3 and GST-Empty Vector	Dr Rick Bagshaw, The Pawson Laboratory, The Samuel Lunenfeld Research Institute, Canada
EGFP-WT Rac1	Professor Christopher Marshall, ICR, London, UK
EGFP-WT RhoG	Dr Len Stephens, Babraham Institute, Cambridge, UK
EGFP-RhoGv12 (Estrach et al., 2002)	Drs Anne Debant and Susanne Schmidt, CRBM, CNRS, Monpellier, France
EGFP-DOCK4 (Kawada et al., 2009)	Dr Vijay Yajnik, Harvard Medical School, Massachusetts, US
Flag WT DOCK4 and deletion constructs (Ueda et al., 2013)	Dr Hironori Katoh, University of Tokyo, Japan
Flag WT DOCK9 (Meller et al., 2008)	Professor Martin Schwartz, University of Virginia, US

Table 2.3 List of DNA plasmid constructs used through this thesis.

2.2 Nucleic acid techniques

2.2.1 Bacterial transformation and DNA plasmid preparation

BL21 pLYsS *E.coli* competent cells were quickly thawed on ice. 500ng of plasmid (containing Amp^R) was mixed with competent BL21 cells (50µl of 10^6cfu/ml) and the mixture was left for 10 minutes on ice. Cells were heat-shocked for 1 minute at 42°C and immediately placed on ice for 5 minutes. Cells were then re-suspended in 500µl of Super Optimal Broth (SOC, Fisher Scientific), incubated for 1 hour at 37°C with shaking, after which a bacterial streak was made on a LB agar plate containing 100µg/ml ampicillin and incubated inverted overnight at 37°C. A single bacterial colony was then used to inoculate an overnight culture of 3mls LB medium containing ampicillin (100µg/ml). Glycerol stocks were made for long-term storage by mixing 1ml of overnight bacterial culture with 20% glycerol and stored at -80°C. The remainder of the bacterial culture was centrifuged for 10 minutes at 4000rpm to pellet the bacteria.

The supernatant was removed and the pellet re-suspended in 200µl lysis buffer (50 mM Tris-HCl, 10 mM EDTA, 100 µg/ml RNase A, pH 8.0). DNA extraction was then performed using Qiagen DNA kit following manufacturer's protocol. Plasmid DNA was resuspended in 150µl of TE and quantified by UV spectrophotometry using the NanoDrop ND-1000 spectrophotometer.

2.2.2 RNA isolation and quantitation of siRNA mediated knockdown by qRT-PCR

Total cellular RNA was isolated from cultured cells using PerfectPure™ RNA Cultured cell kit (5 Prime GmbH, Hamburg) according to the manufacturer's protocol, with the working area pretreated with RNAse Zap (Ambion). The final yield of RNA and purity were quantified using the NanoDrop ND-1000 spectrophotometer. Real time qRT-PCR analysis to determine the degree of siRNA-mediated knockdown for genes where there was no antibody available. This was performed using the one step BRILLIANT II SYBR Green qRT-PCR Master Mix Kit (Applied Biosystems). Reactions were performed in triplicate using 50 ng of RNA per sample in a total volume of 20µl. The housekeeping gene GAPDH

was used as endogenous control for all qRT-PCR assays. Relative quantification was performed using the $\Delta\Delta C_t$ method (Fleige and Pfaffl, 2006). qRT-PCR primer pairs were purchased from Qiagen and were supplied as a lyophilized mix of forward and reverse primers. Each primer was reconstituted in TE (10mM Tris, 1mM EDTA, pH8.0) and stored at the final concentration of 20μM. The final reaction mix (12.5μl 2x Brilliant II SYBR Green master mix, 300nM primer mix, 300nM reference Dye, Nuclease free water) was loaded onto a 96 well optical reaction plate (Applied Biosystems) in which RNA (50ng) was previously added and covered by an optically clear adhesive cover (Thermo Scientific). The reaction was performed in an Applied Biosystem 7900 real-time PCR cycler. Fluorescence data were analyzed using Applied Biosystems SDS software.

2.3 Protein techniques

2.3.1 Expression of recombinant GST fusion proteins

BL21 pLYsS *E.coli* were transformed with the pGEX PAK-CRIB, pGEX ELMO 1, pGEX DOCK4-SH_3 or empty vector expression constructs as described in Section 2.2.1.

Transformants were grown in 500 ml of LB medium containing 100μg/ml ampicillin (for ELMO 1, DOCK4-SH_3 and empty vector expression construct) or 100μg/ml ampicillin and 50μg/ml chloramphenicol (Sigma-Aldrich; for PAK1-CRIB expression construct) until the cultures reached an OD_{600} of 0.3. Expression of the exogenous protein was induced with 0.3 mM isopropylthiogalactoside (IPTG, Sigma-Aldrich) for 3 hours (PAK-CRIB) or 1mM IPTG for 5 hours (ELMO 1, DOCK4-SH_3 and empty vector) at 37^{o}C. Subsequently, bacterial cultures were centrifuged at 4000 rpm for 20 minutes at 4^0 C and the pellets were snap frozen on dry ice and stored at -80^0 C. To verify the expression of the fusion proteins, pre- and post-IPTG induction samples were taken. Bacteria were pelleted at 13000rpm for 5 minutes, the supernatant was removed and the pellet mixed with 30 μl Loading Buffer (4x, NuPAGE, Invitrogen) with addition of 50mM DTT before subjecting to SDS-PAGE (sodium dodecyl sulfate polyacrylamide gel electrophoresis) alongside bovine serum albumin (BSA) standards (1, 2, 5, 10 μg, Sigma-Aldrich). Protein expression was visualized after gel electrophoresis by Coomassie Brilliant Blue staining.

2.3.2 Purification of recombinant proteins and coupling with agarose sepharose beads

Pelleted bacterial cultures were resuspended in 25 ml ice-cold TBS containing 10mM $MgCl_2$, 1mM PMSF (Thermo Scientific), 1mM DTT (Sigma-Aldrich) and lysed by sonication on ice using a 12 mm probe, 3x 1 minute bursts (Soniprep MSE 150). 10% Triton X-100 (Sigma-Aldrich) was added to the lysate and incubated with rocking at 4^0 C for 30 minutes, then centrifuged at 13000 rpm for 30 minutes in a Sorvall RC5B centrifuge using a SS-34 rotor. The supernatants, containing the recombinant proteins, were snap frozen in 5ml aliquots and stored at -80^0 C. Glutathione pre-coated agarose sepharose beads (0.5 ml, GE Healthcare Bio-Sciences AB) were washed once with 10ml TBS and then twice with 5 ml of wash buffer (TBS, 10mM $MgCl_2$, EDTA-free Complete protease inhibitors (Roche), 1mM DTT) and pelleted at 1200 rpm for 5 minutes. The beads were incubated with bacterial lysates containing recombinant GST-tagged proteins at 4^0 C for 1 hour before centrifuged at 1200 rpm at 4^0 C for 5 minutes. The beads/GST fusion complex was then washed 4x with wash buffer to remove contaminating bacterial proteins, pelleted and then re-suspended in a total volume of 750μl of wash buffer and stored at 4^0 C. The immobilized proteins were used for pulldown assays within two weeks.

2.3.3 Protein quantification by BCA (bicinchoninic acid) protein assay

Proteins were quantified using the BCA (bicinchoninic acid) method (Smith et al., 1985). The method combines the biuret reaction with the violet-colored complex formation of copper ions by bicinchoninic acid. To determine protein concentration, the assay uses a standard curve created by different concentrations of BSA ranging from 25 μg to 2 mg. An aliquot of 25 μl of protein sample and BSA standards were pipetted in triplicate into a 96 well plate. 200μl of the BCA reagent (Thermo Scientific) was added to each well and the reaction allowed to proceed at 37^{o}C for 30 minutes. Protein concentration was measured using a spectrophotometer at 562nm wavelength and calculated using the SkanIt Software.

2.3.4 SDS-PAGE

To visualize proteins of interest from cell lysates, immunoprecipitation assays or pulldown assays, Sodium Dodecyl Sulfate Polyacrylamide Gel Electrophoresis (SDS-PAGE) analysis was performed. Samples (protein solutions (Section 2.3.7), agarose sepharose beads (Section 2.3.7) or protein G beads (Section 2.3.8) were re-suspended in 4x loading buffer (NuPAGE, Invitrogen) with 50mM DTT and heated at 70^0 C for 10 minutes. For detection of proteins up to 100 kDa, 10% acrylamide pre-cast gels (Invitrogen) were used; 3-8% acrylamide pre-cast gels were used for higher molecular weight proteins. Electrophoresis was performed at 150V in either 1x MES (2-N-morpholino ethanesulfonic acid, Invitrogen) running buffer (1hour) or 1x MOPS (3-N-morpholino propanesulfonic acid, Invitrogen) running buffer (3 hours) in the presence of NuPAGE Antioxidant (Invitrogen, 1:500). 10µl of tracking marker (Dual Colour Marker, BioRad, 10-250 kDa) was used to track electrophoresis.

2.3.5 Blotting and protein detection

Following electrophoresis, SDS-PAGE gels were transferred to PVDF (Polyvinylidenfluoride) membranes using 4 sheets of Whatman paper equilibrated in Transfer buffer (25mM Tris, 190mM glycine, 20% methanol, 0.01% SDS) to sandwich the gel to the membrane; electroblotting was in Transfer buffer at 1A for 2 hours at 4^0 C. For Li-COR visualization, membranes were blocked in Li-COR blocking buffer (Li-COR Biosciences) at RT for 1 hour. For enhanced chemiluminescence (ECL) visualization, membranes were blocked in a solution of 5% low fat dried milk in TBS with addition of 1% Tween (TBST) for 1 hour at RT and incubated overnight at 4^0C with the appropriate primary antibody in 1% BSA in TBST. Membranes were then washed 3x 5 minutes with TBST and incubated for 1 hour at RT with either IRDye fluorescent secondary antibodies (Li-COR Biosciences) or with horseradish peroxidase enzyme secondary antibody conjugated (ECL). Primary and secondary antibodies are listed in Table 2.4. Membranes were then washed 3x 5minutes each with TBST and visualized either using Li-COR Odyssey scanner or exposure to X-ray film (Amersham Hyperfilm™) for ECL. For data

analysis, band intensity was captured through Image J 1.46 software (http://rsbweb.nih.gov/ij/). Further analysis and statistical analysis are performed using Microsoft Excel.

2.3.6 Stripping and reprobing

When probing the same PVDF membrane with a different antibody was needed, a stripping Buffer (ultra pure water containing 0.2M Glycine, 3mM SDS, pH 2.2) was added to the membrane and the membrane was incubated a RT for 10 minutes. The solution was then discarded. Subsequently, the membrane was washed 2x10 minutes with TBS and 2x5 minutes with TBST. The membrane was then re-blocked in a solution of 5% low fat dried milk and incubated overnight at 4^0C with the appropriate primary antibody in 1% BSA in TBST.

2.3.7 Pulldown assays

$0.5x10^6$ HUVEC, were transfected as described in Section 2.1.6.2. 24 hours after transfection HUVEC medium (LVEM) was replaced with Optimized medium with the addition of supplements and antibiotics. After a further 24 hours, HUVEC were serum-starved using serum-free Optimized medium for 5 hours prior to treatment with the appropriate growth factor where necessary. Where cells were not transfected, LVEM was replaced with Optimised medium 24 hours after plating and cells were growth factor stimulated the following day. Following treatments, cells were lysed in Rho GTPase lysis buffer (100mM NaCl, 50 mM Tris-HCl pH 7.4, 10% Glycerol, 1% NP-40, 5mM $MgCl_2$, EDTA-Free Complete protease inhibitors (Roche), 1mM DTT) and harvested in a final volume of 1ml. The lysate was cleared by centrifugation at 13000rpm at 4^0C for 15 minutes. 70% of the final volume of cell lysate was added to 60μl of a suspension of agarose-sepharose beads

Primary antibody	**Company**	**Dilution/ Concentration**
Mouse anti-Rac1, clone 23A8	Millipore	1/1000
Mouse anti-RhoG, clone 1F3B	Millipore	1/1000
Mouse anti Cdc42	Sigma-Aldrich	1/250
Mouse p-ERK 1/2 (12D4) sc-81492	Santa Cruz	1/500
Rabbit ERK 1/2 (C-16) sc-93	Santa Cruz	1/500
Rabbit DOCK9 A300-531A	Bethyl	1µg/150µl lysate (Co-IP) or 1:1000
Mouse DOCK4 Ab 85723	Abcam	1µg/250µl lysate (Co-IP) or 1:1000
Rabbit IgG P120-101	Bethyl	1µg/150µl lysate (Co-IP) or 1:1000
Mouse anti GAPDH	Sigma-Aldrich	1/1000
Mouse anti Flag	Sigma-Aldrich	1µg/250µl lysate (Co-IP) or 1:1000
Secondary antibody	**Company**	**Dilution**
Goat Anti-Mouse IgG (H+L), HRP	Promega	1/10000
Goat Anti-Rabbit IgG (H+L), HRP	Promega	1/10000
Goat Anti-Mouse, Alexa Fluor 680	Invitrogen	1/10000
Goat Anti-Rabbit, Alexa Fluor 800	Invitrogen	1/10000

Table 2.4 Antibodies used in this thesis to perform immunoprecipitations, pulldown assays and immunoblot assays.

coupled to GST-PAK CRIB or GST-ELMO prepared as described in Section 2.3.2. Lysates were incubated with agarose-sepharose beads for 45 minutes at 4^0 C; beads and bound protein were then collected by centrifugation at 1200 rpm for 5 minutes. Agarose-sepharose beads/bound protein then were washed twice with Rho GTPases wash buffer (TBS containing 10mM $MgCl_2$, EDTA-free complete protease inhibitors, 1mM DTT) and stored at -80^{o}C prior to analysis.

$1x10^6$ HEK 293T cells transfected as described in Section 2.1.6.2, Section 2.1.6.3 and Section 2.1.6.4 were lysed 48 hours after transfection in Rho GTPase lysis buffer and pulldown assays were performed as described above.

2.3.8 Co-Immunoprecipitation (Co-IP) assay

$3x10^6$ HUVEC were plated onto 150mm fibronectin-coated dishes. The following day LVEM was replaced by complete Optimized medium and the following day, HUVEC were serum starved for 5 hours and treated with VEGF (25ng/ml). Cells were harvested by washing 1x with PBS and lysed on ice using 1ml of NP-40 lysis buffer (150nM NaCl, 20mM Tris-Cl pH 7.5, 1% NP-40, EDTA-free complete protease inhibitors, 0.1% phosphatase inhibitor cocktail 2 (Sigma-Aldrich)). Cells were then centrifuged at 12000rpm for 20 minutes at 4^0 C and the supernatant was decanted into fresh tubes. 50µl of the total lysate was removed and stored for future analysis and the rest of the lysate was used for the Co-IP assay. Protein G beads (Invitrogen) were equilibrated with NP-40 buffer before being used. A pre-clearing step was performed adding Protein G beads to the lysate (~950µl) for 30 minutes at 4^0 C. Each sample was then centrifuged for 2 minutes at 1200rpm and supernatant was split into two aliquots (~500 µl each) for Co-IP with an antibody against the protein of interest and IgG control. 3µg of each antibody was added to the lysate and binding was allowed to take place for 2 hours at 4^{o}C. 30µl of Protein G beads was then added to each sample and allowed to bind at 4^0 C for 30 minutes. The beads were then centrifuged at 1200 rpm, the supernatant was removed and the beads were carefully washed 3x with 300µl Lysis Buffer. After the last wash, beads were re-suspended in in 4x

loading buffer (NuPAGE, Invitrogen) with 50mM DTT and heated at 70^0 C for 10 minutes prior to SDS-PAGE or stored at -80^{o}C

For HEK 293T Co-IPs, $1x10^6$ HEK 293T cells were plated onto 100mm fibronectin-coated dishes and transfected as described in Section 2.1.6.2, Section 2.1.6.3 and Section 2.1.6.4. Co-IPs were performed 48 hours after transfection as described above with the following modifications: 2μg of antibody were used both for endogenous proteins and over-expressed proteins; where EGFP (enhanced green fluorescent protein) tagged proteins were overexpressed, IPs were performed using 20μl GFP-Trap® an EGFP antibody conjugated with agarose beads (Chromotek).

2.4 Organotypic angiogenesis assay

$2x10^4$ HDFs were plated on plastic or gelatin-coated glass-bottomed 24 well plates and cultured for 7 days without change of medium to create a confluent monolayer. $8.5x10^3$ HUVEC were then seeded on-to the confluent monolayers of HDF and cultured for a further 5 days (Hetheridge et al., 2011). The co-culture assays were performed with HUVEC manipulated such that genes of interest were knocked-down using siRNA transfection, in order to identify their effect on angiogenesis. Evaluation of the phenotype resulting from a gene knockdown was always performed in parallel with non targeting siRNA control for comparison. VEGF treatment varied according to the analysis being performed:

- detection of filopodia: VEGF (25ng/ml) was added to the culture medium 24 hours prior to analysis;
- detection of branch formation: HUVEC were re-suspended in medium containing VEGF (25ng/ml) and seeded onto confluent HDF. VEGF-containing medium was replenished 3 days after seeding.

Co-cultures were fixed after 5 days of culture, using 70% ethanol for 30 minutes at RT and then subjected to immunostaining for CD31 using Angiogenesis Tubule Staining Kit (TCS CellWorks) according to the manufacturer's protocol. Anti-human CD31 was applied at 1:400 dilution for 1hr at 37^0C followed by washing (3x 10 minutes each at RT). An alkaline

phosphatase conjugated secondary antibody (TCS CellWorks) was applied at 1:500 and left for 1hr at 37^0C. The chromogenic substrate (BCIP/NBT) was diluted in H_2O (1 table in 10mls of water) and applied to the fixed co-culture for ~10 minutes at 37^oC. When tubules were visibly coloured, the plate was washed with H_2O and images of the co-cultures were captured using a 40x object of a compound microscope. For long term storage plates were kept at 4^oC and PBS was added in each well to preserve the staining. Tube formation was quantified using the Angiosys software (TCS CellWorks). The software calculates the number of pixels generated through the staining against the background (unstained) intensity of the captured images and quantifies the following parameters: number of tubules, number of branches and total tubule length. Quantification of angiogenesis parameters (number of branches or tubule length) and analysis of capillary formation were performed as previously described (Hetheridge et al., 2011). Because of consistencies between batches of ECs and their passage number, this assay has an inherent degree of variability; however, trends in quantification were consistently noted and the assay shwos an highly reproducibility.

2.5 Filopodia quantifications

Filopodia generated by a single cell that has assumed a leading position in a tubule are referred to throughout this thesis as “tip filopodia”. Filopodia generated by any cell either than the leading cell are referred to throughout this thesis as “lateral filopodia”. CD31 stains HUVEC cell junctions, so immunostaining fixed co-cultures allows tip cells to be distinguished from neighboring cells (Appendix, Figure 1).

In order to quantitate filopodia, co-cultures were fixed and immunostained for CD31 prior to imaging using a 40x object of a compound microscope. Images were acquired and processed using the Image J 1.46 software (http://rsbweb.nih.gov/ij/). Background was subtracted using the Image J 1.46 software to minimize interference resulting from the underlying fibroblast layer; tubules were enlarged for a clearer view of cell junctions (Appendix, Figure 1). Four or more tubules of comparable length were chosen from each image co-culture and the total length of tubule (expressed in cm) was manually calculated.

The total number of filopodia (tip and lateral) were counted and expressed as the number of filopodia per cm of tubule.

2.6 Retrovirus infection

To visualize HUVEC morphology and follow the cells by time-lapse microscopy HUVEC stably expressing EGFP were generated by means of retroviral transduction using preparations of amphotropic retrovirus harbouring EGFP that was available in the laboratory (Mavria et al., 2006). HUVEC media were changed 24 hours before infection. Cells were infected at 80% confluency in the presence of 8 μg/ml Polybrene (Sigma-Aldrich). Cells were maintained in culture for 6 hours before the viral particles were washed off and replaced with fresh medium. 72 hours later EGFP positive cells were isolated by FACS (fluorescence activated cell sorting). EGFP positive HUVEC were then cultured for 48h before being used to ensure that cells were contamination free.

2.7 Microscopy

2.7.1 Time-lapse microscopy

Time-lapse movies or single snapshots of EGFP expressing cells were obtained using a Zeiss inverted microscope attached to an Orca ER (Hamamatsu), MAC 5000 automation controller system, digital camera and a motorised XYZ stage. 10x or 20X objectives were used. Volocity software (Improvision/ Perkin Elmer) was used for 3D images and 4D time-lapse. The microscope was equipped with temperature and CO_2 controller to maintain the surrounding chamber for cell culture.

2.7.2 Confocal microscopy

HEK 293T cells or HUVEC-EGFP were imaged using a Nikon TE2000 inverted confocal microscope using the Nikon D-eclipse C1 software and attached to an Orca ER (Hamamatsu). Pictures were captured using a 20X and 60X oil objective.

2.7.3 Phase contrast microscopy

Phase contrast images of tube formation in the organotypic assay were obtained with a Nikon light microscope (4x objective) or an Olympus CKX41 inverted microscope (x40 objective).

2.7.4 Phalloidin staining of HEK 293T cells

After transfection (Sections 2.1.6.2, Section 2.1.6.3 and Section 2.1.6.4), HEK 293T cells were washed with PBS and fixed with 4% PFA (paraformaldehyde) for 20 minutes at 4^{o}C. Cells were then permeabilized using 0.5% Triton X-100 in PBS containing 1% BSA (Blocking Buffer) for 1 hour at RT prior adding Phalloidin-tetramethylrhodamine (TRITC, Sigma-Aldrich) for 30 minutes 4^{o}C at a dilution of 1:200 in Blocking Buffer. Cells were then washed 3x with PBS and either imaged immediately or stored at 4^{o}C prior to imaging.

2.8 Statistical Methods

Statistical significance was determined using the two-tailed student's T-test on Microsoft Excel assuming a two-tailed distribution with unequal variance between sample means.

Chapter 3

The Role of RhoG in Angiogenesis and Regulation by Guanine Nucleotide Exchange Factors (GEFs)

3.1 Introduction

Numerous proteins have been reported to play a role in the regulation of endothelial cell behaviours such as cell migration, spreading, proliferation and cell-cell adhesion during both physiological and pathological angiogenesis. Signaling pathways, from cell surface receptors to intracellular signaling components, are crucial to the co-ordination and control of all these cellular functions (Herbert and Stainier, 2011; Weis and Cheresh, 2011). One class of proteins that are key regulators of these processes, through control of the actin cytoskeleton, is the Rho family of small GTPases. Preliminary data have shown that RhoG is a key regulator of vessel formation in the co-culture assay as determined through knockdown experiments (Preliminary Data, Section 1.8.3). However, despite some findings on the regulation of EC polarity induced by RhoG under bFGF stimulation (Elfenbein et al., 2009), little else is known regarding the function of RhoG in ECs and its role in vessel formation remains to be elucidated.

The aim of the work described in this chapter was to determine which steps of VEGF signaling cascade are controlled by RhoG to regulate angiogenesis and to elucidate molecular mechanisms involved in its regulation.

3.2 Assessing Angiogenesis in an Organotypic Co-culture Assay

In order to study the role of Rho GTPases and their regulators in angiogenesis, an organotypic angiogenesis assay was used; this relies on the co-culture of endothelial cells with fibroblasts, which enables EC tube formation (Bishop et al., 1999; Donovan et al., 2001). In this assay, the behaviour of ECs is guided by the underlying dynamic matrix formed by fibroblasts and a number of growth factors released by both the fibroblasts and co-cultured ECs (Bishop et al., 1999; Mavria et al., 2006). This results in the recreation of a 3-dimensional environment, in which ECs form tubes that resemble small capillaries *in vivo,* embedded in a natural matrix produced by the fibroblasts.

Following seeding onto the fibroblasts, ECs migrate guided by the underlying matrix and form cell-cell contacts by extending cellular protrusions towards each other. An example of this co-culture model, visualized by lapse-lapse microscope, is shown in Movie 1 (EGFP

Non targeting, attached CD).

The optimal number of fibroblasts needed in this assay was determined by varying the number of seeded fibroblasts while keeping the number of ECs constant. Different numbers of fibroblasts resulted in a diverse EC morphology. The optimum ratio where tubules appeared to be fully formed and the fibroblasts were evenly distributed was $2x10^4$ HDF : $8.5x10^3$ HUVEC, shown in Figure 3.1. All subsequent experiments were performed in triplicate using this ratio of HDF: HUVEC and cells of the same passage number (HUVEC up to passage 5 and HDF up to passage 11) to ensure consistency in the basal level of tube formation throughout the assays.

To visualize tube morphology, the co-culture was analysed for expression of CD31, an adhesion molecule expressed by ECs but not by fibroblasts. A minimum of 9 representative images were then taken from the triplicates (3 pictures per well). These images were then used to measure the following angiogenic parameters using Angiosys software: i. number of tubules; ii. total tubule length and iii. branch points were quantified, as described in Section 2.4. The co-culture assay was performed with cells where expression of different Rho GTPases had been knocked-down using siRNA transfection (Section 2.1.6.2) to identify their effect on angiogenesis. Evaluation of a phenotype resulting from a gene knockdown was always carried out in comparison to a non targeting siRNA control. To rule out false positives resulting from off-target effects of the siRNA, the level of knockdown of the targeted genes was assessed by qRT-PCR (as described in Section 2.2.2) or by protein expression when the antibody was available for Western blotting, and normalized against the housekeeping gene GAPDH which was unaffected by siRNA activity. Figure 3.2 shows an example of qRT-PCR raw data (Table 3.1) and protein expression visualized through Western blotting (Section 2.3.5) (B) of SGEF and Rac1 respectively.

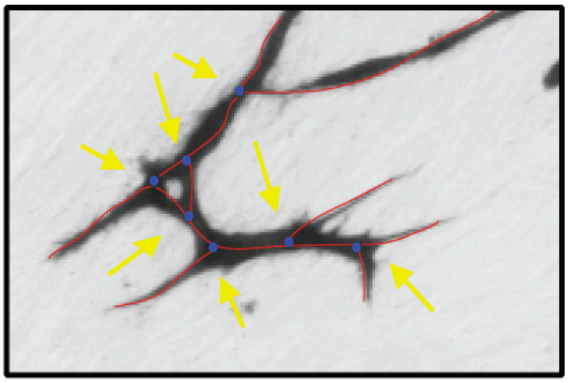

$$\text{Branch Point Index} = \frac{\text{Number of branch points}}{\text{Vessel length}}$$

Figure 3.1 Tube formation in HUVEC-HDF co-cultures
$8.5x10^3$ HUVEC were seeded onto $2x10^4$ fibroblasts and 5 days after seeding the cultures were fixed and stained for the endothelial marker CD31 to visualize tube formation. The number of tubules (objects between consecutive branch points), branch points (blue dots, highlighted by yellow arrows) and total tubule length (outlined in red) were determined using the Angiosys software (Section 2.4). The branch point index is defined as the number of branch points divided by total tubule length.

A

Sample Name	Target Name	RQ	RQ Min	RQ Max	CT	CT Mean	CT SD	ΔCT Mean
Non targeting Control	SGEF	1	0.933149	1.071641	23.34979	23.27396	0.067939	10.368378
Non targeting Control	SGEF	1	0.933149	1.071641	23.21863	23.27396	0.067939	10.368378
Non targeting Control	SGEF	1	0.933149	1.071641	23.25346	23.27396	0.067939	10.368378
SGEF OnTarget 5	SGEF	0.373071	0.4153	0.538879	26.21007	26.17519	0.084825	11.448249
SGEF OnTarget 5	SGEF	0.373071	0.4153	0.538879	26.07849	26.17519	0.084825	11.448249
SGEF OnTarget 5	SGEF	0.373071	0.4153	0.538879	26.23701	26.17519	0.084825	11.448249
Non targeting Control	GAPDH				12.9028	12.90558	0.038221	
Non targeting Control	GAPDH				12.94354	12.90558	0.038221	
Non targeting Control	GAPDH				12.8407	12.90558	0.038221	
SGEF OnTarget 5	GAPDH				14.69396	14.72694	0.046642	
SGEF OnTarget 5	GAPDH				14.75992	14.72694	0.046642	
SGEF OnTarget 5	GAPDH				14.53444	14.49996	0.07419	

B

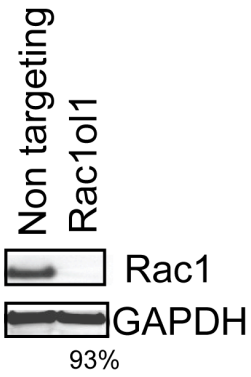

Figure 3.2 Methods to quantify knockdown of Rho GTPases
Members of the Rho GTPase family knocked-down in HUVEC 48 hours or 72 hours after transfection with Standard Pool siRNAs or On-Target oligonucleotides as described in Section 2.1.6.2. Table 3.1 (A) shows qRT-PCR data for SGEF gene knocked-down using SGEF On-Target oligonucleotide 5 after normalization against the housekeeping gene GAPDH. Raw data were generated by Applied Biosystem SDS software and show the Relative Quantifications (RT) and the Ct values. (B) Level of Rac1 protein expression was assessed by western blotting where expression of Rac1 in Rac1 knockdown sample (Rac1ol1) was compared to expression of Rac1 in control sample (non targeting). Given values are reported after normalization against the housekeeping gene GAPDH.

3.3 Requirement of RhoG for Angiogenesis in an Organotypic Tissue Culture Assay

The Rho GTPase Rac1 has been extensively characterized for its roles in angiogenesis (Tan et al., 2008), cell migration (Katoh et al., 2006) and cell division (Michaelson et al., 2008). Given the importance of Rac1 in endothelial cell behaviour outlined in Chapter 1 (Section 1.5.5.4), the study described here aimed to characterize signaling pathways that control Rac1 activation, focusing on RhoG which has previously been shown to exert an effect on Rac1 (Katoh and Negishi, 2003).

To visualize and compare the morphology of cells lacking Rac1 and RhoG, HUVEC were transfected with individual siRNA Standard pool molecules against Rac1 and RhoG or non targeting control siRNA and used in the angiogenesis co-culture assay to determine their effects. The results obtained showed that tubules formed by ECs lacking Rac1 or RhoG appeared much shorter and were fewer in number (Figure 3.3), and branch formation was absent (Figure 3.3). These observations confirmed previous findings shown in Section 1.8.3 and suggest that as with Rac1, RhoG controls EC sprouting and because of the similarity in phenotype, RhoG and Rac1 may operate in the same signaling pathway. Based on these findings and given that RhoG had not been characterized extensively, subsequent studies described in this chapter focused on understanding the role of RhoG in angiogenesis and regulation by guanine nucleotide exchange factors (GEFs).

3.4 Assessment of role of RhoG in endothelial cell behaviour by timelapse microscopy

In order to gain a better understanding of the role of RhoG in angiogenesis, time-lapse microscopy was used to analyze the effect of RhoG knockdown in the EC-fibroblasts co-culture system. To visualize ECs growing upon the fibroblasts, the two cell types needed to be distinguished. HUVEC were infected with a retrovirus harboring EGFP expressing control vector (Section 2.5). Two days after infection, approximately 50% of the infected HUVEC were EGFP positive (termed HUVEC-EGFP).

HUVEC-EGFP were isolated by FACS and cultured in plastic bottomed T75 cm^2 flask until 80% confluent. HUVEC-EGFP were then transfected with Standard pool

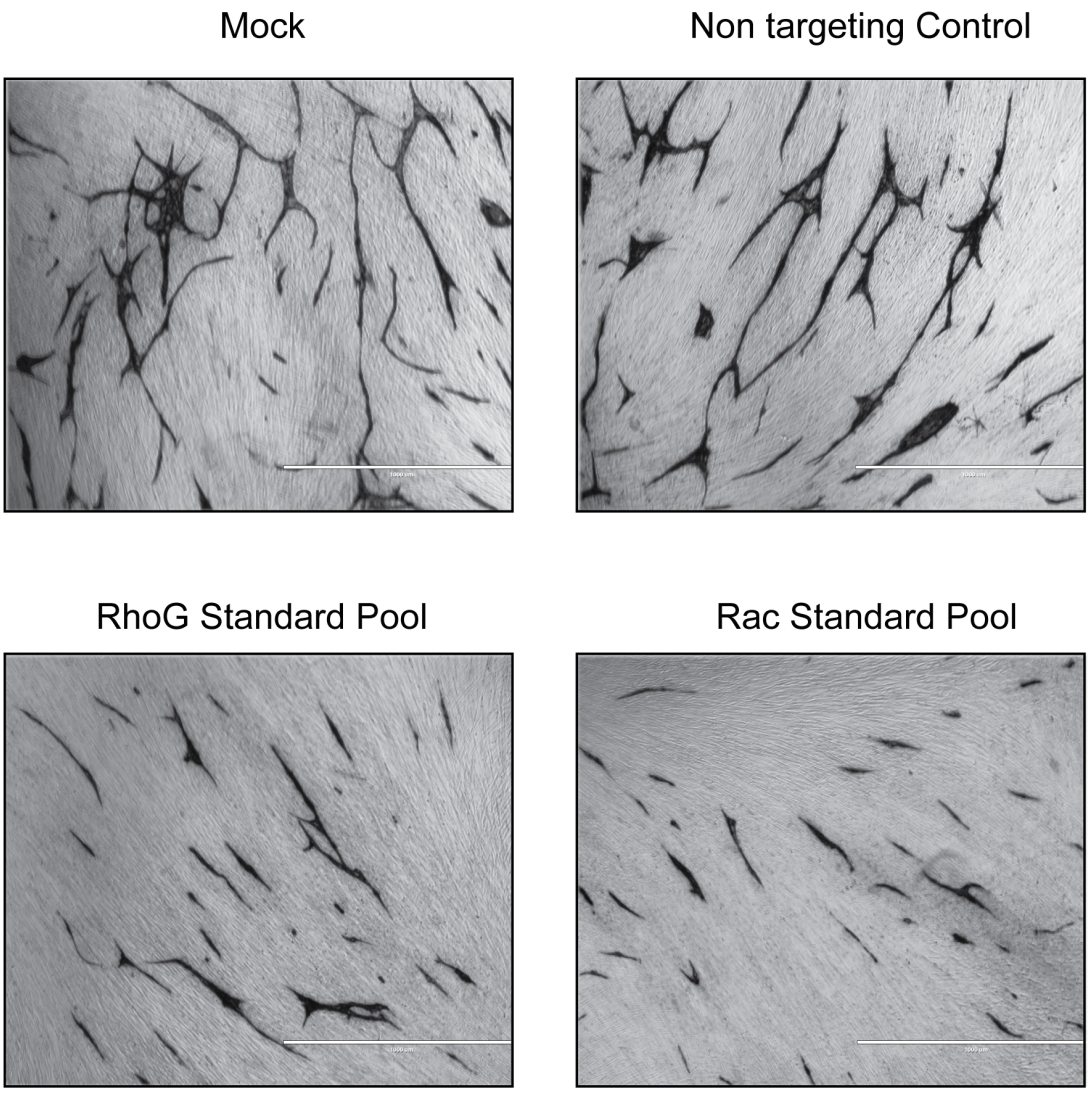

Figure 3.3 Knockdown of RhoG and Rac1 reduces endothelial cells tube formation

HUVEC were transfected with Standard pool siRNAs or mock transfected, and after 24 hours cells were seeded onto confluent fibroblasts as described in Chapter 2 (Section 2.4). Tube formation was assessed by CD31 staining 5 days after seeding. Representative phase-contrast images of tubule morphology are shown. Scale bar: 100μm. Straight tubule morphology was observed with knockdown of Rac1 or RhoG. This experiment shows that knockdown of Rac1 or RhoG reduces tube formation and leads to down-regulation of the branch point index according to results shown in Section 1.8.3 of Preliminary Data.

siRNAs against RhoG, non targeting control or mock transfected HUVEC and seeded onto confluent fibroblasts. Cells were then visualized by timelapse microscopy (see Movies 1, EGFP Non targeting and 2, EGFP RhoG - attached CD) or still images were captured at 1, 3 and 5 days after seeding (Figure 3.4). Control cells (mock transfected HUVEC or non targeting control siRNA transfected HUVEC) appeared locate for one another after adhesion on the fibroblast matrix and subsequently formed clusters (Figure 3.4, day 1). Spindly shaped HUVEC then elongated and started branching out (day 3). The process was completed with an initial step of vessel pruning (day 5). As seen by time-lapse microscopy, absence of RhoG affected more then one angiogenic step including cell migration, elongation and sprouting. EGFP-HUVEC lacking RhoG appeared to be fewer, compared to control cells and the initial cluster, cell-cell adhesion and migration was impaired at 24 hours after seeding (48 hours after transfection; Movie 2, attached CD). Following absence of cluster formation, ECs lacking RhoG lost directionality and moved randomly in circles. By day 5 after seeding, the cells that eventually coalesced formed very short tubes, deficient in lateral branching (by eye) in contrast to the elongated and fully branched control cells. Cells that remained single either assumed a spindle cell shape and migrated along the fibroblasts, or rounded up and detached. These results agreed with the data obtained using the endpoint assays shown in Figure 3.3.

3.5 Activation of RhoG by angiogenic growth factors

VEGF and bFGF stimulate cell survival and proliferation. FGFs and VEGFs exert their effects *via* binding to specific cell surface-expressed receptor tyrosine kinases. Binding activates the kinase activity that in turn activates signaling pathways that regulate proliferation, migration and differentiation of endothelial cells.

Previous studies have shown that tube formation in the co-culture assay is stimulated by endogenous bFGF in the culture media and by VEGF that is released by the human dermal fibroblasts (Mavria et al., 2006). In a number of studies, blocking bFGF and VEGF has been reported to disrupt tube formation in the co-culture assay suggesting that this organotypic assay models at least some aspects of physiological angiogenesis (Bishop et al., 1999; Mavria et al., 2006).

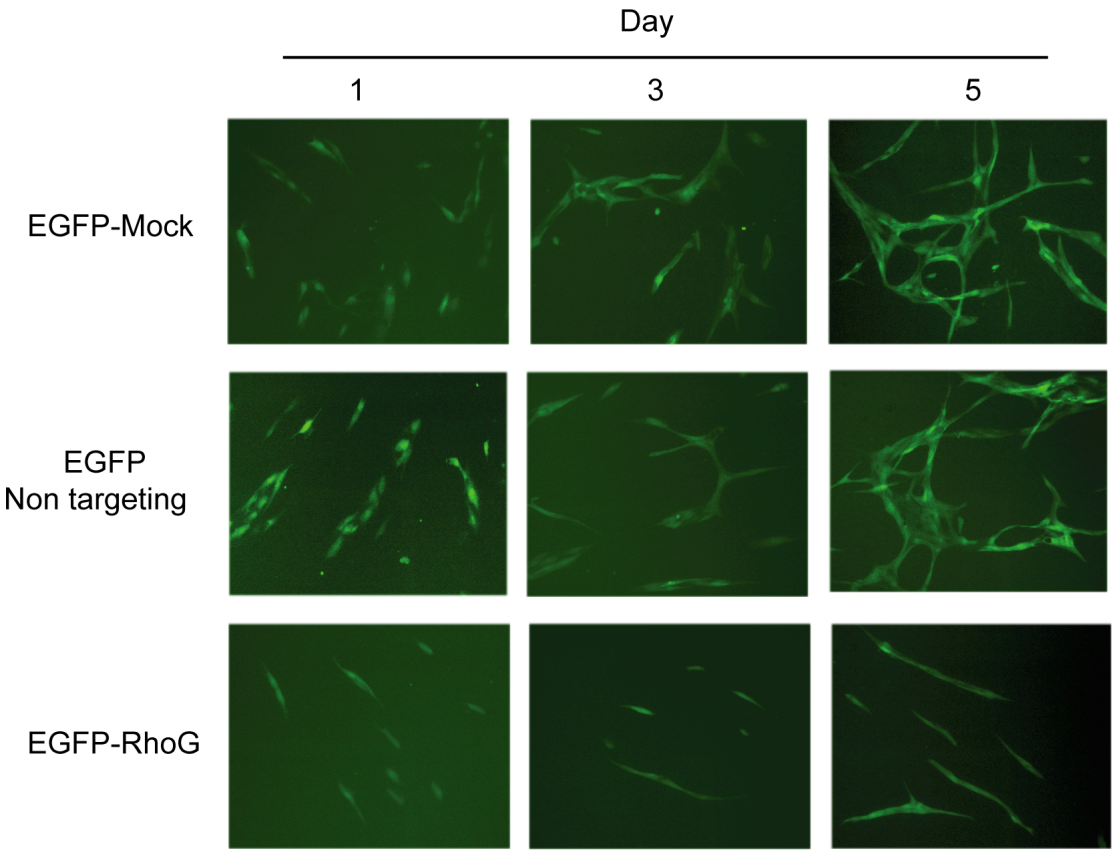

Figure 3.4 Role of RhoG in angiogenesis assessed in real-time
HUVEC expressing EGFP were transfected with RhoG Standard pool (EGFP-RhoG) or non targeting control siRNAs (EGFP Non targeting) or mock transfected EGFP-HUVEC (EGFP-Mock) as discussed in Section 2.1.6.2, and after 24 hours were seeded onto confluent fibroblasts as described in Section 2.4. Images show representative ECs and tubule morphologies at 1, 3 and 5 days after seeding. Images were acquired with a 10x objective of a Zeiss inverted microscope. Scale bar: 200μm.

Regulation of RhoG by bFGF in ECs has already been reported (Elfenbein et al., 2009) although there is no evidence to date describing whether RhoG is activated downstream of VEGF signaling cascade. In order to investigate whether VEGF and bFGF can activate RhoG in HUVEC, a RhoG pulldown assay was used. The RhoG pulldown assay, described in Section 2.3.7, is based on the known interaction between the GTP-bound activated form of RhoG and its downstream effector ELMO (Katoh and Negishi, 2003). In the pulldown assay, recombinant ELMO is used as a capture reagent for the GTP-bound RhoG described in Section 2.3.1.

Production of the GST-ELMO fusion protein in *E.coli* first had to be optimised. Both IPTG concentration and length of induction were kept constant (Section 2.3.1); the optimisation steps addressed the methodology used to lyse the bacteria and purify the recombinant protein. Purification of recombinant proteins followed by coupling with agarose sepharose beads for optimal protein pulldown is described in Section 2.3.2 Figure 3.5 shows an example of successful recombinant GST-ELMO expression before and after IPTG induction.

GST-ELMO pulldowns were used to analyze VEGF and bFGF-dependent RhoG activation in HUVEC. HUVEC were serum starved to down-regulate basal levels of active Rho GTPases, and then stimulated with VEGF or bFGF for different lengths of time. The RhoG pulldown assay was then used to compare levels of activated RhoG in VEGF stimulated compared to un-stimulated serum-starved HUVEC. Time points were chosen based on the observation that RhoG was not rapidly activated (2 minutes and 5 minutes) by VEGF in HUVEC (Samson et al., 2010). Furthermore, unpublished data from this laboratory had previously shown that active Rac1 was upregulated following stimulation of HUVEC with VEGF and bFGF at the same time points (15, 30 and 60 minutes; data not shown). As shown in Figure 3.6A and B, there was no significant RhoG activation after 5 minutes of VEGF stimulation, in agreement with the previously published report (Samson et al., 2010). However, stimulation for 10, 15 and 30 minutes showed increasing level of activated RhoG, with approximately 3.2-fold activated RhoG

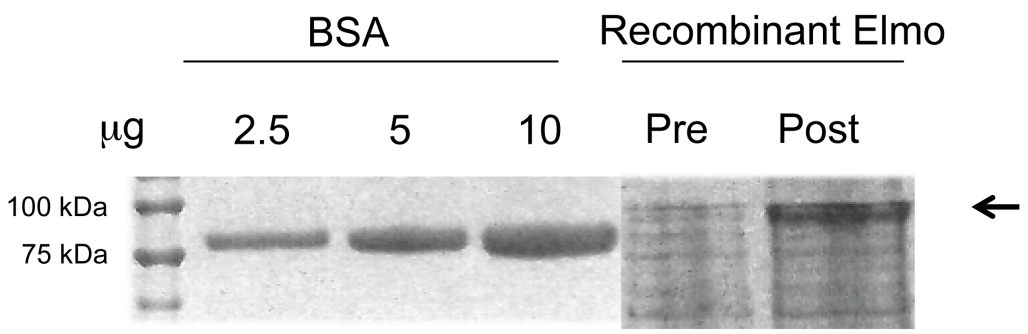

Figure 3.5 Visualization of recombinant GST-ELMO before and after IPTG induction
BL21 pLys bacteria were transfected with pGEX-ELMO and aliquots were taken before (pre) and after (post) IPTG induction. Bacteria were spun down, resuspended in loading buffer and loaded on a 10% acrylamide gel alongside different amounts of BSA (2.5μg, 5μg and 10μg). The gel was stained with Coomassie Blue to visualize the proteins. Arrow points to induction of GST-ELMO expression.

A

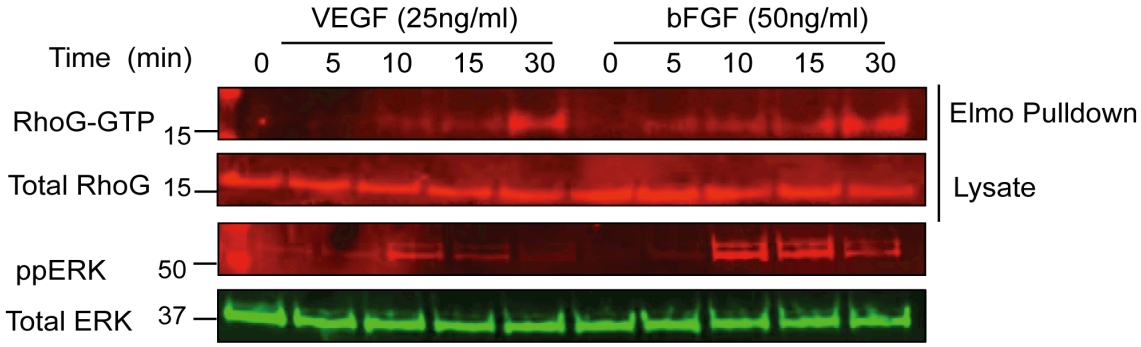

B

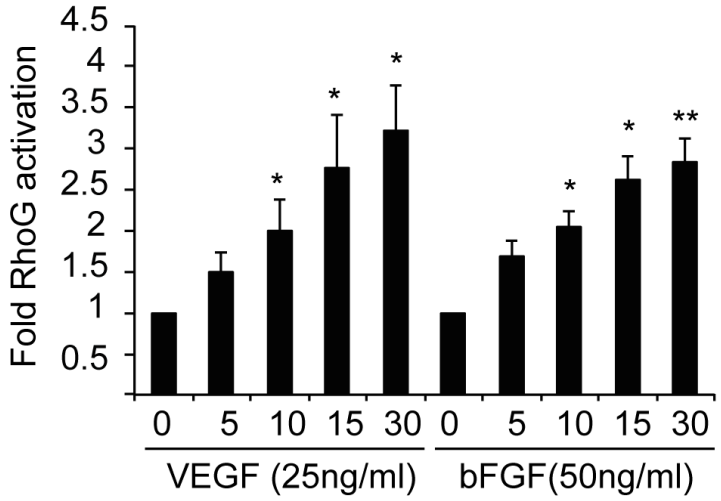

Figure 3.6 Activation of RhoG by angiogenic growth factors
HUVEC growing on fibronectin-coated dishes for 2 days were serum starved for 3 hours and stimulated with VEGF (25ng/ml) and bFGF (50ng/ml) for 5, 10, 15 and 30 minutes. After stimulation cells were lysed and RhoG activation was analysed using the RhoG pulldown assay (Section 2.3.7). (A) Representative Western Blots from one experiment show RhoG-GTP, total RhoG, ppERK and total ERK. (B) Bar chart shows quantification of RhoG pulldowns from three independent experiments performed using the Li-COR Odyssey system. RhoG activation was calculated as fold increase compared to unstimulated control after normalization for total RhoG for each condition. Error bars are S.E.M., p values from unpaired student's t-test compared to unstimulated (0 timepoint). *, $P<0.05$; **, $P<0.01$.

stimulation at 30 minutes. As with VEGF, bFGF stimulation also increased the levels of active RhoG after 10 minutes of stimulation, resulting in approximately 2-fold activation compared with the unstimulated control, whereas a 2.8 fold stimulation was achieved in 30 minutes. Levels of activation of the ERK pathway (detected by ERK phosphorylation) were used to confirm serum starvation and responsiveness of the cells to VEGF and bFGF stimulation. In agreement with previously published literature, ERK phosphorylation peaked at 10 minutes after VEGF and bFGF stimulation and was reduced after 15 minutes (Mor et al., 2004). Overall, these data show that both VEGF and bFGF activate RhoG with similar kinetics.

The intensity of each band was captured by ImageJ 1.46 software; this generates a peak and translates it into a value after subtraction of the background. To analyze a possible RhoG activation, stimulated samples were compared to the un-stimulated control. Samples were also normalized against the basal level of RhoG in the total lysate. This approach can, for example, discriminate between increases in activated RhoG compared to an increased signal due to variations in loading of the blot.

These data reveal that the activation of RhoG by both VEGF and bFGF is significant after 10, 15 and 30 minutes of stimulation.

3.6 RhoG controls Rac-1 activation downstream of VEGF signaling

It has been reported in a number of cell systems including NIH3T3 fibroblasts, A431 tumour cells (a human epithelial carcinoma cell line) and MDA-MB-231 cells (a breast cancer cell line) that RhoG mediates its effects through activation of Rac1 *via* the GEFs DOCK180 and DOCK4 (Hiramoto et al., 2006; Samson et al., 2010). Given that VEGF activates both Rac1 (Garrett et al., 2007) and RhoG (data presented in Section 3.5) in HUVEC, the RhoG-dependent activation of Rac1 in ECs was investigated.

A Rac1 pulldown assay (Section 2.3.7) was used to investigate Rac1 activation. This assay is based on the known interaction between active GTP-bound Rac1 and its downstream effector PAK (Thompson et al., 1998). The CRIB domain of PAK was expressed in *E.coli* as a GST-PAK-CRIB recombinant protein (Section 2.3.1). The GST-PAK-CRIB fusion protein before and after induction with IPTG is shown in Figure 3.7.

HUVEC were transfected with a siRNA Standard pool targeting RhoG or mock transfected HUVEC and stimulated with VEGF (25ng/ml). Active Rac1 was then pulled-down and measured in presence or absence of RhoG. The results of the activated Rac1 pulldown assay (Figure 3.8A and B) show that the active, GTP bound Rac1, was detected 15, 30 and 60 minutes after VEGF stimulation in the mock transfected cells and that the induction of activated Rac1 was dependent upon RhoG expression.

Results generated using a Standard pool siRNA were corroborated using individual On-Target siRNA molecules that bind to different regions of the mRNA of interest. HUVEC were transfected with two On-Target siRNA oligonucleotides (RhoGot5 and ot7) that had previously been shown by qRT-PCR to give good knockdown of RhoG (give the 79% and 64% knockdowns respectively). Cells were then serum starved, stimulated with VEGF and the level of active Rac1 was assessed using the GST-PAK-CRIB pulldown assay.

The results obtained with these individual siRNA molecules (Figure 3.9) confirmed the data using the siRNA pool (Figure 3.8A and B), namely that reduced levels of Rac1 activation were observed following knockdown of RhoG expression at 15, 30 and 60 minutes post-VEGF stimulation. Collectively, these data show that in HUVEC, RhoG acts upstream of Rac1 following VEGF stimulation. This finding suggests that RhoG may co-ordinate Rac1-driven endothelial cell responses to VEGF stimulation.

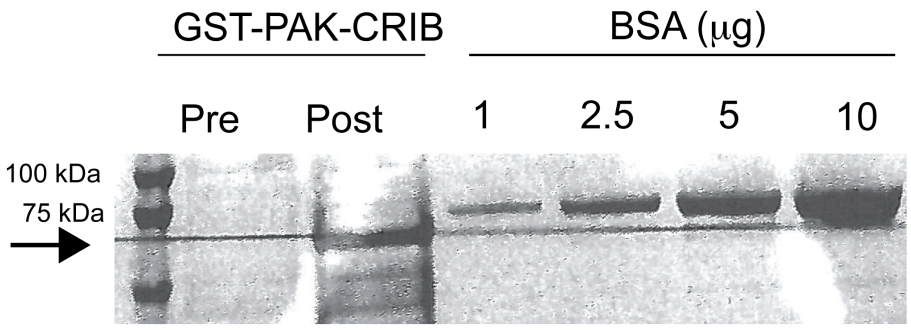

Figure 3.7 Visualization of recombinant GST-PAK-CRIB before and after IPTG induction
BL21 pLys bacteria were transfected with pGEX-GST-PAK-CRIB and aliquots were taken before (pre) and after (post) IPTG induction. Bacteria were spun down, re-suspended in loading buffer and loaded on a 10% acrylamide gel alongside different amounts of BSA (2.5μg, 5μg and 10μg). The gel was stained with Coomassie Blue to visualize the proteins. Arrow points to induction of GST-PAK-CRIB expression.

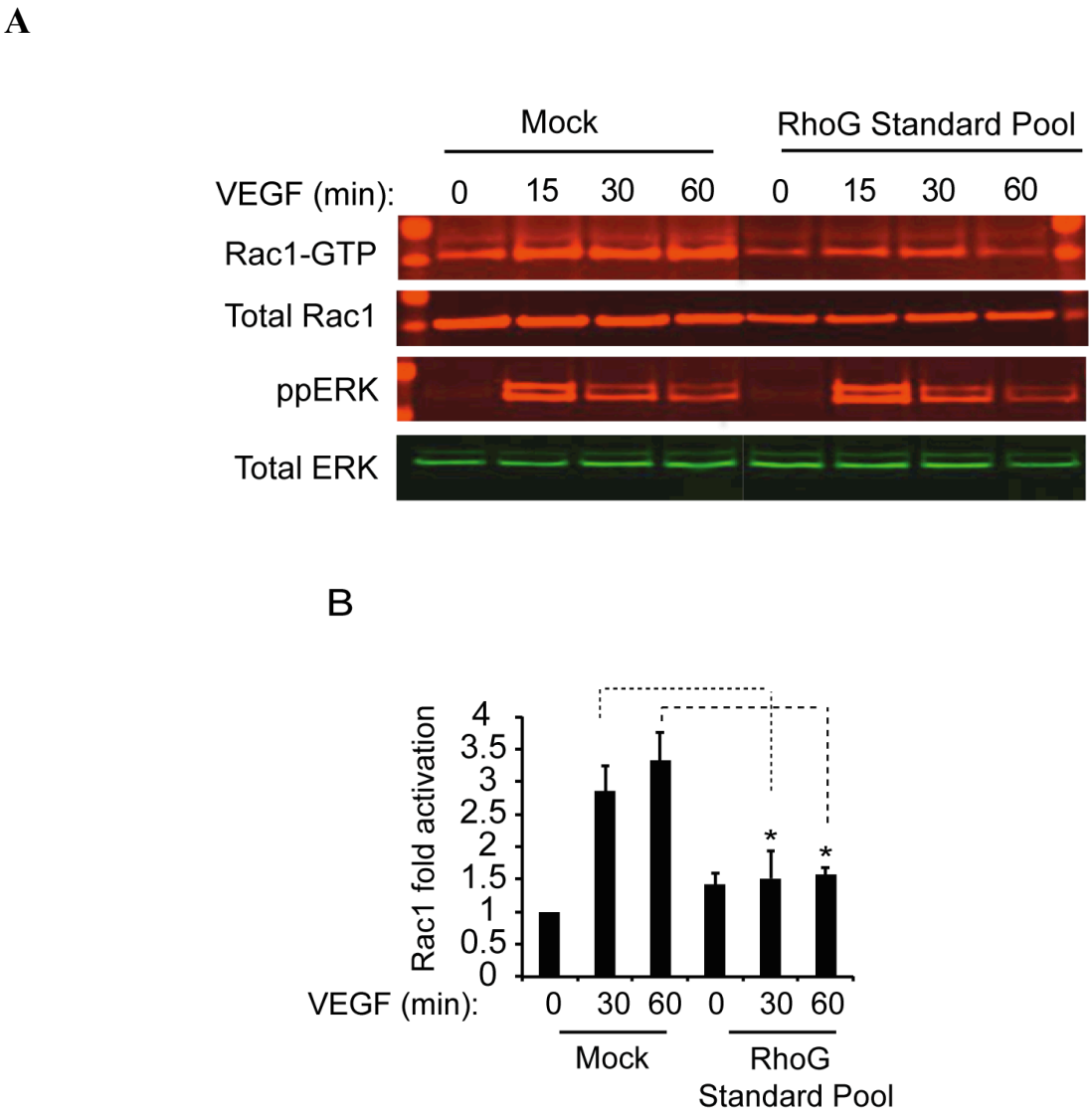

Figure 3.8 Rac1 activation downstream VEGF signaling is regulated by RhoG
HUVEC growing on fibronectin-coated dishes were transfected using RhoG Standard pool siRNA or mock transfected HUVEC. Cells were then serum starved for 3 hours and stimulated with VEGF (25ng/ml) for 15, 30 and 60 minutes. After stimulation the cells were lysed and Rac1 activation was analysed using the Rac1 pulldown assay (Section 2.3.7). (A) Representative Western Blots of Rac1-GTP, total Rac1, ppERK and total ERK are shown. (B) Bar chart shows quantification of Rac1 pulldowns from three independent experiments performed using the Li-COR Odyssey system. Rac1 activation was calculated as fold increase compared to un-stimulated control after normalization for total Rac1 for each condition. Error bars are S.E.M., p values from unpaired student's t-test compared to un-stimulated (0 timepoint) control. RhoG Standard pool knockdown was quantified by qRT-PCR as 86% (Appendix, Figure 2). *, $P<0.05$.

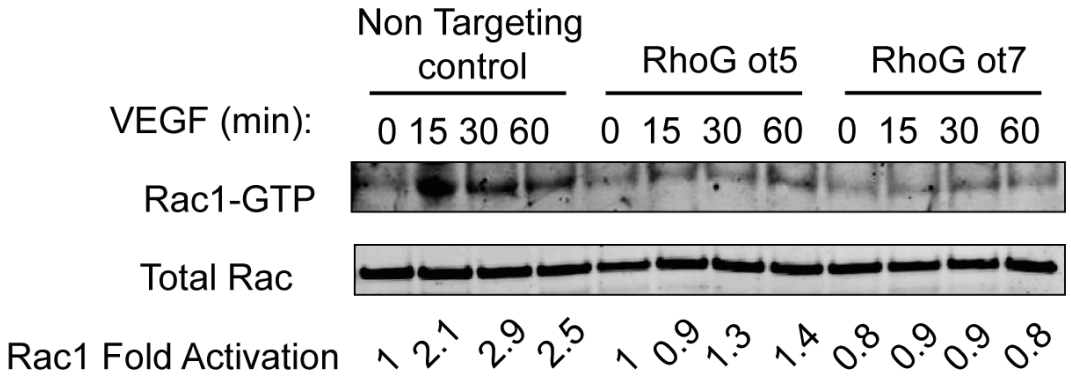

Figure 3.9 Validation of RhoG activity upstream of Rac1
HUVEC growing on fibronectin-coated dishes were transfected using RhoG On-Target oligonucleodites siRNAs against RhoG (RhoG ot5 and RhoG ot7) or non targeting control HUVEC. Cells were serum starved, stimulated with VEGF (25ng/ml, 15, 30 and 60 minutes) and active Rac1 was pulled-down with GST-PAK-CRIB. Western Blots from one experiment performed using the Li-COR Odyssey system show Rac1-GTP and total Rac1. Levels of Rac1-GTP are shown as fold stimulation compared to un-stimulated control after normalization for total Rac1 (Rac1 Fold Activation). RhoG ot5 and RhoG ot7 knockdowns were quantified by qRT-PCR as 78% and 64% respectively (Appendix, Figure 1).
.

3.7 SGEF and Trio activate RhoG downstream of VEGF signaling

RhoG can be activated by different stimuli (Figure 3.6) and its activation and role may vary depending on the cell type (Elfenbein et al., 2009; Hiramoto-Yamaki et al., 2010; Samson et al., 2010).

The data presented here show that VEGF stimulation leads to RhoG dependent Rac1 activation. In order to define the RhoG positive regulators (GEFs) that activate RhoG downstream of VEGF in endothelial cells, HUVEC were transfected with siRNAs against putative RhoG GEFs (SGEF, Trio and FLJ10665) and tested for their effect on RhoG activation. SGEF and Trio were found to activate RhoG in endothelial cells (van Buul et al., 2007; van Rijssel et al., 2012) while FLJ10665 contributes to RhoG activation in A431 breast tumor cells (D'Angelo et al., 2007; Samson et al., 2010). Standard pool siRNA oligonucleotides used were against SGEF, Trio and FLJ10665 or a non targeting control.

This screen was performed using the RhoG pulldown with GST-ELMO following treatment with VEGF for 30 minutes.

The 30 minutes time-point was chosen based on the data shown in Figure 3.6 in which RhoG activation was significantly upregulated 30 minutes after VEGF stimulation. The VEGF treated cells transfected with the non targeting siRNA control showed significant RhoG activation after 30 minutes (Figure 3.10). Expression of active RhoG was not reduced in HUVEC lacking FLJ10665 at the time point observed; in addition the level of active RhoG in this sample was quite variable throughout the three experiments performed although consistently higher than control HUVEC. This explains such a high error bar associated with FLJ10665 transfected HUVEC shown in Figure 3.10B. RhoG activation was partially reduced when Trio expression was inhibited and blocked when SGEF was targeted (Figure 3.10A and B).

These results suggest that, in HUVEC, RhoG is activated by SGEF and, to a lesser extent, by Trio during VEGF stimulation.

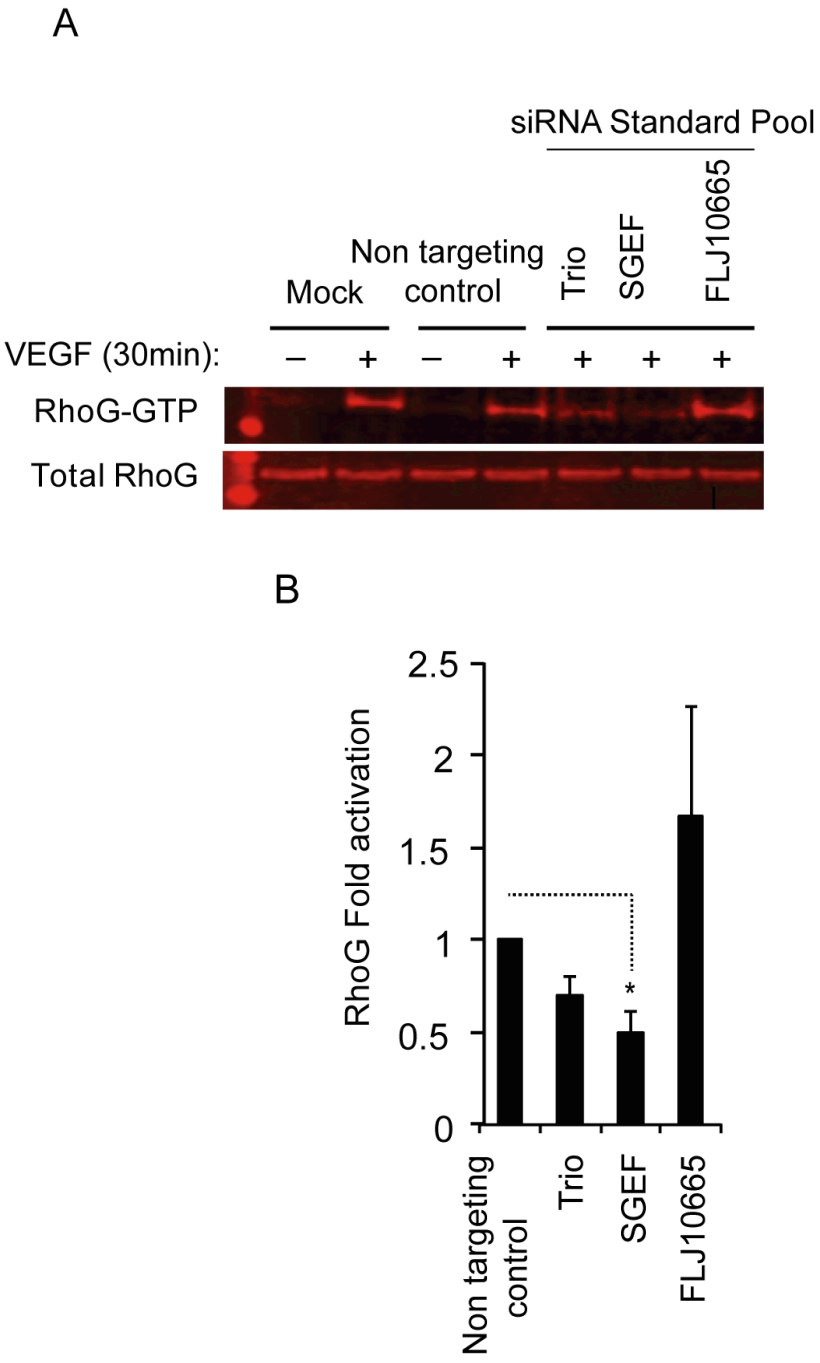

Figure 3.10 SGEF activates RhoG downstream of VEGF
HUVEC growing on fibronectin-coated dishes were transfected with SGEF, Trio, FLJ10665 or non targeting control siRNAs, or mock transfected, and after 48 hours they were serum starved and stimulated with VEGF (25ng/ml). Cells were lysed and RhoG activation was analysed using the RhoG pulldown assay (Secton 2.3.7). (A) Western Blots from one experiment show RhoG-GTP and total RhoG. (B) Bar chart shows quantification of RhoG pulldown from three independent experiments performed using the Li-COR Odyssey system. RhoG activation was calculated as fold increase compared to unstimulated control after normalization for total RhoG for each condition. Error bars are S.E.M., p values from unpaired student's t-test compared to unstimulated (0 timepoint). *, $P<0.05$.

To validate the role of SGEF in RhoG activation, the same experiment was performed using On-Target oligonucleotides to knockdown SGEF. Four different On-Target siRNAs were used (SGEFot5, SGEFot6, SGEFot7 and SGEFot8). First, the On-Target siRNAs were assessed to determine which gave the greatest inhibition of SGEF expression. HUVEC were transfected with the four SGEF On-Target siRNAs or a non targeting control and SGEF mRNA expression analysed by qRT-PCR. The two On-Target oligonucleotides (SGEFot5 and SGEFot6) that provided the greatest knockdown were selected for use in the RhoG pulldown assay. Knockdown levels for SGEFot5 and SGEF ot6 are reported in Appendix (Figure 3). The results in Figure 3.11 show that RhoG activation was indeed SGEF dependent, corroborating the results obtained with the siRNA pool.

3.8 Trio activates RhoG downstream of bFGF signaling

The results above show that SGEF and Trio are both involved in RhoG activation downstream of VEGF. SGEF and Trio are very dissimilar GEFs and it is possible that both GEFs are located downstream of the VEGF receptor to mediate different cellular activities *via* RhoG. When activated by bFGF, a signaling cascade is initiated that dissociates RhoG from binding to the RhoGDI. RhoG is thus released and freed to activate Rac1 through its downstream effector ELMO (Elfenbein et al., 2009).

In order to identify the positive regulators of RhoG downstream of bFGF, the same approach described above was used to look at the effect of bFGF on RhoG signaling. Similar to the findings with VEGF stimulation, knockdown of FLJ10665 had no effect on RhoG activation after 30 minutes of bFGF stimulation (Figure 3.12A and B). RhoG activation by VEGF required SGEF (Figure 3.10 and Figure 3.11); however, for bFGF stimulation, SGEF was not required (Figure 3.12A and B). bFGF mediated activation of RhoG required Trio since inhibition of Trio activity abolished RhoG activation (Figure 3.12A and B). This result was validated using siRNA On-Target oligonucleotides.

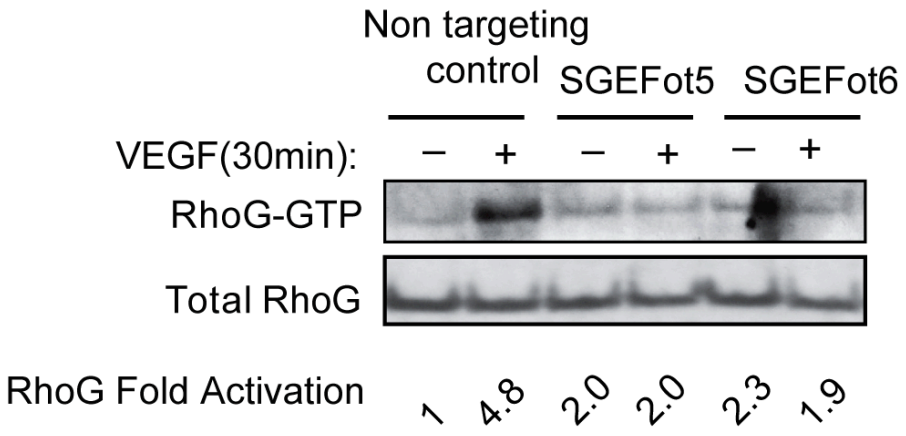

Figure 3.11 Validation of SGEF activity upstream of RhoG
HUVEC growing on fibronectin-coated dishes were transfected with SGEF On-Target oligonucleotides against SGEF (ot5 and ot6) or non targeting control siRNA, serum starved and stimulated with VEGF (25ng/ml). Cells were lysed and RhoG activation was analysed using the RhoG pulldown assay (Section 2.3.7). Western Blots from one experiment performed using the Li-COR Odyssey system show RhoG-GTP and total RhoG. Levels of RhoG-GTP are shown as fold stimulation compared to un-stimulated control after normalization for total RhoG (RhoG Fold Activation). Knockdown of SGEF ot5 and SGEF ot6 was quantitated as 63% and 51% respectively (Appendix, Figure 3).

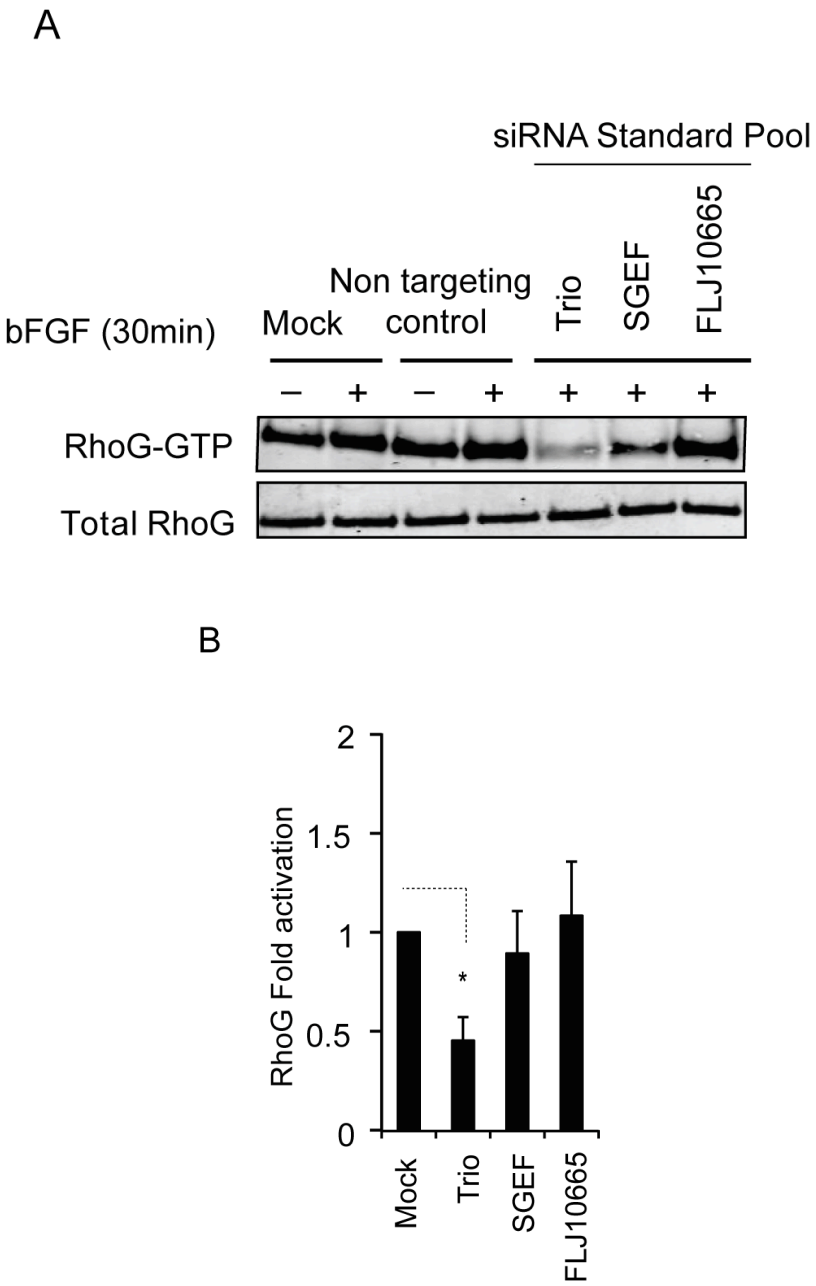

Figure 3.12 RhoG is activated through Trio downstream of bFGF signaling
HUVEC growing on fibronectin-coated dishes were transfected with SGEF, Trio, FLJ10665, non targeting control siRNAs or mock transfected, serum starved and stimulated with bFGF (50ng/ml). Cells were lysed and RhoG activation was analysed using the RhoG pulldown assay (Section 2.3.7). (A) Representative Western Blots from one experiment show RhoG-GTP and total RhoG. (B) Bar chart shows quantification of RhoG pulldowns from three independent experiments performed using the Li-COR Odyssey system. RhoG activation was calculated as fold increase compared to unstimulated control after normalization for total RhoG for each condition. Error bars are S.E.M., p values from unpaired student's t-test compared to unstimulated (0 timepoint). *, $P<0.05$.

The knockdown level achieved was: Trio ot5, 52%, Trio ot6, 32% and Trio ot7, 50% (Appendix, Figure 4). As described above for SGEF and VEGF stimulation, the two siRNA molecules (Trio ot5 and ot7) that gave the largest knockdown of mRNA expression were selected from four tested. These two siRNA molecules (and a non targeting control) were transfected into HUVEC, the cells serum starved, stimulated with bFGF for 30 minutes and RhoG activation determined using the pulldown assay.

These assays showed reduced levels of RhoG activation following knockdown of Trio with the On-Target oligonucleotides after 30 minutes of bFGF stimulation (Figure 3.13), corroborating the result with the siRNA pool (Figure 3.12A and B). This revealed that Trio was required for RhoG activation downstream of bFGF signaling in endothelial cells.

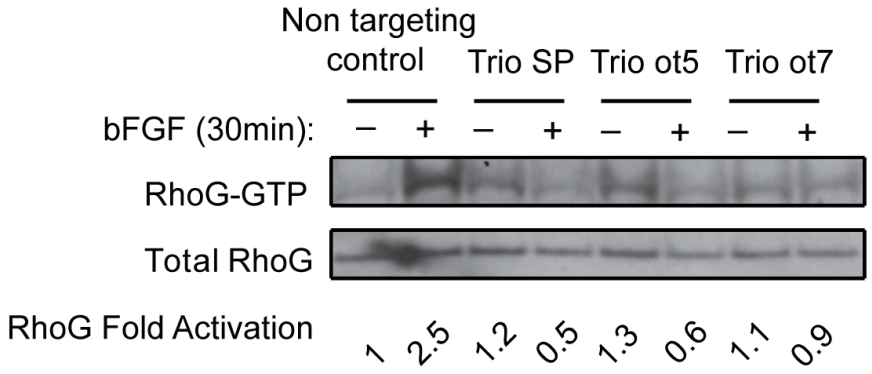

Figure 3.13 Validation of Trio activity upstream of RhoG
HUVEC growing on fibronectin-coated dishes were transfected with Trio Standard Pool siRNA, On-Target oligonucleotides against Trio (ot5 and ot7) or non targeting control siRNA, serum starved and stimulated with bFGF (50ng/ml). Cells were lysed and RhoG activation was analysed using the RhoG pulldown assay (Section 2.3.7). Western Blots from one experiment performed using the Li-COR Odyssey system of RhoG-GTP and total RhoG are shown. Levels of RhoG-GTP are shown as fold stimulation compared to un-stimulated control after normalization for total RhoG (RhoG Fold Activation). Knockdown of Trio pool siRNA, Trio ot5 and ot7 were quantitated as 43%, 52% and Trio ot7, 50% (Appendix, Figure 4).

3.9 Discussion

Angiogenesis, the formation of new blood vessels from pre-existing ones, is crucial for embryo development and is induced by tumours for their development. In order to form new blood vessels, endothelial cells need to migrate, establish cell-cell junctions, form lumens and sprout. These processes require changes in the actin cytoskeleton regulated by the Rho family of small GTPases.

The Rho GTPase prototypical members Rho, Rac and Cdc42 have been implicated in endothelial cell migration and cell junction formation; however, the role of other family members and their regulation are less characterized. The siRNA mini-screens performed in these studies showed that knockdown of Rho GTPases impacts on tubule formation leading to changes in the levels and/or morphology of tubules formed in the organotypic angiogenesis assay. Amongst the less characterized Rho GTPases, RhoG has attracted attention due to its interaction with the DOCK family GEFs DOCK180, DOCK3 and DOCK4 in the context of neuronal cell function (Katoh et al., 2000; Katoh et al., 2006; Hiramoto-Yamaki et al., 2010). The contribution of RhoG to endothelial cell behaviour has not been established and, to date, the only report shows that RhoG regulates endothelial docking structure of the endothelium facilitating inflammation (van Rijssel et al., 2012).

Data presented in this chapter have demonstrated that: i) RhoG is activated by VEGF and bFGF and has an essential role in controlling endothelial lateral branching and tube formation; ii) RhoG activates Rac1 downstream of VEGF signaling cascade; iii) SGEF and Trio act as RhoG positive regulators downstream VEGF and bFGF respectively.

The siRNA mini-screen was a good tool to visualize tube morphology in cells lacking RhoG. As shown using CD31 stained ECs or *via* live imaging, control HUVEC recreated a number of phenotypes similar to those seen in an *in vivo* environment. As shown through still images (Figure 3.4) and time-lapse microscopy (CD, movies 1) HUVEC-EGFP developed fully formed tubules that were stabilized by day 5, whereas in the absence of RhoG (movie 2) a number of defects were witnessed including reduction in cell number. As described in Section 3.4, HUVEC lacking RhoG showed reduced number of cells compared

to control HUVEC. Cells viability of RhoG knocked down HUVEC was not assessed in the organotypic angiogenesis assay. However the number of ECs transfected with RhoG siRNA growing on fibronectin or plastic dishes was comparable to non targeting control transfected HUVEC as determined by cell counting 48hrs or 72hrs following transfection. Because neither Tunnel assay for cell death quantification or KI67 staining to assess cell proliferation were carried out, it cannot be excluded that RhoG might promote cell survival or attachment to the fibroblast produced extracellular matrix. However the CD31 staining in Figure 3.3 shows a high number of black dots in RhoG siRNA transfected HUVEC. It could therefore be hypothesized that HUVEC with a reduced expression of RhoG did attach to the extracellular matrix but the growth did now progress and cells did not cluster but remained as single cell. It is also possible to speculate that cell-cell interaction stimulates cell division. If that is the case, it might be that cell-cell contact may act to upregulate VEGF mRNA within the ECs. A second hypothesis is that the cluster acts on the layer of fibroblasts to induce an increase of the concentration of matrix produced VEGF. Tubules formed by HUVEC lacking RhoG were shorter than control tubules and branch free. These data therefore highlighted that importance of RhoG in tube formation *in vitro*.

The angiogenic factors VEGF and bFGF significantly activated RhoG in endothelial cells (Figure 3.6). Samson and co-workers showed absence of a VEGF-induced activation of RhoG (Samson et al., 2010) since early stimulation (2 minutes and 5 minutes) did not upregulate the expression of active RhoG in HUVEC. However in my study, whilst no significant activation was seen after 5 minutes of stimulation (consistent with data published by Samson et al), longer stimulation (for 10, 15 and 30 minutes) strongly upregulated RhoG. Activation of RhoG by bFGF has been shown to be stronger after 10 minutes of stimulation compared to 20 minutes (Elfenbein et al., 2009); however, in my study, RhoG activation was further activated by longer bFGF stimulation for 30 minutes. The endothelial cell type investigated by Elfenbein et al. was isolated from the rat fat pad. It is documented that ECs from different tissues show different phenotypes: this might be an example of a tissue specific EC response.

In some cell systems, RhoG mediates its effects through the activation of Rac1 *via* the GEFs DOCK180 and DOCK4 (Hiramoto et al., 2006; Hiramoto-Yamaki et al., 2010). My study showed that RhoG is necessary for Rac1 activation in endothelial cells. Given the similarity in phenotypes of RhoG and Rac1 knockdown, this finding suggests that the defect in tube formation (shown in Figure 3.3) in response to knockdown of RhoG is mediated by the blockade of Rac1 activation. To prove this, it would be necessary to over-express Rac1 and determine if the phenotype of reduced tube formation and decrease in branch point index in response to knockdown of RhoG could be rescued. Although this was attempted as part of my study, the experiments were not successful because of the low transfection efficiency of HUVEC with plasmid DNA (typically < 20%). It has been reported previously that RhoG can also act in a Rac1 independent (Mouse Embryo Fibroblast and HUVEC, Meller et al., 2008; van Rijssel et al., 2012) as well as a Rac1 dependent manner (Rat Embryo Fibroblast, Blangy et al., 2000) and accordingly, RhoG can interact with only some of the Rac1 downstream effectors (IQGAP2, MLK-3, PLD1), but not with others (e.g. PAKs, POSH, WASP, Par-6, IRSp53) (Wennerberg et al., 2002). It will be important in future studies to establish whether there are Rac1-independent functions downstream of RhoG in endothelial cells and which downstream effectors are part of the RhoG signaling pathways.

The studies presented here showed that VEGF activates RhoG through SGEF and to a lesser extent through Trio, whereas bFGF activates RhoG exclusively through SGEF. Van Buul and co-workers first described a role for SGEF in endothelial cup formation, the extension of dynamic membrane protrusions that surround leucocytes during their endothelial transmigration (van Buul et al., 2007). Trio is a complex molecule since it has 2 DH-PH domains for Rho and RhoG/Rac1 activation. As with SGEF, Trio has been shown to control leukocyte trans-endothelial cell migration through the control of RhoG-driven endothelial protrusions and clustering of the adhesion molecule ICAM1, although the latter was thought to be independent of RhoG activation but dependent on Rac1 (van Rijssel et al., 2012). These published studies, together with the current study of regulation of RhoG downstream of VEGF and bFGF, suggest that Trio and SGEF may play important roles in tubule formation through control of endothelial cell protrusive activity. In addition to SGEF

and Trio, previous reports showed that FLJ10665 plays an important role in RhoG activation, microvilli and membrane ruffle formation in A431 epithelial cells downstream of EGF signaling (Samson et al., 2010), and that it acted through its interaction with ELMO. FLJ10665 was shown to be in a ternary complex with RhoG and ELMO (Samson et al., 2010). Down-regulation of FLJ10665 showed no changes in RhoG activation downstream of VEGF or bFGF signaling; therefore it would be interesting to find out whether it acts as GEF downstream of EGF in endothelial cells. Previous reports have established that the DOCK family GEFs controls Rac1 activation downstream of RhoG in other cell systems (Katoh and Negishi, 2003; Katoh et al., 2006; Namekata et al., 2012). Additional RNAi screens of GEFs performed in this laboratory (Preliminary Data, Section 1.8.1) showed that DOCK4 is necessary for tube formation in the organotypic angiogenesis assay. Moreover DOCK4 acted as a Rac1 GEF downstream of VEGF (Preliminary Data, Section 1.8.2) suggesting that RhoG activates Rac1 through DOCK4 in endothelial cells. Interestingly, DOCK180 was not found to play a role in tube formation in the co-culture system although DOCK180 has been described as a Rac1 GEF in endothelial cells (Sanematsu et al., 2010; Brugnera et al., 2002; Lu and Ravichandran, 2006; Côté and Vuori, 2007). This suggests that the role of each component of a signaling pathway can be highly influenced by many parameters. For an accurate analysis of a potential biological role, it should always be considered that the same molecule might change behaviour in a different cell type and under different stimuli.

Chapter 4

RhoG-DOCK4-Rac1-Cdc42: a Signaling Module That Controls Filopodia Formation

4.1 Introduction

The studies presented in chapter 3 showed that down-regulation of RhoG and Rac1 in ECs resulted in a similar phenotype (Figure 3.3) and, as seen in some other cell systems, RhoG controls Rac1 activation. RhoG is regulated by SGEF and to a lesser extent by Trio, downstream of the VEGF signaling pathway (Figure 3.10). In *vivo* VEGF promotes branch formation through stimulation of the endothelial cell filopodia protrusions required for sprouting (Gerhardt et al., 2003). Previous work in this laboratory had shown that DOCK4, the Rac1 nucleotide exchange factor, controls lateral filopodia formation in the organotypic angiogenesis system whereas tip filopodia persisted in absence of DOCK4 (Preliminary Data, Section 1.8.1). Given that in other cell systems RhoG controls Rac1 activation through DOCK4 (Hiramoto et al., 2006), it was hypothesized that RhoG controls lateral branching through the control of filopodia formation. As described above (Section 1.5.5.5 and 1.5.5.6), Cdc42 controls filopodia formation in many cell types including fibroblasts, cancer cells and neuronal cells (Allen et al., 1997; Calvo et al., 2011; Gauthier-Campbell et al., 2004). However, it is not known whether Cdc42 controls filopodia formation in endothelial cells. Therefore, I set out to test the hypothesis that Cdc42 controls filopodia formation in ECs and whether there is a link between SGEF, RhoG, Cdc42 activation and filopodia formation.

4.2 Filopodia formation in the organotypic co-culture assay

Previous work in this laboratory has shown that sprouting in the organotypic co-culture assay is preceded by filopodia formation, as visualized by confocal microscopy in HUVEC stably expressing EGFP (unpublished data). During development, filopodia formation is driven by VEGF (Gerhardt et al., 2003); hence the first point addressed was to confirm that filopodia formation in the co-culture system is VEGF dependent.

The method adopted to image ECs filopodia on the organotypic assay relies on fixation and staining of the co-cultures with a CD31 staining kit (Section 2.4). An example of visualizing filopodia in endothelial cells using this staining method is shown in Figure 4.1. The basal level of filopodia formation in non targeting control cells can vary depending on

the individual performance of the two cell types co-cultured (HDF and HUVEC). When the assay was performed by different individuals, the VEGF-dependent increase in filopodia number and distribution around the cell body was observed consistently, indicating an high reliability of the assay and reproducibility of the data. The pictures selected for analysis are those in which the background was reduced to a very low level, which is necessary to guarantee precise counting of filopodia. Prior to statistical analysis filopodia were also counted by an independent observer to ensure that protrusions were clearly distinguished by inexpert eye.

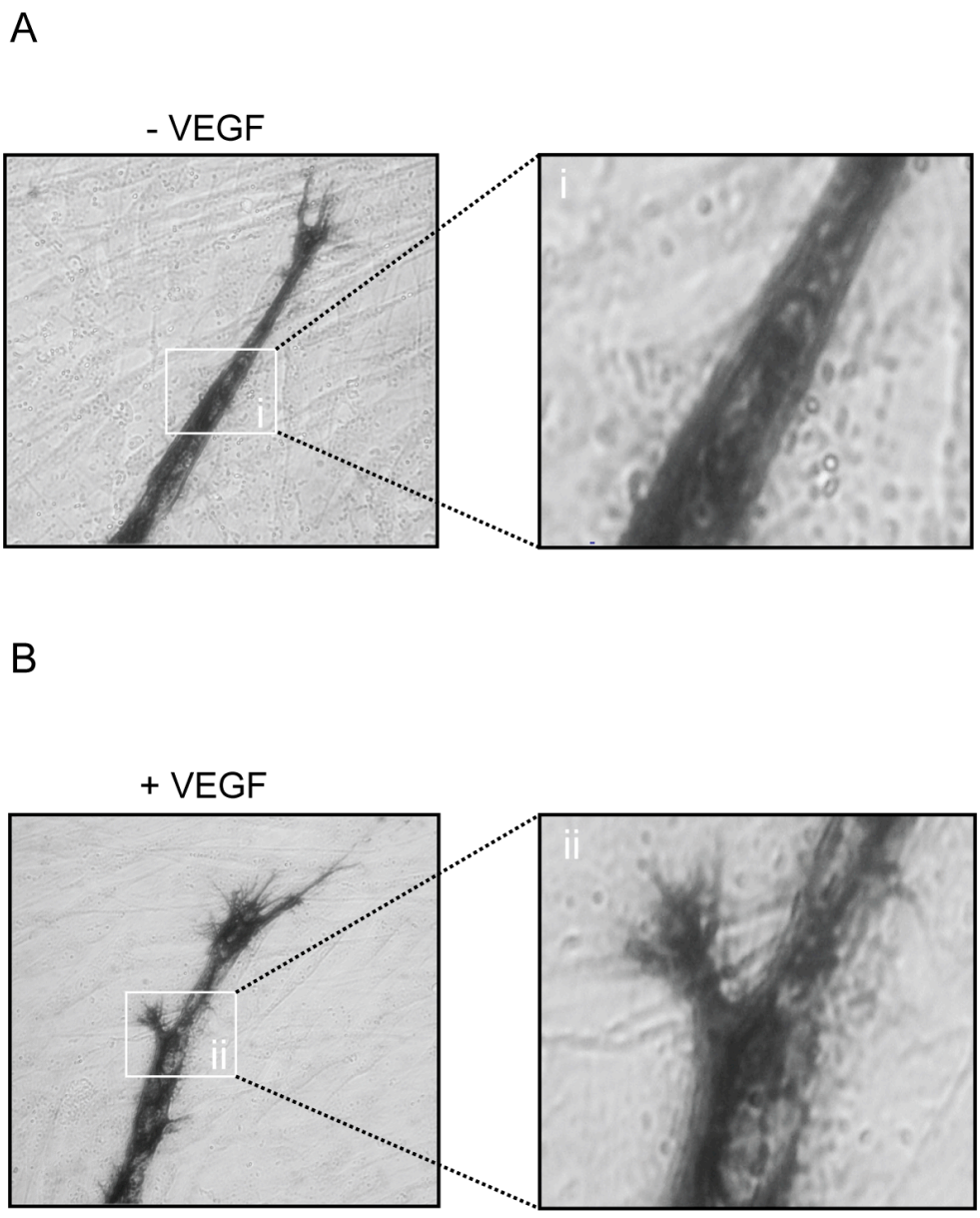

Figure 4.1 VEGF-driven filopodia formation in the organotypic angiogenesis assay
HUVEC were seeded onto confluent fibroblasts in the organotypic angiogenesis assay in the presence or absence of VEGF (25ng/ml) as described in Section 2.4. In control treated cultures, VEGF was refreshed 3 days after seeding and 48 hours later cultures were fixed, stained and endothelial cells imaged using the 40x objective of a compound microscope. Scale bar: 50μm. Representative images show tube morphology and appearance of filopodia in the absence (A) or presence of VEGF (B). Marked areas in each sample show a manual enlargement of lateral regions where filopodia localize.

Using this method, filopodia are stable for long period when stored with PBS at 4^{o}C. However, as with other immuno-staining procedures, background staining due to interaction between the chromogenic reporter bound to the secondary antibody and the substrate, may confound counting the filopodia. In the experiments described below, the total number of filopodia was quantified by a blinded, manual count and reported as number of filopodia divided per tubule length.

4.3 RhoG and its exchange factor SGEF control VEGF-driven endothelial cell filopodia formation

Data presented in chapter 3 (Section 3.7) showed that SGEF and Trio regulate RhoG activation, downstream of VEGF signaling. To investigate whether RhoG, SGEF and Trio play a role in the control of endothelial cell filopodia formation, filopodia formation in the co-culture system was analysed in the presence or absence of RhoG, SGEF or Trio using the siRNA technique described previously (Section 2.1.6.2).

HUVEC were transfected with siRNA oligonucletides against RhoG (previously validated in this laboratory), On-Target oligonucleotides against SGEF (ot5 and ot6) or Trio (ot5 and ot7) or non targeting control siRNA. Following transfection and seeding onto confluent fibroblasts, tube formation was allowed to proceed in the presence of VEGF for 5 days. The cultures were then immuno-stained for CD31 and filopodia were visualized using a 40x objective of a compound microscope (Figure 4.2). Quantification of the total number of filopodia per vessel length was assessed as described in Section 3.3 and shown in Figure 4.2B. The results show that inhibition of RhoG expression abolished VEGF-driven filopodia. Knockdown of SGEF produced a similar phenotype, showing reduction in number of filopodia. Inhibition of both RhoG and SGEF generate similar tubule morphologies which is consistent with them acting in the same pathway and agrees with the data presented in chapter 3, showing that SGEF acts as a RhoG GEF downstream of VEGF signaling.

Analysis of the role of Trio showed that the majority of cells with reduced level of Trio formed shorter tubules.

A

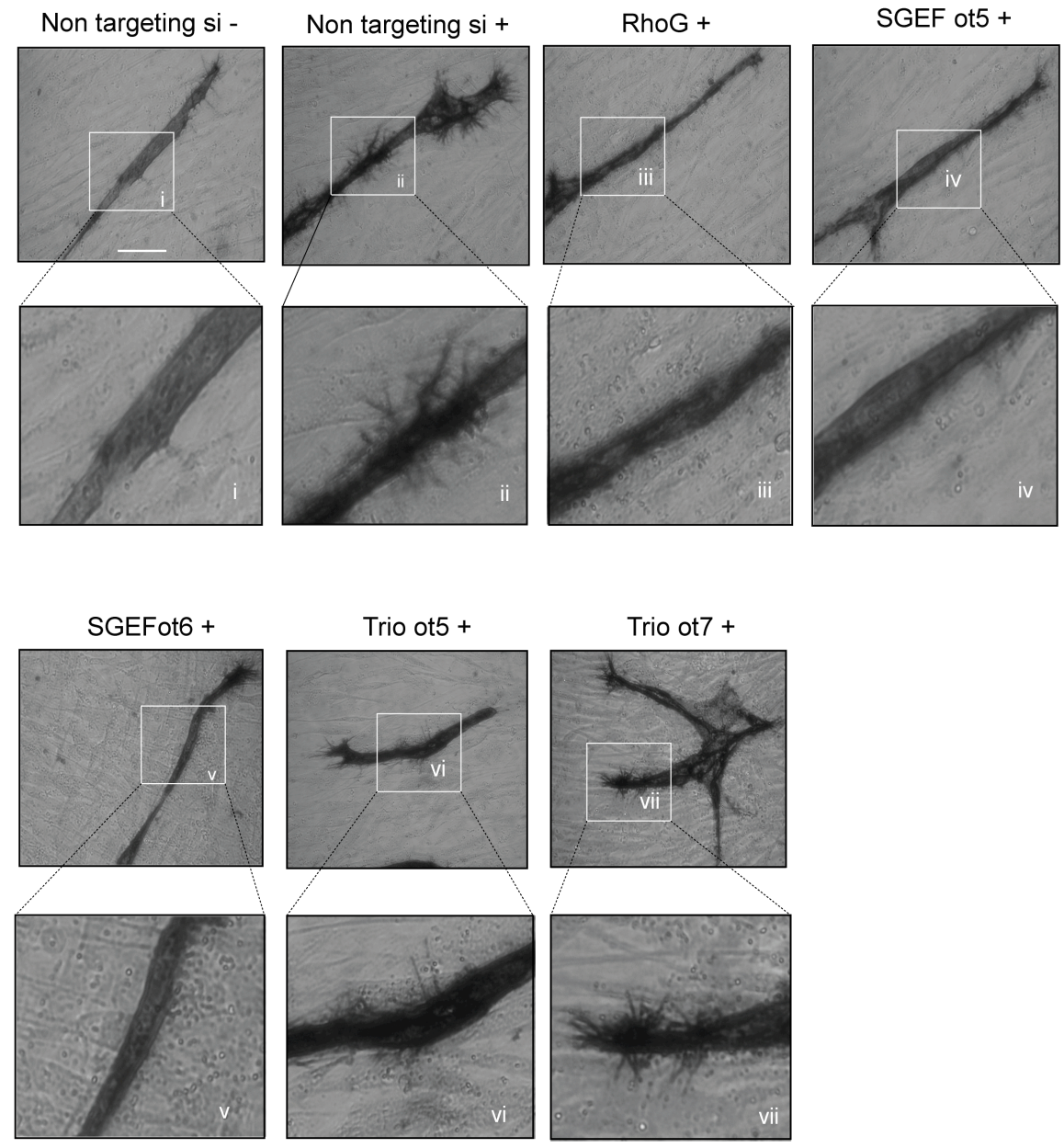
siRNA:
Non targeting si -
Non targeting si +
RhoG +
SGEF ot5 +
i
ii
iii
iv
SGEFot6 +
Trio ot5 +
Trio ot7 +
v
vi
vii

B

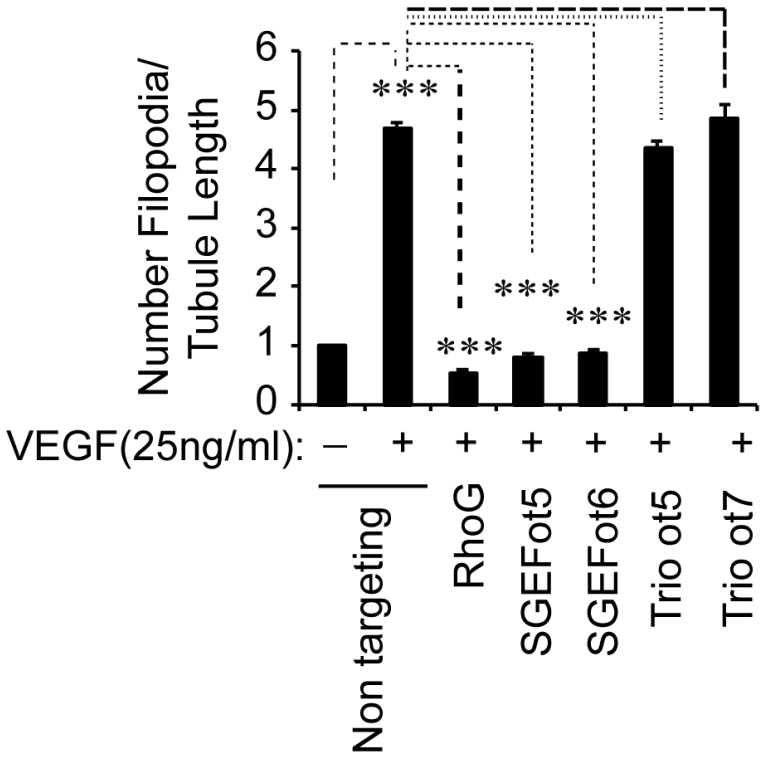

Figure 4.2 RhoG and SGEF control VEGF-driven filopodia formation
HUVEC were transfected with siRNAs against RhoG (Standard pool siRNA), SGEF and Trio (ot; On-Target siRNAs) or non targeting control siRNA. 24 hours after transfection cells were seeded onto confluent fibroblasts in the presence (+) or absence (-) of VEGF (25ng/ml). The media with VEGF were replenished after 72 hours and the cultures were stained for CD31 48 hours later.
(A) Representative phase-contrast images of filopodia formation taken at 40x magnification. Scale bar: 50μm. The marked area in each sample shows a manual enlargement of tip or lateral regions where filopodia localize. (B) Bar chart shows number of filopodia per tubule length as fold increase compared to unstimulated, non targeting control. Error bars represent S.E.M., p values from unpaired student's t-test; ***, P<0.001. Percentage of knockdown assessed through qRT-PCR is shown in Appendix (Figure 5).

The overall number of filopodia and the distribution pattern around the cell body in Trio knocked-down with the two On-Target oligonucleotides was comparable to non targeting control sample (Figure 4.2B). Trio therefore appears to be involved in endothelial cell elongation but plays no role in VEGF-driven filopodia formation.

Overall, results in Figure 4.2A and B show that RhoG and SGEF are key regulators of filopodia formation. Analysis of spatial distribution of filopodia (filopodia located at tip sides compared to lateral sides) in un-stimulated or VEGF-stimulated endothelial cells was performed. Lateral and tip filopodia were counted and reported as number/length (Figure 4.3A and B). Quantification showed that there was a greater increase in lateral filopodia in response to VEGF (approx. 14-fold) compared to tip filopodia (<2-fold) and that in both sites the number of filopodia was dramatically reduced by knockdown of RhoG or SGEF (<4-fold at tip sides) although lateral filopodia formation was affected to a greater extent than tip filopodia (~70 –fold for RhoG and ~ 22 fold for SGEF).

This could suggest that a different regulatory pathway controls tip and lateral filopodia formation and the pathway so far described appears to be involved in controlling filopodia formation at lateral sites in endothelial cells.

A

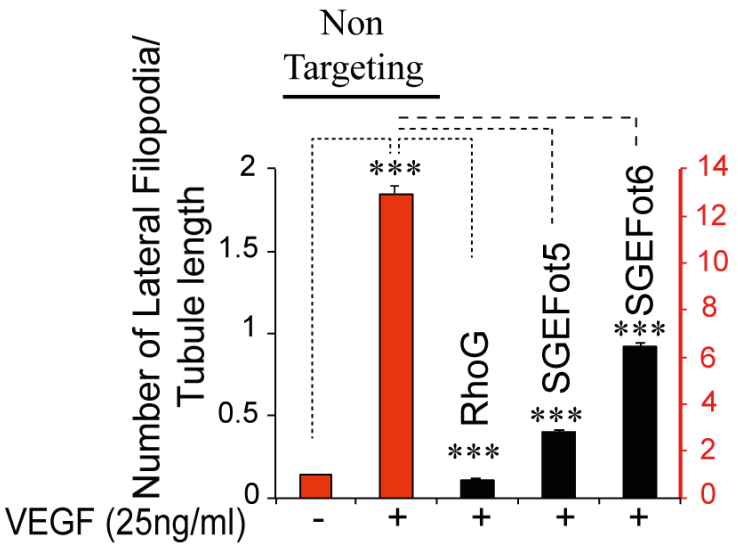

B

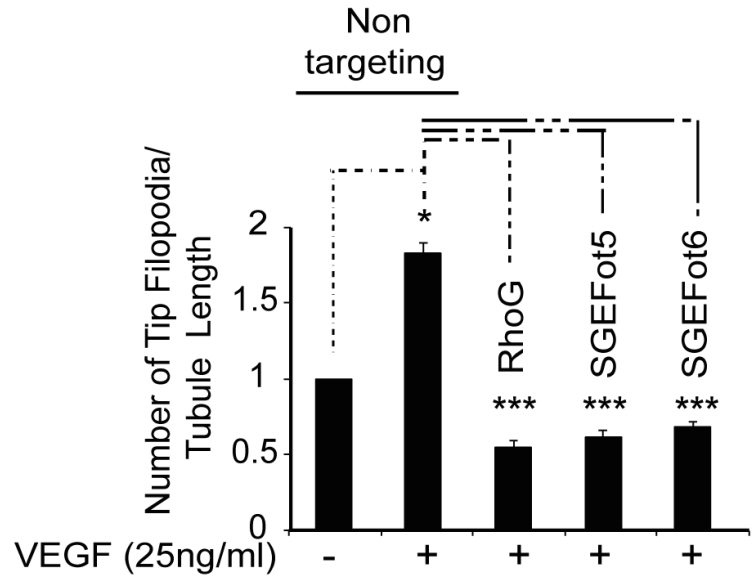

Figure 4.3 Analysis of tip and lateral filopodia in absence of RhoG and its regulator SGEF in VEGF treated ECs

Analysis of tip filopodia compared to lateral filopodia formation from the experiment shown in Figure 4.2. Lateral (A) and tip (B) filopodia were counted in each sample (n=9), divided per tubule length and shown as fold increase compared to unstimulated, non targeting control. Error bars represent S.E.M., p values from unpaired student's t-test; *, P<0.05; ***, P<0.001. Red column values are reported on the red axis.

4.4 SGEF but not Trio is necessary for VEGF-driven branch formation

Since SGEF and Trio are both involved in controlling RhoG activation in response to VEGF stimulation, assays were performed to establish how knockdown of SGEF or Trio affects branching in the co-culture assay. HUVEC were transfected with On-Target oligonucleotides against SGEF (ot5 and ot6), Trio (ot5 and ot7) or non targeting control siRNA and used in co-cultures. VEGF significantly stimulated branch formation in the co-culture assay (Figure 4.4). This phenotype was reduced dramatically in absence of SGEF but not Trio. In agreement with SGEF controlling lateral filopodia, HUVEC with SGEF knockdown lacked lateral branches (Figure 4.4A and B). In contrast, cells lacking Trio showed short tubules with several branches (Figure 4.4A and B). These data show that SGEF is required for branch formation downstream of VEGF whereas Trio appears to play a role in VEGF-dependent tubule growth *via* a different mechanism.

4.5 RhoG and Rac1 drive Cdc42 dependent filopodia in 293T cells

It has been previously shown that RhoG and DOCK4 control VEGF induced filopodia formation in endothelial cells (Figure 4.2 and Figure 1.10). It has also been reported that RhoG signals through DOCK4 to control several cellular activities (Hiramoto et al., 2006; Hiramoto-Yamaki et al., 2010). To investigate whether activation of RhoG results in increased filopodia formation and whether this happens in a DOCK4-dependent manner, HEK 293T cells were plated on fibronectin-coated dishes and transfected with combination of DNA plasmids and siRNAs as described in Section 2.1.6.4. DNA plasmids used were EGFP empty vector (Vector) or EGFP constitutively active RhoG (RhoGv12 (Table 2.3)) while siRNA oligonucleotides employed were against DOCK4 or non targeting control siRNA.

Representative confocal images are shown in Figure 4.5A. Cells transfected with empty vector control showed a smooth surface contrasting with the pronounced phenotype obtained in cells expressing RhoGv12 where numerous filopodia protrusions (white arrows) were seen. The phenotype induced by RhoGv12 expressing cells was consistent

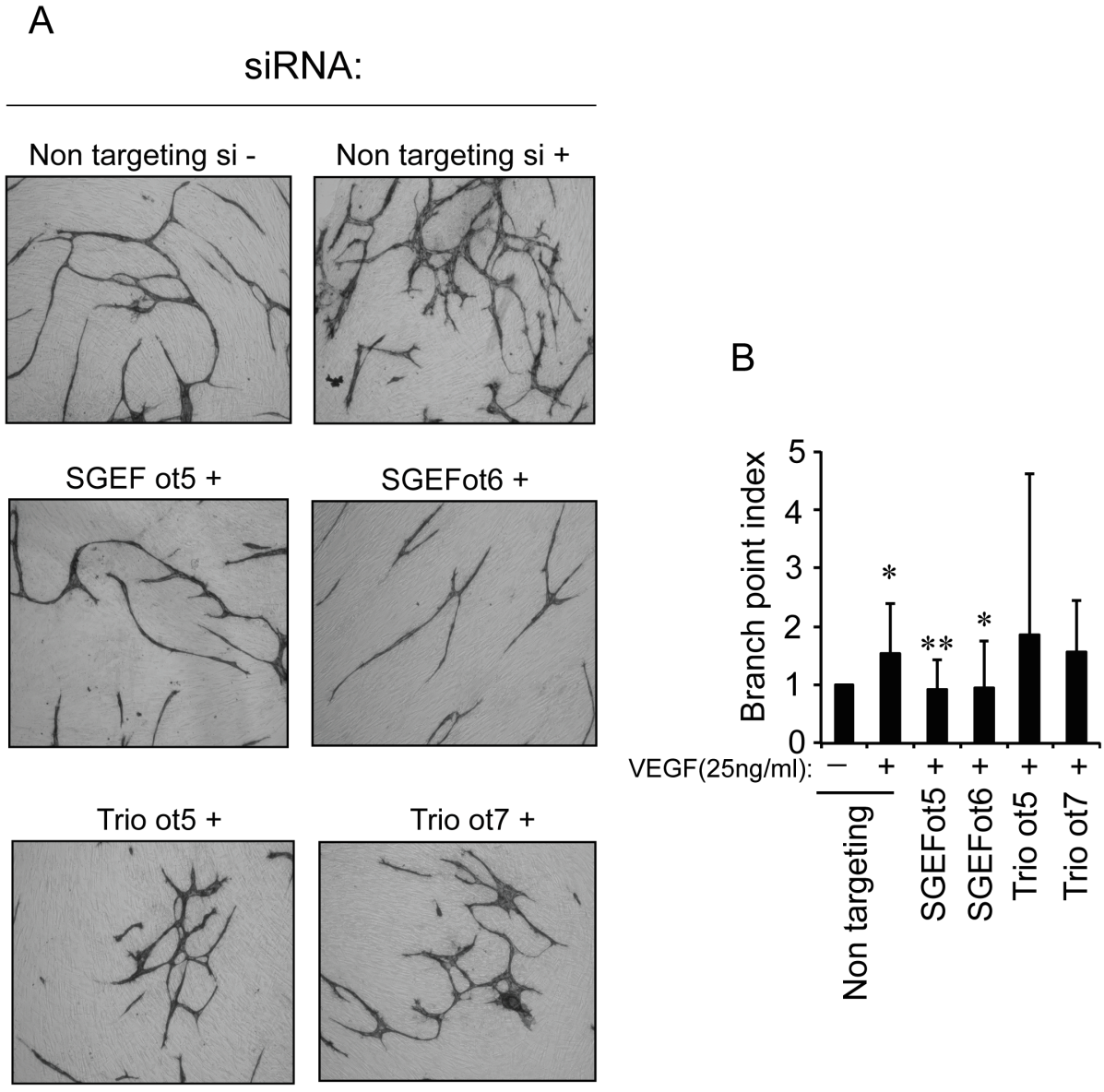

Figure 4.4 SGEF is necessary for VEGF-driven branching
HUVEC were transfected with siRNAs against SGEF or Trio (ot; On-Target siRNA oligonucleotides) or non targeting control siRNA. 24 hours after transfection cells were seeded onto confluent fibroblasts in the organotypic angiogenesis assay as described in Section 2.4 in the presence (+) or absence (-) of VEGF (25ng/ml). The media with VEGF were replenished after 72 hours and the cultures were stained for CD31 48 hours later. (A) Representative phase-contrast images of tubule morphology taken at 10x magnification are shown. Scale bar: 200μm. (B) Bar chart represents the branch point index (number of branch points/ total vessel length) as thefold increase compared to unstimulated non targeting control. Error bars represent S.E.M., p values from unpaired student's t-test; *, $P<0.05$; **, $P<0.01$. VEGF-stimulated SGEF and Trio were compared against stimulated non targeting control.

A

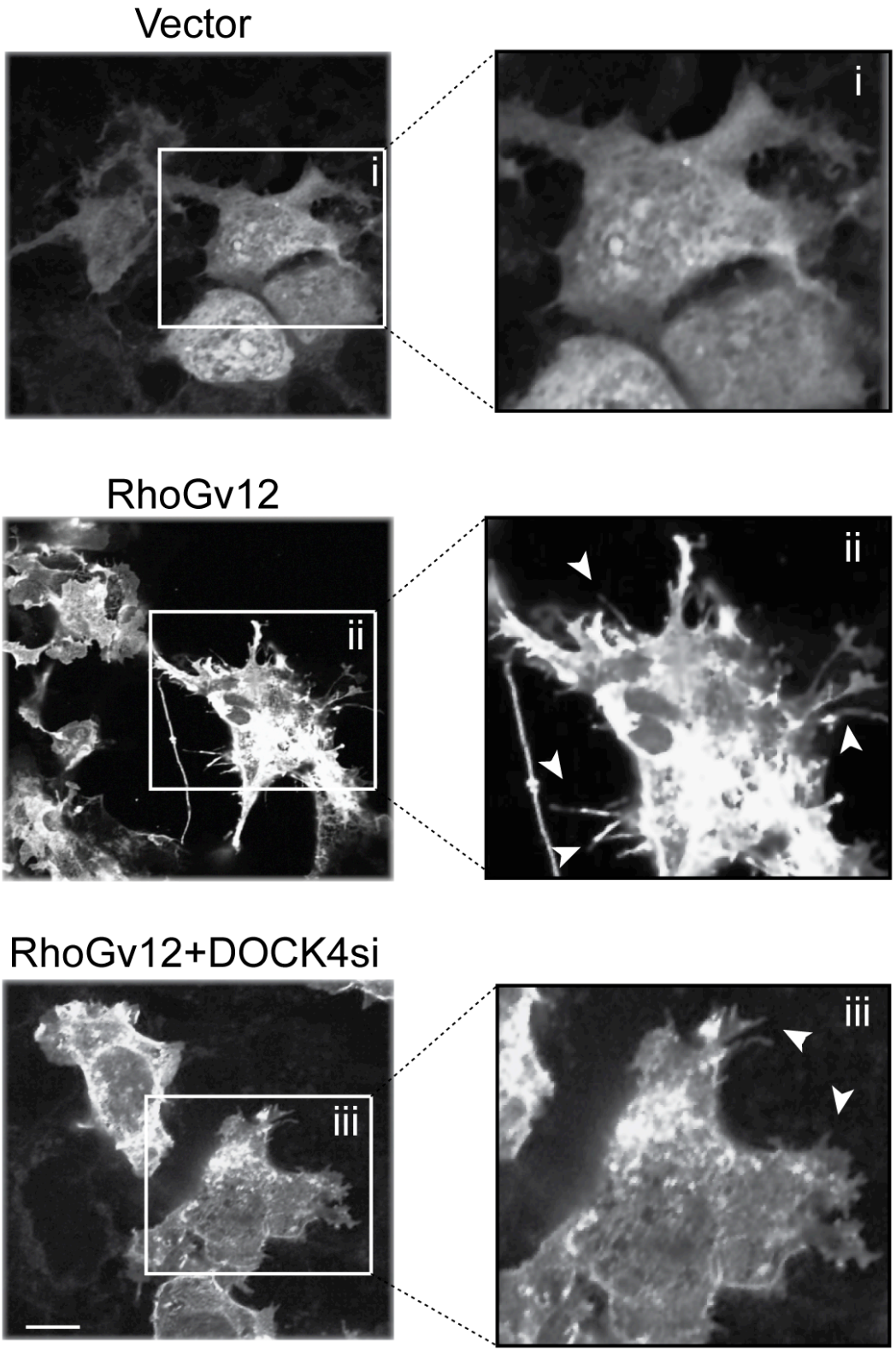

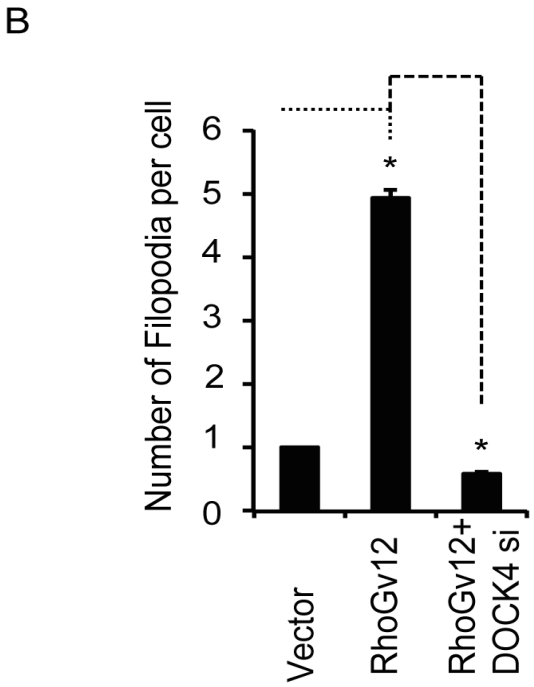

Figure 4.5 RhoG-driven filopodia are dependent on the Rac1 GEF DOCK4
HEK 293T cells growing on fibronectin were transfected with RhoGv12 in the presence or absence of DOCK4 siRNA. Two days after transfection the cultures were visualized using a 60x objective on a confocal microscope. (A) Representative images of empty vector (Vector), constitutively active RhoG in presence (RhoGv12) or absence of DOCK4 (RhoGv12+DOCK4 Standard pool siRNA) are shown. Note the induction of filopodia with RhoGv12 overexpression (arrowheads) and ablation of filopodia in RhoGv12 overexpressing cells in which DOCK4 was knocked-down. The marked area in each sample shows a manual enlargement of regions of interest containing filopodia. Scale bar: 50μm. (B) Graph shows number of filopodia/per cell ±S.E.M. The graph was generated after manual counting of filopodia formed on EGFP cells (20 per sample). *, $P<0.01$.

with the phenotype reported by Blangy and colleagues when RhoGv12 was overexpressed in fibroblasts (Blangy et al., 2000). HEK 293T cells in which RhoGv12 protein was overexpressed but lacked DOCK4 assumed different morphology: cells were spread as seen with the control but filopodia formation was significantly reduced and those filopodia that did persist looked shorter and thinner by eye compared to RhoGv12-expressing cells (Figure 4.5A). These results suggest that RhoG acts upstream of DOCK4 to control filopodia formation in HEK 293T cells.

As seen for RhoG, Rac1 has been demonstrated to control filopodia formation in endothelial cells (Preliminary Data, Section 1.8.1). Experiments were therefore performed in HEK 293T cells to establish whether Rac1 stimulates filopodia formation in a Cdc42 dependent manner in a non-endothelial cell type. DNA plasmids used were EGFP empty vector (Vector) or EGFP wild-type Rac1 (Rac1, (Table 2.3)) while siRNA oligonucleotides employed were against Cdc42 or non targeting control siRNA. Cells were cultured for further 48 hours prior to fixation and imaging by confocal microscopy. TRITC-phalloidin dye was used to visualize the cytoskeleton, resulting in F-actin staining in red. As shown in Figure 4.6, overexpression of Rac1 promoted a high number of filopodia around the cell membrane compared to control. Overexpression of Rac1 in cells lacking Cdc42 showed a reduced number of protrusions compared to control cells and cells adopted a different phenotype with a pronounced number of swelling projections. These results confirmed that Rac1 acts upstream of Cdc42 and suggested that formation of filopodia protrusions is regulated by Rac1 in HEK 293T cell.

4.6 Rac1 and its GEF DOCK4 control Cdc42 activation in ECs

It is well established that Cdc42 controls filopodia formation in a variety of cell types including fibroblasts (Nobes and Hall, 1995), macrophages (Allen et al., 1997; Kozma et al., 1995) and tumour cells (Reymond et al., 2012). In addition, it has been reported that Cdc42 controls filopodia-like protrusions in endothelial cells under certain conditions (Kouklis et al., 2003). Previous work in this laboratory has shown that Rac1 and its GEF

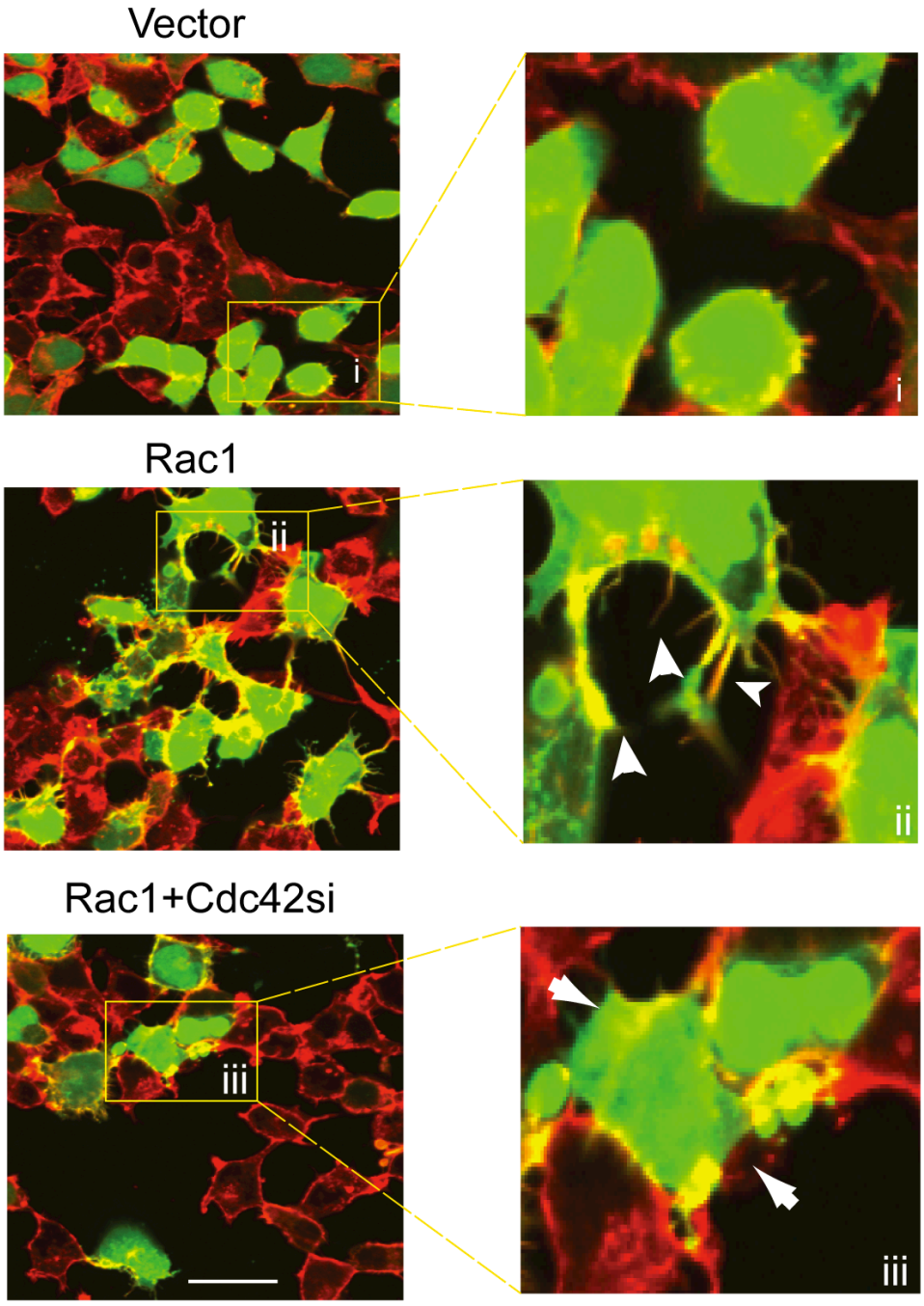

Figure 4.6 Rac1-driven filopodia are Cdc42 dependent
HEK 293T cells growing on fibronectin were transfected with empty vector (Vector, green cells) or wild type Rac1 (Rac1, green cells) in the presence or absence of Cdc42. Two days after transfection the cultures were stained for phalloidin (red) and visualized using a 20x objective on a confocal microscope. Representative images are shown. Note the induction of filopodia with Rac1 overexpression (arrowheads) and ablation of filopodia and disruption of cortical actin in the absence of Cdc42 (arrows). Scale bar: 50μm. The marked area in each sample shows a manual enlargement of regions of interest containing filopodia.

DOCK4 control filopodia formation (Preliminary Data, Section 1.8.1).

It has also been shown that Rac1 acts upstream of Cdc42 to control filopodia formation in HEK 293T cells (Figure 4.6). In order to establish whether Rac1 acts upstream of Cdc42 in endothelial cells experiments were performed in HUVEC. Cells were plated on fibronectin-coated dishes and transfected with siRNA Standard Pool against Rac1 or non targeting control siRNA. Cells were then treated with VEGF and active Cdc42 was pulled down as described in Section 2.3.7. Cdc42 activation was upregulated after stimulation with VEGF compared to un-stimulated control (Figure 4.7A). The result was reversed in absence of Rac1, with a significant reduction of Cdc42 activation at all time points of VEGF stimulation. To confirm the result obtained, the same experiment was performed where HUVEC were transfected with non targeting control, On-Target oligonucleotide against Rac1 (Rac ot1) or mock transfected. Active Cdc42 was then pulled down. The result (Figure 4.7B) suggests that Rac1ot1 down-regulates active Cdc42 stimulation by VEGF, consistent with results seen using the Rac1 Standard pool siRNA (Figure 4.7A). This is a striking result since Cdc42 is thought to act upstream of Rac1 and that filopodia protrusions precede lamellipodia formation (Nemethova et al., 2008; El-Sibai et al., 2007). To find out whether there is a Rac1-Cdc42 positive loop in endothelial cells stimulated by VEGF and whether Cdc42 can therefore regulate Rac1, activation of Rac1 was measured in presence or absence of Cdc42. As expected, expression of active Rac1 was upregulated in VEGF stimulated HUVEC while, in the absence of Cdc42, Rac1 activation was unaffected throughout the time course followed (Figure 4.8). To ensure knockdown had been achieved, Cdc42 protein levels were determined in siRNA transfected cells by Western Blot that showed 93% loss of Cdc42 expression in cells transfected with Cdc42 siRNA. These data show that in HUVEC, Cdc42 is dispensable for Rac1 activation downstream of VEGF.

Altogether the data show that Rac1 operates upstream of Cdc42 to control its activation in endothelial cells as also demonstrated in HEK 293T cells.

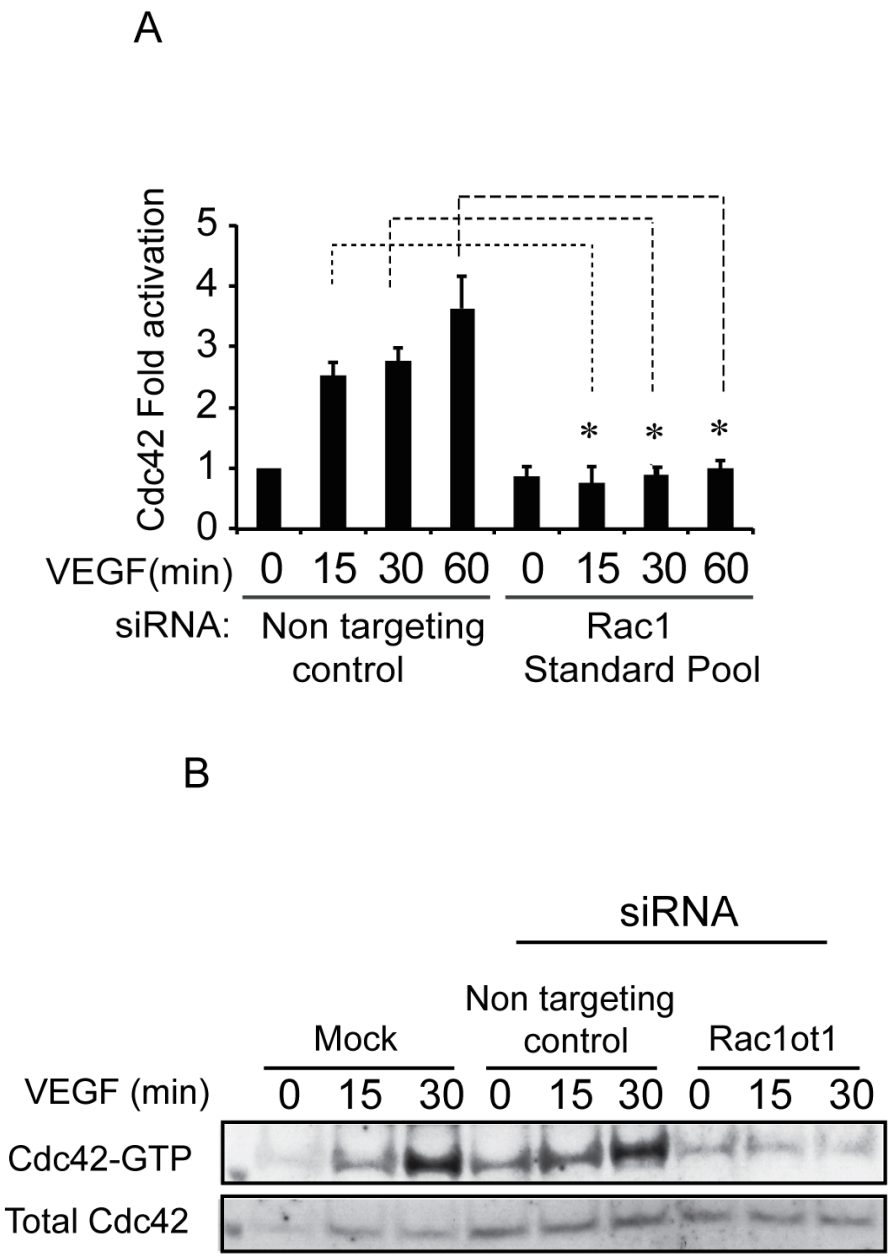

Figure 4.7 Rac1 controls Cdc42 activation downstream of VEGF signaling
HUVEC growing on fibronectin-coated dishes were transfected with Rac1 Standard Pool or non targeting control siRNAs, serum starved and stimulated with VEGF (25ng/ml). Cells were lysed and Cdc42 activation was analysed using the Cdc42 pulldown assay (Section 2.3.7). (A) Bar chart shows quantification of Cdc42 pulldown from three independent experiments performed using the ECL system. Cdc42 activation was calculated as fold increase compared to unstimulated control after normalization for total Cdc42 for each condition. Error bars are S.E.M., p values from unpaired student's t-test compared to unstimulated (0 timepoint) control. *, $P<0.05$.
(B) Representative Western Blots showing Cdc42-GTP and total Cdc42 in ECs with or without Rac1. Rac1 protein expression was knockdown of 97% with Rac ot1 (Appendix, Figure 6).

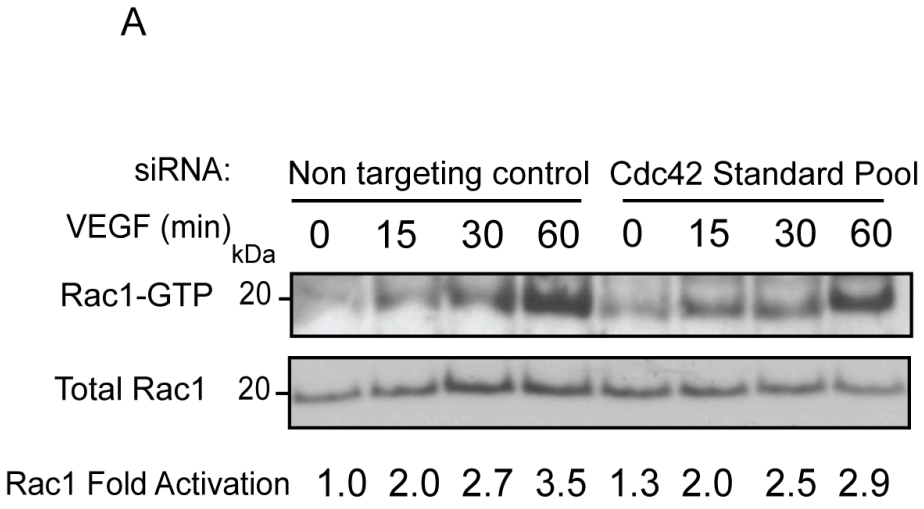

Figure 4.8 Cdc42 activity is not essential for Rac1 activation
HUVEC growing on fibronectin-coated dishes were transfected with Cdc42 Standard pool or non targeting control siRNAs and after 48 hours they were serum starved and stimulated with VEGF (25ng/ml). Cells were lysed and Rac1 activation was analysed using the Rac1 pulldown assay (Section 2.3.7). Representative Western Blots from one experiment performed using the ECL system show Rac1-GTP and total Rac. Rac1 activation was calculated as fold increase compared to unstimulated non targeting control after normalization for total Rac1 (Rac1 Fold Activation). Cdc42 protein expression was knocked-down by 93% (Appendix, Figure 7).

4.7 Rac1 and DOCK4 control Cdc42 activation in ECs

DOCK4 is a Rac1 GEF downstream of VEGF that, amongst its different contributions to many cellular activities, regulates Rac1 and controls filopodia formation in endothelial cells (Preliminary Data, Section 1.8.1) and HEK 293T cells (Figure 4.6). Given that Rac1 acts upstream of Cdc42 in VEGF-stimulated HUVEC, it was hypothesized that DOCK4 controls Cdc42 activation downstream of the same signaling cascade. A Cdc42 pulldown assay (Section 2.3.7) was performed and the level of active Cdc42 was determined in the presence and absence of VEGF and DOCK4. As shown in Figure 4.9, while VEGF upregulates Cdc42 activation, levels of GTP-Cdc42 were significantly reduced in absence of DOCK4 after 30 and 60 minutes of stimulation (Figure 4.9A). To further corroborate the result obtained, the experiment was repeated using an On-Target oligonucleotide against DOCK4 (ot11, Figure 4.9B). Ablation of DOCK4 through use of the siRNA On-Target oligonucleotides maintained the same trend shown by use of the Standard pool. To quantify DOCK4 knockdown, small amounts of protein lysates from cells transfected with DOCK4ot11 or non targeting control siRNAs were probed with DOCK4 antibody and protein expression was assessed.

Taken together, the results suggest that DOCK4 controls Cdc42 activation downstream of VEGF signalling cascade in ECs.

4.8 RhoG both regulates Cdc42 basal level and participates in Cdc42 activation downstream of VEGF signalling pathway

In endothelial cells, the signaling cascade activated by VEGF places RhoG upstream of DOCK4 which in turn regulates the activation of Rac1. Rac1 is responsible for Cdc42 activation downstream of VEGF. To date, there are no reports linking RhoG to filopodia formation or Cdc42 activation in ECs. However, data show in Section 4.2 suggested that down-regulation of RhoG dramatically diminished the number of filopodia protrusions in

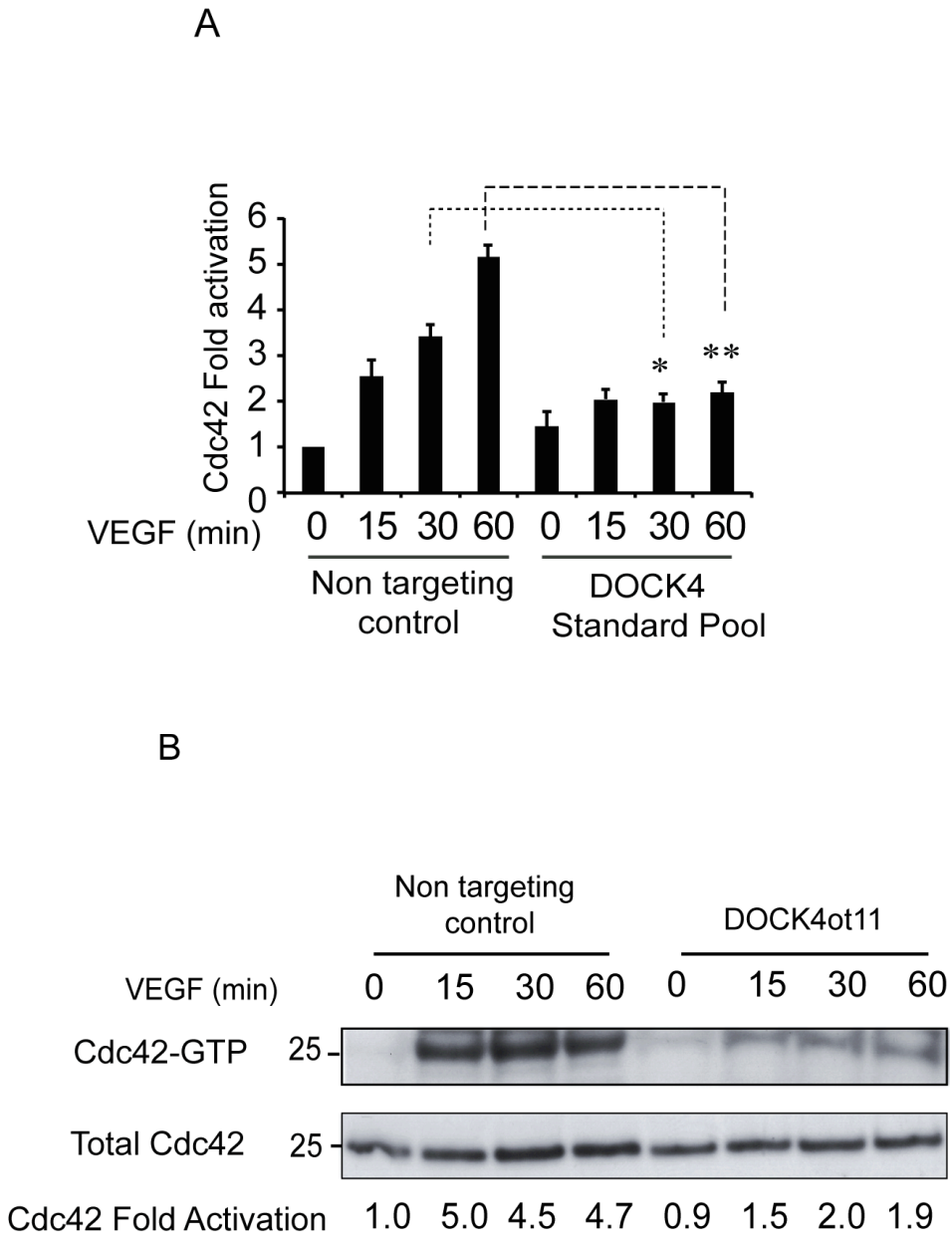

Figure 4.9 DOCK4 controls Cdc42 activation
HUVEC growing on fibronectin-coated dishes were transfected with Rac1 or non targeting control siRNA or mock transfected, serum starved and stimulated with VEGF (25ng/ml). Cells were lysed and Cdc42 activation was analysed using the Cdc42 pulldown assay (Section 2.3.7). (A) Bar chart shows quantification of Cdc42 pulldown from three independent experiments. Cdc42 activation was calculated as fold increase compared to unstimulated control after normalization for total Cdc42 for each condition. Error bars are S.E.M., p values from unpaired student's t-test compared to unstimulated (0 timepoint) control. *, $P<0.05$; **, $P<0.01$. (B) Western Blots from one independent experiment performed using the ECL system show Cdc42-GTP and total Cdc42. Cdc42 activation was calculated as fold increase compared to unstimulated control after normalization for total Cdc42 (Cdc42 Fold Activation). DOCK4 knockdown levels are reported in Appendix (Figure 8).

VEGF stimulated HUVEC. It was therefore hypothesized that RhoG controls the regulation of Cdc42 in endothelial cells. To test this hypothesis, HUVEC were transfected using siRNA Standard pool against RhoG or non targeting control siRNA. Active Cdc42 was consequentially pulled-down after stimulation with VEGF. As shown in the Figure 4.10, in un-stimulated RhoG siRNA transfected HUVEC the level of active Cdc42 was downregulated, suggesting the RhoG might control VEGF independent Cdc42 basal activity. VEGF-stimulated Cdc42 activation was also down-regulated when RhoG expression was reduced (71% knockdown) compared to VEGF stimulated non targeting control cells at all the time points tested although Cdc42 activity remained responsive to VEGF.

Altogether, the results suggest that the small GTPase RhoG and the exchange factor DOCK4 control Cdc42 activation downstream of VEGF signaling pathway in endothelial cells to regulate filopodia formation and that RhoG might also play a role in controlling Cdc42 basal activity.

4.9 RhoG promotes DOCK4 dependent Rac1 activation in HEK 293T cells

It has been shown that RhoG controls filopodia protrusions in endothelial cells and HEK 293T cells *via* DOCK4. Given that Rac1 controls Cdc42 activation and DOCK4 is a Rac1 positive regulator, it was hypothesized that RhoG controls Rac1 activation downstream of DOCK4. To test this hypothesis, HEK 293T cells were plated on fibronectin-coated dishes and transfected with combination of DNA plasmids and siRNAs as described in Section 2.1.6.4. The DNA plasmids used for transfection were: EGFP empty vector (Vector) or EGFP wild-type RhoG (RhoG). The siRNA oligonucleotides used were against DOCK4 or non targeting control siRNA.

As shown by Western Blot analysis (Figure 4.11A), the level of active Rac1 was upregulated by overexpression of RhoG compared to Vector. When RhoG was overexpressed in the absence of DOCK4, Rac1 activation was reduced back to basal level suggesting that DOCK4 is necessary for RhoG dependent Rac1 activation. Also, to rule out

the possibility that the down-regulation of Rac1 was due to an off target effect of the oligonucleotide, the cell lysates was analysed by western blotting for expression of DOCK4 (Figure 4.11B).

These results show that RhoG controls Rac1 activation through DOCK4 in HEK 293T cell as previously demonstrated in HUVEC.

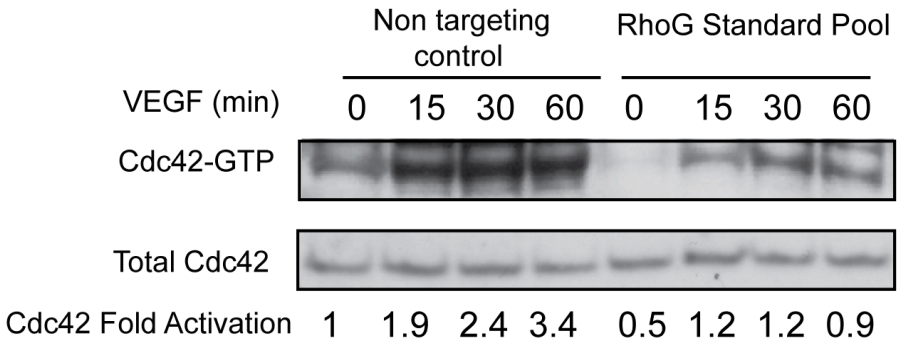

Figure 4.10 RhoG knockdown reduces Cdc42 basal level and affects active Cdc42 in response to VEGF

HUVEC transfected with RhoG Standard pool and non targeting control siRNAs HUVEC were serum starved and stimulated with VEGF (25ng/ml). Western Blots from one independent experiment performed using the ECL system show Cdc42-GTP and total Cdc42. Levels of Cdc42-GTP are shown as the fold increase compared to unstimulated non targeting control after normalization for total Cdc42 (Cdc42 Fold Activation). RhoG protein expression knockdown was 71% (Appendix, Figure 9).

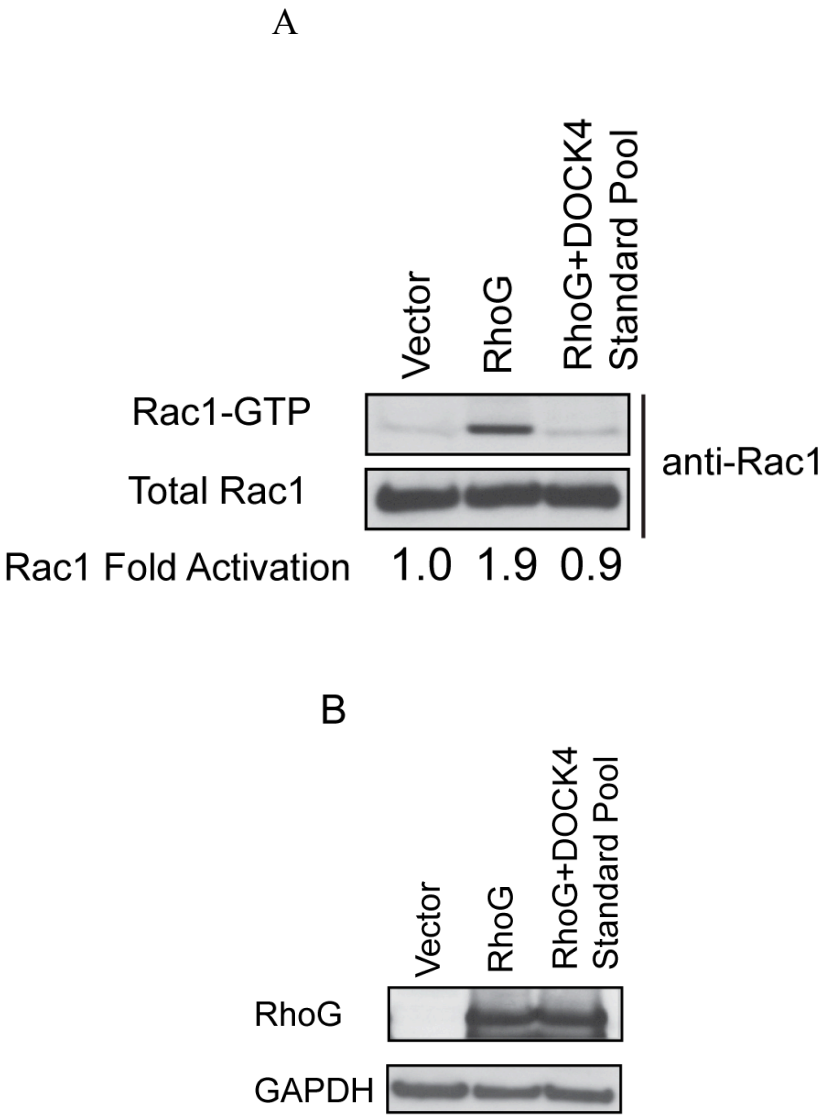

Figure 4.11 RhoG promotes DOCK4 dependent Rac1 activation
HEK 293T cells plated on fibronectin-coated dishes were co-transfected (DNA/siRNA) and lysed 2 days after. Level of active Rac1 was detected by pulldown assay (Section 2.3.7). (A) Western Blots from one independent experiment performed using the ECL system show Rac1 activation (Rac1-GTP) following RhoG overexpression (RhoG) and DOCK4 depletion (RhoG+DOCK4 Standar pool siRNA) in HEK 293T cells. (B) Immunoblots of RhoG show equal level of RhoG protein overexpression in total lysates. DOCK4 protein expression knockdown was 72% (Appendix, Figure 10).

4.10 Discussion

Data presented in this chapter show that i) RhoG is activated downstream of VEGF signaling cascade *via* SGEF; ii) Rac1 acts upstream of Cdc42 and iii) RhoG activates Cdc42 *via* DOCK4. Unravelling this signaling axis is an important step in understanding the kinetics and the regulation of biological phenomena. Although the components of the signaling cascade proposed in this thesis are known, their sequential activation (SGEF→RhoG→DOCK4→Rac1→Cdc42) and the ultimate phenotype (control of filopodia formation and branching) in endothelial cells is described here for the first time.
Experiments shown in this chapter have emphasised VEGF-driven filopodia formation in endothelial cells and described a signaling cascade that controls this process. Once activated, the positive regulators SGEF and DOCK4 activate a signaling pathway that ultimately controls the overall number of filopodia (both lateral and tip) leading to ablation of lateral filopodia and reduction of tip filopodia when SGEF and DOCK4 are knocked-down in HUVEC. It has been demonstrated that Cdc42 controls filopodia formation in ECs (De Smet et al., 2003). Experiments performed in this laboratory revealed that Cdc42 knockdown blocks filopodia formation and greatly reduces endothelial cells viability. Given that the signaling axis described here (SGEF-RhoG-DOCK4-Rac1) leads to Cdc42 regulation it could be hypothesized that Cdc42 is responsible for lateral filopodia downstream of the signaling cascade delineated in this thesis and control tip filopodia formation through a different mechanism.

It has been shown that RhoG is responsible for filopodia formation in ECs and lack of RhoG expression in HUVEC ablates lateral filopodia formation. The RhoG positive regulator SGEF has been associated with rearrangement of the endothelial cytoskeleton and induction of docking structures involved in leucocytes trans-endothelium migration upstream of RhoG (van Buul et al., 2007). SGEF has also been linked with human prostate cancer progression and development (Wang et al., 2012). Data reported in this thesis are the first pieces of evidence linking RhoG and its regulator SGEF to filopodia formation in ECs. In the previous chapter, pulldown experiments were used to show that Trio is a RhoG GEF downstream of VEGF. Although Trio controls cytoskeleton dynamics in fibroblasts (Bellanger et al., 2000) and dendrite morphogenesis in *Drosophila* sensory neurons (Iyer et

al., 2012) its roles in ECs are still to be clarified. As shown in Figure 4.2, under VEGF stimulation, HUVEC lacking Trio showed an unusual phenotype. Cells showed numerous branches and the number of filopodia induced by exogenous VEGF was not reduced. Tubules lacking Trio were very short compared to control tubules. However, the level of knockdown achieved using Trio Standard pool or the On-Target oligonucleotides (ot5 and ot7) siRNAs was only around 50% and it could therefore be argued that a dose effect is being seen: depletion of half protein expression was sufficient to control cell elongation but not filopodia formation. However, Trio Standard pool or On-Target siRNAs were sufficient to down-regulate RhoG activation significantly as shown by pulldown assay in Figure 3.12 and Figure 3.13.

Overexpression of constitutively active RhoG was associated with upregulation of protrusions in REF-52 fibroblasts (Blangy et al., 2000) through a signaling cascade that involves Rac1 and Cdc42 activation. Figure 4.5 shows that overexpression of RhoG in HEK 293T cells was not only translated in filopodia formation but there was a second phenotype in which lamella-type structures were seen, consistent with previous data (Blangy et al., 2000). This might indicate that, in some cell types or under specific stimuli, RhoG controls Rac1 and Cdc42activation through independent signaling pathways.

In some cell types filopodia form early after Cdc42 activation to facilitate formation of lamellipodia structures. Studies presented in this chapter demonstrate that in HUVEC, VEGF regulates filopodia formation through a novel mechanism in which, unexpectedly, Rac1 is activated to regulate the small GTPase Cdc42. Absence of Rac1 totally ablated Cdc42 activation (Figure 4.7) and filopodia formation as discussed in Preliminary Data (Section 1.8.1). There is however evidence showing that Cdc42-deficient fibroblastoid and Embryonic Stem (ES) cells are capable of constitutive filopodium and lamellipodium formation, demonstrating that Cdc42 is not required for the formation of these protrusion (Czuchra et al., 2005). However, there are many Rho GTPase family members that show a high sequence similarity and therefore it can be speculated that here is a degree of redundancy. It has been reported previously that DOCK4 mediates RhoG-driven Rac1 activation. It has been reported that RhoG binds its downstream effector ELMO (Hiramoto et al., 2006; Hiramoto-Yamaki et al., 2010), which itself has no catalytic effect and acts as a

scaffolding protein, binding to the SH_3 domain of DOCK4; this binding is necessary to translocate DOCK4 from the cytosol to the plasma membrane (Hiramoto et al., 2006). Following translocation of DOCK4, Rac1 is activated by direct binding with the DOCK4 DHR2 domain (Section 1.7.1.1). This mechanism, or at least part of it, seems to be preserved to mediate filopodia formation in endothelial cells and HEK 293T cells as suggested by phenotype analysis and biochemical data. Filopodia formation is a necessary step during development and therefore, as expected, Rac1 and Cdc42 knockout mice are embryonic lethal. SGEF knockout mice (Samson et al., 2013) as well as RhoG knockout mice (Vigorito et al., 2003) are viable and fertile although SGEF and RhoG play a crucial role in the formation of atherosclerosis (Samson et al., 2013). DOCK4 knockout mice are not yet available. This highlights that the signaling cascade described is dispensable during development, but it might be critical during pathological conditions, for instance to drive aberrant vessel formation, invasion and metastasis.

Chapter 5

A Novel Interaction Between DOCK Family GEFs and the RhoG effector ELMO

5.1 Introduction

As outlined in chapter 1 (Section 1.5.5.5 and 1.5.5.6), the small GTPase Cdc42 has been associated with the formation of protrusions around the plasma membrane in a variety of cell types. Given this important role, a more detailed understanding of the mechanism through which Cdc42 is activated is needed. There are a number of putative Cdc42 positive regulators described including members of the FGD (Huber et al., 2008; Hayakawa t al., 2008) and DOCK family (Meller et al., 2004; Nishikimi et al., 2005; Gadea et al., 2008) members. The experiments discussed in this chapter were performed to establish which positive regulator determines Cdc42 activation downstream of VEGF. As previously discussed (Section 1.7), DOCK members are not as well characterized as GEFs and to date important information about their biological roles and mechanisms of activation are still lacking. It is known that they require RhoG activated ELMO to move between different subcellular compartments. The role of ELMO is to date still unclear since in *vitro* data are not consistent with knockout model outcomes. This final chapter shows biochemical data generated in order to determine whether 1) ELMO binds to DOCK4 or other DOCKs; 2) ELMO participates in regulation of filopodia in ECs and 3) to provide a better understanding of the signaling and kinetics of the events the lead to filopodia formation in HUVEC downstream the VEGF driven signaling axis SGEF-RhoG-DOCK4-Rac1-Cdc42.

5.2 DOCK9 is a Cdc42 GEF downstream of VEGF signaling

As described in Chapter 1 (Section 1.5.5.5 and Section 1.5.5.6), Cdc42 controls several cellular activities. Data obtained in our laboratory have shown that when Cdc42 expression is down-regulated using siRNA, HUVEC showed a number of severe defects that ultimately led to cell detachment and death (data not shown). Data presented in Chapter 4 showed that Cdc42 mediates filopodia formation (Section 4.5). However, a positive regulator for Cdc42 in endothelial cells has not yet been identified, despite a reports of few putative Cdc42 exchange factors including DOCK9, DOCK10 and DOCK11 (Meller et al., 2004; Nishikimi et al., 2005; Gadea et al., 2008), members of the FGD family (Huber et al., 2008; Hayakawa t al., 2008) and SPATA13 (Hamann et al., 2007; Kawasaki et al., 2007).

In order to find out which regulator activates Cdc42 downstream of VEGF in endothelial cells, DOCK9, DOCK10, DOCK11, FGD3, FGD6, SPATA 13 were targeted in HUVEC plated on fibronectin-coated dishes using the RNA interference technology described in Chapter 2 (Section 2.1.6.2). siRNA oligonucleotides used to perform this set of experiments were Standard pools.

Cells were serum starved and stimulated with VEGF before Cdc42 pulldown assays were performed. In chapter 4 (Figure 4.7) it was shown that Cdc42 activation peaked after 30 minutes of stimulation with VEGF; therefore, this time point, was used to investigate the effect of knockdown of Cdc42 regulators in HUVEC. As shown in figure 5.1A, the VEGF treated cells transfected with non targeting control siRNA showed significant Cdc42 activation after 30 minutes. This activation was not dependent on SPATA13 or DOCK11 expression at the time point observed but was partially reduced when FGD3, FGD6 and DOCK10 expression was inhibited and blocked when DOCK9 was targeted. Cdc42 activity in cells lacking DOCK9 was monitored in a number (n=3) of experiments and quantified as shown in Figure 5.1B. To ensure knockdown had been achieved, DOCK9 mRNA levels were determined in siRNA transfected cells by qRT-PCR that showed 85% loss of DOCK9 expression in cells transfected with DOCK9 siRNA compared to non targeting control transfected cells (Figure 5.1B).

Altogether, these data suggest that in HUVEC, it is likely that DOCK9 is a GEF that activates Cdc42 downstream of VEGF stimulation.

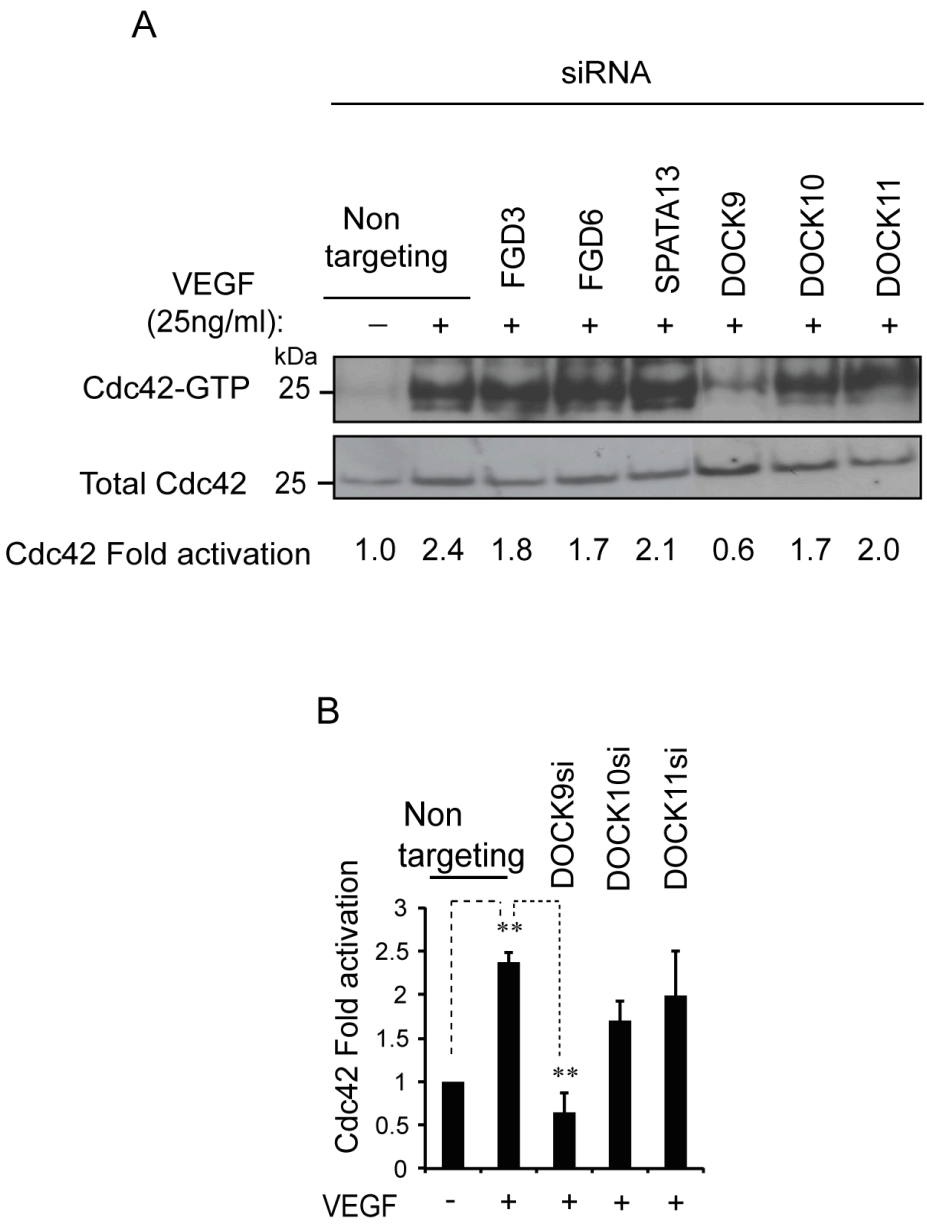

Figure 5.1 DOCK9 is necessary for Cdc42 activation downstream of VEGF signaling
HUVEC growing on fibronectin-coated dishes were transfected with FGD3 and 6, SPATA13, DOCK9, 10, 11 or non targeting control siRNAs. After 48 hours they were serum starved and stimulated with VEGF (25ng/ml). Cells were lysed and Cdc42 activation was analysed using the Cdc42 pulldown assay (Section 2.3.7). (A) Representative Western Blots from one experiment shows Cdc42-GTP and total Cdc42. Cdc42 activation was calculated as fold increase compared to unstimulated control after normalization for total Cdc42. (B) Bar chart shows quantification of Cdc42 pulldowns from three independent experiments performed using the ECL system. Cdc42 activation was calculated as fold increase compared to unstimulated control after normalization for total Cdc42 for each condition. Error bars are S.E.M., p values from unpaired student's t-test compared to unstimulated (0 timepoint) control. **, $P<0.01$. DOCK9 knockdown was quantitated by qRT-PCR as 85% (Appendix, Figure 11).

5.3 DOCK9 regulates filopodia formation in the organotypic angiogenesis assay

Cdc42 controls many cellular activities each of which may require a different guanine exchange factor to activate Cdc42 downstream of extracellular signaling pathways. To investigate whether Cdc42-driven filopodia formation relies on DOCK9 activation in endothelial cells, filopodia formation was visualized in the co-culture system in the presence or absence of DOCK9. Two different On-Target oligonucleotides were used to reduce DOCK9 expression (ot10 and ot11). Following transfection and seeding onto confluent fibroblasts, co-cultures were treated with VEGF and the media including VEGF replenished three days after seeding, as described in Chapter 2 (Section 2.4). Tube formation was allowed to proceed for a total of five days. The cultures were then stained for CD31 and filopodia were visualized under 10x magnification (Figure 5.2A). Tubules were able to form and grow in the absence of DOCK9 but VEGF-driven filopodia formation was abolished (Figure 5.2B) as also seen in absence of SGEF (Chapter 4, Section 4.3) and DOCK4 (Preliminary Data, Section 1.8.1). HUVEC with reduced expression of DOCK9 were able to form tubules which were comparable to control cells, although overall tubules appeared thinner by eye. To ensure knockdown had been achieved, DOCK9 expression levels were determined in DOCK9ot10 and DOCK9ot11 siRNA transfected cells through qRT-PCR which showed 68.5% (DOCK9ot10) and 74.5% (DOCK9ot11) loss of DOCK9 expression in cells transfected with On-Target oligonucleotide siRNAs.

Overall, these data suggest that DOCK9 activates Cdc42 to control VEGF-induced filopodia formation in HUVEC. Analysis of the spatial distribution of filopodia (filopodia located at tip sides and lateral sides) in un-stimulated or VEGF-stimulated endothelial cells was performed. Lateral and tip filopodia were counted and reported as number/total tubule length (Figure 5.2B and C). As described in chapter 4 (Section 4.3), VEGF stimulates filopodia formation at lateral sites to a higher extent than at the tip. As shown in Figure 5.2 B and C, DOCK9 knockdown ablated lateral filopodia formation and significantly reduced tip filopodia. However, in VEGF treated HUVEC with DOCK9 knockdown, a degree of tip filopodia persisted as also seen with SGEF knockdown (Chapter 4, Section 4.3) and DOCK4 knockdown in HUVEC (Preliminary Data, Section 1.8.1) following VEGF treatment. Overall, the data shown suggest that DOCK9 controls filopodia formation downstream of VEGF signaling pathway in the co-culture model.

A

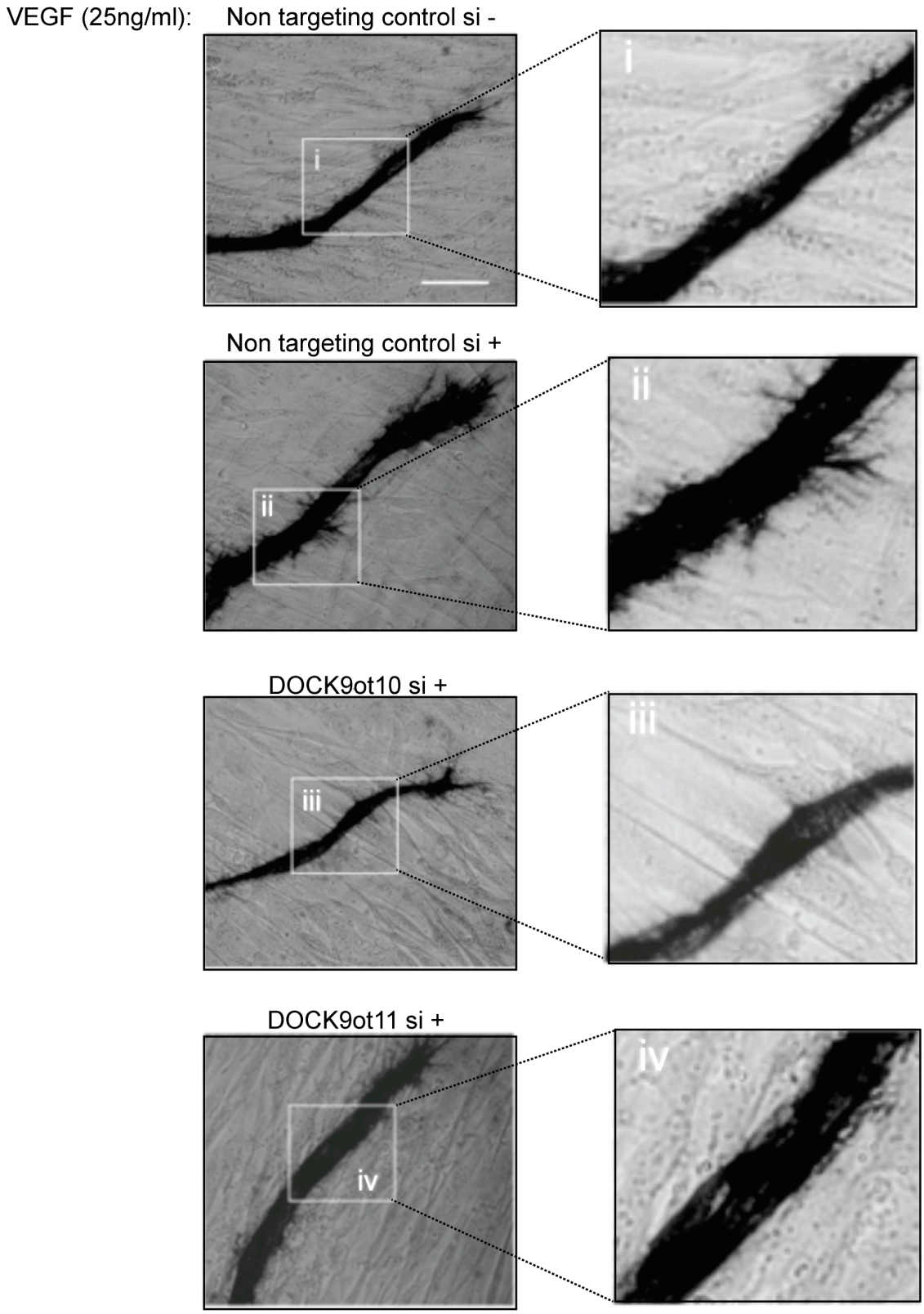
VEGF (25ng/ml):
Non targeting control si -
i
Non targeting control si +
ii
DOCK9ot10 si +
iii
DOCK9ot11 si +
iv

B

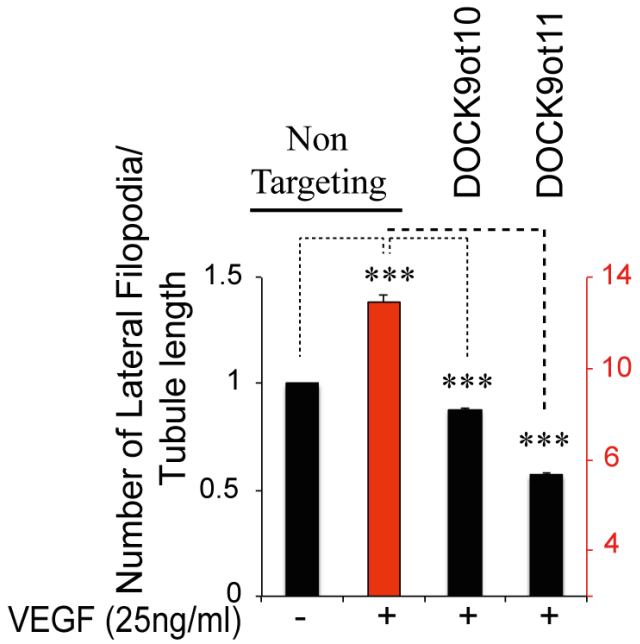

C

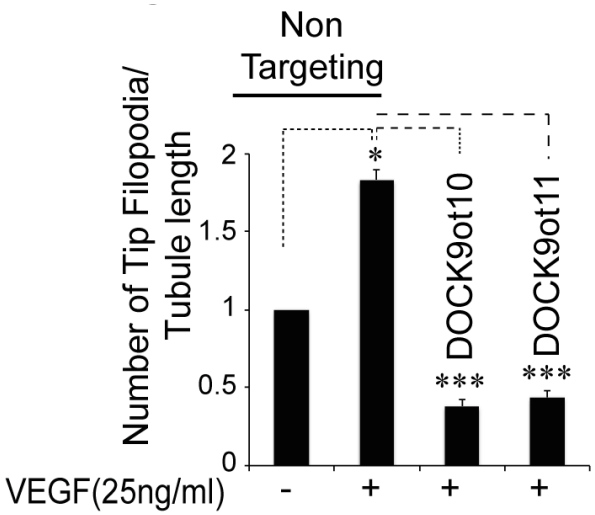

Figure 5.2 DOCK9 controls VEGF-driven filopodia formation
HUVEC were transfected with DOCK9 On-Target oligonucleotide siRNAs or non targeting control siRNA. 24 hours after transfection, cells were seeded onto confluent fibroblasts in the organotypic angiogenesis assay (Section 2.4) in the presence (+) or absence (-) of VEGF (25 ng/ml). The media containing VEGF were replenished after 72 hours and the cultures were stained for CD31 after an additional 2 days. (A) Representative phase-contrast images of filopodia were taken at 40x magnification. Scale bar: 200μm. The marked area in each sample shows a manual enlargement of regions of interest containing lateral filopodia. Knockdown of DOCK9ot10 and DOCK9ot11 were quantitated by qRT-PCR as 68.5% and 74.5% respectively (Appendix, Figure 12). Lateral (B) and tip (C) filopodia were counted in each sample (n=9), divided per tubule length and shown as fold increase compared to unstimulated, non targeting control. The red axis refers to the red column. Error bars represent S.E.M., p values from unpaired student's t-test; *, $P<0.05$; ***, $P<0.001$.

5.4 RhoG controls Cdc42 activation in a DOCK9-dependent manner

Activation of the signaling axis described in this thesis begins when endothelial cells are stimulated by VEGF. Upon binding to its receptor the VEGF downstream signaling cascade activates SGEF and thereby RhoG (chapter 3, Figure 3.10). Once activated, RhoG-GTP, through is effector ELMO, promotes localization of DOCK4 to the plasma membrane (this has been demonstrated in other cell types) and activation of Rac1. Rac1 then promotes Cdc42-driven filopodia formation. In the previous section (Section 5.2), it was shown that DOCK9 is a Cdc42 GEF that controls filopodia formation in the organotypic angiogenesis assay. To find out whether DOCK9 is activated downstream of the signaling cascade described above or whether it controls Cdc42 activation downstream of a different signaling pathway, biochemical assays were performed in HEK 293T cells. Cells were plated on fibronectin-coated dishes and transfected with a combination of DNA plasmids and siRNAs as described in Section 2.1.6.4. The DNA plasmids used were EGFP empty vector (Vector), EGFP wild-type Rac1 (Rac1) or EGFP wild-type RhoG (RhoG) (Table 2.3) while siRNA oligonucleotides employed were Standard pools against DOCK4, DOCK9 or non targeting control siRNA. After transfection, cells were grown for further 48 hours before being lysed. Active Cdc42 was then pulled down as described previously. As shown by Western Blot analysis (Figure 5.3A), the level of active Cdc42 was increased by overexpression of Rac1 compared to control vector. Strikingly, when the protein was overexpressed in the absence of DOCK9, Cdc42 activation was down-regulated to basal levels (Figure 5.3A). This result suggests that DOCK9 is necessary for Rac dependent Cdc42 activation. Overexpression of RhoG resulted in a 3-fold upregulation of active Cdc42. However, when RhoG was overexpressed in cells lacking DOCK4 or DOCK9, expression of active Cdc42 was dramatically reduced, suggesting that RhoG functions upstream of Rac1 in this pathway (Figure 5.3A). To verify that the same amount of plasmid was overexpressed in each sample, 50µl of total lysate for each sample were loaded onto acrylamide gels, transferred and blotted with antibodies against Rac1 (Figure 5.3B) or RhoG (Figure 5.3C). Increased protein expression of Rac1 and RhoG was seen in samples transfected with Rac1 and RhoG DNA plasmids. In addition, DOCK4 and DOCK9 protein levels were determined in siRNA transfected cells by Western Blot (Figure 5.3 D and E). The data shown here suggest

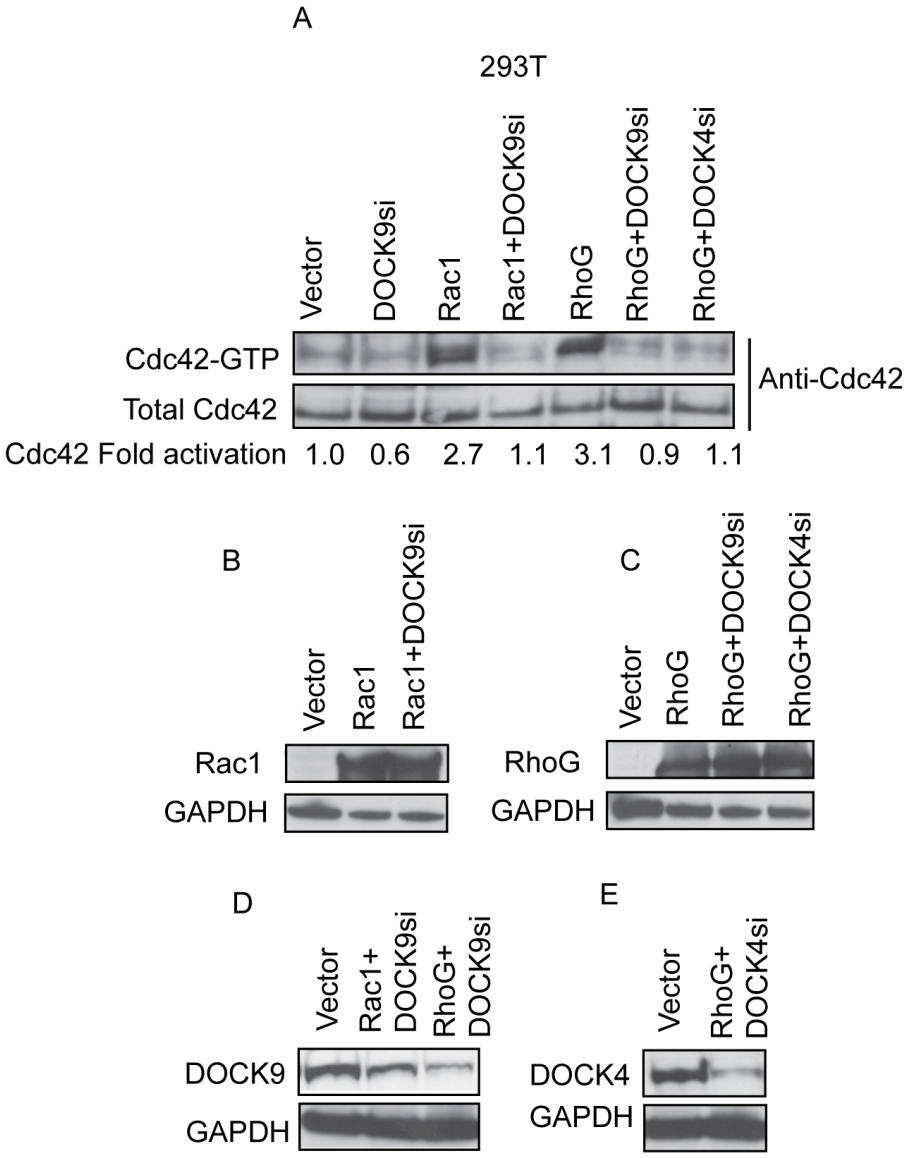

Figure 5.3 RhoG and Rac1 overexpression controls DOCK9-dependent Cdc42 activation
HEK 293T cells plated on fibronectin-coated dishes were co-transfected (DNA/siRNA) and lysed for protein extraction 48 hours later. Level of active Cdc42 was detected by pulldown assay (Section 2.3.7). (A) Western Blots from one independent experiment performed using the ECL system show Cdc42 activation (GTP Cdc42) following Rac1 over-expression and DOCK9 depletion (Standard pool siRNA) or RhoG overexpression and DOCK4 and DOCK9 depletion (Standard pool siRNA) in HEK 293T cells. Cdc42 activation was calculated as fold increase compared to control vector after normalization for total Cdc42. Immunoblots of Rac1 (B) and RhoG (C) show equal protein levels in total lysate where Rac1 and RhoG were overexpressed. Level of DOCK9 knockdown (D) or DOCK4 knockdown (E) were visualized through SDS-PAGE and normalized against total amount of DOCK9 or DOCK4 in control sample. Knockdown of DOCK9 in cells overexpressing Rac1 was quantified as 50% Knockdown of DOCK9 in cells overexpressing RhoG was quantified as 74%. Knockdown of DOCK4 in cells overexpressing RhoG was quantified as 72%. Knockdown levels for Figure 5.3D are reported in Appendix, Figure 13; knockdown levels for Figure 5.3E are reported in Appendix, Figure 14.

that the RhoG-DOCK4-Rac1 signaling axis controls Cdc42 activation and it is not specific for endothelial cells.

5.5 DOCK9 controls filopodia in HEK 293T cells

As previously demonstrated, Cdc42 is activated downstream of Rac1 in HUVEC (Figure 4.7A and B) as well as in HEK 293T cells (Figure 4.6). This mechanism appears to be conserved to regulate filopodia formation. Since DOCK9 acts as a Cdc42 GEF in the control of filopodia formation and is activated downstream of Rac1 in HEK 293T cells, it was reasoned that DOCK9 might control Cdc42-driven filopodia formation downstream of Rac1. To test this hypothesis, HEK 293T cells were plated on fibronectin-coated dishes and transfected with a combination of DNA over-expression plasmids and siRNAs as described in Section 2.1.6.4. The DNA plasmids used were EGFP empty vector (Vector) or EGFP wild-type Rac1 (Rac1, Table 2.3) while siRNA oligonucleotides employed were Standard pool against DOCK9 or non targeting control siRNA. Cells were cultured for further 48 hours prior to fixing and imaging by confocal microscopy. TRITC-phalloidin dye was used to visualize the cytoskeleton, resulting in F-actin staining in red. As shown in Figure 5.4, cells expressing EGFP empty Vector (Vector) alone showed smooth edges and protrusions were not detected. In contrast, overexpression of EGFP wild-type Rac1 (Rac1) stimulated the production of numerous projections all around the cell body, as seen previously (Figure 4.6). Overexpression of Rac1 in cells lacking DOCK9 (DOCK9 Standard pool siRNA) showed a reduced number of such protrusions. Consistent with the phenotype seen in cells lacking Cdc42 (Figure 4.6), knockdown of DOCK9 in HEK 293T cells led to the cortical actin rearrangement resulting in the projection of membrane bulges.

This result supports the hypothesis that DOCK9 is activated downstream of Rac1 to control Cdc42 activation and formation of filopodia.

A

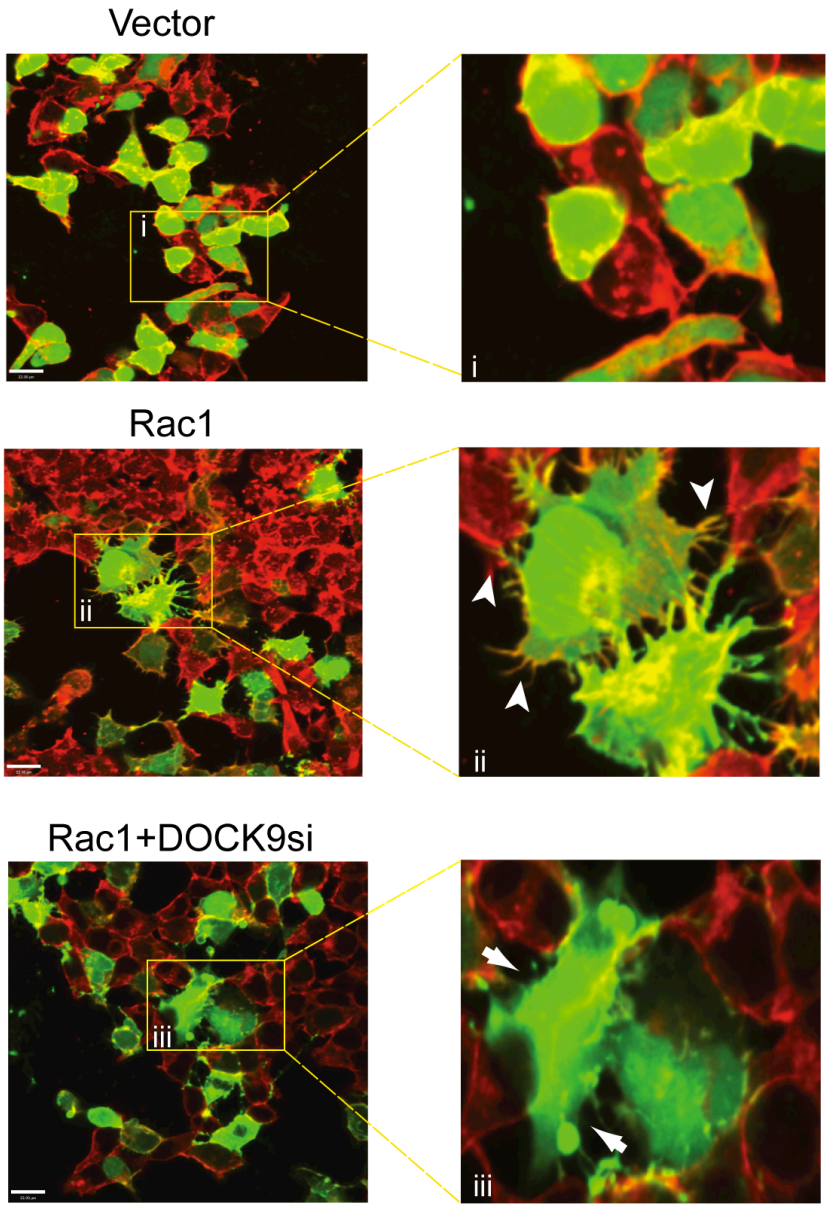

Figure 5.4 Rac1 overexpression controls Cdc42 activation in a DOCK9 dependent fashion
HEK 293T cells growing on fibronectin were transfected with WT Rac1 (Rac1, GFP tagged) in the presence or absence of DOCK9 Standard pool siRNA. Two days after transfection the cultures were stained for TRITC-Phalloidin (red) and visualized using a 20x objective. Representative pictures are shown. The marked area in each sample shows a manual enlargement of regions of interest where filopodia localize. Note the induction of filopodia with Rac1 overexpression (arrowheads) and ablation of filopodia and disruption of cortical actin in the absence of DOCK9 (arrows). Scale bar: 200μm.

5.6 The RhoG effector ELMO interacts with DOCK4 and DOCK9

The RhoG and Rac1 overexpression experiments described previously (Section 5.4) suggest that a RhoG-DOCK4-Rac1-DOCK9-Cdc42 signaling cascade is in operation to control filopodia formation. In order to understand more about how the RhoG-DOCK4-Rac1 cascade and DOCK9-Cdc42 are linked, the role of the RhoG effector ELMO (Section 1.5.6.2) was investigated. Following RhoG activation, ELMO interacts with DOCK4 to promote Rac1 activation as demonstrated in fibroblasts (Hiramoto et al., 2006) and breast cancer cells (Hiramoto-Yamaki et al., 2010). Experiments performed in the laboratory (data not shown) showed that ELMO interacted with over-expressed DOCK4 in HEK 293T cells. DOCK4 and DOCK9 participate in the same signaling pathway that leads to Rac1 and Cdc42 activation in VEGF stimulated HUVEC as well as HEK 293T cells. Therefore, given that DOCK4 interacts with ELMO, the possibility that ELMO forms a complex with DOCK9 was investigated. Flag-tagged DOCK9 was overexpressed in HEK 293T cells (Chapter 2, Table 2.3); as a control, a flag-tagged empty vector was used. Two days later, proteins in the cell lysates were pulled-down using GST-ELMO recombinant protein (Chapter 2, Section 2.3.7). As shown in Figure 5.5A, no binding was visualized between flag-tagged empty vector and ELMO. However, ELMO was found in a complex with over-expressed DOCK9 (Figure 5.5B). Thus, this identifies a novel interaction between the scaffolding protein ELMO and DOCK9.

5.7 The GEF DOCK4 mediates the binding between ELMO and DOCK9

As previously discussed, ELMO-DOCK4 binding is necessary for translocation of DOCK4 to the plasma membrane (Hiramoto et al., 2006). Since ELMO-DOCK9 binding has not previously been reported, experiments were performed in HEK 293T cells to understand more about the nature of the complex. Cells were first plated on fibronectin-coated dishes and transfected with DOCK4 or DOCK9 Standard pool siRNAs or non targeting control siRNA. Transfected cells were lysed two days later and GST recombinant ELMO was used to pulldown ELMO binding partners (Chapter 2, Section 2.3.7). Lysates from cells transfected with DOCK4 or non targeting control siRNA were blotted and probed using a

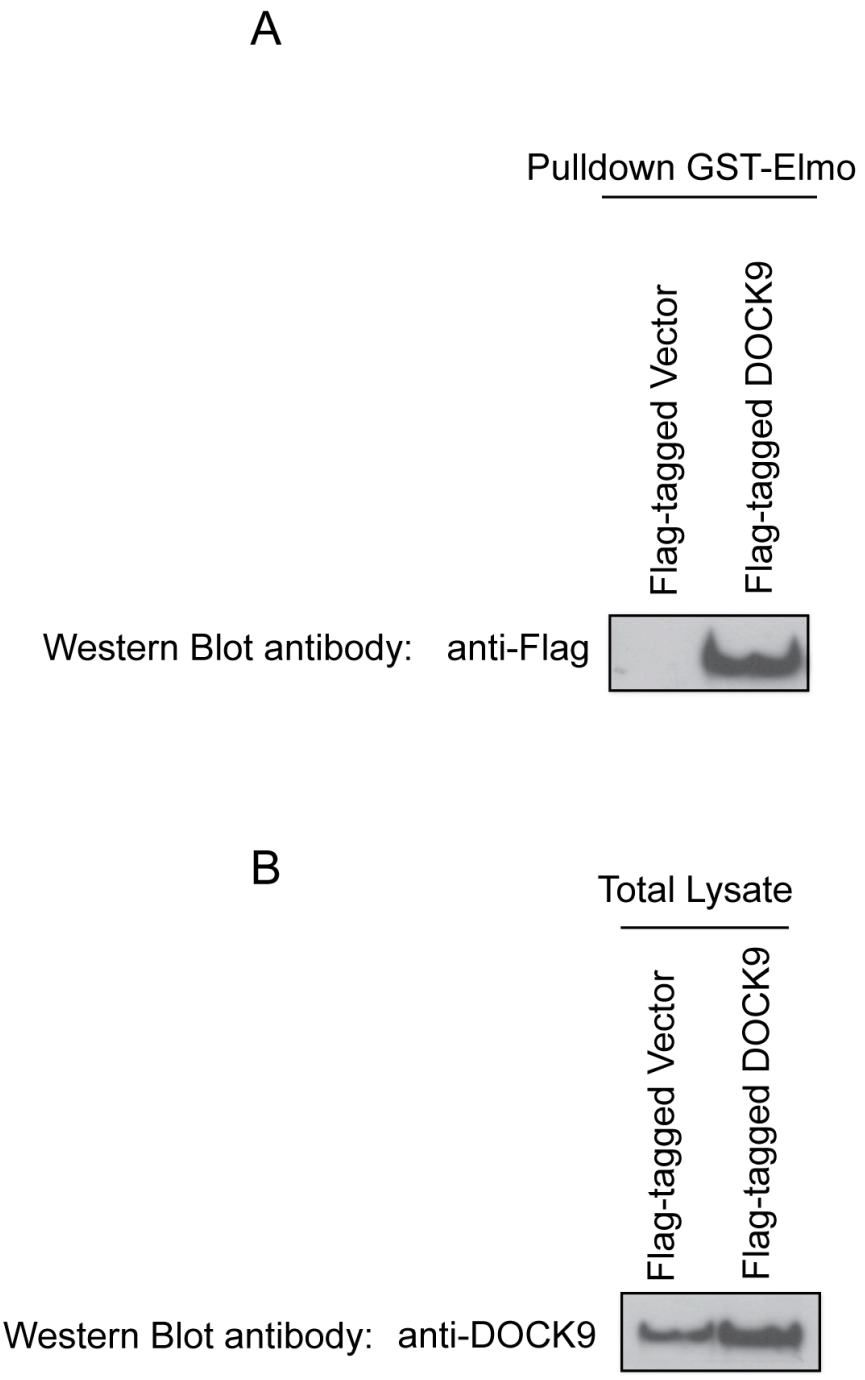

Figure 5.5 ELMO binds DOCK4 and DOCK9 in HEK 293T cells
HEK 293T cells growing on fibronectin were transfected with empty vector control or WT DOCK9. DNA plasmids were flag tagged. Two days after transfection the cultures were lysed and proteins were pulled-down with GST ELMO (Section 2.3.7). Immunoblots (ECL system) show flag-tagged proteins precipitated with GST ELMO (A) and level of endogenous (flag-tagged Vector) and overexpressed (flag-tagged DOCK9) DOCK9 in the total lysate (B).

DOCK9 antibody whereas cells lacking DOCK9 were probed using an antibody against DOCK4. As shown in Figure 5.6A, in the absence of DOCK4, a reduction in DOCK9 binding to ELMO was seen, suggesting that DOCK4 is necessary for this complex formation. DOCK9 knockdown in HEK 293T cells did not affect the binding between ELMO and DOCK4, suggesting that DOCK9 does not mediate the interaction between ELMO and DOCK4. As shown in the Figure 5.6 (A and B) the amount of endogenous DOCK4 in non targeting control cells and cells lacking DOCK9 was comparable. Similarly, non targeting control cells and cells silenced for DOCK4 showed equal amount of DOCK9. In addition, knockdown of protein levels in total lysates was assessed by Western Blot using antibodies against DOCK4 or DOCK9. The level of DOCK4 and DOCK9 knockdown is shown in Figure 5.6 (A and B) and was quantified as 86% and 72% respectively.

5.8 ELMO family members control endothelial filopodia formation in the organotypic co-culture assay

Since DOCK4 and DOCK9 control filopodia formation and they both bind the scaffolding protein ELMO, it was reasoned that ELMO might be involved in controlling filopodia formation in EC. Filopodia were visualized in the co-culture system in presence or absence of VEGF and the ELMO isoforms (ELMO1 and ELMO2, Gumienny et al., 2001; Ho et al., 2010). HUVEC were transfected with siRNAs (Standard pool) against ELMO1, ELMO2 or a non targeting control oligonucleotide (non targeting siRNA). Following transfection and seeding onto confluent fibroblasts, co-cultures were treated with VEGF as described in Chapter 2 (Section 2.4). The cultures were then fixed and stained for CD31 and filopodia visualized under 10x magnification (Figure 5.7A).

As expected, the total number of filopodia (tip and lateral) increased when control cells were stimulated with VEGF compared to control untreated (Figure 5.7B). VEGF stimulated HUVEC that lacked the different ELMO isoforms (knockdown of ELMO 1 and ELMO 2 were quantified as 99% and 75% respectively) showed a reduction of filopodia

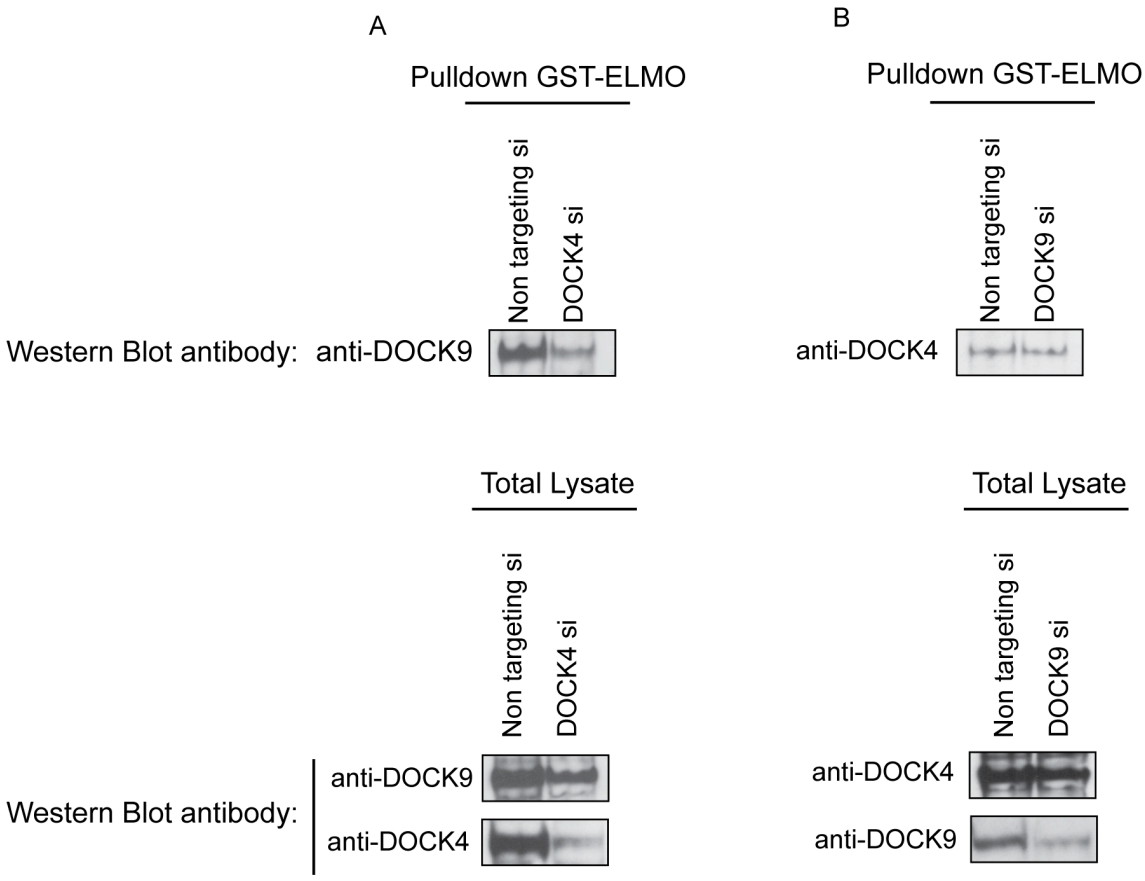

Figure 5.6 DOCK4 is necessary for ELMO-DOCK9 binding
HEK 293T cells growing on fibronectin were transfected with DOCK9 or DOCK4 Standard pool siRNAs (DOCK4si and DOCK9si) or non targeting control siRNA. Two days after transfection cells were lysed and endogenous proteins were pulled-down with GST-ELMO (Section 2.3.7). Immunoblots (ECL system) show binding between ELMO and endogenous DOCK9 in absence of DOCK4 (A) or binding of ELMO to endogenous DOCK4 in absence of DOCK9 (B). Expression of endogenous DOCK9 and DOCK4 in total lysates are shown (A and B) together with knockdown of DOCK9 (quantified as 72% (B)) and DOCK4 (quantified as 86% (A)). Knockdown level for DOCK4 and DOCK9 Standard pool was assessed through western blotting and shown in Appendix, Figure 15 and 16.

A

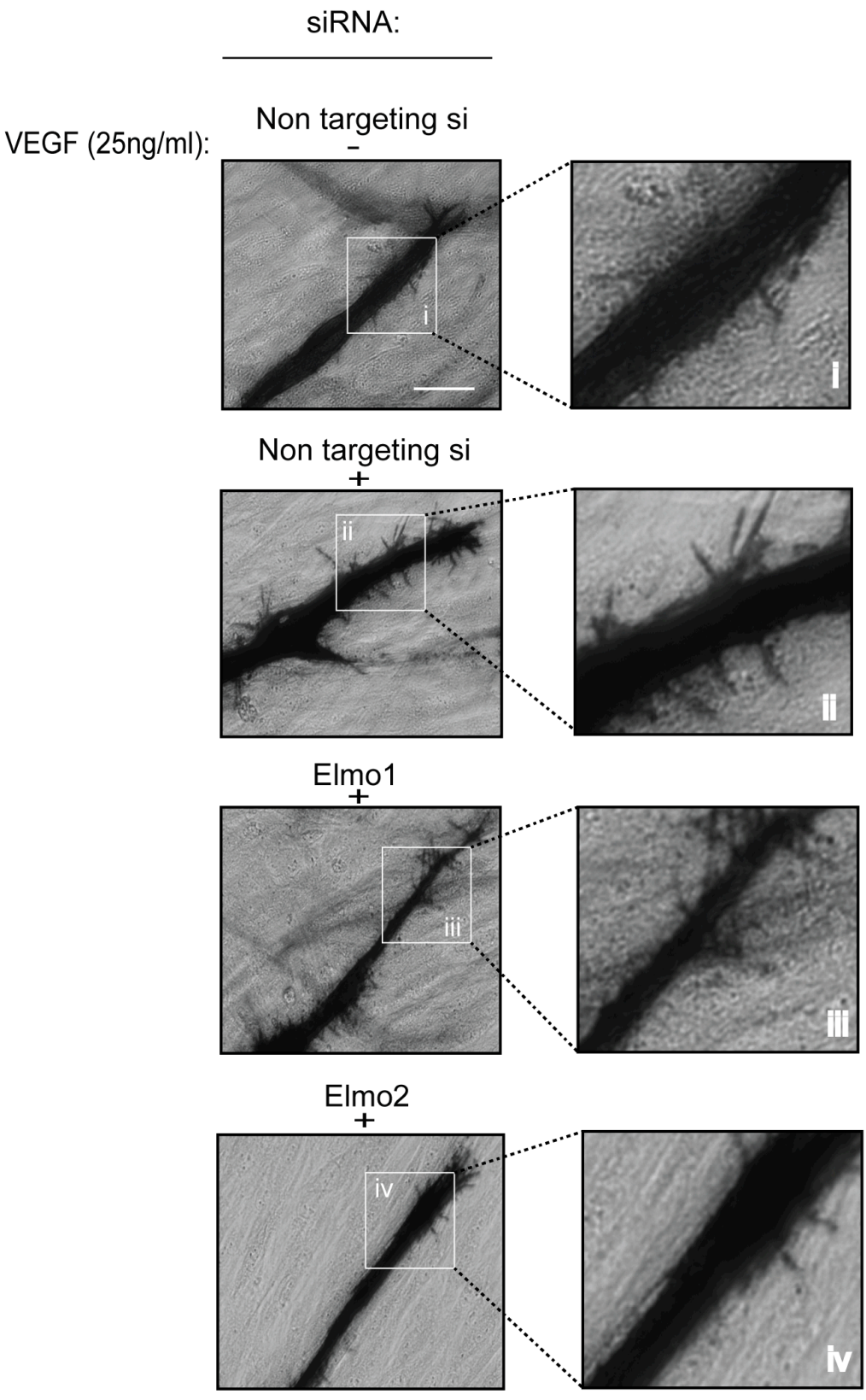
siRNA:
VEGF (25ng/ml):
Non targeting si
-
i
i
Non targeting si
+
ii
ii
Elmo1
+
iii
iii
Elmo2
+
iv
iv

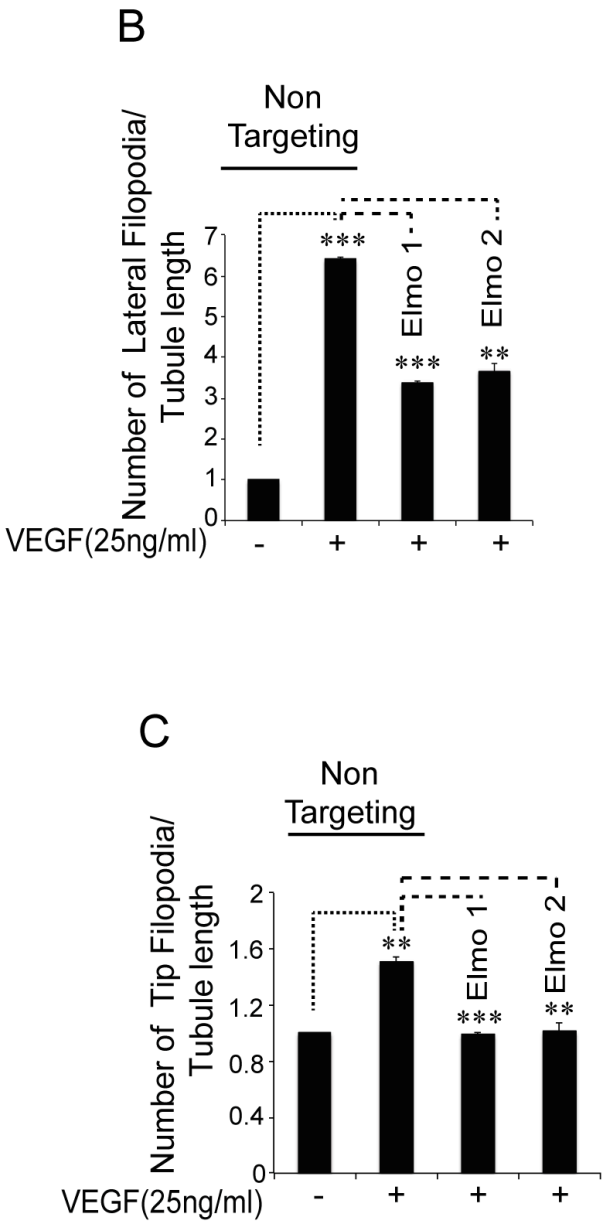

Figure 5.7 Knockdown of ELMO family members reduces filopodia formation
HUVEC were transfected with siRNAs Standard pool against ELMO 1, ELMO 2 or non targeting control siRNA. 24 hours after transfection cells were seeded onto confluent fibroblasts in the organotypic angiogenesis assay as described in Section 2.4 in the presence (+) or absence (-) of VEGF (25 ng/ml). The media with VEGF were replenished after 72 hours and the cultures were stained for CD31 2 days later. (A) Representative phase-contrast images of filopodia formation taken at 10x magnification are shown. Scale bar: 200μm. The marked area in each sample shows a manual enlargement of regions of interest where lateral filopodia localize. (B) Bar charts show number of lateral (B) and tip (C) filopodia counted in each sample (n=6), divided per tubule length and shown as fold increase compared to unstimulated, non targeting control. Error bars represent S.E.M., p values from unpaired student's t-test. **, $P<0.05$; ***, $P<0.001$. ELMO 1 and ELMO 2 knockdown levels are shown in Appendix (Figure 17).

formation to a similar degree within the different isoforms (~ 1.5 fold compared to VEGF treated non targeting control siRNA; Figure 5.7B). Visual observations suggested that a greater effect was seen on lateral as opposed to tip filopodia in the absence of ELMO. This phenotype is consistent with those seen when SGEF, DOCK4 or DOCK9 are down-regulated in VEGF treated HUVEC (Figure 4.3, Figure 1.11 and Figure 5.2).

Overall the results suggest that cells lacking ELMO cannot form filopodia as normal. Therefore ELMO plays a role in the generation or maintenance of EC protrusions downstream of the VEGF signaling cascade.

5.9 VEGF stimulates the binding between endogenous DOCK4 and DOCK9 in ECs

Figure 5.5 shows that the scaffolding protein ELMO binds the GEFs DOCK4 and DOCK9. Results shown in Figure 5.6 suggest that the interaction between ELMO and DOCK9 is mediated by DOCK4. It was therefore hypothesized that ELMO, DOCK4 and DOCK9 form a ternary complex; if this is the case, DOCK4 and DOCK9 might interact directly which would be a novel observation as there is no published evidence of binding between different subgroups of DOCKs (although homodimerisation of DOCK members has been observed) (Terasawa et al., 2012; Kulkami et al., 2011).

To investigate whether DOCK4 and DOCK9 form a complex in ECs, co-immunoprecipitation experiments (CO-IPs) were performed using lysates from HUVEC (Section 2.3.8). Precipitated proteins (Figure 5.8) were then eluted from the beads, detected by Western Blot (Section 2.3.4), quantified and normalized against the total amount of the protein of interest in the whole lysate.

Rac1 and Cdc42 VEGF-driven activation occurs at an early time point (after 15 minutes of VEGF stimulation both proteins were upregulated, Figure 3.8 and Figure 4.7) and both proteins are still active after 30 minutes of stimulation. Based on this knowledge, it was reasoned that the DOCK4-DOCK9 binding might occur prior to the stimulation of these Rho GTPases. Complex formation was therefore evaluated after 5 and 15 minutes of

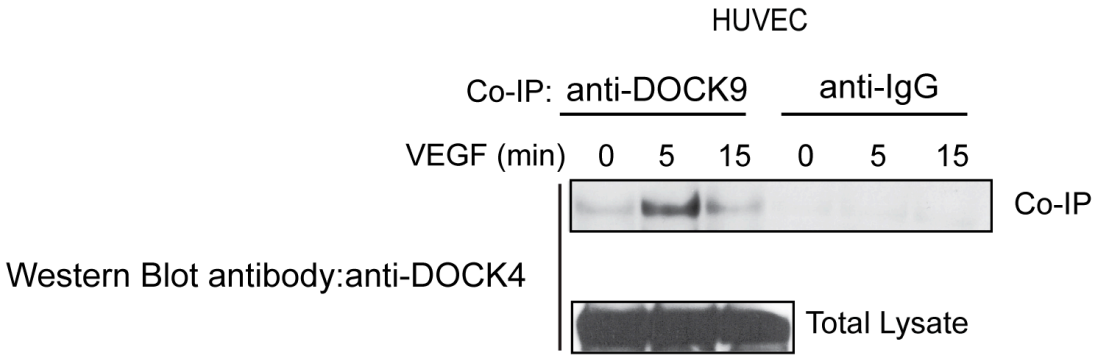

Figure 5.8 VEGF stimulates a complex between DOCK family members
HUVEC were plated on fibronectin-coated dishes. Two days later cells were serum starved, stimulated with VEGF (25ng/ml) at the time point shown and lysed after stimulation. Proteins were immuno-precipitated using a DOCK9 or an IgG antibody (chapter 2, Table 2.4). Western Blots were probed with a DOCK4 antibody (chapter 2, Table 2.4). Immunoblots (ECL system) show binding between endogenous DOCK4 and DOCK9 proteins at different time points after stimulation with VEGF and the level of endogenous DOCK4 in the total lysates.

binding of the antibody, equal amounts of protein lysates was mixed with IgG antibody, as a control. Protein lysates bound to the beads were analysed by western blotting using DOCK4 antibodies to identify the endogenous protein. Figure 5.8 shows an example of VEGF-driven DOCK4-DOCK9 binding.

As shown, binding between endogenous DOCK4 and endogenous DOCK9 occurred following VEGF stimulation, although the result underlined the transient nature of the complex. DOCK4 and DOCK9 bound at an early time point (5 minutes) and the intensity of the binding diminished 10 minutes later. To confirm that any differences seen were due to differential binding of the proteins rather than to differences in overall DOCK4 expression, DOCK4 protein levels were detected and compared using western blotting. Equal amounts of DOCK4 protein were present in each lysate.

Taken together these data suggests that we have identified a new, VEGF-driven complex formation not previously described, activated upstream of filopodia formation in HUVEC.

5.10 The Rac1 GEF DOCK4 and the Cdc42 GEF DOCK9 complex in HEK 293T cells

Binding between DOCK4 and DOCK9 is a "non canonical" mechanism not previously reported for any cell type. In Chapter 4 and in Figure 5.3 it was shown that the signaling module RhoG→DOCK4→Rac1→DOCK9→Cdc42 is conserved in both endothelial cells and HEK 293T cells. To test whether DOCK4-DOCK9 binding is unique to endothelial cells when appropriately stimulated or whether the complex formation also occurs in HEK 293T, Co-IP assays were repeated in HEK 293T cells. As shown in Figure 5.9A, immunoblotting using an anti-DOCK9 antibody showed a binding between DOCK4 and DOCK9 in HEK 293T cells expressing EGFP DOCK4 (EGFP-tagged DOCK4, A). No binding was visualized using Vector alone (EGFP-tagged Vector, A). To validate these results, expression of DOCK9 protein was evaluated in each sample by western blotting of 50μl of total lysate. Figure 5.9A, bottom panel, shows equal expression of the DOCK9

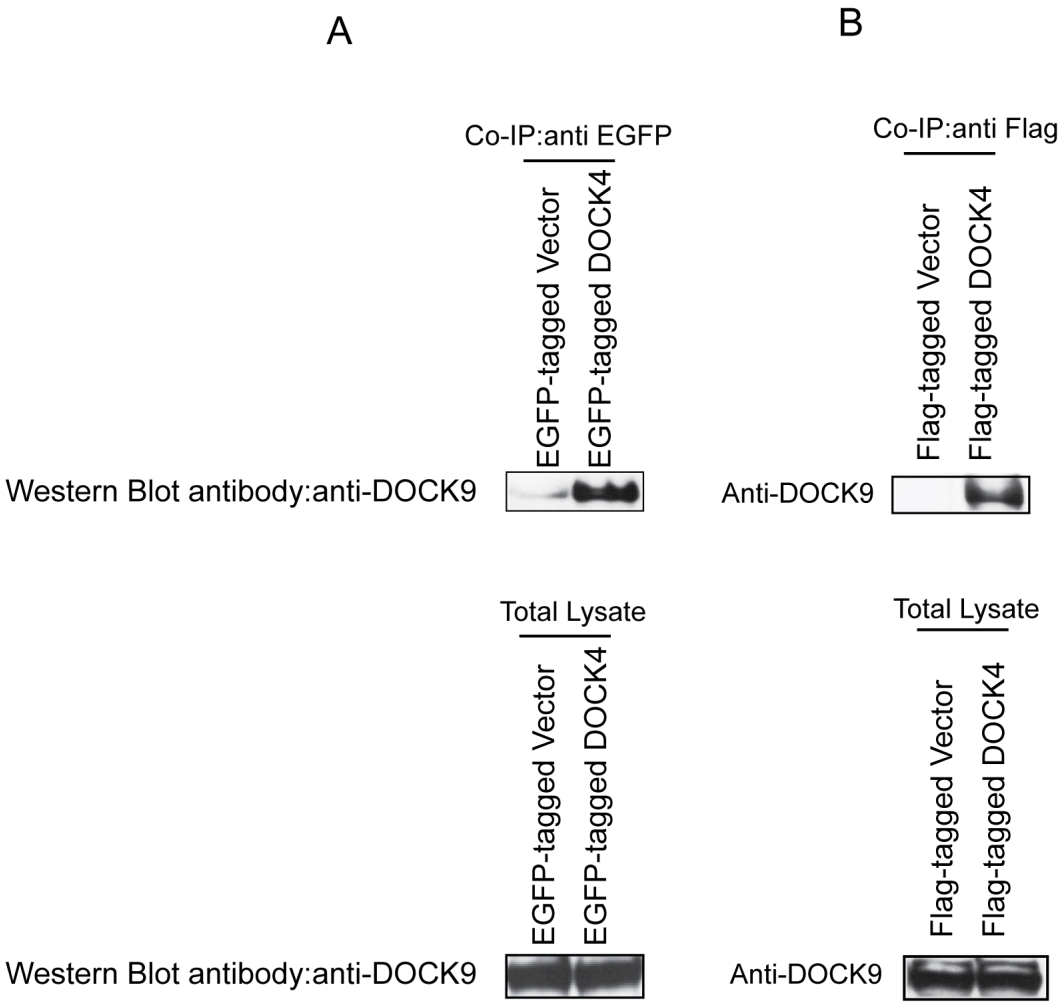

Figure 5.9 Binding between DOCK4 and DOCK9 in HEK 293T cells
HEK 293T cells were plated on fibronectin-coated dished and transfected using an empty vector control (Vector) or a WT DOCK4 constructs (EGFP tagged or flag tagged, A and B). Two days later cells were lysed and proteins were immuno-precipitated using a GFP trap (A) or an anti-flag antibody (B). Binding partners were visualized (ECL system) using a DOCK9 antibody that detected the endogenous protein (A and B) or expression of endogenous DOCK9 in total lysates (A and B, lower panel.

protein in each lysate. To ensure that the result was not an artefact due to the EGFP tag linked to the plasmid, the experiment was repeated using flag-tagged DNA plasmids. As shown in Figure 5.9B, binding between DOCK4 and DOCK9 was solely visualized in the sample where DOCK4 was overexpressed (Flag-tagged DOCK4, B). In contrast, binding between DOCK9 and DOCK4 was not detected when DOCK4 was not overexpressed (Flag-tagged Vector, B). Overall the results show that DOCK4 and DOCK9 form a complex that is not unique to endothelial cells.

5.11 The DOCK4 SH_3 and DHR2 domains are necessary for the binding with DOCK9

The DOCK4-DOCK9 interaction described above is the first example of DOCK protein heterodimerization that we are aware of. As this is a novel finding, it is interesting to determine how this binding occurs and which domains of both proteins are involved. The strategy adopted to answer this question relied on using DOCK4 mutant plasmids (Chapter 2, Table 2.3), in which specific domains of the DOCK4 protein were deleted.

The DHR2 domain of DOCK4 directly binds and activates Rac1 (Chapter 1, Section 1.7.1) while the SH_3 domain could potentially be necessary for the binding with DOCK9, based on the high affinity towards the PH domain of DOCK9 (Pawson and Schlessingert, 1998). To assess whether these domains are involved in the binding between DOCK4 and DOCK9, Co-IP assays were performed using deletion constructs for DOCK4 (Figure 5.10A). HEK 293T cells were plated on fibronectin-coated dishes and transfected the following day. Empty vector (Vector), WT DOCK4 (DOCK4), DOCK4 lacking DHR2 domain (ΔDHR2) or the SH_3 domain (ΔSH_3) were overexpressed. All exogenous proteins were flag-tagged. After transfection, cells were grown for two further days before being lysed. Endogenous DOCK9 was immuno-precipitated using the DOCK9 antibody listed in Table 2.4 (Chapter 2). The ability of DOCK9 to bind DOCK4 was visualized by western blotting using an antibody to detect DOCK4 (Figure 5.10B). While no binding was visualized between DOCK9 and the empty vector construct, DOCK9 strongly bound overexpressed DOCK4 protein. DOCK4-DOCK9 binding was reduced in the absence of

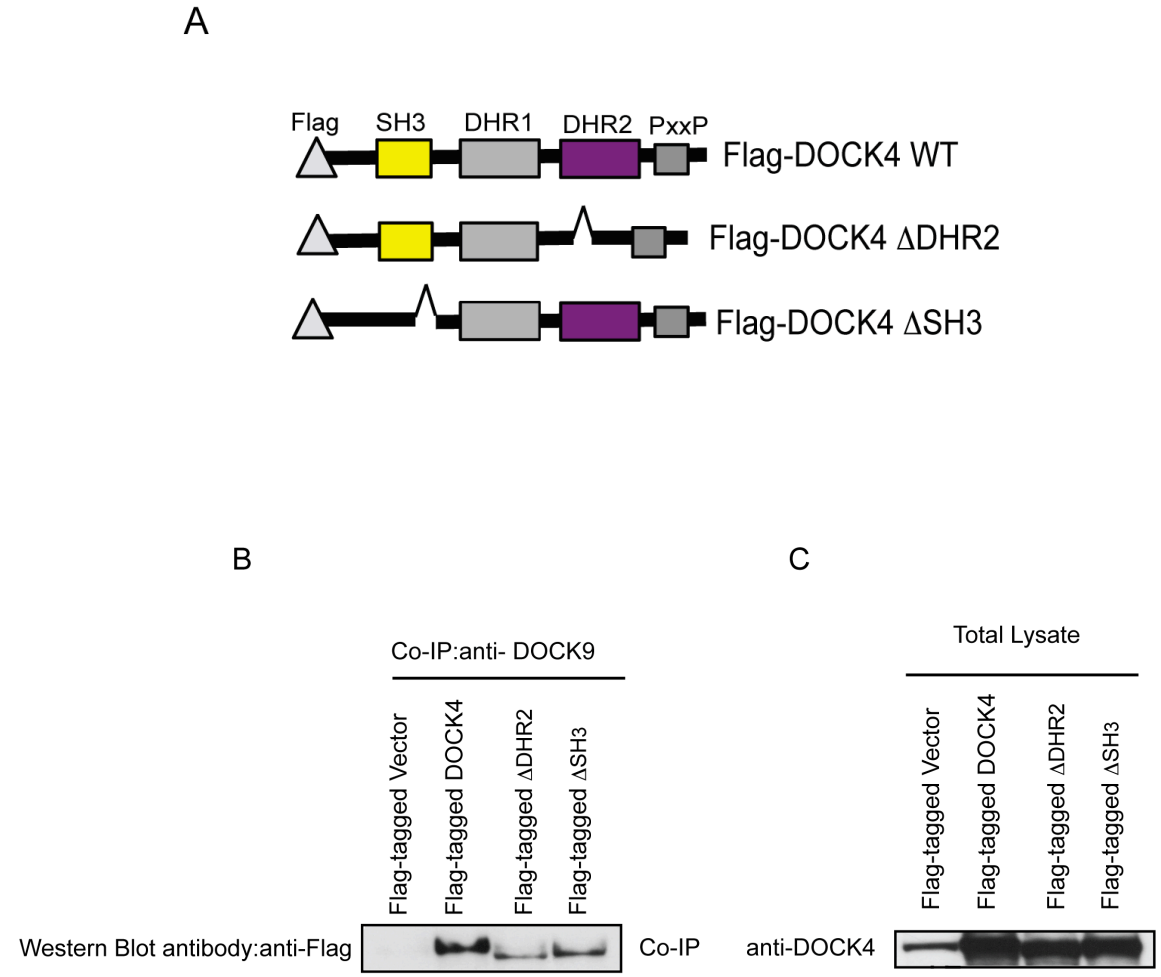

Figure 5.10 The DHR2 and SH_3 domain of DOCK4 are necessary to mediate DOCK4-DOCK9 complex formation

Schematic representation of WT-DOCK4 protein and DOCK4 deletion constructs used to perform co-immunoprecipitation (A).

HEK 293T cells were plated on fibronectin-coated dished and transfected with empty vector control (Vector), WT DOCK4 (flag tagged DOCK4) or deletion constructs (flag tagged, (B)). Two days later cells were lysed and proteins were immuno-precipitated using a DOCK9 antibody. Immunoblots show DOCK4-DOCK9 binding in HEK 293T cells and loss of the binding in absence of DHR2 and SH_3 domain (B). Immunoblots (ECL system) show expression of endogenous DOCK4 (flag-tagged Vector) and overexpressed DOCK4 (flag-tagged DOCK4, ΔDHR2 and ΔSH_3 domains) in the total lysates.

both the DHR2 and SH_3 domains. To confirm the overexpression of the proteins and show equal loading of proteins into the samples, protein lysates were probed with an antibody against DOCK4 (Figure 5.10C) that recognizes a region of the PH domain, with motifs uniquely possessed by DOCK4 (aa 1725-1775).

Overall the results suggest that both the DHR2 and SH_3 domains of DOCK4 partecipate to the formation of a complex involving DOCK4 and DOCK9.

5.12 The DOCK4 SH_3 domain is sufficient to mediate DOCK4-DOCK9 binding

As described in Chapter 1 (Section 1.7.1), the DOCK family DHR2 domain possesses catalytic activity which facilitates nucleotide exchange of Rho GTPase molecules (Yang et al., 2009). The SH_3 domain has not been fully characterized, but its high affinity towards proline-rich regions suggests that it might mediate protein-protein interactions (Alexandropoulos et al., 1995). Since it has been demonstrated that the DHR2 and SH_3 domains are bound together to maintain the DOCK in the inactive conformation (Lu et al., 2005), it was reasoned that the DOCK4 DHR2 domain could be involved in maintenance of the DOCK4 open conformation whilst the SH_3 domain is responsible for the direct binding with DOCK9. To test this hypothesis, a GST empty vector construct (Vector) and a GST-DOCK4 SH_3 (DOCK4-SH_3, Table 2.3) domain were expressed in bacteria to produce recombinant protein (Chapter 2 (Section 2.3.1 and 2.3.2)). Following induction with IPTG, proteins were purified from the bacteria. The pulldown experiment shown in Figure 5.11 was performed using recombinant proteins purified after 5h of induction with 1mM IPTG. Protein concentration was measured (chapter 2, Section 2.3.3) and equal concentrations of GST-empty vector and GST-DOCK4-SH_3 recombinant proteins were used to pulldown endogenous DOCK9 from HEK 293T cells plated on fibronectin-coated dishes. GST-empty vector or GST-DOCK4-SH_3 domain binding partners were eluted, analysed by western blotting and probed using an antibody against DOCK9. As shown in Figure 5.11, no endogenous DOCK9 was visualized in samples in which empty vector was overexpressed (top panel); in contrast, when proteins were pulled down using the recombinant GST-DOCK4-SH_3 domain, DOCK9 was detected. These data suggest that the DOCK4 SH_3 domain has high enough affinity towards DOCK9 to pulldown the endogenous protein.

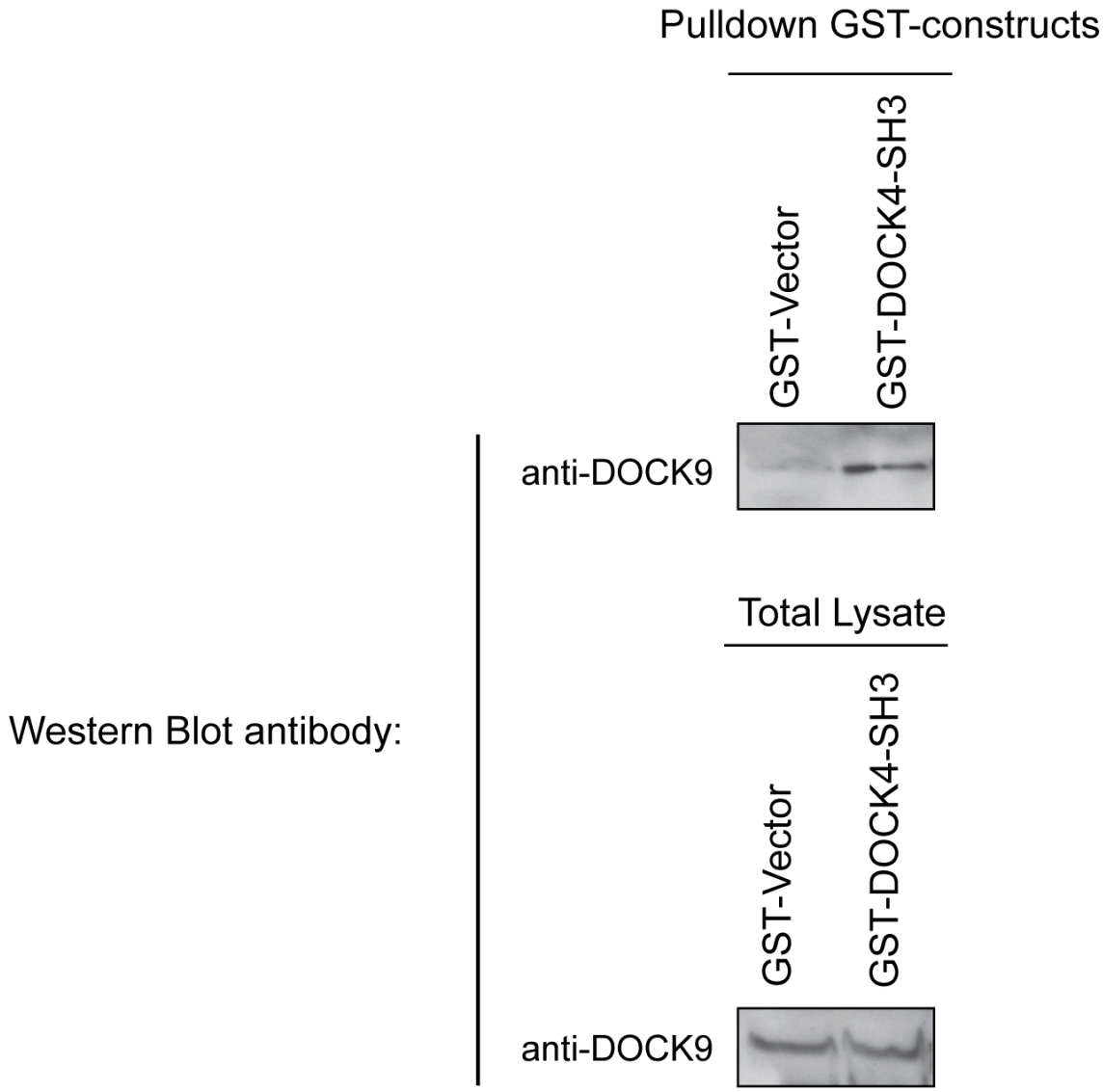

Figure 5.11 The DOCK4-SH_3 domain is sufficient to mediate the binding with DOCK9
HEK 293T cells were plated on fibronectin-coated dished. 48 hours later cells were lysed and proteins were pulled-down using a GST-empty vector control or a GST-DOCK4-SH_3 domain construct. Immunoblots (ECL system) show that endogenous DOCK9 and the SH_3 domain of GST-DOCK4 are in a complex (top panel) and that endogenous DOCK9 is equally expressed in the total lysates (bottom panel).

5.13 Discussion

There are only few previous reports regarding DOCK9 and its function, with the first only in 2002 (Meller et al., 2002). A major advance came in 2009 when a detailed description of DOCK9-Cdc42 binding sites was reported (Yang et al., 2009). That DOCK9 is a Cdc42 positive regulator has been suggested for both primary and secondary cells. For instance, it was shown that dendrite outgrowth of hippocampal neurons is mediated by the DOCK9-activated Cdc42 (Kuramoto et al. 2009). More recently, it was reported that DOCK9 is involved in glioblastoma cell spreading and invasion (Hirata et al., 2012). Glioblastoma cells are highly invasive and penetrate the brain parenchyma using pseudopodia to intercalate through tissues; a metastatic glioblastoma cell line has been shown to have very high levels of both Rac1 and Cdc42. Silencing of DOCK9 in these cancer cells reduced cell spreading and invasion due to a lack of cellular protrusions (Hirata et al., 2012). However, to date, the role of DOCK9 in endothelial cells has not been investigated.

This chapter reports evidence of DOCK9 mediated filopodia formation in endothelial cells through control of Cdc42.

The screen of putative Cdc42 regulators (Figure 5.1) showed that DOCK9 was the only GEF that controlled Cdc42 activation after 30 minutes of stimulation with VEGF. This finding does not exclude the possibility that the other GEFs might play a role in Cdc42 activation at earlier or at later time points.

In this chapter, it was demonstrated that DOCK9 participates in controlling endothelial cells filopodia formation in the co-culture assay. In this 3-dimensional model tubules do not grow towards a directional VEGF gradient as occurs *in vivo*. Instead, spatial and temporal control of tubule growth might be mediated by the adjacent extracellular matrix produced by the fibroblasts below. Lateral filopodia are not involved in cell viability or attachment to the ECM. If this were the case, cells lacking lateral filopodia formation would rapidly detach, and we do not see this in our model. However, lateral filopodia are necessary for cell-cell interactions and vessel thickening. Consistent with this, in the absence of DOCK9, endothelial cell spreading and migration are maintained but lateral thickening and filopodia formation are reduced, similarly to observations in the absence of DOCK4 and SGEF.

As demonstrated in this chapter, both DOCK4 and DOCK9 are in a complex with ELMO. The ELMO-DOCK4 complex was established previously (Hiramoto et al., 2006) whereas the ELMO-DOCK9 complex has not been previously reported. ELMO is a very intriguing molecule. A variety of receptors in organisms ranging from worms to humans can activate the ELMO/DOCK180 complex, including integrins, cell death receptors, and 7-TMRs (7-TransMembrane Receptor) (Côté et al., 2007). Exactly how the ELMO/DOCK180 complex functions in cells has yet to be determined. Some data implicate ELMO as functioning as a scaffold, with additional roles in localizing the GEF activity performed by DOCK180 (Lu et al., 2005). Other work suggests that ELMO is required for DOCK180-mediated nucleotide exchange on Rac1, where ELMO, nucleotide-free Rac1 and DOCK180 form a ternary structure (Grimsley et al., 2004). In 2010, it was shown that ELMO1 influences the formation of both blood and lymphatic vessels in zebrafish (Epting et al., 2010). In particular, it was shown that ELMO is crucial to the formation and function of the dorsal aorta, posterior cardinal vein, intersomitic vessels and parachordal vessels. In *Drosophila* embryos, ELMO is involved in myoblast fusion (Geisbrecht et al., 2008). However, knockout mouse model showed that animals were viable and fertile (Elliott et al., 2010). It is important to remember that while *Drosophila* and zebrafish express just one ELMO isoform, in human and mouse there are three isoforms. Therefore, absence of one member might be compensated by an other of the same family and the phenotype is rescued.

In CHO cell line (Chinese Hamster Ovary) ELMO is associated with formation of protrusions as well as their maintenance, stabilizing the microtubule through direct interaction with ACF7 (Actin Crosslinking Family 7) (Margaron et al., 2013). In this thesis it is shown that ELMO is involved in filopodia formation. The mechanism through which ELMO promotes filopodia formation is thought to be through translocation of pre-existing DOCK4-DOCK9 complex. Alternately ELMO is responsible for DOCK4 translocation to the plasma membrane where interaction with DOCK9 follows and ELMO is rapidly released. A number of studies converge to show that ELMO has a role at the leading edge of the cell. In *Drosophila,* ELMO is responsible for Rac1 activation during border cell migration (Duchek et al., 2001; Erickson et al., 1997). During this process, border cells collectively start to move toward the egg chamber. ELMO activity is required for the lead

cell of the cluster to adopt an elongated morphology, and as such, to drive a mesenchymal-like mode of migration (Bianco et al., 2007). Expression of an open conformation and active mutant of ELMO1 is sufficient to promote cell elongation leading to DOCK180/Rac-dependent directed cell motility (Patel et al., 2010). It has been shown in Section 5.7 that DOCK4 mediates the binding between DOCK9 and ELMO. Published reports show that binding between ELMO and DOCK family occurs through the PH domain of ELMO and the first 200 amino acid of the SH_3 domain at the N-terminus of the relevant DOCK (Komander et al., 2008). However DOCK9 lacks the SH_3 domain and this could explain why DOCK4 mediates the ELMO-DOCK9 interaction.

The DOCK4-DOCK9 binding is a novel finding. Interaction between these two DOCK members is a new mechanism to control activation of Rho GTPases and filopodia formation. As shown in Figure 5.10, both DHR2 and SH_3 domains are necessary for the complex to form. Data produced in the laboratory provided evidence that DOCK4 (as well as other GEFs, as shown in literature (Kulkarni et al., 2011), homodimerizes through the DHR2 domain (data not shown). It is possible therefore to speculate that after DOCK4 activates Rac1 through the DHR2 domain, the DOCK4 SH_3 domain is directly involved in the binding with DOCK9. Analysis of the DOCK9 structure has highlighted 9 proline rich regions. Proteomic studies demonstrated that the SH_2 and SH_3 domains (Scr homology domain) have a very high affinity towards to proline rich regions (Kay et al., 2000). This explains the involvement of the DOCK4 SH_3 domain in binding DOCK9 and the result shown in Figure 5.11, where endogenous DOCK9 is pulled-down by the SH_3 domain of this DOCK. It has also been shown that VEGF-driven filopodia formation is dramatically affected in absence of Rac1. It is still unclear whether Rac1 plays a role in DOCK4-DOCK9 complex formation and further work should be carried out to unravel the precise role of each component described in this thesis. Ultimately, targeting of the DOCK4-DOCK9 complex could represent a pharmacological tool to diminish aberrant angiogenesis, and therefore cancer growth, in those highly vascularized tumours.

Chapter 6

Final Discussion

6.1 Overview and possible therapeutical outcomes

It has been over 40 years since Judah Folkman published a paper titled "Tumour angiogenesis: therapeutic implications" which put forward the concepts that i. the growth of blood vessels is necessary for the development of tumours; ii. tumours express pro-angiogenic factors to promote the growth of blood vessels and iii. inhibiting angiogenesis represents a potential therapeutic strategy for treating cancer (Folkman, 1971). Although taking several decades, these concepts are now widely accepted and are the subject of intense research activity.

VEGF was originally identified as Vascular Permeability factor (VPF; Dvorak et al., 1991) but was subsequently shown to be a potent pro-angiogenic factor with broad roles. The vascularization of tumours varies together with vessel function and that determines the response to chemotherapy drugs. Malignant cells regulate the release of VEGF and other growth factors at a transcriptional level and through hypoxia-induced mechanisms. As a result, VEGF is expressed at abnormally high levels and acts rapidly on endothelial cells in vessels to induce vascular permeability and, over a longer time frame, endothelial cell proliferation and angiogenesis.

As a result of VEGF activity the vascular network in tumours is abnormal and tortuous, with leaking and dysfunctional vessels that create a highly disorganized endothelium (Jain, 2005; Mazzone et al., 2009).

Blockage of the VEGF downstream signaling cascade causes tumour regression (Beck et al., 2010); therefore targeting tumour angiogenesis has been considered a useful strategy in reducing the tumour mass and in improving the therapeutic spectrum. Angiogenesis inhibitors interfere with various steps during tumour angiogenesis and some have been tested in clinical trials (Kerbel and Folkman, 2002; Herbst et al., 2002; Srishar et al., 2003). A number of anti-VEGF drugs are now available and licenced for use in the clinic. These include antibodies against VEGF-A (Bevacizumab (Avastin)) or its receptors (Pazopanib (AV-951),) and receptor tyrosine kinase (RTK) inhibitors (Sorafenib (Nexavar) or Sunitinib (Votrient)) that preferentially target VEGFR2 with high affinity (Ferrara et al., 2004; Harris et al., 2008; Wilhelm et al., 2006; O'Farrell et al., 2003). The Food and Drug Administration (FDA) has approved the use of anti-angiogenesis inhibitors as therapy in

cancer. Bevacizumab is currently used as a single agent for the treatment of glioblastoma (where other chemotherapeutic drugs have failed) and in combination with other drugs for the treatment of metastatic colorectal cancer and renal carcinoma. Sorafenib is approved for hepatocellular carcinoma and kidney cancer; Sunitinib for both kidney cancer and neuroendocrine tumours, and Pazopanib for kidney cancer.

Although anti-VEGF therapy has been beneficial in some cases as mentioned above, overall the benefits of the treatment seen in mouse tumour xenograft models have not been translated to the clinic. This is due to an increase in hypoxia and the resulting tumour angiogenesis that occurs in tumours where vessels have been disrupted through therapeutic intervention. In addition, an increasing number of reports show that the tumour micro-environment sustains tumour growth and augments chemotherapy resistance (Loges et al., 2010).

It has been demonstrated that the anti-angiogenic therapy could transiently normalize the tumor vasculature (normalization window, Jain et al., 2001) and thus improve the delivery and effectiveness of therapeutic agents given during the normalization window (Jain, 2005). New generation drugs are being developed to extend the normalization window and therefore offer an opportunity to reduce anticancer resistance (Goel et al., 2011).

VEGF, through its tyrosine kinase receptors, activates a plethora of signaling cascade including PI3K/AKT (involved in cell survival, Abid et al., 2004) and MAP kinase (involved in cell proliferation, Olsoon et al., 2006). More recently, VEGF has been identified as inducing cytoskeletal changes in the endothelium through activation of Rho GTPases, leading to cell migration and metastasis.

Data presented in this thesis have identified a new signaling module activated downstream of VEGF in endothelial cells and highlighted some novel findings in VEGF-stimulated endothelial cells:

i. Rac1 acts upstream of Cdc42 to control filopodia formation.
ii. DOCK4 and DOCK9 form a complex to regulate filopodia formation.
iii. The signaling axis SGEF-RhoG-DOCK4-Rac1-DOCK9-Cdc42 controls lateral filopodia formation and branches downstream of VEGF.

These findings delineate some new VEGF-dependent signaling modules, which themselves may represent some novel therapeutic targets.

Although it was previously known that Rac1 is involved in filopodia formation, acting through Cdc42, it was thought that Cdc42 acted upstream of Rac1. However, the use of dominant negative mutants in mammalian cells as well as genetic studies in *C. elegans* suggested that Rac1 operates downstream of Cdc42 (Nobes and Hall, 1995; Demarco et al., 2012). The knockdown studies presented in this thesis strongly support Rac1 having a role upstream of Cdc42, at least in the process of filopodia formation. It is possible that different signaling modules, with different cellular endpoints, may place Cdc42 and Rac1 in different hierarchies. As for Cdc42, Rac1 has been reported to be upstream or downstream of RhoG depending on the cell type and cellular activity. For instance, Rac1 is activated downstream of RhoG to mediate neurite outgrowth in PC12 stimulated with BDNF (Brain Derived Neurotrophic Factor, Namekata et al., 2013) while Rac1 is activated by Trio upstream of RhoG in endothelial cell to induce remodeling of F-actin and formation of endothelial docking structure to favour leukocyte transmigration (Van Buul et al., 2012).

The interaction between DOCK4 and DOCK9 is described here for the first time. DOCK4 is known as a Rac1 GEF and DOCK9 is known as a Cdc42 GEF. The activation of DOCK4-Rac1-DOCK9-Cdc42 signaling downstream of VEGF may be through an association of DOCK4 with VEGFR2, either directly or through an adaptor molecule. Similar mechanisms of activation have been shown for other GEFs. For instance RTKs stimulate the phosphorylation of the Rac1 and RhoG positive regulator Vavs (Hunter et al., 2006; Samson et al., 2010) through phosphorylation of Tyr^{172} residue in the N-terminal of the DH domain (Aghazadeh et al., 1998). Another example is represented by SOS (a Rac1 GEF), which is recruited in the cytosol and anchored to RTKs by the adaptor molecule Grb (McKay and Morrison, 2007).

The results generated using the co-culture model suggest that endothelial cells lacking DOCK4 and DOCK9 still create a vascular network, but one that is defective as it lacks branches. Vessels appeared thinner and unable to sprout. This is because the VEGF-driven signaling cascade here reported spatially controls the distribution of endothelial cell

filopodia since knockdown of any of the positive regulators mentioned (SGEF, DOCK4 and DOCK9) dramatically affects tip filopodia while the effect on tip cells is milder (Figure 4.3, Figure 1.10, Figure 5.2).

In support of this finding, independent work by collaborators in the Pawson laboratory have shown DOCK4-DOCK9 complex formation in HEK 293T cells and identified Elmo as a common DOCK4 and DOCK9 binding partner through proteomic studies (personal communication).

In vivo experiments selectively targeting DOCK4 expression in tumor vasculature showed reduction of vessel calibre in those lacking DOCK4 compared to control vessels (data not shown), suggesting an impairment in cell-cell interaction, consistent with observations *in vitro*. It will be interesting to perform the same experiment with DOCK9 knockdown and analyse tumour angiogenesis. Based on the results shown in this thesis, knockdown of DOCK9 in the vasculature might be expected to show a reduction in filopodia formation and therefore sprouting angiogenesis and ultimately lumen calibre as seen for DOCK4 knockdown.

Whilst the work described here identified the DOCK4 SH_3 domain as required for interaction with DOCK9, it is still unclear which domain is used by DOCK9 in this context. Further studies are therefore necessary to pinpoint the amino acids required for DOCK9 binding to DOCK4. One approach would be to use DOCK9 deletion mutants, as previously used for DOCK4, to determine which domain is involved in the binding. Analysis of the DOCK9 amino acid sequence has shown that there are 9 proline rich regions in the DOCK9 structure. Due to the high affinity of proline to the SH_3 domain it might be that binding between SH_3-PxxP mediates DOCK4-DOCK9 complex formation. If this were the case, disruption of the SH_3-proline interaction could contribute to reduction of tumour angiogenesis in a number of vascularized tumours and thus potentially represents a new therapeutic target in addition to existing anti-VEGF therapies. A number of reports has shown that blockage of the SH_3-proline binding can be beneficial in tumours. For instance the GEF-ARF6 effector AMAP1 binds SH_3 domain of cortactin via its proline-rich peptide

to control cancer cell invasion (Hashimoto et al., 2006). Disruption of the SH_3 domain proline-rich ligand blocked metastasis in a variety of tumours including breast cancer, glioblastoma and lung carcinoma in mouse models (Hashimoto et al., 2006). UCS15A, also designed to disrupt the binding between SH_3 and proline (Oneyama et al., 2002), has shown reduction of breast cancer invasion (Hashimoto et al., 2006).

The findings described in this thesis show a VEGF-driven signaling cascade, summarized in Figure 6.1. There are however a number of questions still to address. It would interesting to determine the precise mechanism through which Rac1 controls filopodia formation and activation of DOCK9 and whether Rac1 plays a role in DOCK4-DOCK9 binding complex. How SGEF is activated downstream VEGFR and whether SGEF activation impacts on DOCK4-DOCK9 complex formation also need to be clarified.

Overall this thesis gives evidence of a novel signaling axis that mediates VEGF-driven filopodia formation and lateral branching in vessels and provides possible new therapeutic targets when targeting tumour angiogenesis.

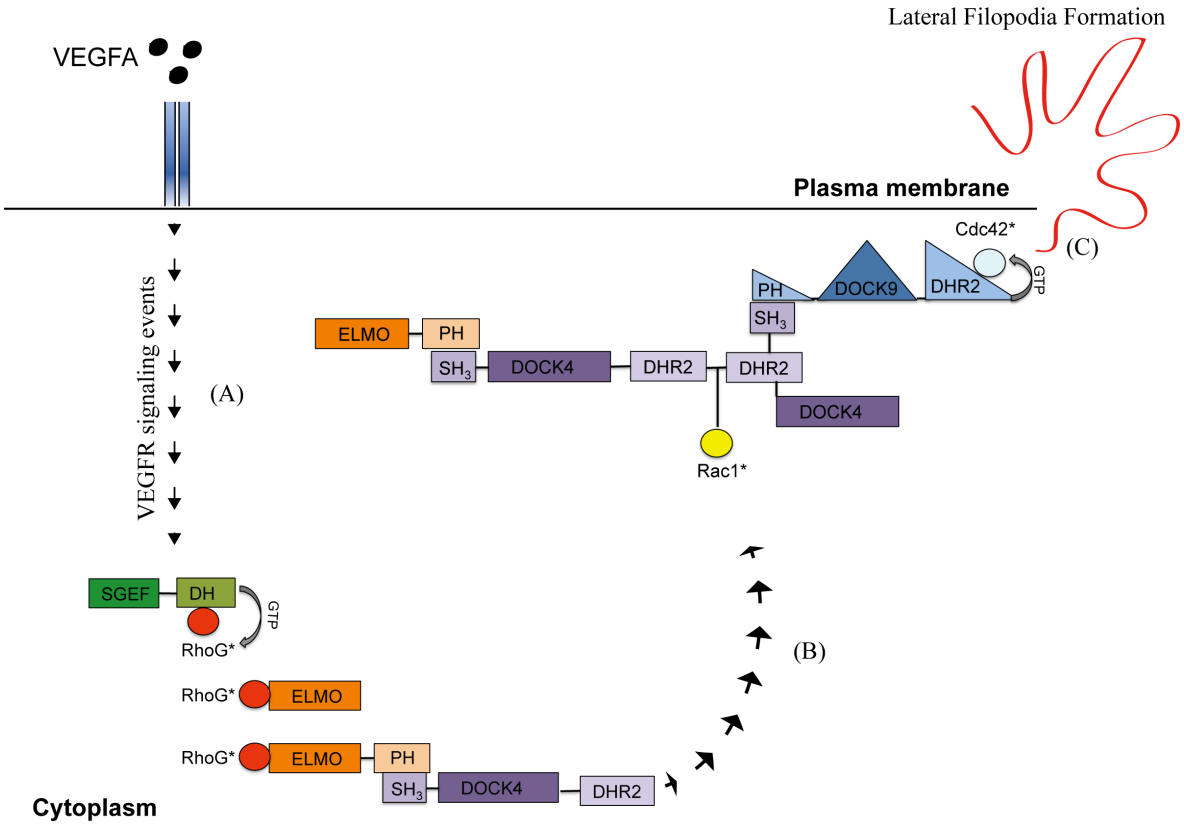

Figure 6.1 Model of interaction of signaling components controlling lateral filopodia downstream of VEGF

(A) Interaction between VEGFA and its receptor triggers a signaling cascade that activates the guanine nucleotide exchange factor SGEF (in green). SGEF, through the DH domain, switches RhoG in the active state (RhoG*). Once activated, RhoG* binds the scaffolding protein Elmo (in orange) and (B) mediates the translocation of DOCK4 (in purple) from the cytoplasm to the plasma membrane where it activates Rac1 (in yellow) *via* the DHR2 domain and bind DOCK9 (in blue) through the SH_3 domain. Activation of GTP-Rac1 (Rac1*) leads to Cdc42 dependent filopodia formation downstream of DOCK9.

APPENDIX

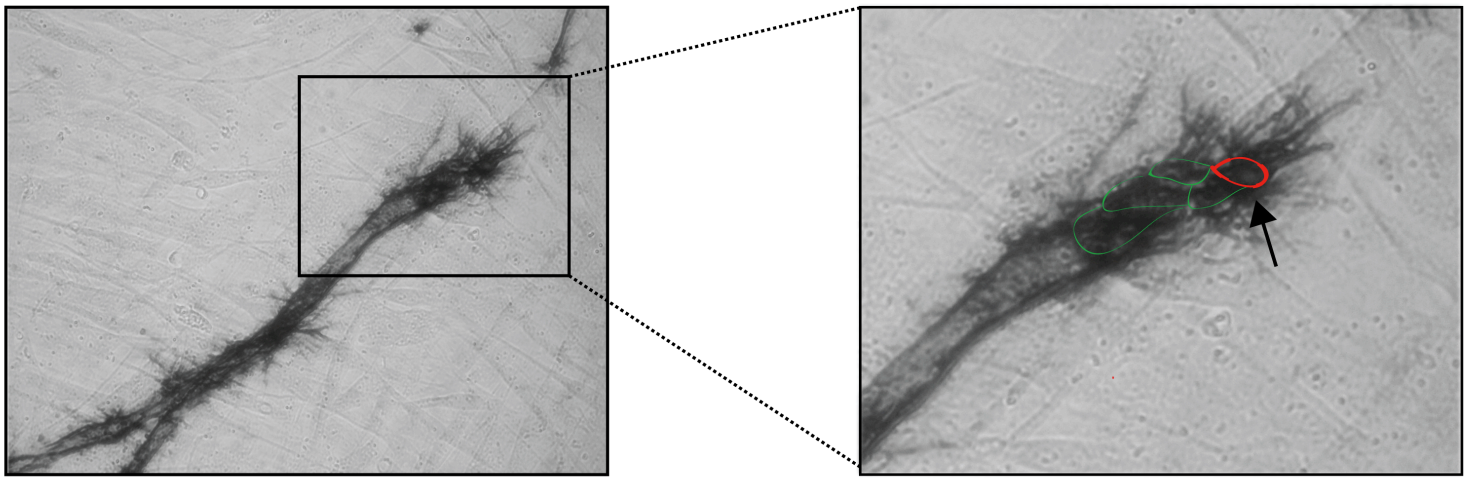

Figure 1 Tip and lateral filopodia quantification
HUVEC were seeded onto confluent fibroblasts and the co-cultures were stained for CD31 (dark stain) 5 days after seeding. For tip and lateral filopodia counting, 40x images from a compound microscope were enlarged and the background was reduced using ImageJ software (Section 2.5). The CD31 staining solely marked the ECs making a clear distinction between one cell and the neighboring ones. The first cell of the tubule (in red) is called tip cell and filopodia quantified as tip filopodia. Cells that follow the tip cell are called lateral cells (in green) and filopodia are quantified as lateral filopodia.

Sample	Target name	RQ	RQ Min	RQ Max	Ct	Ct Mean	Ct SD	ΔCt Mean
Non targeting	RHO G	1	0.76013273	1.3155597	23.49265	23.42940	0.10659374	5.26290
Non targeting	RHO G	1	0.76013273	1.3155597	23.83848	23.42940	0.10659374	5.26290
Non targeting	RHO G	1	0.76013273	1.3155597	23.47839	23.42940	0.10659374	5.26290
RhoG SP	RHO G	0.13890883	0.118490554	0.16284558	25.90994	25.86396	0.03223337	7.29866
RhoG SP	RHO G	0.13890883	0.118490554	0.16284558	25.88010	25.86396	0.03223337	7.29866
RhoG SP	RHO G	0.13890883	0.118490554	0.16284558	25.80184	25.86396	0.03223337	7.29866
RhoG ot5	RHO G	0.21150732	0.18795753	0.23800775	24.88338	24.89592	0.03450741	7.50412
RhoG ot5	RHO G	0.21150732	0.18795753	0.23800775	24.96097	24.89592	0.03450741	7.50412
RhoG ot5	RHO G	0.21150732	0.18795753	0.23800775	24.84342	24.89592	0.03450741	7.50412
RhoG ot7	RHO G	0.3587027	0.39607316	0.53123564	24.53796	24.88679	0.01620757	7.38727
RhoG ot7	RHO G	0.3587027	0.39607316	0.53123564	24.57105	24.88679	0.01620757	7.38727
RhoG ot7	RHO G	0.3587027	0.39607316	0.53123564	24.99399	24.88679	0.01620757	7.38727
Non targeting	GAPDH				18.32118	18.167	0.09459098	
Non targeting	GAPDH				18.18349	18.167	0.09459098	
Non targeting	GAPDH				17.99483	18.167	0.09459098	
RhoG SP	GAPDH				17.89777	17.753	0.07606357	
RhoG SP	GAPDH				17.72217	17.753	0.07606357	
RhoG SP	GAPDH				17.63984	17.753	0.07606357	
RhoG ot5	GAPDH				17.49269	17.392	0.05071054	
RhoG ot5	GAPDH				17.33236	17.392	0.05071054	
RhoG ot5	GAPDH				17.35035	17.392	0.05071054	
RhoG ot7	GAPDH				17.63895	17.500	0.07454021	
RhoG ot7	GAPDH				17.47550	17.500	0.07454021	
RhoG ot7	GAPDH				17.38411	17.500	0.07454021	

Figure 2 RhoG knockdown in HUVEC

HUVEC were lysed for RNA extraction 72hrs after transfection and gene knockdown was assessed through qRT-PCR (Section 2.2.2). Raw data (relative quantification of the amplified RhoG mRNA product (RQ); minimum and maximum quantification of the amplified RhoG mRNA product (RQmin and RQmax); relative quantification of threshold cycle numbers of the amplified RhoG mRNA (Ct); average cycle numbers (Ct Mean); cycle number standard deviation (Ct SD) and average of cycle numbers of the amplified RhoG mRNA compared to average of cycle numbers of the reference gene GAPDH (ΔCT Mean) were generated by Applied Biosystem 7900 SDS software. Relative quantification (RQ) was performed using the ΔΔCt method (Fleige and Pfaffl, 2006). qRT-PCR analysis was performed using the one step BRILLIANT II SYBR Green qRT-PCR MasterMix Kit (Applied Biosystems). RhoG knockdown in RhoG Standard pool siRNA or RhoG On-Target transfected sample was quantified as 86%, 79% or 64% respectively. Knockdown percentages were generated by comparing RhoG mRNA levels in RhoG transfected sample (RhoG SP RQ=0.139; RhoG ot5 RQ=0.211; RhoG ot7 RQ=0.36) to RhoG mRNA level in non targeting control sample (non targeting RQ=1).

Sample	Target name	RQ	RQ Min	RQ Max	Ct	Ct Mean	Ct SD	ΔCt Mean
Non targeting	SGEF	1	0.933148503	1.07164085	23.34979057	23.27396202	0.06793944	10.36837769
Non targeting	SGEF	1	0.933148503	1.07164085	23.21863365	23.27396202	0.06793944	10.36837769
Non targeting	SGEF	1	0.933148503	1.07164085	23.25345993	23.27396202	0.06793944	10.36837769
SGEF ot5	SGEF	0.373071158	0.415299803	0.53887898	26.21006966	26.17518806	0.08482528	11.44824886
SGEF ot5	SGEF	0.373071158	0.415299803	0.53887898	26.07848549	26.17518806	0.08482528	11.44824886
SGEF ot5	SGEF	0.373071158	0.415299803	0.53887898	26.23701477	26.17518806	0.08482528	11.44824886
SGEF ot6	SGEF	0.487143505	0.609231412	0.77501947	25.44344139	25.40965271	0.04778306	10.90969467
SGEF ot6	SGEF	0.487143505	0.609231412	0.77501947	25.37586594	25.40965271	0.04778306	10.90969467
Non targeting	GAPDH				12.90279579	12.90558338	0.03822112	
Non targeting	GAPDH				12.94354057	12.90558338	0.03822112	
Non targeting	GAPDH				12.84070396	14.72694111	0.04664206	
SGEF ot5	GAPDH				14.69396019	14.72694111	0.04664206	
SGEF ot5	GAPDH				14.75992203	14.49995899	0.07419027	
SGEF ot6	GAPDH				14.53443718	14.49995899	0.07419027	
SGEF ot6	GAPDH				14.4148035	14.49995899	0.07419027	
SGEF ot6	GAPDH				14.55063629	14.49995899	0.07419027	

Figure 3 SGEF knockdown in HUVEC

HUVEC were lysed for RNA extraction 72hrs after transfection and gene knockdown was assessed through qRT-PCR (Section 2.2.2). Raw data (relative quantification of the amplified SGEF mRNA product (RQ); minimum and maximum quantification of the amplified SGEF mRNA product (RQmin and RQmax); relative quantification of threshold cycle numbers of the amplified SGEF mRNA (Ct); average cycle numbers (Ct Mean); cycle number standard deviation (Ct SD) and average of cycle numbers of the amplified SGEF mRNA compared to average of cycle numbers of the reference gene GAPDH (ΔCT Mean) were generated by Applied Biosystem 7900 SDS software. Relative quantification (RQ) was performed using the ΔΔCt method (Fleige and Pfaffl, 2006). qRT-PCR analysis was performed using the one step BRILLIANT II SYBR Green qRT-PCR Master Mix Kit (Applied Biosystems).

SGEF knockdown in SGEF On-Target transfected sample (ot5 and ot6) was quantified as 63% and 51% respectively. Knockdown percentages were generated by comparing SGEF mRNA levels in SGEF transfected sample (SGEF ot5 RQ=0.37; SGEF ot6 RQ=0.48) to SGEF mRNA level in non targeting control sample (non targeting RQ=1).

Sample	Target name	RQ	RQ Min	RQ Max	Ct	Ct Mean	Ct SD	ΔCt Mean
Mock	TRIO	1	0.927463889	1.07820916	15.73671913	15.70692158	0.02593889	3.512927294
Mock	TRIO	1	0.927463889	1.07820916	15.69465065	15.70692158	0.02593889	3.512927294
Mock	TRIO	1	0.927463889	1.07820916	15.68939495	15.70692158	0.02593889	3.512927294
TRIO 5	TRIO	0.480319142	0.458491385	0.50318611	16.70581436	16.70410347	0.00900911	4.570862293
TRIO 5	TRIO	0.480319142	0.458491385	0.50318611	16.71213341	16.70410347	0.00900911	4.570862293
TRIO 5	TRIO	0.480319142	0.458491385	0.50318611	16.69436073	16.70410347	0.00900911	4.570862293
TRIO 6	TRIO	0.684248745	0.572124481	0.8183471	16.29487228	16.39024544	0.15411034	4.060334682
TRIO 6	TRIO	0.684248745	0.572124481	0.8183471	16.56803894	16.39024544	0.15411034	4.060334682
TRIO 6	TRIO	0.684248745	0.572124481	0.8183471	16.30782318	16.39024544	0.15411034	4.060334682
TRIO 7	TRIO	0.49935922	0.442798197	0.56314504	16.61058998	16.52986336	0.07814369	4.51477766
TRIO 7	TRIO	0.49935922	0.442798197	0.56314504	16.52441406	16.52986336	0.07814369	4.51477766
TRIO 7	TRIO	0.49935922	0.442798197	0.56314504	16.45458794	16.52986336	0.07814369	4.51477766
TRIO SP	TRIO	0.572685063	0.402935445	0.81394714	16.4777298	16.6128006	0.27423295	4.3171134
TRIO SP	TRIO	0.572685063	0.402935445	0.81394714	16.92836952	16.6128006	0.27423295	4.3171134
TRIO SP	TRIO	0.572685063	0.402935445	0.81394714	16.43230247	16.6128006	0.27423295	4.3171134
Non targeting	TRIO	1.019278646	0.775304973	1.34002614	16.12660789	15.85708332	0.2359824	3.485378981
Non targeting	TRIO	1.019278646	0.775304973	1.34002614	15.68760967	15.85708332	0.2359824	3.485378981
Non targeting	TRIO	1.019278646	0.775304973	1.34002614	15.75703049	15.85708332	0.2359824	3.485378981
Mock	GAPDH				12.22466564	12.19399357	0.06261149	
Mock	GAPDH				12.12196064	12.19399357	0.06261149	
Mock	GAPDH				12.23535633	12.19399357	0.06261149	
TRIO 5	GAPDH				12.09714794	12.1332407	0.04087771	
TRIO 5	GAPDH				12.17763042	12.1332407	0.04087771	
TRIO 5	GAPDH				12.12494373	12.1332407	0.04087771	
TRIO 6	GAPDH				12.28602791	12.32991028	0.04683474	
TRIO 6	GAPDH				12.37922382	12.32991028	0.04683474	
TRIO 6	GAPDH				12.3244791	12.32991028	0.04683474	
TRIO 7	GAPDH				11.93314457	12.01508617	0.07482591	
TRIO 7	GAPDH				12.03232861	12.01508617	0.07482591	
TRIO 7	GAPDH				12.0797863	12.01508617	0.07482591	
TRIO SP	GAPDH				12.45118046	12.29568768	0.15782639	
TRIO SP	GAPDH				12.30025387	12.29568768	0.15782639	
TRIO SP	GAPDH				12.13562679	12.29568768	0.15782639	
Non targeting	GAPDH				12.44339657	12.3717041	0.07031908	
Non targeting	GAPDH				12.30284405	12.3717041	0.07031908	
Non targeting	GAPDH				12.36887074	12.3717041	0.07031908	

Figure 4 Trio knockdown in HUVEC

HUVEC were lysed for RNA extraction 72hrs after transfection and gene knockdown was assessed through qRT-PCR (Section 2.2.2). Raw data (relative quantification of the amplified Trio mRNA product (RQ); minimum and maximum quantification of the amplified Trio mRNA product (RQmin and RQmax); relative quantification of threshold cycle numbers of the amplified Trio mRNA (Ct); average cycle numbers (Ct Mean); cycle number standard deviation (Ct SD) and average of cycle numbers of the amplified Trio mRNA compared to average of cycle numbers of the reference gene GAPDH (ΔCT Mean) were generated by Applied Biosystem 7900 SDS software. Relative quantification (RQ) was performed using the $\Delta\Delta C_t$ method (Fleige and Pfaffl, 2006). qRT-PCR analysis was performed using the one step BRILLIANT II SYBR Green qRT-PCR Master Mix Kit (Applied Biosystems).

Trio knockdown in Trio On-Target oligonucleotide transfected samples (Trio ot5, ot6, ot7 and Trio Standand pool (SP)) was quantified as 52%, 32%, 50% and 43% respectively. Knockdown percentages were generated by comparing Trio mRNA level in Trio transfected samples (Trio ot5 RQ=0.48; Trio ot6 RQ=0.68; Trio ot7 RQ=0.50; Trio SP RQ=0.57) to non targeting control sample (non targeting RQ=1).

Sample	Target name	RQ	RQ Min	RQ Max	Ct	Ct Mean	Ct SD	ΔCt Mean
Non targeting	RhoG	1	0.860964298	1.16148841	33.71115875	33.62428284	0.1228584	10.71870041
Non targeting	RhoG	1	0.860964298	1.16148841	33.53741074	33.62428284	0.1228584	10.71870041
RhoG	RhoG	0.211134736	0.375805944	1.52539647	36.36075211	36.64456558	0.40137288	11.12007904
RhoG	RhoG	0.211134736	0.375805944	1.52539647	36.92837906	36.64456558	0.40137288	11.12007904
Non targeting	GAPDH				12.90449047	12.90558338	0.03822112	
Non targeting	GAPDH				12.94517994	12.90558338	0.03822112	
Non targeting	GAPDH				12.89678955	12.90558338	0.03822112	
RhoG	GAPDH				14.79572392	14.52448654	0.24667729	
RhoG	GAPDH				14.4641819	14.52448654	0.24667729	
RhoG	GAPDH				14.31355286	14.52448654	0.24667729	
Non targeting	SGEF	1	0.933148503	1.07164085	23.34979057	23.27396202	0.06793944	10.36837769
Non targeting	SGEF	1	0.933148503	1.07164085	23.21863365	23.27396202	0.06793944	10.36837769
Non targeting	SGEF	1	0.933148503	1.07164085	23.25345993	23.27396202	0.06793944	10.36837769
SGEF OT5	SGEF	0.373071158	0.415299803	0.53887898	26.21006966	26.17518806	0.08482528	11.44824886
SGEF OT5	SGEF	0.373071158	0.415299803	0.53887898	26.07848549	26.17518806	0.08482528	11.44824886
SGEF OT5	SGEF	0.373071158	0.415299803	0.53887898	26.23701477	26.17518806	0.08482528	11.44824886
SGEF OT6	SGEF	0.487143505	0.609231412	0.77501947	25.44344139	25.40965271	0.04778306	10.90969467
SGEF OT6	SGEF	0.487143505	0.609231412	0.77501947	25.37586594	25.40965271	0.04778306	10.90969467
Non targeting	GAPDH				12.90279579	12.90558338	0.03822112	
Non targeting	GAPDH				12.94354057	12.90558338	0.03822112	
Non targeting	GAPDH				12.84070396	12.90558338	0.03822112	
SGEF OT5	GAPDH				14.69396019	14.72694111	0.04664206	
SGEF OT5	GAPDH				14.75992203	14.72694111	0.04664206	
SGEF OT6	GAPDH				14.53443718	14.49995899	0.07419027	
SGEF OT6	GAPDH				14.4148035	14.49995899	0.07419027	
SGEF OT6	GAPDH				14.55063629	14.49995899	0.07419027	
Non targeting	TRIO	1	0.915171981	1.09269083	19.39157104	19.3487606	0.03788137	5.684366703
Non targeting	TRIO	1	0.915171981	1.09269083	19.33512306	19.3487606	0.03788137	5.684366703
Non targeting	TRIO	1	0.915171981	1.09269083	19.31958389	19.3487606	0.03788137	5.684366703
TRIO OT5	TRIO	0.572206616	0.498669475	0.65658802	20.27345467	20.27721405	0.05287479	6.489758492
TRIO OT5	TRIO	0.572206616	0.498669475	0.65658802	20.33186913	20.27721405	0.05287479	6.489758492
TRIO OT5	TRIO	0.572206616	0.498669475	0.65658802	20.22632027	20.27721405	0.05287479	6.489758492
TRIO OT7	TRIO	0.522552752	0.587812662	0.65934598	19.94623375	19.93004036	0.01917526	6.368098736
TRIO OT7	TRIO	0.522552752	0.587812662	0.65934598	19.93502426	19.93004036	0.01917526	6.368098736
TRIO OT7	TRIO	0.522552752	0.587812662	0.65934598	19.90886688	19.93004036	0.01917526	6.368098736
Non targeting	GAPDH				13.76395988	13.66439342	0.12115951	
Non targeting	GAPDH				13.69110203	13.66439342	0.12115951	
Non targeting	GAPDH				13.81225586	13.66439342	0.12115951	
TRIO OT5	GAPDH				13.69795322	13.78745651	0.11194279	
TRIO OT5	GAPDH				13.75144196	13.78745651	0.11194279	
TRIO OT5	GAPDH				13.9129734	13.78745651	0.11194279	
TRIO OT7	GAPDH				13.5992012	13.56194305	0.04798929	
TRIO OT7	GAPDH				13.57883644	13.56194305	0.04798929	
TRIO OT7	GAPDH				13.50779152	13.56194305	0.04798929	

Figure 5 RhoG, SGEF and Trio knockdown in HUVEC

HUVEC were lysed for RNA extraction 72hrs after transfection and gene knockdown was assessed through qRT-PCR (Section 2.2.2). Raw data (relative quantification of the amplified mRNA product (RQ); minimum and maximum quantification of the amplified mRNA product (RQmin and RQmax); relative quantification of threshold cycle numbers of the amplified mRNA (Ct); average cycle numbers (Ct Mean); cycle number standard deviation (Ct SD) and average of cycle numbers of the amplified mRNA compared to average of cycle numbers of the reference gene GAPDH (ΔCT Mean) were generated by Applied Biosystem 7900 SDS software. Relative quantification (RQ) was performed using the $\Delta\Delta C_t$ method (Fleige and Pfaffl, 2006). qRT-PCR analysis was performed using the one step BRILLIANT II SYBR Green qRT-PCR Master Mix Kit (Applied Biosystems). RhoG knockdown in RhoG Standard pool siRNA was quantified as 79%. SGEF knockdown in SGEF On-Target oligonucleotide transfected samples (SGEF ot5 and ot6) was quantified as 63% and 52%, respectively. Trio knockdown in Trio On-Target oligonucleotide transfected samples (Trio ot5, and ot7) was quantified as 43% and 48% respectively. Knockdown percentages were generated by comparing mRNA level of the gene of interest in RhoG, SGEF and Trio siRNA transfected samples (RhoG SP RQ=0.21; SGEF ot5 RQ=0.37; SGEF ot6 RQ=0.48; Trio ot5 RQ=0.57; Trio ot7 RQ=0.57) to non targeting control sample (non targeting RQ=1).

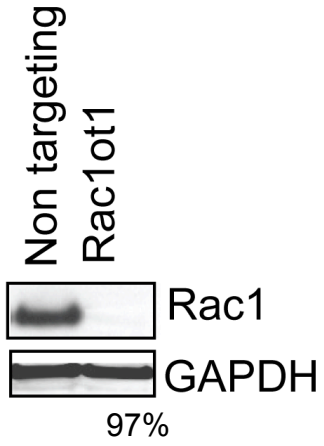

Figure 6 Rac1 knockdown in HUVEC
Level of Rac1 protein expression was assessed by western blotting, comparing knockdown using Rac1 On-Target 1 (Rac1 ot1) to the non targeting control, after normalization against the housekeeping gene GAPDH. Rac1 knockdown in Rac1 On-Target oligonucleotide transfected sample was quantified as 97% using Image j 1.46 software 48hrs after transfection.

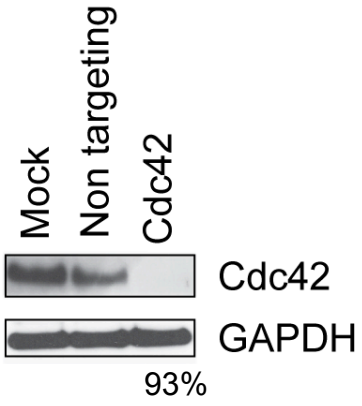

Figure 7 Cdc42 knockdown in HUVEC
Level of Cdc42 protein expression was assessed by western blotting, comparing knockdown using Cdc42 Standard pool (Cdc42) to the non targeting control, after normalization against the housekeeping gene GAPDH. Cdc42 knockdown in Cdc42 siRNA transfected sample was quantified as 93% using Image j 1.46 software 48hrs after transfection.

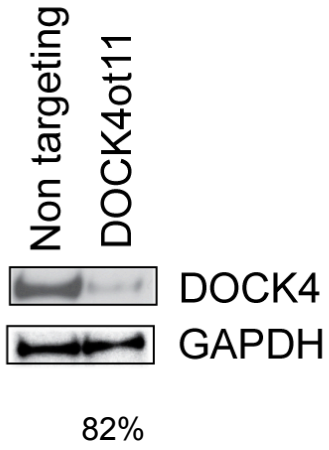

Figure 8 DOCK4 knockdown in HUVEC
Level of DOCK4 protein expression was assessed by western blotting, comparing knockdown using DOCK4 On-Target oligonucleotide 11 (DOCK4ot11) to the non-targeting control after normalization against the housekeeping gene GAPDH. DOCK4 knockdown in DOCK4 On-Target oligonucleotide transfected sample was quantified as 82% using Image j 1.46 software 48hrs after transfection.

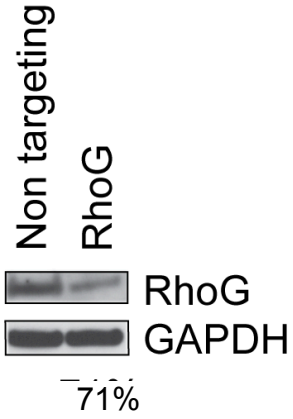

Figure 9 RhoG knockdown in HUVEC
Level of RhoG protein expression was assessed by western blotting, comparing knockdown using RhoG Standard pool siRNA (RhoG) to the non-targeting control after normalization against the housekeeping gene GAPDH. RhoG knockdown in RhoG transfected sample was quantified as 71% using Image j 1.46 software 48hrs after transfection.

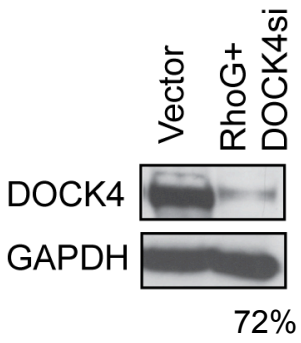

Figure 10 DOCK4 knockdown in RhoG overexpressed HEK 293T cells
Level of DOCK4 protein expression was assessed by western blotting, comparing knockdown using DOCK4 Standard pool siRNA in sample in which RhoG was overexpressed (RhoG+DOCK4si) to the non-targeting control. Samples were normalized against the housekeeping gene GAPDH. DOCK4 knockdown in DOCK4 transfected sample was quantified as 72% using Image j 1.46 software 48hrs after transfection.

Sample	Target name	RQ	RQ Min	RQ Max	Ct	Ct Mean	Ct SD	ΔCt Mean
Non targeting	DOCK9	1	0.827924132	1.2078402	20.7674408	20.83288574	0.09255178	7.053389072
Non targeting	DOCK9	1	0.827924132	1.2078402	20.89832878	20.83288574	0.09255178	7.053389072
DOCK9	DOCK9	0.154463604	0.097559407	0.24455875	24.95564651	24.78483772	0.30187598	9.74805069
DOCK9	DOCK9	0.154463604	0.097559407	0.24455875	24.43628502	24.78483772	0.30187598	9.74805069
DOCK9	DOCK9	0.154463604	0.097559407	0.24455875	24.96258354	24.78483772	0.30187598	9.74805069
Non targeting	GAPDH				13.80911636	13.77949524	0.09557876	
Non targeting	GAPDH				13.67261314	13.77949524	0.09557876	
Non targeting	GAPDH				13.85675716	13.77949524	0.09557876	
DOCK9	GAPDH				14.92270947	15.03678799	0.16133139	
DOCK9	GAPDH				14.0711956	14.23545456	0.23229657	
DOCK9	GAPDH				14.39971256	14.23545456	0.23229657	

Figure 11 DOCK9 knockdown in HUVEC
HUVEC were lysed for RNA extraction 72hrs after transfection and gene knockdown was assessed through qRT-PCR (Section 2.2.2). Raw data (relative quantification of the amplified DOCK9 mRNA product (RQ); minimum and maximum quantification of the amplified mRNA product (RQmin and RQmax); relative quantification of threshold cycle numbers of the amplified DOCK9 mRNA (Ct); average cycle numbers (Ct Mean); cycle number standard deviation (Ct SD) and average of cycle numbers of the amplified DOCK9 mRNA compared to average of cycle numbers of the reference gene GAPDH (ΔCT Mean) were generated by Applied Biosystem 7900 SDS software. Relative quantification (RQ) was performed using the $\Delta\Delta C_t$ method (Fleige and Pfaffl, 2006). qRT-PCR analysis was performed using the one step BRILLIANT II SYBR Green qRT-PCR Master Mix Kit (Applied Biosystems). DOCK9 knockdown in DOCK9 Standard pool siRNA transfected samples was quantified as 85% respectively. Knockdown percentages were generated by comparing DOCK9 mRNA level in DOCK9 transfected samples (DOCK9 RQ=0.15) to non targeting control sample (non targeting RQ=1).

Sample	Target name	RQ	RQ Min	RQ Max	Ct	Ct Mean	Ct SD	ΔCt Mean
Non targeting	DOCK9	1	0.873518765	1.14479506	19.42149734	19.43644905	0.11437042	5.772056103
Non targeting	DOCK9	1	0.873518765	1.14479506	19.55755997	19.43644905	0.11437042	5.772056103
Non targeting	DOCK9	1	0.873518765	1.14479506	19.33028984	19.43644905	0.11437042	5.772056103
DOCK9 ot10	DOCK9	0.315160745	0.368162274	0.4681589	20.44569969	20.3782444	0.06517408	7.040314198
DOCK9 ot10	DOCK9	0.315160745	0.368162274	0.4681589	20.37341309	20.3782444	0.06517408	7.040314198
DOCK9 ot10	DOCK9	0.315160745	0.368162274	0.4681589	20.31562042	20.3782444	0.06517408	7.040314198
DOCK9 ot11	DOCK9	0.254363388	0.183521345	0.35255152	20.49860954	20.77949524	0.2455747	7.747093201
DOCK9 ot11	DOCK9	0.254363388	0.183521345	0.35255152	20.95361519	20.77949524	0.2455747	7.747093201
DOCK9 ot11	DOCK9	0.254363388	0.183521345	0.35255152	20.88626289	20.77949524	0.2455747	7.747093201
	DOCK9				31.78017807			
	DOCK9				31.7446003			
	DOCK9				31.71156311			
Non targeting	GAPDH				13.66892147	13.66439342	0.12115951	
Non targeting	GAPDH				13.49297142	13.66439342	0.12115951	
Non targeting	GAPDH				13.55714607	13.66439342	0.12115951	
DOCK9 ot10	GAPDH				13.27685547	13.33792973	0.0862795	
DOCK9 ot10	GAPDH				13.43663311	13.33792973	0.0862795	
DOCK9 ot10	GAPDH				13.30030155	13.33792973	0.0862795	
DOCK9 ot11	GAPDH				13.07478428	13.03240204	0.05993687	
DOCK9 ot11	GAPDH				12.99002075	13.03240204	0.05993687	

Figure 12 DOCK9 knockdown HUVEC

HUVEC were lysed for RNA extraction 72hrs after transfection and gene knockdown was assessed through qRT-PCR (Section 2.2.2). Raw data (relative quantification of the amplified DOCK9 mRNA product (RQ); minimum and maximum quantification of the amplified DOCK9 mRNA product (RQmin and RQmax); relative quantification of threshold cycle numbers of the amplified DOCK9 mRNA (Ct); average cycle numbers (Ct Mean); cycle number standard deviation (Ct SD) and average of cycle numbers of the amplified DOCK9 mRNA compared to average of cycle numbers of the reference gene GAPDH (ΔCT Mean) were generated by Applied Biosystem 7900 SDS software. Relative quantification (RQ) was performed using the ΔΔCt method (Fleige and Pfaffl, 2006). qRT-PCR analysis was performed using the one step BRILLIANT II SYBR Green qRT-PCR Master Mix Kit (Applied Biosystems).

DOCK9 knockdown in DOCK9 On-Target oligonucleotide transfected samples (DOCK9 ot10 and DOCK9 ot11) was quantified as 69% and 75% respectively. Knockdown percentages were generated by comparing DOCK9 mRNA level in DOCK9 transfected samples (DOCK9 ot10 RQ=0.31; DOCK9 ot11 RQ=0.25) to non targeting control sample (non targeting RQ=1).

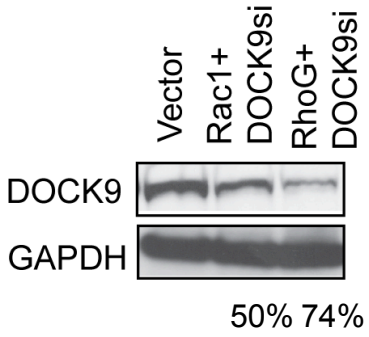

Figure 13 DOCK4 knockdown in RhoG overexpressed HEK 293T cells
Level of DOCK9 protein expression was assessed by western blotting, comparing knockdown using DOCK9 Standard pool siRNA in samples in which Rac1 (Rac1+DOCK9si) or RhoG (RhoG+DOCK9si) was overexpressed. Samples were normalized against the housekeeping gene GAPDH. DOCK9 knockdown in DOCK9 transfected sample was quantified as 50% and 74% respectively using Image j 1.46 software 48hrs after transfection.

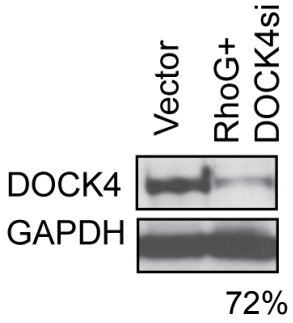

Figure 14 DOCK4 knockdown in RhoG overexpressed HEK 293T cells
Level of DOCK4 protein expression was assessed by western blotting, comparing knockdown using DOCK4 Standard pool siRNA in samples in which RhoG (RhoG+DOCK4si) where expressed. Samples were normalized against the housekeeping gene GAPDH. DOCK4 knockdown in DOCK4 transfected sample was quantified as 72% using Image j 1.46 software 48hrs after transfection.

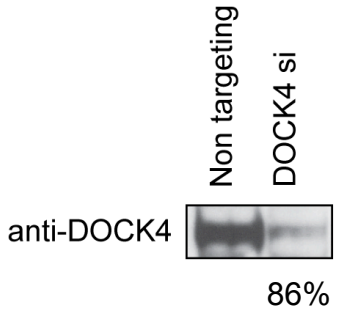

Figure 15 DOCK4 knockdown in HEK 293T cells
Level of DOCK4 protein expression was assessed by western blotting, comparing knockdown using DOCK4 Standard pool (DOCK4 si) to the non targeting control. DOCK4 knockdown in DOCK4 Standard pool oligonucleotide transfected sample was quantified as 86% using Image j 1.46 software 48hrs after transfection.

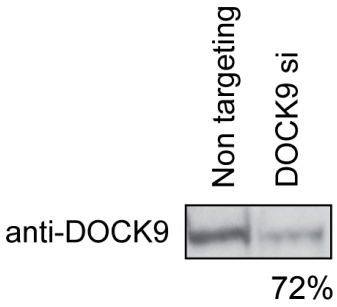

Figure 16 DOCK9 knockdown in HEK 293T cells
Level of DOCK9 protein expression was assessed by western blotting, comparing knockdown using DOCK9 Standard pool (DOCK9 si) to the non targeting control. DOCK9 knockdown in DOCK9 Standard pool oligonucleotide transfected sample was quantified as 86% using Image j 1.46 software 48hrs after transfection.

Sample	Target name	RQ	RQ Min	RQ Max	Ct	Ct Mean	Ct SD	ΔCt Mean
Non targeting	ELMO	1	0.697654307	1.43337464	23.02001381	22.81668854	0.18616492	6.573273182
Non targeting	ELMO	1	0.697654307	1.43337464	22.77545357	22.81668854	0.18616492	6.573273182
Non targeting	ELMO	1	0.697654307	1.43337464	22.65459824	22.81668854	0.18616492	6.573273182
ELMO 1	ELMO	0.090721391	0.078520216	0.10481849	27.29046249	27.40221596	0.10543501	10.03568649
ELMO 1	ELMO	0.090721391	0.078520216	0.10481849	27.4162674	27.40221596	0.10543501	10.03568649
ELMO 1	ELMO	0.090721391	0.078520216	0.10481849	27.49992371	27.40221596	0.10543501	10.03568649
Non targeting	ELMO	1	0.715232372	1.39814699	29.54163361	29.62888908	0.14368448	13.38547325
Non targeting	ELMO	1	0.715232372	1.39814699	29.79472542	29.62888908	0.14368448	13.38547325
Non targeting	ELMO	1	0.715232372	1.39814699	29.55030632	29.62888908	0.14368448	13.38547325
ELMO 2	ELMO	0.2479873	0.140235901	0.43853036	31.08125305	31.64766502	0.49583983	15.39713478
ELMO 2	ELMO	0.2479873	0.140235901	0.43853036	32.00325775	31.64766502	0.49583983	15.39713478
ELMO 2	ELMO	0.2479873	0.140235901	0.43853036	31.85848618	31.64766502	0.49583983	15.39713478
Non targeting	GAPDH				16.47580719	16.24341583	0.26521453	
Non targeting	GAPDH				15.95449352	16.24341583	0.26521453	
Non targeting	GAPDH				16.29994583	16.24341583	0.26521453	
ELMO 1	GAPDH				17.32262993	17.36653137	0.07603953	
ELMO 1	GAPDH				17.32262993	17.36653137	0.07603953	
ELMO 1	GAPDH				17.45433426	17.36653137	0.07603953	
ELMO 2	GAPDH				16.19051743	16.25053024	0.13177159	
ELMO 2	GAPDH				16.15944862	16.25053024	0.13177159	
ELMO 2	GAPDH				16.40162659	16.25053024	0.13177159	

Figure 17 ELMO knockdown in HUVEC

HUVEC were lysed for RNA extraction 72hrs after transfection and gene knockdown was assessed through qRT-PCR (Section 2.2.2). Raw data (relative quantification of the amplified ELMO mRNA product (RQ); minimum and maximum quantification of the amplified ELMO mRNA product (RQmin and RQmax); relative quantification of threshold cycle numbers of the amplified ELMO mRNA (Ct); average cycle numbers (Ct Mean); cycle number standard deviation (Ct SD) and average of cycle numbers of the amplified ELMO mRNA compared to average of cycle numbers of the reference gene GAPDH (ΔCT Mean) were generated by Applied Biosystem 7900 SDS software. Relative quantification (RQ) was performed using the ΔΔCt method (Fleige and Pfaffl, 2006). qRT-PCR analysis was performed using the one step BRILLIANT II SYBR Green qRT-PCR Master Mix Kit (Applied Biosystems).

ELMO knockdown in ELMO1 and ELMO 2 Standard pool siRNA transfected samples was quantified as 99% and 75% respectively. Knockdown percentages were generated by comparing ELMO mRNA level in ELMO 1 and ELMO 2 transfected samples (ELMO 1 RQ=0.09; ELMO 2 RQ=0.25) to non targeting control sample (non targeting RQ=1).

References

Abdel-Malak, N.A., Srikant, C.B., Kristof, A.S., Magder, S.A., Di Battista, J.A., and Hussain, S.N. (2008). Angiopoietin-1 promotes endothelial cell proliferation and migration through AP-1-dependent autocrine production of interleukin-8. Blood *111*, 4145-4154.

Abid, M.R., Guo, S., Minami, T., Spokes, K.C., Ueki, K., Skurk, C., Walsh, K., and Aird, W.C. (2004). Vascular endothelial growth factor activates PI3K/Akt/forkhead signaling in endothelial cells. Arteriosclerosis, thrombosis, and vascular biology *24*, 294-300.

Abraham, S., Yeo, M., Montero-Balaguer, M., Paterson, H., Dejana, E., Marshall, C.J., and Mavria, G. (2009). VE-Cadherin-mediated cell-cell interaction suppresses sprouting via signaling to MLC2 phosphorylation. Current biology : CB *19*, 668-674.

Adams, R.H., and Alitalo, K. (2007). Molecular regulation of angiogenesis and lymphangiogenesis. Nature reviews Molecular cell biology *8*, 464-478.

Aghazadeh, B., Zhu, K., Kubiseski, T.J., Liu, G.A., Pawson, T., Zheng, Y., and Rosen, M.K. (1998). Structure and mutagenesis of the Dbl homology domain. Nature structural biology *5*, 1098-1107.

Aird, W.C. (2007). Phenotypic heterogeneity of the endothelium: II. Representative vascular beds. Circulation research *100*, 174-190.

Alexandropoulos, K., Cheng, G., and Baltimore, D. (1995). Proline-rich sequences that bind to Src homology 3 domains with individual specificities. Proceedings of the National Academy of Sciences of the United States of America *92*, 3110-3114.

Alitalo, K., and Carmeliet, P. (2002). Molecular mechanisms of lymphangiogenesis in health and disease. Cancer cell *1*, 219-227.

Allegra, J.R., Brennan, J., Lanier, V., Lavery, R., and MacKenzie, B. (1999). Storage temperatures of out-of-hospital medications. Academic emergency medicine : official journal of the Society for Academic Emergency Medicine *6*, 1098-1103.

Allen, W.E., Jones, G.E., Pollard, J.W., and Ridley, A.J. (1997). Rho, Rac and Cdc42 regulate actin organization and cell adhesion in macrophages. Journal of cell science *110 (Pt 6)*, 707-720.

Amano, M., Fukata, Y., and Kaibuchi, K. (2000). Regulation and functions of Rho-associated kinase. Experimental cell research *261*, 44-51.

Amano, M., Mukai, H., Ono, Y., Chihara, K., Matsui, T., Hamajima, Y., Okawa, K., Iwamatsu, A., and Kaibuchi, K. (1996). Identification of a putative target for Rho as the serine-threonine kinase protein kinase N. Science *271*, 648-650.

Arias-Romero, L.E., and Chernoff, J. (2008). A tale of two Paks. Biol Cell *100*, 97-108.

Arima, S., Nishiyama, K., Ko, T., Arima, Y., Hakozaki, Y., Sugihara, K., Koseki, H., Uchijima, Y., Kurihara, Y., and Kurihara, H. (2011). Angiogenic morphogenesis driven by dynamic and heterogeneous collective endothelial cell movement. Development *138*, 4763-4776.

Augustin, H.G., Koh, G.Y., Thurston, G., and Alitalo, K. (2009). Control of vascular morphogenesis and homeostasis through the angiopoietin-Tie system. Nature reviews Molecular cell biology *10*, 165-177.

Ausprunk, D.H., Falterman, K., and Folkman, J. (1978). The sequence of events in the regression of corneal capillaries. Laboratory investigation; a journal of technical methods and pathology *38*, 284-294.

Ballestrem, C., Wehrle-Haller, B., Hinz, B., and Imhof, B.A. (2000). Actin-dependent lamellipodia formation and microtubule-dependent tail retraction control-directed cell migration. Molecular biology of the cell *11*, 2999-3012.

Bayless, K.J., and Davis, G.E. (2004). Microtubule depolymerization rapidly collapses capillary tube networks in vitro and angiogenic vessels in vivo through the small GTPase Rho. The Journal of biological chemistry *279*, 11686-11695.

Bear, J.E., Rawls, J.F., and Saxe, C.L., 3rd (1998). SCAR, a WASP-related protein, isolated as a suppressor of receptor defects in late Dictyostelium development. The Journal of cell biology *142*, 1325-1335.

Bellanger, J.M., Astier, C., Sardet, C., Ohta, Y., Stossel, T.P., and Debant, A. (2000). The Rac1- and RhoG-specific GEF domain of Trio targets filamin to remodel cytoskeletal actin. Nature cell biology *2*, 888-892.

Benjamin, L.E., Golijanin, D., Itin, A., Pode, D., and Keshet, E. (1999). Selective ablation of immature blood vessels in established human tumors follows vascular endothelial growth factor withdrawal. The Journal of clinical investigation *103*, 159-165.

Benner, G.E., Dennis, P.B., and Masaracchia, R.A. (1995). Activation of an S6/H4 kinase (PAK 65) from human placenta by intramolecular and intermolecular autophosphorylation. The Journal of biological chemistry *270*, 21121-21128.

Bernatchez, P.N., Soker, S., and Sirois, M.G. (1999). Vascular endothelial growth factor effect on endothelial cell proliferation, migration, and platelet-activating factor synthesis is Flk-1-dependent. The Journal of biological chemistry *274*, 31047-31054.

Bianco, A., Poukkula, M., Cliffe, A., Mathieu, J., Luque, C.M., Fulga, T.A., and Rorth, P. (2007). Two distinct modes of guidance signalling during collective migration of border cells. Nature *448*, 362-365.

Bishop, A.L., and Hall, A. (2000). Rho GTPases and their effector proteins. The Biochemical journal *348 Pt 2*, 241-255.

Bishop, E.T., Bell, G.T., Bloor, S., Broom, I.J., Hendry, N.F., and Wheatley, D.N. (1999). An in vitro model of angiogenesis: basic features. Angiogenesis *3*, 335-344.

Blangy, A., Vignal, E., Schmidt, S., Debant, A., Gauthier-Rouviere, C., and Fort, P. (2000). TrioGEF1 controls Rac- and Cdc42-dependent cell structures through the direct activation of rhoG. Journal of cell science *113 (Pt 4)*, 729-739.

Blum, Y., Belting, H.G., Ellertsdottir, E., Herwig, L., Luders, F., and Affolter, M. (2008). Complex cell rearrangements during intersegmental vessel sprouting and vessel fusion in the zebrafish embryo. Developmental biology *316*, 312-322.

Bohil, A.B., Robertson, B.W., and Cheney, R.E. (2006). Myosin-X is a molecular motor that functions in filopodia formation. Proc Natl Acad Sci U S A *103*, 12411-12416.

Boilly, B., Vercoutter-Edouart, A.S., Hondermarck, H., Nurcombe, V., and Le Bourhis, X. (2000). FGF signals for cell proliferation and migration through different pathways. Cytokine Growth Factor Rev *11*, 295-302.

Boulton, M.E., Cai, J., and Grant, M.B. (2008). gamma-Secretase: a multifaceted regulator of angiogenesis. J Cell Mol Med *12*, 781-795.

Bourne, H.R., Sanders, D.A., and McCormick, F. (1990). The GTPase superfamily: a conserved switch for diverse cell functions. Nature *348*, 125-132.

Bretscher, A. (1991). Microfilament structure and function in the cortical cytoskeleton. Annual review of cell biology *7*, 337-374.

Briggs, M.W., and Sacks, D.B. (2003). IQGAP1 as signal integrator: Ca2+, calmodulin, Cdc42 and the cytoskeleton. FEBS letters *542*, 7-11.

Brindle, N.P., Saharinen, P., and Alitalo, K. (2006). Signaling and functions of angiopoietin-1 in vascular protection. Circulation research *98*, 1014-1023.

Broadley, K.N., Aquino, A.M., Woodward, S.C., Buckley-Sturrock, A., Sato, Y., Rifkin, D.B., and Davidson, J.M. (1989). Monospecific antibodies implicate basic fibroblast growth factor in normal wound repair. Laboratory investigation; a journal of technical methods and pathology *61*, 571-575.

Brugnera, E., Haney, L., Grimsley, C., Lu, M., Walk, S.F., Tosello-Trampont, A.C., Macara, I.G., Madhani, H., Fink, G.R., and Ravichandran, K.S. (2002). Unconventional Rac-GEF activity is mediated through the Dock180-ELMO complex. Nature cell biology *4*, 574-582.

Bryan, B.A., and D'Amore, P.A. (2007). What tangled webs they weave: Rho-GTPase control of angiogenesis. Cell Mol Life Sci *64*, 2053-2065.

Bryan, B.A., Dennstedt, E., Mitchell, D.C., Walshe, T.E., Noma, K., Loureiro, R., Saint-Geniez, M., Campaigniac, J.P., Liao, J.K., and D'Amore, P.A. (2010). RhoA/ROCK

signaling is essential for multiple aspects of VEGF-mediated angiogenesis. FASEB journal : official publication of the Federation of American Societies for Experimental Biology *24*, 3186-3195.

Brzostowski, J.A., Fey, P., Yan, J., Isik, N., and Jin, T. (2009). The Elmo family forms an ancient group of actin-regulating proteins. Communicative & integrative biology *2*, 337-340.

Burridge, K., and Connell, L. (1983a). A new protein of adhesion plaques and ruffling membranes. The Journal of cell biology *97*, 359-367.

Burridge, K., and Connell, L. (1983b). Talin: a cytoskeletal component concentrated in adhesion plaques and other sites of actin-membrane interaction. Cell motility *3*, 405-417.

Calvo, F., Sanz-Moreno, V., Agudo-Ibanez, L., Wallberg, F., Sahai, E., Marshall, C.J., and Crespo, P. (2011). RasGRF suppresses Cdc42-mediated tumour cell movement, cytoskeletal dynamics and transformation. Nature cell biology *13*, 819-826.

Carmeliet, P. (2003). Angiogenesis in health and disease. Nature medicine *9*, 653-660.

Carmeliet, P., Ferreira, V., Breier, G., Pollefeyt, S., Kieckens, L., Gertsenstein, M., Fahrig, M., Vandenhoeck, A., Harpal, K., Eberhardt, C.*, et al.* (1996). Abnormal blood vessel development and lethality in embryos lacking a single VEGF allele. Nature *380*, 435-439.

Carmeliet, P., and Jain, R.K. (2000). Angiogenesis in cancer and other diseases. Nature *407*, 249-257.

Cascone, I., Giraudo, E., Caccavari, F., Napione, L., Bertotti, E., Collard, J.G., Serini, G., and Bussolino, F. (2003). Temporal and spatial modulation of Rho GTPases during in vitro formation of capillary vascular network. Adherens junctions and myosin light chain as targets of Rac1 and RhoA. The Journal of biological chemistry *278*, 50702-50713.

Chen, F., Ma, L., Parrini, M.C., Mao, X., Lopez, M., Wu, C., Marks, P.W., Davidson, L., Kwiatkowski, D.J., Kirchhausen, T.*, et al.* (2000). Cdc42 is required for PIP(2)-induced actin polymerization and early development but not for cell viability. Current biology : CB *10*, 758-765.

Cheng, C., Haasdijk, R., Tempel, D., van de Kamp, E.H., Herpers, R., Bos, F., Den Dekker, W.K., Blonden, L.A., de Jong, R., Burgisser, P.E.*, et al.* (2012). Endothelial cell-specific FGD5 involvement in vascular pruning defines neovessel fate in mice. Circulation *125*, 3142-3158.

Cheresh, D.A., Leng, J., and Klemke, R.L. (1999). Regulation of cell contraction and membrane ruffling by distinct signals in migratory cells. The Journal of cell biology *146*, 1107-1116.

Cherfils, J., and Chardin, P. (1999). GEFs: structural basis for their activation of small GTP-binding proteins. Trends in biochemical sciences *24*, 306-311.

Chhabra, E.S., and Higgs, H.N. (2007). The many faces of actin: matching assembly factors with cellular structures. Nature cell biology *9*, 1110-1121.

Chimini, G., and Chavrier, P. (2000). Function of Rho family proteins in actin dynamics during phagocytosis and engulfment. Nature cell biology *2*, E191-196.

Chrzanowska-Wodnicka, M., and Burridge, K. (1996). Rho-stimulated contractility drives the formation of stress fibers and focal adhesions. The Journal of cell biology *133*, 1403-1415.

Conway, E.M., Collen, D., and Carmeliet, P. (2001). Molecular mechanisms of blood vessel growth. Cardiovascular research *49*, 507-521.

Cote, J.F., Motoyama, A.B., Bush, J.A., and Vuori, K. (2005). A novel and evolutionarily conserved PtdIns(3,4,5)P3-binding domain is necessary for DOCK180 signalling. Nature cell biology *7*, 797-807.

Cote, J.F., and Vuori, K. (2002). Identification of an evolutionarily conserved superfamily of DOCK180-related proteins with guanine nucleotide exchange activity. Journal of cell science *115*, 4901-4913.

Cote, J.F., and Vuori, K. (2007). GEF what? Dock180 and related proteins help Rac to polarize cells in new ways. Trends in cell biology *17*, 383-393.

Couper, L.L., Bryant, S.R., Eldrup-Jorgensen, J., Bredenberg, C.E., and Lindner, V. (1997). Vascular endothelial growth factor increases the mitogenic response to fibroblast growth factor-2 in vascular smooth muscle cells in vivo via expression of fms-like tyrosine kinase-1. Circulation research *81*, 932-939.

Czuchra, A., Wu, X., Meyer, H., van Hengel, J., Schroeder, T., Geffers, R., Rottner, K., and Brakebusch, C. (2005). Cdc42 is not essential for filopodium formation, directed migration, cell polarization, and mitosis in fibroblastoid cells. Molecular biology of the cell *16*, 4473-4484.

D'Souza-Schorey, C., Boshans, R.L., McDonough, M., Stahl, P.D., and Van Aelst, L. (1997). A role for POR1, a Rac1-interacting protein, in ARF6-mediated cytoskeletal rearrangements. The EMBO journal *16*, 5445-5454.

Dachs, G.U., and Tozer, G.M. (2000). Hypoxia modulated gene expression: angiogenesis, metastasis and therapeutic exploitation. Eur J Cancer *36*, 1649-1660.

Davis, G.E., and Camarillo, C.W. (1996). An alpha 2 beta 1 integrin-dependent pinocytic mechanism involving intracellular vacuole formation and coalescence regulates capillary lumen and tube formation in three-dimensional collagen matrix. Experimental cell research *224*, 39-51.

Davis, G.E., Koh, W., and Stratman, A.N. (2007). Mechanisms controlling human endothelial lumen formation and tube assembly in three-dimensional extracellular matrices. Birth defects research Part C, Embryo today : reviews *81*, 270-285.

De Smet, F., Segura, I., De Bock, K., Hohensinner, P.J., and Carmeliet, P. (2009). Mechanisms of vessel branching: filopodia on endothelial tip cells lead the way. Arterioscler Thromb Vasc Biol *29*, 639-649.

Defilippi, P., Olivo, C., Venturino, M., Dolce, L., Silengo, L., and Tarone, G. (1999). Actin cytoskeleton organization in response to integrin-mediated adhesion. Microscopy research and technique *47*, 67-78.

del Toro, R., Prahst, C., Mathivet, T., Siegfried, G., Kaminker, J.S., Larrivee, B., Breant, C., Duarte, A., Takakura, N., Fukamizu, A.*, et al.* (2010). Identification and functional analysis of endothelial tip cell-enriched genes. Blood *116*, 4025-4033.

Demarco, R.S., Struckhoff, E.C., and Lundquist, E.A. (2012). The Rac GTP exchange factor TIAM-1 acts with CDC-42 and the guidance receptor UNC-40/DCC in neuronal protrusion and axon guidance. PLoS genetics *8*, e1002665.

Dent, E.W., Kwiatkowski, A.V., Mebane, L.M., Philippar, U., Barzik, M., Rubinson, D.A., Gupton, S., Van Veen, J.E., Furman, C., Zhang, J.*, et al.* (2007). Filopodia are required for cortical neurite initiation. Nature cell biology *9*, 1347-1359.

Der, C.J., Finkel, T., and Cooper, G.M. (1986). Biological and biochemical properties of human rasH genes mutated at codon 61. Cell *44*, 167-176.

Devreotes, P.N., and Zigmond, S.H. (1988). Chemotaxis in eukaryotic cells: a focus on leukocytes and Dictyostelium. Annual review of cell biology *4*, 649-686.

Djonov, V., Schmid, M., Tschanz, S.A., and Burri, P.H. (2000). Intussusceptive angiogenesis: its role in embryonic vascular network formation. Circulation research *86*, 286-292.

Donovan, D., Brown, N.J., Bishop, E.T., and Lewis, C.E. (2001). Comparison of three in vitro human 'angiogenesis' assays with capillaries formed in vivo. Angiogenesis *4*, 113-121.

Downs, K.M. (2003). Florence Sabin and the mechanism of blood vessel lumenization during vasculogenesis. Microcirculation *10*, 5-25.

Downs, K.M., Inman, K.E., Jin, D.X., and Enders, A.C. (2009). The Allantoic Core Domain: new insights into development of the murine allantois and its relation to the primitive streak. Developmental dynamics : an official publication of the American Association of Anatomists *238*, 532-553.

Duchek, P., Somogyi, K., Jekely, G., Beccari, S., and Rorth, P. (2001). Guidance of cell migration by the Drosophila PDGF/VEGF receptor. Cell *107*, 17-26.

Dvorak, H.F., Sioussat, T.M., Brown, L.F., Berse, B., Nagy, J.A., Sotrel, A., Manseau, E.J., Van de Water, L., and Senger, D.R. (1991). Distribution of vascular permeability factor (vascular endothelial growth factor) in tumors: concentration in tumor blood vessels. The Journal of experimental medicine *174*, 1275-1278.

Eilken, H.M., and Adams, R.H. (2010). Dynamics of endothelial cell behavior in sprouting angiogenesis. Current opinion in cell biology *22*, 617-625.

El-Sibai, M., Nalbant, P., Pang, H., Flinn, R.J., Sarmiento, C., Macaluso, F., Cammer, M., Condeelis, J.S., Hahn, K.M., and Backer, J.M. (2007). Cdc42 is required for EGF-stimulated protrusion and motility in MTLn3 carcinoma cells. Journal of cell science *120*, 3465-3474.

Elfenbein, A., Rhodes, J.M., Meller, J., Schwartz, M.A., Matsuda, M., and Simons, M. (2009). Suppression of RhoG activity is mediated by a syndecan 4-synectin-RhoGDI1 complex and is reversed by PKCalpha in a Rac1 activation pathway. The Journal of cell biology *186*, 75-83.

Elliott, M.R., Zheng, S., Park, D., Woodson, R.I., Reardon, M.A., Juncadella, I.J., Kinchen, J.M., Zhang, J., Lysiak, J.J., and Ravichandran, K.S. (2010). Unexpected requirement for ELMO1 in clearance of apoptotic germ cells in vivo. Nature *467*, 333-337.

Engelse, M.A., Laurens, N., Verloop, R.E., Koolwijk, P., and van Hinsbergh, V.W. (2008). Differential gene expression analysis of tubule forming and non-tubule forming endothelial cells: CDC42GAP as a counter-regulator in tubule formation. Angiogenesis *11*, 153-167.

Epting, D., Wendik, B., Bennewitz, K., Dietz, C.T., Driever, W., and Kroll, J. (2010). The Rac1 regulator ELMO1 controls vascular morphogenesis in zebrafish. Circulation research *107*, 45-55.

Ergun, S., Kilic, N., Wurmbach, J.H., Ebrahimnejad, A., Fernando, M., Sevinc, S., Kilic, E., Chalajour, F., Fiedler, W., Lauke, H*., et al.* (2001). Endostatin inhibits angiogenesis by stabilization of newly formed endothelial tubes. Angiogenesis *4*, 193-206.

Erickson, J.W., and Cerione, R.A. (2001). Multiple roles for Cdc42 in cell regulation. Current opinion in cell biology *13*, 153-157.

Erickson, J.W., and Cerione, R.A. (2004). Structural elements, mechanism, and evolutionary convergence of Rho protein-guanine nucleotide exchange factor complexes. Biochemistry *43*, 837-842.

Estrach, S., Schmidt, S., Diriong, S., Penna, A., Blangy, A., Fort, P., and Debant, A. (2002). The Human Rho-GEF trio and its target GTPase RhoG are involved in the NGF pathway, leading to neurite outgrowth. Current biology : CB *12*, 307-312.

Etienne-Manneville, S. (2004). Cdc42--the centre of polarity. Journal of cell science *117*, 1291-1300.

Etienne-Manneville, S., and Hall, A. (2002). Rho GTPases in cell biology. Nature *420*, 629-635.

Eva, A., Vecchio, G., Rao, C.D., Tronick, S.R., and Aaronson, S.A. (1988). The predicted DBL oncogene product defines a distinct class of transforming proteins. Proceedings of the National Academy of Sciences of the United States of America *85*, 2061-2065.

Fantin, A., Vieira, J.M., Gestri, G., Denti, L., Schwarz, Q., Prykhozhij, S., Peri, F., Wilson, S.W., and Ruhrberg, C. (2010). Tissue macrophages act as cellular chaperones for vascular anastomosis downstream of VEGF-mediated endothelial tip cell induction. Blood *116*, 829-840.

Feng, J., Ito, M., Kureishi, Y., Ichikawa, K., Amano, M., Isaka, N., Okawa, K., Iwamatsu, A., Kaibuchi, K., Hartshorne, D.J.*, et al.* (1999). Rho-associated kinase of chicken gizzard smooth muscle. The Journal of biological chemistry *274*, 3744-3752.

Ferguson, J.E., 3rd, Kelley, R.W., and Patterson, C. (2005). Mechanisms of endothelial differentiation in embryonic vasculogenesis. Arteriosclerosis, thrombosis, and vascular biology *25*, 2246-2254.

Ferrara, N. (2004). Vascular endothelial growth factor: basic science and clinical progress. Endocr Rev *25*, 581-611.

Ferrara, N., Carver-Moore, K., Chen, H., Dowd, M., Lu, L., O'Shea, K.S., Powell-Braxton, L., Hillan, K.J., and Moore, M.W. (1996). Heterozygous embryonic lethality induced by targeted inactivation of the VEGF gene. Nature *380*, 439-442.

Ferrara, N., Gerber, H.P., and LeCouter, J. (2003). The biology of VEGF and its receptors. Nature medicine *9*, 669-676.

Ferrara, N., Hillan, K.J., Gerber, H.P., and Novotny, W. (2004). Discovery and development of bevacizumab, an anti-VEGF antibody for treating cancer. Nature reviews Drug discovery *3*, 391-400.

Feuerstein, J., Goody, R.S., and Webb, M.R. (1989). The mechanism of guanosine nucleotide hydrolysis by p21 c-Ha-ras. The stereochemical course of the GTPase reaction. The Journal of biological chemistry *264*, 6188-6190.

Flamme, I., Frolich, T., and Risau, W. (1997). Molecular mechanisms of vasculogenesis and embryonic angiogenesis. Journal of cellular physiology *173*, 206-210.

Folkman, J. (1971). Tumor angiogenesis: therapeutic implications. The New England journal of medicine *285*, 1182-1186.

Folkman, J., and D'Amore, P.A. (1996). Blood vessel formation: what is its molecular basis? Cell *87*, 1153-1155.

Franke, K., Otto, W., Johannes, S., Baumgart, J., Nitsch, R., and Schumacher, S. (2012). miR-124-regulated RhoG reduces neuronal process complexity via ELMO/Dock180/Rac1 and Cdc42 signalling. The EMBO journal *31*, 2908-2921.

Gadea, G., Sanz-Moreno, V., Self, A., Godi, A., and Marshall, C.J. (2008). DOCK10-mediated Cdc42 activation is necessary for amoeboid invasion of melanoma cells. Current biology : CB *18*, 1456-1465.

Galbraith, C.G., Yamada, K.M., and Galbraith, J.A. (2007). Polymerizing actin fibers position integrins primed to probe for adhesion sites. Science *315*, 992-995.

Gallo, G., and Letourneau, P.C. (2004). Regulation of growth cone actin filaments by guidance cues. J Neurobiol *58*, 92-102.

Gardiner, E.M., Pestonjamasp, K.N., Bohl, B.P., Chamberlain, C., Hahn, K.M., and Bokoch, G.M. (2002). Spatial and temporal analysis of Rac activation during live neutrophil chemotaxis. Current biology : CB *12*, 2029-2034.

Garrett, T.A., Van Buul, J.D., and Burridge, K. (2007). VEGF-induced Rac1 activation in endothelial cells is regulated by the guanine nucleotide exchange factor Vav2. Experimental cell research *313*, 3285-3297.

Garvalov, B.K., Flynn, K.C., Neukirchen, D., Meyn, L., Teusch, N., Wu, X., Brakebusch, C., Bamburg, J.R., and Bradke, F. (2007). Cdc42 regulates cofilin during the establishment of neuronal polarity. The Journal of neuroscience : the official journal of the Society for Neuroscience *27*, 13117-13129.

Gauthier-Campbell, C., Bredt, D.S., Murphy, T.H., and El-Husseini Ael, D. (2004). Regulation of dendritic branching and filopodia formation in hippocampal neurons by specific acylated protein motifs. Molecular biology of the cell *15*, 2205-2217.

Gauthier-Rouviere, C., Vignal, E., Meriane, M., Roux, P., Montcourier, P., and Fort, P. (1998). RhoG GTPase controls a pathway that independently activates Rac1 and Cdc42Hs. Molecular biology of the cell *9*, 1379-1394.

Geisbrecht, E.R., Haralalka, S., Swanson, S.K., Florens, L., Washburn, M.P., and Abmayr, S.M. (2008). Drosophila ELMO/CED-12 interacts with Myoblast city to direct myoblast fusion and ommatidial organization. Developmental biology *314*, 137-149.

Gerber, H.P., McMurtrey, A., Kowalski, J., Yan, M., Keyt, B.A., Dixit, V., and Ferrara, N. (1998). Vascular endothelial growth factor regulates endothelial cell survival through the phosphatidylinositol 3'-kinase/Akt signal transduction pathway. Requirement for Flk-1/KDR activation. The Journal of biological chemistry *273*, 30336-30343.

Gerhardt, H. (2008). VEGF and endothelial guidance in angiogenic sprouting. Organogenesis *4*, 241-246.

Gerhardt, H., and Betsholtz, C. (2005). How do endothelial cells orientate? Exs, 3-15.

Gerhardt, H., Golding, M., Fruttiger, M., Ruhrberg, C., Lundkvist, A., Abramsson, A., Jeltsch, M., Mitchell, C., Alitalo, K., Shima, D.*, et al.* (2003). VEGF guides angiogenic sprouting utilizing endothelial tip cell filopodia. The Journal of cell biology *161*, 1163-1177.

Goel, S., Duda, D.G., Xu, L., Munn, L.L., Boucher, Y., Fukumura, D., and Jain, R.K. (2011). Normalization of the vasculature for treatment of cancer and other diseases. Physiological reviews *91*, 1071-1121.

Graham, F.L., Smiley, J., Russell, W.C., and Nairn, R. (1977). Characteristics of a human cell line transformed by DNA from human adenovirus type 5. J Gen Virol *36*, 59-74.

Grimsley, C.M., Kinchen, J.M., Tosello-Trampont, A.C., Brugnera, E., Haney, L.B., Lu, M., Chen, Q., Klingele, D., Hengartner, M.O., and Ravichandran, K.S. (2004). Dock180 and ELMO1 proteins cooperate to promote evolutionarily conserved Rac-dependent cell migration. The Journal of biological chemistry *279*, 6087-6097.

Gualandris, A., Urbinati, C., Rusnati, M., Ziche, M., and Presta, M. (1994). Interaction of high-molecular-weight basic fibroblast growth factor with endothelium: biological activity and intracellular fate of human recombinant M(r) 24,000 bFGF. Journal of cellular physiology *161*, 149-159.

Gumienny, T.L., Brugnera, E., Tosello-Trampont, A.C., Kinchen, J.M., Haney, L.B., Nishiwaki, K., Walk, S.F., Nemergut, M.E., Macara, I.G., Francis, R.*, et al.* (2001). CED-12/ELMO, a novel member of the CrkII/Dock180/Rac pathway, is required for phagocytosis and cell migration. Cell *107*, 27-41.

Guo, F., Debidda, M., Yang, L., Williams, D.A., and Zheng, Y. (2006). Genetic deletion of Rac1 GTPase reveals its critical role in actin stress fiber formation and focal adhesion complex assembly. The Journal of biological chemistry *281*, 18652-18659.

Gupton, S.L., and Gertler, F.B. (2007). Filopodia: the fingers that do the walking. Sci STKE *2007*, re5.

Haeusler, L.C., Blumenstein, L., Stege, P., Dvorsky, R., and Ahmadian, M.R. (2003). Comparative functional analysis of the Rac GTPases. FEBS Lett *555*, 556-560.

Hall, A. (1998). Rho GTPases and the actin cytoskeleton. Science *279*, 509-514.

Hamann, M.J., Lubking, C.M., Luchini, D.N., and Billadeau, D.D. (2007). Asef2 functions as a Cdc42 exchange factor and is stimulated by the release of an autoinhibitory module from a concealed C-terminal activation element. Molecular and cellular biology *27*, 1380-1393.

Harris, A.L. (2002). Hypoxia--a key regulatory factor in tumour growth. Nature reviews Cancer *2*, 38-47.

Harris, P.A., Boloor, A., Cheung, M., Kumar, R., Crosby, R.M., Davis-Ward, R.G., Epperly, A.H., Hinkle, K.W., Hunter, R.N., 3rd, Johnson, J.H.*, et al.* (2008). Discovery of 5-[[4-[(2,3-dimethyl-2H-indazol-6-yl)methylamino]-2-pyrimidinyl]amino]-2-methyl-b enzenesulfonamide (Pazopanib), a novel and potent vascular endothelial growth factor receptor inhibitor. Journal of medicinal chemistry *51*, 4632-4640.

Hart, M.J., Eva, A., Evans, T., Aaronson, S.A., and Cerione, R.A. (1991). Catalysis of guanine nucleotide exchange on the CDC42Hs protein by the dbl oncogene product. Nature *354*, 311-314.

Hasegawa, H., Kiyokawa, E., Tanaka, S., Nagashima, K., Gotoh, N., Shibuya, M., Kurata, T., and Matsuda, M. (1996). DOCK180, a major CRK-binding protein, alters cell morphology upon translocation to the cell membrane. Molecular and cellular biology *16*, 1770-1776.

Hashimoto, S., Hirose, M., Hashimoto, A., Morishige, M., Yamada, A., Hosaka, H., Akagi, K., Ogawa, E., Oneyama, C., Agatsuma, T.*, et al.* (2006). Targeting AMAP1 and cortactin binding bearing an atypical src homology 3/proline interface for prevention of breast cancer invasion and metastasis. Proceedings of the National Academy of Sciences of the United States of America *103*, 7036-7041.

Hayakawa, M., Matsushima, M., Hagiwara, H., Oshima, T., Fujino, T., Ando, K., Kikugawa, K., Tanaka, H., Miyazawa, K., and Kitagawa, M. (2008). Novel insights into FGD3, a putative GEF for Cdc42, that undergoes SCF(FWD1/beta-TrCP)-mediated proteasomal degradation analogous to that of its homologue FGD1 but regulates cell morphology and motility differently from FGD1. Genes to cells : devoted to molecular & cellular mechanisms *13*, 329-342.

Hellstrom, M., Phng, L.K., Hofmann, J.J., Wallgard, E., Coultas, L., Lindblom, P., Alva, J., Nilsson, A.K., Karlsson, L., Gaiano, N.*, et al.* (2007). Dll4 signalling through Notch1 regulates formation of tip cells during angiogenesis. Nature *445*, 776-780.

Henderson, A.M., Wang, S.J., Taylor, A.C., Aitkenhead, M., and Hughes, C.C. (2001). The basic helix-loop-helix transcription factor HESR1 regulates endothelial cell tube formation. The Journal of biological chemistry *276*, 6169-6176.

Herbert, S.P., and Stainier, D.Y. (2011). Molecular control of endothelial cell behaviour during blood vessel morphogenesis. Nature reviews Molecular cell biology *12*, 551-564.

Herbst, R.S., Hidalgo, M., Pierson, A.S., Holden, S.N., Bergen, M., and Eckhardt, S.G. (2002). Angiogenesis inhibitors in clinical development for lung cancer. Seminars in oncology *29*, 66-77.

Hiramoto, K., Negishi, M., and Katoh, H. (2006). Dock4 is regulated by RhoG and promotes Rac-dependent cell migration. Experimental cell research *312*, 4205-4216.

Hiramoto-Yamaki, N., Takeuchi, S., Ueda, S., Harada, K., Fujimoto, S., Negishi, M., and Katoh, H. (2010). Ephexin4 and EphA2 mediate cell migration through a RhoG-dependent mechanism. The Journal of cell biology *190*, 461-477.

Hirata, E., Yukinaga, H., Kamioka, Y., Arakawa, Y., Miyamoto, S., Okada, T., Sahai, E., and Matsuda, M. (2012). In vivo fluorescence resonance energy transfer imaging reveals differential activation of Rho-family GTPases in glioblastoma cell invasion. Journal of cell science *125*, 858-868.

Hirshberg, M., Stockley, R.W., Dodson, G., and Webb, M.R. (1997). The crystal structure of human rac1, a member of the rho-family complexed with a GTP analogue. Nature structural biology *4*, 147-152.

Hoang, M.V., Whelan, M.C., and Senger, D.R. (2004). Rho activity critically and selectively regulates endothelial cell organization during angiogenesis. Proceedings of the National Academy of Sciences of the United States of America *101*, 1874-1879.

Hoelzle, M.K., and Svitkina, T. (2012). The cytoskeletal mechanisms of cell-cell junction formation in endothelial cells. Molecular biology of the cell *23*, 310-323.

Hu, G.D., Chen, Y.H., Zhang, L., Tong, W.C., Cheng, Y.X., Luo, Y.L., Cai, S.X., and Zhang, L. (2011). The generation of the endothelial specific cdc42-deficient mice and the effect of cdc42 deletion on the angiogenesis and embryonic development. Chin Med J (Engl) *124*, 4155-4159.

Huber, C., Martensson, A., Bokoch, G.M., Nemazee, D., and Gavin, A.L. (2008). FGD2, a CDC42-specific exchange factor expressed by antigen-presenting cells, localizes to early endosomes and active membrane ruffles. The Journal of biological chemistry *283*, 34002-34012.

Hunter, S.G., Zhuang, G., Brantley-Sieders, D., Swat, W., Cowan, C.W., and Chen, J. (2006). Essential role of Vav family guanine nucleotide exchange factors in EphA receptor-mediated angiogenesis. Molecular and cellular biology *26*, 4830-4842.

Huveneers, S., and Danen, E.H. (2009). Adhesion signaling - crosstalk between integrins, Src and Rho. Journal of cell science *122*, 1059-1069.

Ihara, K., Muraguchi, S., Kato, M., Shimizu, T., Shirakawa, M., Kuroda, S., Kaibuchi, K., and Hakoshima, T. (1998). Crystal structure of human RhoA in a dominantly active form complexed with a GTP analogue. The Journal of biological chemistry *273*, 9656-9666.

Im, E., and Kazlauskas, A. (2006). New insights regarding vessel regression. Cell Cycle *5*, 2057-2059.

Iyer, S.C., Wang, D., Iyer, E.P., Trunnell, S.A., Meduri, R., Shinwari, R., Sulkowski, M.J., and Cox, D.N. (2012). The RhoGEF trio functions in sculpting class specific dendrite morphogenesis in Drosophila sensory neurons. PloS one *7*, e33634.

Izzard, C.S. (1974). Contractile filopodia and in vivo cell movement in the tunic of the ascidian, Botryllus schlosseri. Journal of cell science *15*, 513-535.

Jackson, B., Peyrollier, K., Pedersen, E., Basse, A., Karlsson, R., Wang, Z., Lefever, T., Ochsenbein, A.M., Schmidt, G., Aktories, K.*, et al.* (2011). RhoA is dispensable for skin development, but crucial for contraction and directed migration of keratinocytes. Molecular biology of the cell *22*, 593-605.

Jaffe, A.B., and Hall, A. (2005). Rho GTPases: biochemistry and biology. Annual review of cell and developmental biology *21*, 247-269.

Jain, R.K. (2001). Normalizing tumor vasculature with anti-angiogenic therapy: a new paradigm for combination therapy. Nature medicine *7*, 987-989.

Jain, R.K. (2003). Molecular regulation of vessel maturation. Nature medicine *9*, 685-693.

Jain, R.K. (2005). Normalization of tumor vasculature: an emerging concept in antiangiogenic therapy. Science *307*, 58-62.

Jakobsson, L., Franco, C.A., Bentley, K., Collins, R.T., Ponsioen, B., Aspalter, I.M., Rosewell, I., Busse, M., Thurston, G., Medvinsky, A.*, et al.* (2010). Endothelial cells dynamically compete for the tip cell position during angiogenic sprouting. Nature cell biology *12*, 943-953.

Kaibuchi, K., Kuroda, S., and Amano, M. (1999). Regulation of the cytoskeleton and cell adhesion by the Rho family GTPases in mammalian cells. Annual review of biochemistry *68*, 459-486.

Kanda, S., Landgren, E., Ljungstrom, M., and Claesson-Welsh, L. (1996). Fibroblast growth factor receptor 1-induced differentiation of endothelial cell line established from tsA58 large T transgenic mice. Cell growth & differentiation : the molecular biology journal of the American Association for Cancer Research *7*, 383-395.

Katoh, H., Hiramoto, K., and Negishi, M. (2006). Activation of Rac1 by RhoG regulates cell migration. Journal of cell science *119*, 56-65.

Katoh, H., and Negishi, M. (2003). RhoG activates Rac1 by direct interaction with the Dock180-binding protein Elmo. Nature *424*, 461-464.

Katoh, H., Yasui, H., Yamaguchi, Y., Aoki, J., Fujita, H., Mori, K., and Negishi, M. (2000). Small GTPase RhoG is a key regulator for neurite outgrowth in PC12 cells. Molecular and cellular biology *20*, 7378-7387.

Kawada, K., Upadhyay, G., Ferandon, S., Janarthanan, S., Hall, M., Vilardaga, J.P., and Yajnik, V. (2009). Cell migration is regulated by platelet-derived growth factor receptor endocytosis. Molecular and cellular biology *29*, 4508-4518.

Kawano, Y., Fukata, Y., Oshiro, N., Amano, M., Nakamura, T., Ito, M., Matsumura, F., Inagaki, M., and Kaibuchi, K. (1999). Phosphorylation of myosin-binding subunit (MBS) of myosin phosphatase by Rho-kinase in vivo. The Journal of cell biology *147*, 1023-1038.

Kawasaki, Y., Sagara, M., Shibata, Y., Shirouzu, M., Yokoyama, S., and Akiyama, T. (2007). Identification and characterization of Asef2, a guanine-nucleotide exchange factor specific for Rac1 and Cdc42. Oncogene *26*, 7620-7267.

Kerbel, R., and Folkman, J. (2002). Clinical translation of angiogenesis inhibitors. Nature reviews Cancer *2*, 727-739.

Khan, S.A., Nelson, M.S., Pan, C., Gaffney, P.M., and Gupta, P. (2008). Endogenous heparan sulfate and heparin modulate bone morphogenetic protein-4 signaling and activity. American journal of physiology Cell physiology *294*, C1387-1397.

Kiosses, W.B., Hood, J., Yang, S., Gerritsen, M.E., Cheresh, D.A., Alderson, N., and Schwartz, M.A. (2002). A dominant-negative p65 PAK peptide inhibits angiogenesis. Circulation research *90*, 697-702.

Kiyokawa, E., Hashimoto, Y., Kurata, T., Sugimura, H., and Matsuda, M. (1998). Evidence that DOCK180 up-regulates signals from the CrkII-p130(Cas) complex. The Journal of biological chemistry *273*, 24479-24484.

Klemke, R.L., Leng, J., Molander, R., Brooks, P.C., Vuori, K., and Cheresh, D.A. (1998). CAS/Crk coupling serves as a "molecular switch" for induction of cell migration. The Journal of cell biology *140*, 961-972.

Knezevic, II, Predescu, S.A., Neamu, R.F., Gorovoy, M.S., Knezevic, N.M., Easington, C., Malik, A.B., and Predescu, D.N. (2009). Tiam1 and Rac1 are required for platelet-activating factor-induced endothelial junctional disassembly and increase in vascular permeability. The Journal of biological chemistry *284*, 5381-5394.

Kobayashi, S., Shirai, T., Kiyokawa, E., Mochizuki, N., Matsuda, M., and Fukui, Y. (2001). Membrane recruitment of DOCK180 by binding to PtdIns(3,4,5)P3. The Biochemical journal *354*, 73-78.

Komander, D., Patel, M., Laurin, M., Fradet, N., Pelletier, A., Barford, D., and Cote, J.F. (2008). An alpha-helical extension of the ELMO1 pleckstrin homology domain mediates direct interaction to DOCK180 and is critical in Rac signaling. Molecular biology of the cell *19*, 4837-4851.

Kottakis, F., Polytarchou, C., Foltopoulou, P., Sanidas, I., Kampranis, S.C., and Tsichlis, P.N. (2011). FGF-2 regulates cell proliferation, migration, and angiogenesis through an NDY1/KDM2B-miR-101-EZH2 pathway. Molecular cell *43*, 285-298.

Kouklis, P., Konstantoulaki, M., and Malik, A.B. (2003). VE-cadherin-induced Cdc42 signaling regulates formation of membrane protrusions in endothelial cells. The Journal of biological chemistry *278*, 16230-16236.

Kozma, R., Ahmed, S., Best, A., and Lim, L. (1995). The Ras-related protein Cdc42Hs and bradykinin promote formation of peripheral actin microspikes and filopodia in Swiss 3T3 fibroblasts. Molecular and cellular biology *15*, 1942-1952.

Krause, M., Dent, E.W., Bear, J.E., Loureiro, J.J., and Gertler, F.B. (2003). Ena/VASP proteins: regulators of the actin cytoskeleton and cell migration. Annu Rev Cell Dev Biol *19*, 541-564.

Krauthammer, M., Kong, Y., Ha, B.H., Evans, P., Bacchiocchi, A., McCusker, J.P., Cheng, E., Davis, M.J., Goh, G., Choi, M.*, et al.* (2012). Exome sequencing identifies recurrent somatic RAC1 mutations in melanoma. Nature genetics *44*, 1006-1014.

Kress, H., Stelzer, E.H., Holzer, D., Buss, F., Griffiths, G., and Rohrbach, A. (2007). Filopodia act as phagocytic tentacles and pull with discrete steps and a load-dependent velocity. Proceedings of the National Academy of Sciences of the United States of America *104*, 11633-11638.

Kulkarni, K., Yang, J., Zhang, Z., and Barford, D. (2011). Multiple factors confer specific Cdc42 and Rac protein activation by dedicator of cytokinesis (DOCK) nucleotide exchange factors. The Journal of biological chemistry *286*, 25341-25351.

Kuramoto, K., Negishi, M., and Katoh, H. (2009). Regulation of dendrite growth by the Cdc42 activator Zizimin1/Dock9 in hippocampal neurons. J Neurosci Res *87*, 1794-1805.

Kureishy, N., Sapountzi, V., Prag, S., Anilkumar, N., and Adams, J.C. (2002). Fascins, and their roles in cell structure and function. BioEssays : news and reviews in molecular, cellular and developmental biology *24*, 350-361.

Kurogane, Y., Miyata, M., Kubo, Y., Nagamatsu, Y., Kundu, R.K., Uemura, A., Ishida, T., Quertermous, T., Hirata, K., and Rikitake, Y. (2012). FGD5 mediates proangiogenic action of vascular endothelial growth factor in human vascular endothelial cells. Arteriosclerosis, thrombosis, and vascular biology *32*, 988-996.

Kusuhara, S., Fukushima, Y., Fukuhara, S., Jakt, L.M., Okada, M., Shimizu, Y., Hata, M., Nishida, K., Negi, A., Hirashima, M.*, et al.* (2012). Arhgef15 promotes retinal angiogenesis by mediating VEGF-induced Cdc42 activation and potentiating RhoJ inactivation in endothelial cells. PloS one *7*, e45858.

Kwiatkowski, A.V., Rubinson, D.A., Dent, E.W., Edward van Veen, J., Leslie, J.D., Zhang, J., Mebane, L.M., Philippar, U., Pinheiro, E.M., Burds, A.A.*, et al.* (2007). Ena/VASP Is Required for neuritogenesis in the developing cortex. Neuron *56*, 441-455.

Kwofie, M.A., and Skowronski, J. (2008). Specific recognition of Rac2 and Cdc42 by DOCK2 and DOCK9 guanine nucleotide exchange factors. The Journal of biological chemistry *283*, 3088-3096.

Lang, R.A., and Bishop, J.M. (1993). Macrophages are required for cell death and tissue remodeling in the developing mouse eye. Cell *74*, 453-462.

Laurin, M., Fradet, N., Blangy, A., Hall, A., Vuori, K., and Cote, J.F. (2008). The atypical Rac activator Dock180 (Dock1) regulates myoblast fusion in vivo. Proceedings of the National Academy of Sciences of the United States of America *105*, 15446-15451.

le Noble, F., Fleury, V., Pries, A., Corvol, P., Eichmann, A., and Reneman, R.S. (2005). Control of arterial branching morphogenesis in embryogenesis: go with the flow. Cardiovascular research *65*, 619-628.

Lei, M., Lu, W., Meng, W., Parrini, M.C., Eck, M.J., Mayer, B.J., and Harrison, S.C. (2000). Structure of PAK1 in an autoinhibited conformation reveals a multistage activation switch. Cell *102*, 387-397.

Leslie, J.D., Ariza-McNaughton, L., Bermange, A.L., McAdow, R., Johnson, S.L., and Lewis, J. (2007). Endothelial signalling by the Notch ligand Delta-like 4 restricts angiogenesis. Development *134*, 839-844.

Liu, S.C., Yang, J.J., Shao, K.N., and Chueh, P.J. (2008). RNA interference targeting tNOX attenuates cell migration via a mechanism that involves membrane association of Rac. Biochemical and biophysical research communications *365*, 672-677.

Lobov, I.B., Renard, R.A., Papadopoulos, N., Gale, N.W., Thurston, G., Yancopoulos, G.D., and Wiegand, S.J. (2007). Delta-like ligand 4 (Dll4) is induced by VEGF as a negative regulator of angiogenic sprouting. Proceedings of the National Academy of Sciences of the United States of America *104*, 3219-3224.

Loges, S., Schmidt, T., and Carmeliet, P. (2010). Mechanisms of resistance to anti-angiogenic therapy and development of third-generation anti-angiogenic drug candidates. Genes & cancer *1*, 12-25.

Lu, M., Kinchen, J.M., Rossman, K.L., Grimsley, C., deBakker, C., Brugnera, E., Tosello-Trampont, A.C., Haney, L.B., Klingele, D., Sondek, J.*, et al.* (2004). PH domain of ELMO functions in trans to regulate Rac activation via Dock180. Nat Struct Mol Biol *11*, 756-762.

Lu, M., Kinchen, J.M., Rossman, K.L., Grimsley, C., Hall, M., Sondek, J., Hengartner, M.O., Yajnik, V., and Ravichandran, K.S. (2005). A Steric-inhibition model for regulation of nucleotide exchange via the Dock180 family of GEFs. Current biology : CB *15*, 371-377.

Lu, M., and Ravichandran, K.S. (2006). Dock180-ELMO cooperation in Rac activation. Methods in enzymology *406*, 388-402.

Luo, L. (2002). Actin cytoskeleton regulation in neuronal morphogenesis and structural plasticity. Annual review of cell and developmental biology *18*, 601-635.

Luttun, A., Tjwa, M., and Carmeliet, P. (2002). Placental growth factor (PlGF) and its receptor Flt-1 (VEGFR-1): novel therapeutic targets for angiogenic disorders. Annals of the New York Academy of Sciences *979*, 80-93.

Machacek, M., Hodgson, L., Welch, C., Elliott, H., Pertz, O., Nalbant, P., Abell, A., Johnson, G.L., Hahn, K.M., and Danuser, G. (2009). Coordination of Rho GTPase activities during cell protrusion. Nature *461*, 99-103.

Madaule, P., and Axel, R. (1985). A novel ras-related gene family. Cell *41*, 31-40.

Madaule, P., Furuyashiki, T., Reid, T., Ishizaki, T., Watanabe, G., Morii, N., and Narumiya, S. (1995). A novel partner for the GTP-bound forms of rho and rac. FEBS letters *377*, 243-248.

Margaron, Y., Fradet, N., and Cote, J.F. (2013). ELMO recruits actin cross-linking family 7 (ACF7) at the cell membrane for microtubule capture and stabilization of cellular protrusions. The Journal of biological chemistry *288*, 1184-1199.

Martin, G.R. (1998). The roles of FGFs in the early development of vertebrate limbs. Genes & development *12*, 1571-1586.

Matsuda, M., Ota, S., Tanimura, R., Nakamura, H., Matuoka, K., Takenawa, T., Nagashima, K., and Kurata, T. (1996). Interaction between the amino-terminal SH3 domain of CRK and its natural target proteins. The Journal of biological chemistry *271*, 14468-14472.

Mattila, P.K., and Lappalainen, P. (2008). Filopodia: molecular architecture and cellular functions. Nature reviews Molecular cell biology *9*, 446-454.

Mavria, G., Vercoulen, Y., Yeo, M., Paterson, H., Karasarides, M., Marais, R., Bird, D., and Marshall, C.J. (2006). ERK-MAPK signaling opposes Rho-kinase to promote endothelial cell survival and sprouting during angiogenesis. Cancer cell *9*, 33-44.

Mayer, B.J., and Baltimore, D. (1993). Signalling through SH2 and SH3 domains. Trends in cell biology *3*, 8-13.

Mazzone, M., Dettori, D., Leite de Oliveira, R., Loges, S., Schmidt, T., Jonckx, B., Tian, Y.M., Lanahan, A.A., Pollard, P., Ruiz de Almodovar, C*., et al.* (2009). Heterozygous deficiency of PHD2 restores tumor oxygenation and inhibits metastasis via endothelial normalization. Cell *136*, 839-851.

McAvoy, J.W., and Chamberlain, C.G. (1989). Fibroblast growth factor (FGF) induces different responses in lens epithelial cells depending on its concentration. Development *107*, 221-228.

McKay, M.M., and Morrison, D.K. (2007). Integrating signals from RTKs to ERK/MAPK. Oncogene *26*, 3113-3121.

McKenzie, J.A., and Ridley, A.J. (2007). Roles of Rho/ROCK and MLCK in TNF-alpha-induced changes in endothelial morphology and permeability. Journal of cellular physiology *213*, 221-228.

Medley, Q.G., Buchbinder, E.G., Tachibana, K., Ngo, H., Serra-Pages, C., and Streuli, M. (2003). Signaling between focal adhesion kinase and trio. The Journal of biological chemistry *278*, 13265-13270.

Melendez, J., Stengel, K., Zhou, X., Chauhan, B.K., Debidda, M., Andreassen, P., Lang, R.A., and Zheng, Y. (2011). RhoA GTPase is dispensable for actomyosin regulation but is essential for mitosis in primary mouse embryonic fibroblasts. The Journal of biological chemistry *286*, 15132-15137.

Meller, J., Vidali, L., and Schwartz, M.A. (2008). Endogenous RhoG is dispensable for integrin-mediated cell spreading but contributes to Rac-independent migration. Journal of cell science *121*, 1981-1989.

Meller, N., Irani-Tehrani, M., Kiosses, W.B., Del Pozo, M.A., and Schwartz, M.A. (2002). Zizimin1, a novel Cdc42 activator, reveals a new GEF domain for Rho proteins. Nature cell biology *4*, 639-647.

Meller, N., Irani-Tehrani, M., Ratnikov, B.I., Paschal, B.M., and Schwartz, M.A. (2004). The novel Cdc42 guanine nucleotide exchange factor, zizimin1, dimerizes via the Cdc42-binding CZH2 domain. The Journal of biological chemistry *279*, 37470-37476.

Meller, N., Merlot, S., and Guda, C. (2005). CZH proteins: a new family of Rho-GEFs. Journal of cell science *118*, 4937-4946.

Merks, R.M., Brodsky, S.V., Goligorksy, M.S., Newman, S.A., and Glazier, J.A. (2006). Cell elongation is key to in silico replication of in vitro vasculogenesis and subsequent remodeling. Developmental biology *289*, 44-54.

Michaelson, D., Abidi, W., Guardavaccaro, D., Zhou, M., Ahearn, I., Pagano, M., and Philips, M.R. (2008). Rac1 accumulates in the nucleus during the G2 phase of the cell cycle and promotes cell division. The Journal of cell biology *181*, 485-496.

Millard, T.H., and Martin, P. (2008). Dynamic analysis of filopodial interactions during the zippering phase of Drosophila dorsal closure. Development *135*, 621-626.

Miller, P.J., and Johnson, D.I. (1997). Characterization of the Saccharomyces cerevisiae cdc42-1ts allele and new temperature-conditional-lethal cdc42 alleles. Yeast *13*, 561-572.

Miyamoto, Y., Yamauchi, J., Sanbe, A., and Tanoue, A. (2007). Dock6, a Dock-C subfamily guanine nucleotide exchanger, has the dual specificity for Rac1 and Cdc42 and regulates neurite outgrowth. Experimental cell research *313*, 791-804.

Mor, F., Quintana, F.J., and Cohen, I.R. (2004). Angiogenesis-inflammation cross-talk: vascular endothelial growth factor is secreted by activated T cells and induces Th1 polarization. J Immunol *172*, 4618-4623.

Morreale, A., Venkatesan, M., Mott, H.R., Owen, D., Nietlispach, D., Lowe, P.N., and Laue, E.D. (2000). Structure of Cdc42 bound to the GTPase binding domain of PAK. Nature structural biology *7*, 384-388.

Munoz-Chapuli, R., Perez-Pomares, J.M., Macias, D., Garcia-Garrido, L., Carmona, R., and Gonzalez, M. (1999). Differentiation of hemangioblasts from embryonic mesothelial cells? A model on the origin of the vertebrate cardiovascular system. Differentiation *64*, 133-141.

Murakami, M. (2012). Signaling required for blood vessel maintenance: molecular basis and pathological manifestations. International journal of vascular medicine *2012*, 293641.

Nakatsu, M.N., Sainson, R.C., Aoto, J.N., Taylor, K.L., Aitkenhead, M., Perez-del-Pulgar, S., Carpenter, P.M., and Hughes, C.C. (2003). Angiogenic sprouting and capillary lumen formation modeled by human umbilical vein endothelial cells (HUVEC) in fibrin gels: the role of fibroblasts and Angiopoietin-1. Microvascular research *66*, 102-112.

Namekata, K., Watanabe, H., Guo, X., Kittaka, D., Kawamura, K., Kimura, A., Harada, C., and Harada, T. (2012). Dock3 regulates BDNF-TrkB signaling for neurite outgrowth by forming a ternary complex with Elmo and RhoG. Genes to cells : devoted to molecular & cellular mechanisms *17*, 688-697.

Nemethova, M., Auinger, S., and Small, J.V. (2008). Building the actin cytoskeleton: filopodia contribute to the construction of contractile bundles in the lamella. The Journal of cell biology *180*, 1233-1244.

Nishikimi, A., Meller, N., Uekawa, N., Isobe, K., Schwartz, M.A., and Maruyama, M. (2005). Zizimin2: a novel, DOCK180-related Cdc42 guanine nucleotide exchange factor expressed predominantly in lymphocytes. FEBS letters *579*, 1039-1046.

Nobes, C.D., and Hall, A. (1995). Rho, rac, and cdc42 GTPases regulate the assembly of multimolecular focal complexes associated with actin stress fibers, lamellipodia, and filopodia. Cell *81*, 53-62.

O'Brien, S.P., Seipel, K., Medley, Q.G., Bronson, R., Segal, R., and Streuli, M. (2000). Skeletal muscle deformity and neuronal disorder in Trio exchange factor-deficient mouse embryos. Proceedings of the National Academy of Sciences of the United States of America *97*, 12074-12078.

O'Farrell, A.M., Abrams, T.J., Yuen, H.A., Ngai, T.J., Louie, S.G., Yee, K.W., Wong, L.M., Hong, W., Lee, L.B., Town, A.*, et al.* (2003). SU11248 is a novel FLT3 tyrosine kinase inhibitor with potent activity in vitro and in vivo. Blood *101*, 3597-3605.

Oliver, G., and Detmar, M. (2002). The rediscovery of the lymphatic system: old and new insights into the development and biological function of the lymphatic vasculature. Genes & development *16*, 773-783.

Olsson, A.K., Dimberg, A., Kreuger, J., and Claesson-Welsh, L. (2006). VEGF receptor signalling - in control of vascular function. Nature reviews Molecular cell biology *7*, 359-371.

Oneyama, C., Agatsuma, T., Kanda, Y., Nakano, H., Sharma, S.V., Nakano, S., Narazaki, F., and Tatsuta, K. (2003). Synthetic inhibitors of proline-rich ligand-mediated protein-protein interaction: potent analogs of UCS15A. Chemistry & biology *10*, 443-451.

Ornitz, D.M., and Itoh, N. (2001). Fibroblast growth factors. Genome Biol *2*, REVIEWS3005.

Paduch, M., Jelen, F., and Otlewski, J. (2001). Structure of small G proteins and their regulators. Acta Biochim Pol *48*, 829-850.

Pai, E.F., Kabsch, W., Krengel, U., Holmes, K.C., John, J., and Wittinghofer, A. (1989). Structure of the guanine-nucleotide-binding domain of the Ha-ras oncogene product p21 in the triphosphate conformation. Nature *341*, 209-214.

Parrini, M.C., Lei, M., Harrison, S.C., and Mayer, B.J. (2002). Pak1 kinase homodimers are autoinhibited in trans and dissociated upon activation by Cdc42 and Rac1. Molecular cell *9*, 73-83.

Patel, M., Margaron, Y., Fradet, N., Yang, Q., Wilkes, B., Bouvier, M., Hofmann, K., and Cote, J.F. (2010). An evolutionarily conserved autoinhibitory molecular switch in ELMO proteins regulates Rac signaling. Current biology : CB *20*, 2021-2027.

Pawson, T., and Schlessingert, J. (1993). SH2 and SH3 domains. Current biology : CB *3*, 434-442.

Pellegrin, S., and Mellor, H. (2005). The Rho family GTPase Rif induces filopodia through mDia2. Curr Biol *15*, 129-133.

Peng, Y.J., He, W.Q., Tang, J., Tao, T., Chen, C., Gao, Y.Q., Zhang, W.C., He, X.Y., Dai, Y.Y., Zhu, N.C*., et al.* (2010). Trio is a key guanine nucleotide exchange factor coordinating regulation of the migration and morphogenesis of granule cells in the developing cerebellum. The Journal of biological chemistry *285*, 24834-24844.

Pollard, T.D., and Borisy, G.G. (2003). Cellular motility driven by assembly and disassembly of actin filaments. Cell *112*, 453-465.

Presta, M., Dell'Era, P., Mitola, S., Moroni, E., Ronca, R., and Rusnati, M. (2005). Fibroblast growth factor/fibroblast growth factor receptor system in angiogenesis. Cytokine Growth Factor Rev *16*, 159-178.

Qi, H., Fournier, A., Grenier, J., Fillion, C., Labrie, Y., and Labrie, C. (2003). Isolation of the novel human guanine nucleotide exchange factor Src homology 3 domain-containing guanine nucleotide exchange factor (SGEF) and of C-terminal SGEF, an N-terminally

truncated form of SGEF, the expression of which is regulated by androgen in prostate cancer cells. Endocrinology *144*, 1742-1752.

Qutub, A.A., and Popel, A.S. (2009). Elongation, proliferation & migration differentiate endothelial cell phenotypes and determine capillary sprouting. BMC Syst Biol *3*, 13.

Raich, W.B., Agbunag, C., and Hardin, J. (1999). Rapid epithelial-sheet sealing in the Caenorhabditis elegans embryo requires cadherin-dependent filopodial priming. Current biology : CB *9*, 1139-1146.

Ramchandran, R., Mehta, D., Vogel, S.M., Mirza, M.K., Kouklis, P., and Malik, A.B. (2008). Critical role of Cdc42 in mediating endothelial barrier protection in vivo. American journal of physiology Lung cellular and molecular physiology *295*, L363-369.

Reid, T., Furuyashiki, T., Ishizaki, T., Watanabe, G., Watanabe, N., Fujisawa, K., Morii, N., Madaule, P., and Narumiya, S. (1996). Rhotekin, a new putative target for Rho bearing homology to a serine/threonine kinase, PKN, and rhophilin in the rho-binding domain. The Journal of biological chemistry *271*, 13556-13560.

Reymond, N., Im, J.H., Garg, R., Vega, F.M., Borda d'Agua, B., Riou, P., Cox, S., Valderrama, F., Muschel, R.J., and Ridley, A.J. (2012). Cdc42 promotes transendothelial migration of cancer cells through beta1 integrin. J Cell Biol *199*, 653-668.

Ridley, A. (2013). GTPase switch: Ras then Rho and Rac. Nature cell biology *15*, 337.

Ridley, A.J. (2001). Rho GTPases and cell migration. Journal of cell science *114*, 2713-2722.

Ridley, A.J., and Hall, A. (1992). The small GTP-binding protein rho regulates the assembly of focal adhesions and actin stress fibers in response to growth factors. Cell *70*, 389-399.

Risau, W. (1990). Angiogenic growth factors. Prog Growth Factor Res *2*, 71-79.

Risau, W., and Flamme, I. (1995). Vasculogenesis. Annual review of cell and developmental biology *11*, 73-91.

Rossman, K.L., Worthylake, D.K., Snyder, J.T., Siderovski, D.P., Campbell, S.L., and Sondek, J. (2002). A crystallographic view of interactions between Dbs and Cdc42: PH domain-assisted guanine nucleotide exchange. The EMBO journal *21*, 1315-1326.

Rudolph, M.G., Bayer, P., Abo, A., Kuhlmann, J., Vetter, I.R., and Wittinghofer, A. (1998). The Cdc42/Rac interactive binding region motif of the Wiskott Aldrich syndrome protein (WASP) is necessary but not sufficient for tight binding to Cdc42 and structure formation. The Journal of biological chemistry *273*, 18067-18076.

Ruhrberg, C., Gerhardt, H., Golding, M., Watson, R., Ioannidou, S., Fujisawa, H., Betsholtz, C., and Shima, D.T. (2002). Spatially restricted patterning cues provided by

heparin-binding VEGF-A control blood vessel branching morphogenesis. Genes & development *16*, 2684-2698.

Rusnati, M., Dell'Era, P., Urbinati, C., Tanghetti, E., Massardi, M.L., Nagamine, Y., Monti, E., and Presta, M. (1996). A distinct basic fibroblast growth factor (FGF-2)/FGF receptor interaction distinguishes urokinase-type plasminogen activator induction from mitogenicity in endothelial cells. Molecular biology of the cell *7*, 369-381.

Ryan, H.E., Poloni, M., McNulty, W., Elson, D., Gassmann, M., Arbeit, J.M., and Johnson, R.S. (2000). Hypoxia-inducible factor-1alpha is a positive factor in solid tumor growth. Cancer research *60*, 4010-4015.

Sahai, E., and Marshall, C.J. (2002). RHO-GTPases and cancer. Nature reviews Cancer *2*, 133-142.

Samson, T., van Buul, J.D., Kroon, J., Welch, C., Bakker, E.N., Matlung, H.L., van den Berg, T.K., Sharek, L., Doerschuk, C., Hahn, K.*, et al.* (2013). The guanine-nucleotide exchange factor SGEF plays a crucial role in the formation of atherosclerosis. PloS one *8*, e55202.

Samson, T., Welch, C., Monaghan-Benson, E., Hahn, K.M., and Burridge, K. (2010). Endogenous RhoG is rapidly activated after epidermal growth factor stimulation through multiple guanine-nucleotide exchange factors. Molecular biology of the cell *21*, 1629-1642.

Sanematsu, F., Hirashima, M., Laurin, M., Takii, R., Nishikimi, A., Kitajima, K., Ding, G., Noda, M., Murata, Y., Tanaka, Y.*, et al.* (2010). DOCK180 is a Rac activator that regulates cardiovascular development by acting downstream of CXCR4. Circulation research *107*, 1102-1105.

Sanz-Moreno, V., Gadea, G., Ahn, J., Paterson, H., Marra, P., Pinner, S., Sahai, E., and Marshall, C.J. (2008). Rac activation and inactivation control plasticity of tumor cell movement. Cell *135*, 510-523.

Saunders, W.B., Bayless, K.J., and Davis, G.E. (2005). MMP-1 activation by serine proteases and MMP-10 induces human capillary tubular network collapse and regression in 3D collagen matrices. Journal of cell science *118*, 2325-2340.

Scehnet, J.S., Jiang, W., Kumar, S.R., Krasnoperov, V., Trindade, A., Benedito, R., Djokovic, D., Borges, C., Ley, E.J., Duarte, A.*, et al.* (2007). Inhibition of Dll4-mediated signaling induces proliferation of immature vessels and results in poor tissue perfusion. Blood *109*, 4753-4760.

Schneider, M., Othman-Hassan, K., Christ, B., and Wilting, J. (1999). Lymphangioblasts in the avian wing bud. Developmental dynamics : an official publication of the American Association of Anatomists *216*, 311-319.

Seipel, K., O'Brien, S.P., Iannotti, E., Medley, Q.G., and Streuli, M. (2001). Tara, a novel F-actin binding protein, associates with the Trio guanine nucleotide exchange factor and regulates actin cytoskeletal organization. Journal of cell science *114*, 389-399.

Siekmann, A.F., and Lawson, N.D. (2007). Notch signalling and the regulation of angiogenesis. Cell adhesion & migration *1*, 104-106.

Small, J.V., and Celis, J.E. (1978). Direct visualization of the 10-nm (100-A)-filament network in whole and enucleated cultured cells. Journal of cell science *31*, 393-409.

Sridhar, S.S., and Shepherd, F.A. (2003). Targeting angiogenesis: a review of angiogenesis inhibitors in the treatment of lung cancer. Lung Cancer *42 Suppl 1*, S81-91.

Stoletov, K.V., Ratcliffe, K.E., Spring, S.C., and Terman, B.I. (2001). NCK and PAK participate in the signaling pathway by which vascular endothelial growth factor stimulates the assembly of focal adhesions. The Journal of biological chemistry *276*, 22748-22755.

Stradal, T.E., and Scita, G. (2006). Protein complexes regulating Arp2/3-mediated actin assembly. Current opinion in cell biology *18*, 4-10.

Svitkina, T.M., Bulanova, E.A., Chaga, O.Y., Vignjevic, D.M., Kojima, S., Vasiliev, J.M., and Borisy, G.G. (2003). Mechanism of filopodia initiation by reorganization of a dendritic network. The Journal of cell biology *160*, 409-421.

Takenawa, T., and Suetsugu, S. (2007). The WASP-WAVE protein network: connecting the membrane to the cytoskeleton. Nature reviews Molecular cell biology *8*, 37-48.

Tammela, T., and Alitalo, K. (2010). Lymphangiogenesis: Molecular mechanisms and future promise. Cell *140*, 460-476.

Tan, W., Palmby, T.R., Gavard, J., Amornphimoltham, P., Zheng, Y., and Gutkind, J.S. (2008). An essential role for Rac1 in endothelial cell function and vascular development. FASEB journal : official publication of the Federation of American Societies for Experimental Biology *22*, 1829-1838.

Terasawa, M., Uruno, T., Mori, S., Kukimoto-Niino, M., Nishikimi, A., Sanematsu, F., Tanaka, Y., Yokoyama, S., and Fukui, Y. (2012). Dimerization of DOCK2 is essential for DOCK2-mediated Rac activation and lymphocyte migration. PloS one *7*, e46277.

Thomas, W.A., Boscher, C., Chu, Y.S., Cuvelier, D., Martinez-Rico, C., Seddiki, R., Heysch, J., Ladoux, B., Thiery, J.P., Mege, R.M*., et al.* (2013). alpha-Catenin and vinculin cooperate to promote high E-cadherin-based adhesion strength. The Journal of biological chemistry *288*, 4957-4969.

Ueda, S., Negishi, M., and Katoh, H. (2013). Rac GEF Dock4 interacts with cortactin to regulate dendritic spine formation. Molecular biology of the cell.

Van Aelst, L., and D'Souza-Schorey, C. (1997). Rho GTPases and signaling networks. Genes & development *11*, 2295-2322.

van Buul, J.D., Allingham, M.J., Samson, T., Meller, J., Boulter, E., Garcia-Mata, R., and Burridge, K. (2007). RhoG regulates endothelial apical cup assembly downstream from ICAM1 engagement and is involved in leukocyte trans-endothelial migration. The Journal of cell biology *178*, 1279-1293.

van Rijssel, J., Kroon, J., Hoogenboezem, M., van Alphen, F.P., de Jong, R.J., Kostadinova, E., Geerts, D., Hordijk, P.L., and van Buul, J.D. (2012). The Rho-guanine nucleotide exchange factor Trio controls leukocyte transendothelial migration by promoting docking structure formation. Molecular biology of the cell *23*, 2831-2844.

Vasioukhin, V., Bauer, C., Yin, M., and Fuchs, E. (2000). Directed actin polymerization is the driving force for epithelial cell-cell adhesion. Cell *100*, 209-219.

Vega, F.M., and Ridley, A.J. (2008). Rho GTPases in cancer cell biology. FEBS letters *582*, 2093-2101.

Vigil, D., Martin, T.D., Williams, F., Yeh, J.J., Campbell, S.L., and Der, C.J. (2010). Aberrant overexpression of the Rgl2 Ral small GTPase-specific guanine nucleotide exchange factor promotes pancreatic cancer growth through Ral-dependent and Ral-independent mechanisms. J Biol Chem *285*, 34729-34740.

Vigorito, E., Billadeu, D.D., Savoy, D., McAdam, S., Doody, G., Fort, P., and Turner, M. (2003). RhoG regulates gene expression and the actin cytoskeleton in lymphocytes. Oncogene *22*, 330-342.

Vincent, S., Jeanteur, P., and Fort, P. (1992). Growth-regulated expression of rhoG, a new member of the ras homolog gene family. Molecular and cellular biology *12*, 3138-3148.

Wang, H., Wu, R., Yu, L., Wu, F., Li, S., Zhao, Y., Li, H., Luo, G., Wang, J., and Zhou, J. (2012). SGEF is overexpressed in prostate cancer and contributes to prostate cancer progression. Oncology reports *28*, 1468-1474.

Wang, J.K., Gao, G., and Goldfarb, M. (1994). Fibroblast growth factor receptors have different signaling and mitogenic potentials. Molecular and cellular biology *14*, 181-188.

Watanabe, G., Saito, Y., Madaule, P., Ishizaki, T., Fujisawa, K., Morii, N., Mukai, H., Ono, Y., Kakizuka, A., and Narumiya, S. (1996). Protein kinase N (PKN) and PKN-related protein rhophilin as targets of small GTPase Rho. Science *271*, 645-648.

Wehrle-Haller, B. (2012). Structure and function of focal adhesions. Current opinion in cell biology *24*, 116-124.

Weis, S.M., and Cheresh, D.A. (2011). alphav Integrins in Angiogenesis and Cancer. Cold Spring Harb Perspect Med *1*, a006478.

Welch, M.D., and Mullins, R.D. (2002). Cellular control of actin nucleation. Annual review of cell and developmental biology *18*, 247-288.

Wennerberg, K., and Der, C.J. (2004). Rho-family GTPases: it's not only Rac and Rho (and I like it). J Cell Sci *117*, 1301-1312.

Wennerberg, K., Ellerbroek, S.M., Liu, R.Y., Karnoub, A.E., Burridge, K., and Der, C.J. (2002). RhoG signals in parallel with Rac1 and Cdc42. The Journal of biological chemistry *277*, 47810-47817.

Wheeler, A.P., and Ridley, A.J. (2004). Why three Rho proteins? RhoA, RhoB, RhoC, and cell motility. Experimental cell research *301*, 43-49.

Wilhelm, S., Carter, C., Lynch, M., Lowinger, T., Dumas, J., Smith, R.A., Schwartz, B., Simantov, R., and Kelley, S. (2006). Discovery and development of sorafenib: a multikinase inhibitor for treating cancer. Nature reviews Drug discovery *5*, 835-844.

Woolard, J., Wang, W.Y., Bevan, H.S., Qiu, Y., Morbidelli, L., Pritchard-Jones, R.O., Cui, T.G., Sugiono, M., Waine, E., Perrin, R.*, et al.* (2004). VEGF165b, an inhibitory vascular endothelial growth factor splice variant: mechanism of action, in vivo effect on angiogenesis and endogenous protein expression. Cancer research *64*, 7822-7835.

Wu, J., Song, Y., Bakker, A.B., Bauer, S., Spies, T., Lanier, L.L., and Phillips, J.H. (1999). An activating immunoreceptor complex formed by NKG2D and DAP10. Science *285*, 730-732.

Yajnik, V., Paulding, C., Sordella, R., McClatchey, A.I., Saito, M., Wahrer, D.C., Reynolds, P., Bell, D.W., Lake, R., van den Heuvel, S.*, et al.* (2003). DOCK4, a GTPase activator, is disrupted during tumorigenesis. Cell *112*, 673-684.

Yang, J., Zhang, Z., Roe, S.M., Marshall, C.J., and Barford, D. (2009). Activation of Rho GTPases by DOCK exchange factors is mediated by a nucleotide sensor. Science *325*, 1398-1402.

Yuan, X.B., Jin, M., Xu, X., Song, Y.Q., Wu, C.P., Poo, M.M., and Duan, S. (2003). Signalling and crosstalk of Rho GTPases in mediating axon guidance. Nature cell biology *5*, 38-45.

Zheng, J.Q., Wan, J.J., and Poo, M.M. (1996). Essential role of filopodia in chemotropic turning of nerve growth cone induced by a glutamate gradient. The Journal of neuroscience : the official journal of the Society for Neuroscience *16*, 1140-1149.